PHENOTYPIC, CELLULAR AND MOLECULAR CHARACTERIZATION OF THE *CRX*-LCA FELINE MODEL AND POTENTIAL THERAPIES

By

Laurence Mireille Alice Occelli

A DISSERTATION

Submitted to
Michigan State University
in partial fulfillment of the requirements
for the degree of

Comparative Medicine and Integrative Biology — Doctor of Philosophy

2017

ABSTRACT

PHENOTYPIC, CELLULAR AND MOLECULAR CHARACTERIZATION OF THE *CRX*-LCA FELINE MODEL AND POTENTIAL THERAPIES

By

Laurence Mireille Alice Occelli

Leber's congenital amaurosis (LCA) is one of the major inherited causes of childhood blindness. Mutations in the cone-rod homeobox (*CRX*) gene result in severe dominant retinopathies and can be responsible for LCA. CRX is a transcription factor essential for normal photoreceptor development and survival. The Crx^{Rdy} cat has a spontaneous frameshift mutation in *Crx* and represents a model for Class III *CRX* mutations where the mutant *CRX* allele binds DNA but fails to transactivate it. The Crx^{Rdy} cat model is valuable for investigating disease mechanisms as well as potential therapy development.

In this model, early disease stages in the heterozygous cat ($Crx^{Rdy/+}$) mimic severe Leber's congenital amaurosis. This is characterized by a dominant negative effect of the mutant *Crx* mRNA/protein over the wild-type mRNA/protein. This study fully investigated the early phenotype as well as the timing and extent of retinal remodeling during retinal degeneration. There is early halting of photoreceptor development coupled with over expression of the mutant *Crx* allele, accumulation of abnormally high mutant Crx protein levels, resulting in markedly impaired visual function followed by retinal degeneration. During the late stages of the disease, extensive inner retinal remodeling occurred with some retinal pigmentary epithelium (RPE) degeneration in the *area centralis* (macula-like high retinal acuity region of the feline retina) and also vascular remodeling. The homozygous cat ($Crx^{Rdy/Rdy}$) had a different phenotype with halting of photoreceptor development at an earlier stage resulting in complete blindness and total lack of photoreceptor function. This was followed by a slower photoreceptor degeneration and extensive

retinal remodeling that differed from that of the heterozygote cat. Additionally, there was a marked increase in globe size with a severe alteration in refraction.

There is currently no treatment for dominant negative LCA diseases. Yet, the investigation findings on *Crx*$^{Rdy/+}$ cat model and the similarities between the feline eye and the human eye with the presence of a macula-like region make this feline model valuable for preclinical testing of therapies for dominant *CRX* diseases. The detailed phenotyping sheds light on the therapeutic approach needed. Prior to photoreceptor degeneration, a therapeutic approach aiming to restore function to endogenous photoreceptors would need to increase the expression levels of the wild-type allele over the mutant transcript. Following photoreceptor degeneration, therapeutic approaches to replace photoreceptors or to activate light-induced responses in other retinal neurons would need to be performed before retinal remodeling and neuronal cell loss become too extensive. Trial therapy using a gene augmentation approach showed some promise to improve the phenotype but requires further optimization.

The *Crx*^{Rdy} cat is a valuable model for Class III *CRX* mutations, RPE degeneration and deprivation myopia mechanism, and therapy development.

This dissertation is dedicated to my parents who supported me since the beginning and never let me down no matter what. But most importantly it is dedicated to all research animals especially the cats whose lives were used for Human research. Thank you for never giving me grief, for making me smile and for giving the love that kept me going.

ACKNOWLEDGEMENTS

I would like to thank my major advisor Dr Simon Petersen-Jones for giving me that research opportunity and for the endless hours of discussion (animated or not) that we spent together speaking about research; the last 6 years flew!

I also thank my committee members. I would to thank Dr András Komáromy, although always very quiet he always supported me. He knows I owe him a lot for in my future career. I thank Dr Debra Thompson, the only woman of my committee; she was there and took time for me when I needed a major advice. Finally, I would like to acknowledge Dr John Kruger for always being available for medical advice for our animal colonies and for providing scientific and financial support.

I would like to thank all the collaborators far or near this project who helped me develop my skills and knowledge and therefore at a major impact on me and this work:

- Dr Shiming Chen and Dr Nicholas Tran, the mouse experts in *CRX* mutations.
- Dr Patrick Venta and Dr Arthur Weber, always available for scientific advice and discussion.
- Dr Alicia Withrow and Dr Melinda Frame, the electron microscopy and confocal experts.
- The Univeristy of Florida viral vector expert; Dr William Hauswirth, Dr Shannon Boye and Sanford Boye.
- Dr Kristina Narfström, from whom the *Crx* cat colony came.
- Dr Bryan Jones, the retinal remodeling expert.
- The many scientists from the Kellogg Eye Center who were always available for advice notably Dr Patrice Fort and Dr Thomas Gardner.

- Other collaborators such as Dr Don Hood; the OCT expert, Isis Pharmaceuticals, Dr Steve Surh, MPI, Dr Yuzbasivan-Gurkan Lab (Dr Maciej Parys), Dr John Fyfe.
- The RATTS group; Janice Querubin for her endless hours of some kitten ERGs and others, Kristin Koehl for her help and moral support, and Heather Defore for pulling with me and their tremendous understanding those last months.
- The vivarium and ULAR staffs for taking care for our animals especially those who I would like to refer as "my" precious cats to me; Lisa Allen, Kim Williamson, the students. Special thanks to Ramona Stambaugh for all her help with the animal care but mainly her moral support during weekends over the years.
- The CMIB staff for their help and guidance during this PhD expecially Dr Yuzbasivan-Gurkan, Dr Victoria Hoelzer-Maddox and Dimity Palazzola.
- The CVM MSU staff especially Debbie Roman and Whitney Smith for their availability and huge help in administrative matters.
- My major fundings: Myers-Dunlap Endowment, George H. Bird and ''Casper'' Endowment for Feline Initiatives, Michigan State University Center for Feline Health and Well-Being and Michigan State University College of Veterinary Medicine Endowed Research Funds.

On a more personal note, I would like to thank the endless number of people I met and for some work with those last 6 years and family members for their support.

- All my labmates who taught me a lot about working environment and relationships. I am happy to say I gained friends; Dr Paige Winkler, Dr Kara Gornik thanks for being there in my dark hours during my MSU time.

- All the students who worked or were involved at some point in the SPJ lab. A big thank you to Taylor Chambers, Dr Ashlee Bruewer, Nate Parsmanter, Dr Laure Damitio for their understanding and free help.
- Christine Harman and Kristin Koehl for their help with lab stuffs and friendships.
- Previous residents and MSU mentors: a huge thanks to Dr Joshua Bartoe for his help and moral support over the years and Dr Ryan Boyd for sharing a scientific passion.

Finally I would like to thank people how have a huge place in my personal life.

- My parents for their moral and financial support over so many years of studying…. your patient is endless and I love you.
- The rest of my family for believing in me.
- My previous mentors and for some now dear friends who have impacted my career: Dr Jacques Fajardi, Dr Margie Neaderland, Dr Joe Wolfer, Dr Peter Bedford, Dr Hatim Alibhai, my high schools teachers.
- Sanjuanita Perez for driving me back home at 1am after long hours and for all her support and friendship over the years.
- My dear friends who were there on the phone during my darkest hours and make themselves available: Fabien, Damien, Isabelle, Leah, Steph, Pablo, Elodie, Candide, Penny, Wendy.
- Cwen for her last minute tremendous help and support.
- My boyfriend Caleb and his cute clumsy but honest endless support. Thanks for pulling with me and accepting my animated discussions. I love you and hope we will go through many more years together. Thanks to his family to have welcomed me in theirs.

- Last but not the least; all my pets present and past who gave me my vet passion especially the Gus Gus but mostly all the lab animals. To all my research cats I do and will remember every single one of you, whatever people might say you all had your own personality and I miss the ones gone dearly.

TABLE OF CONTENTS

LIST OF TABLES

LIST OF FIGURES

KEY TO ABBREVIATIONS

AAV	Adeno-associated virus
AC	*Area centralis*
AF	Autofluorescence
Arr	Arrestin
bp	Base pair
CBA	Chicken β-actin
CoRD	Cone-rod dystrophy
Crx	Cone-rod homeobox
$Crx^{Rdy/+}$	Heterozygous *Crx* mutant cat
$Crx^{Rdy/rdy}$	Homozygous *Crx* mutant cat
cSLO	Confocal scanning laser ophthalmoscopy
DAPI	4',6-diamidino-2-phenylindole
ELM	External limiting membrane
EM	Electron microscopy
ERG	Electroretinography/Electroretinogram
EZ	Ellipsoid zone
F	Phenylalanine
FA	Fluorescein angiography
FAF	Fundus autofluorescence
GAPDH	Glyceraldehyde-3-phosphate dehydrogenase
GCC	Ganglion cell complex
GCL	Ganglion cell layer

GFAP	Glial fibrillary acidic protein
GFP	Green fluorescent protein
hCAR	Human cone arrestin
IHC	Immunohistochemistry
ILM	Inner limiting membrane
INL	Inner nuclear layer
IPL	Inner plexiform layer
IR	Infrared
IR	Inner retina
IS	Inner photoreceptor segment
IZ	Interdigitation zone
LCA	Leber congenital amaurosis
ML-opsin (MLO)	Medium-Long wavelength opsin
NeuN	Neuronal nuclei
NFL	Nerve fiber layer
NRL	Neural retina-specific leucine zipper protein
NR2E3	Photoreceptor-specific nuclear receptor
OTX2	Orthodenticle homebox 2
ONL	Outer nuclear layer
OS	Outer photoreceptor segment
OPL	Outer plexiform layer
PBS	Phosphate buffered saline
PFA	Paraformaldehyde
PKCα/PKCa	Protein kinase C alpha

PR	Photoreceptor
REC+	Receptor+
Rho	Rhodopsin
RORβ	Orphan nuclear receptor
RP	Retintis pigmentosa
RPE	Retinal pigmentary epithelium
SD-OCT	Spectral Domain – Optical Coherence Tomography
S-opsin (SO)	Short-wavelength opsin
TR	Total retina
TRβ2	Thyroid hormone receptor β2
Tuba1b	Tubulin alpha-1B chain
Y	Tyrosine

CHAPTER 1

INTRODUCTION

ANIMAL MODELS FOR DOMINANT LEBER CONGENITAL AMAUROSIS (LCA) DUE TO *CRX* MUTATIONS – INTRODUCTION OF THE FELINE MODEL AND POTENTIAL THERAPIES

1.1. RETINAL INHERITED DISEASES AND BLINDNESS

Severe impairment of vision and more dramatically blindness is widespread across the globe. The World Health Organization (WHO**;** http://www.who.int/mediacentre/factsheets/fs282/en/ available in the public domain) estimates that impairment of vision affected about 285 million people including 19 million children (under 15) with about 246 million people having low vision and 39 million being blind.[1] Blindness is an important factor affecting the life quality of a significant number of people. Causes of visual impairment and in more severe case blindness can be metabolic (like diabetes mellitus), infectious (like onchocerciasis, leprosy), traumatic or inherited. About 43% of visual impairment is reported to be due to uncorrected refractive errors like myopia, hyperopia or astigmatism, 33% due to unoperated cataract and 2% from glaucoma.[1] Inherited diseases affecting notably the retina are another cause of visual impairment and in worse cases blindness.

Hereditary disorders are a common cause of photoreceptor dysfunction and degeneration resulting in vision loss with a prevalence of 1 in approximately 3,000.[3-5] Currently 293 genes and loci are mapped and 256 identified (Fig.1.1) as being associated with hereditary retinal disease by RetNet, the Retinal Information Network (RetNet[6]; https://sph.uth.edu/retnet; available in the public domain). The known genes are divided into many functional categories reflecting both the complexity of the retina but also the stresses involved in the unique retinal environment with high oxygen requirements and light exposure (Fig. 1.2).[5]

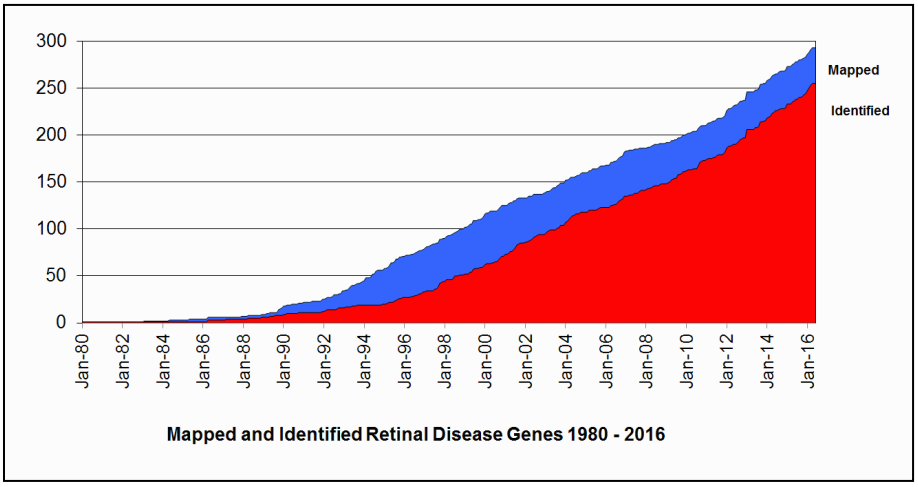

Figure 1.1. Mapped and identified retinal disease genes 1980-2016 (from RetNet 2017 [6]).

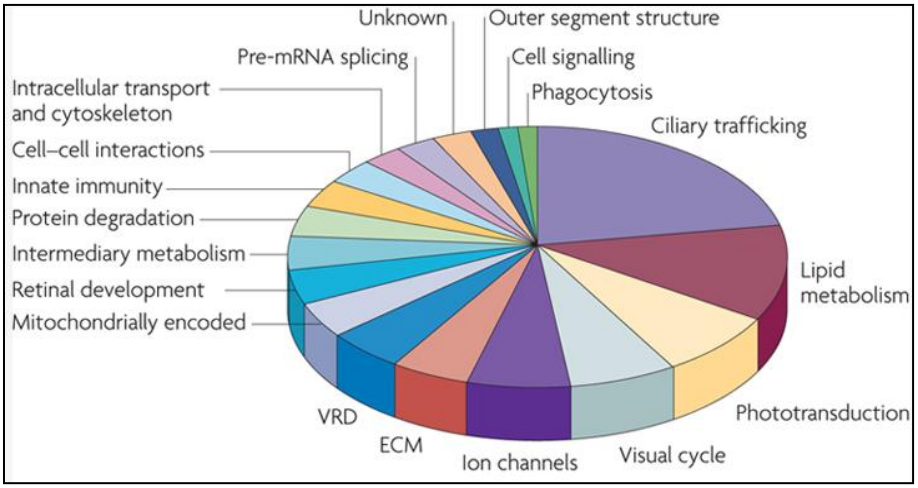

Figure 1.2. Functional categories of retinal disease genes (from Wright et *al*. 2010) [5].

1.2. THE EYE AND ANIMAL MODELS

To understand the underlying mechanisms of single-gene human retinal diseases, animal models are used. Indeed, there is a high degree of homology between genomes and notably mammalian genomes. Many of the human genes are also found in small animal models like rodents (mice and rats) and large animal models like cats, dogs and primates.

1.2.1. General eye and retinal anatomy

1.2.1.1. General eye anatomy and development

The eye is a neurosensitive organ. It acts as the black box of a camera and the retina located at the back of the eye as a sensitive film where the image forms (Fig. 1.3).

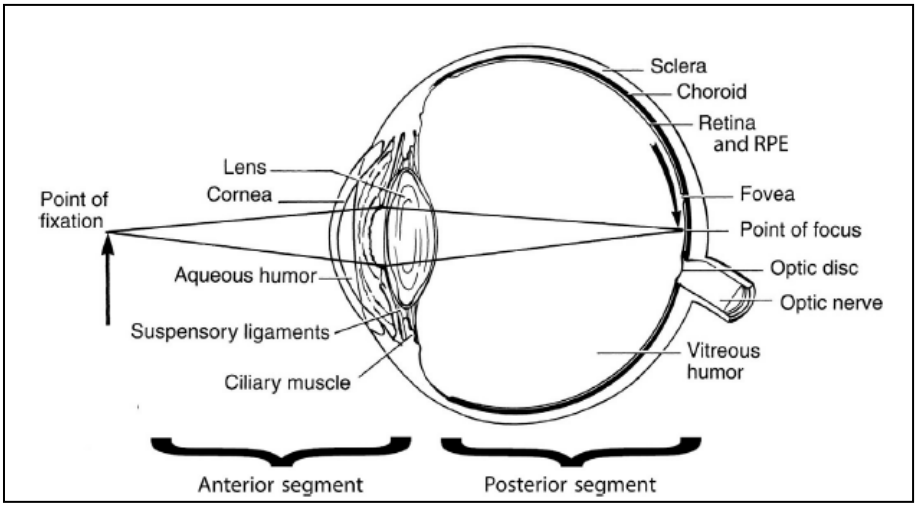

Figure 1.3. Schematic of the eye (from Hejtmancik et *al.*,2015).
The light rays go through the cornea, aqueous humor, lens and vitreous before focusing onto the retina. The viewed object (here indicated as an arrow) will be projected onto the retina as an inverted image, which will be converted into electrical impulse by the retina and transmitted to the brain.[7]

The eye is composed from its front to its back by (Fig. 1.3 above):

The anterior segment including:

- the cornea, transparent structure at the front of the eye

- the aqueous humor in the anterior chamber

- the lens, structure which help to focus the light on the retina

- the posterior chamber between the lens and iris

- The iris and ciliary bodies

The posterior segment including:

- the vitreous

- the retina

- the choroid then sclera

The eye is linked to the brain by the optic nerve, which transmits the information transformed from light to electrical impulse by the retina.

During prenatal development, the different structures of the eye come from the ectoderm (neuroectoderm and surface ectoderm) or the head mesenchyme (neural crest and mesoderm).
The retinal pigmented epithelium, ciliary body and iridal epitheliums, the sensory retina and innermost layer of the ciliary bodies (non-pigmented), the optic nerve, the iris sphincter and dilator muscles and part of the vitreous originate from the neuroectoderm. The surface ectoderm is at the origin of the lens, the corneal epithelium, the conjunctiva and caruncle, the eyelid skin and the lacrimal apparatus (glands and drainage system). The rest of the structures originate from the neural crest and/or mesoderm; blood vessels, corneal stroma and endothelium, stroma of the choroid, ciliary body stroma and part of the iris, ciliary muscle, sclera, optic nerve sheath (meninges), extraocular muscles and fasciase, remainder of the eyelids (i.e. orbicularis oculi muscle, tarsus, orbital septum, etc…) and part of the vitreous (Figs. 1.4 and 1.5).[7, 8]

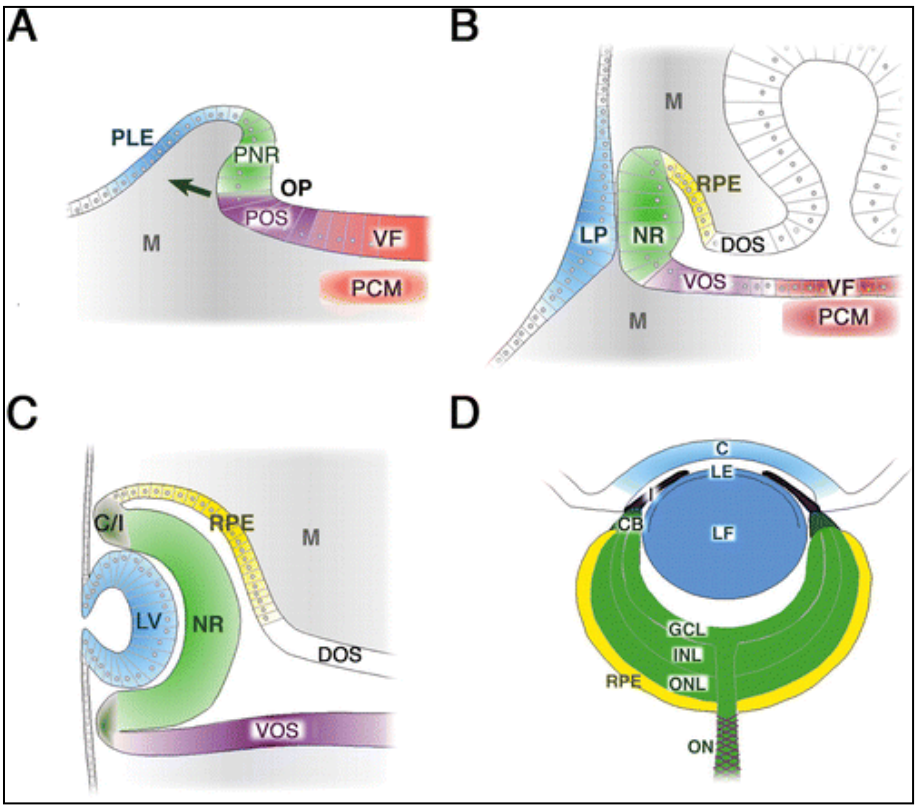

Figure 1.4. Schematic overview of vertebrate eye development (from Chow et *al*., 2001).[9]
In panels **(A–D)**, presumptive or differentiated eye tissues are color-coded in the following manner: *blue*, lens/cornea; *green*, neural retina; *yellow*, retinal pigmented epithelium (RPE); *purple*, optic stalk (for explanation of why only the ventral region of optic stalk is colored, see the text section on defining axes in the developing eye); *red*, ventral forebrain/prechordal mesenchyme; *grey*, mesenchyme.
(A) Formation of the optic vesicle is initiated by an evagination (*indicated by arrow*) of the presumptive forebrain region resulting in the formation of the optic pit (OP). The optic vesicle region is divided into dorso-distal region (*green*), which contains the presumptive neural retina (PNR) and RPE (not shown), and the proximo-ventral region, which gives rise to the presumptive ventral optic stalk (POS); PLE, presumptive lens ectoderm; M, mesenchyme; VF, ventral forebrain; PCM, prechordal mesoderm.
(B) Continued growth of the optic vesicle culminates with a period of close contact between the lens placode (LP) and the presumptive neural retina (NR) during which important inductive signal likely exchange: RPE, presumptive retinal pigmented epithelium; VOS, ventral optic stalk; DOS, dorsal optic stalk.
(C) Invagination of the optic vesicle results in formation of the lens vesicle (LV) and neural retina (NR) and establishes the overall structure of the eye. The point at which the neural retina and RPE meet gives rise to components of the ciliary body and iris (C/I).
(D) Mature eye: C, cornea; LE, lens epithelium; LF, lens fiber cells; I, iris; CB, ciliary body; GCL, ganglion cell layer; INL, inner nuclear layer; ONL, outer nuclear layer; ON, optic nerve.

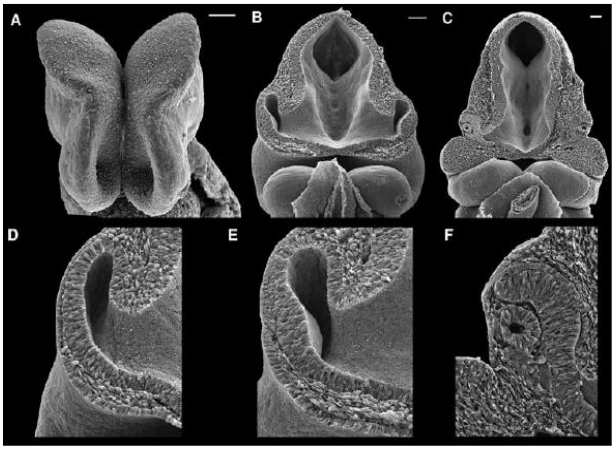

Figure 1.5. Anatomy of embryonic mouse forebrain and eyes (from Heavner et *al.*, 2012).[10]
(A) Frontal view of embryonic day E8.5 forebrain, just before the eye field splits. The optic sulci are the large pits protruding from the ventral neural ectoderm. **(B)** Wide and **(D)** high magnification views of frontal sections of the E9.0 to E9.5 optic vesicle. **(E)** The coordinated invagination of the distal optic vesicle and the surface ectoderm, where the lens placode has thickened, begins at E9.5. **(C)** Wide and **(F)** high magnification views of frontal sections of the E10.5 optic cup and lens vesicle. The retinal pigment epithelium is the thin layer of cells proximal to the neural retina, which is dorsal to the optic stalk. The optic stalk is continuous with the ventral forebrain. The lens vesicle is distal to the neural retina. Dorsal is to the top **(A–F)**, and proximal is to the right **(D–F**). Scale bars, 50 mm (A); 100 mm (B, C). (Photo from Lee Langer)

1.2.1.2. General retinal anatomy and retinogenesis

The retina covers the back of the eye and extends from the optic nerve head to the ora ciliaris. The retinal structure (Figs. 1.6 and 1.7) is composed of 10 layers of very specialized cells. They include from its basal side (referred as "outer" structures) to the side in contact with the vitreous (referred as "inner" structures):

- Retinal pigmentary epithelium (RPE),
- Photoreceptor outer and inners segments (Photoreceptor OS/IS),
- External limiting membrane (ELM),
- Outer nuclear layer (ONL),
- Outer plexiform layer (OPL),
- Inner nuclear layer (INL),

- Inner plexiform layer (IPL),

- Ganglion cell layer (GCL),

- Nerve fiber layers (NFL)

- Internal limiting membrane (ILM).

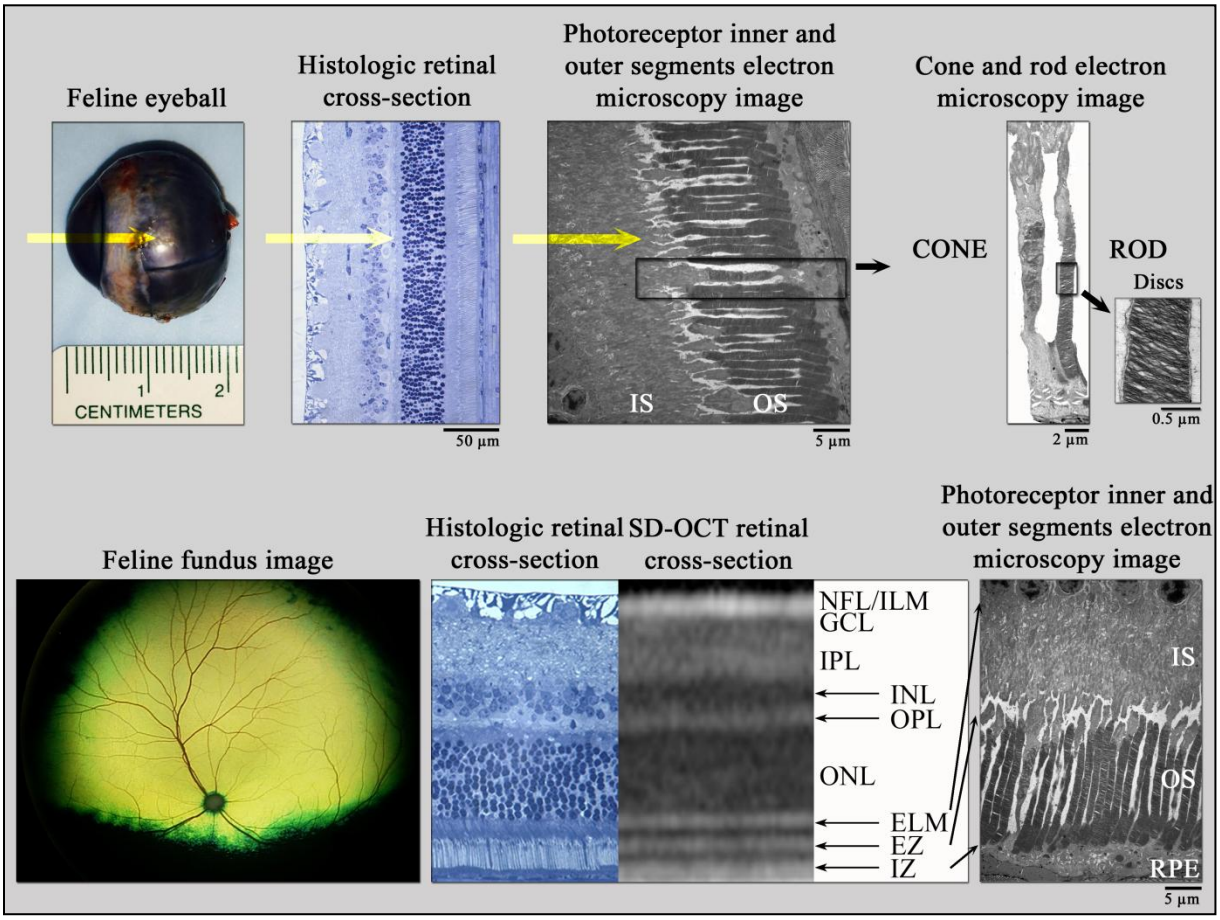

Figure 1.6. Representative photographs and images of a feline eye and retina.
The yellow arrows represent the light path that goes through the eye traversing the cornea, aqueous humor, lens and vitreous before hitting the retina, which is the neural covering the back of the eye. This structure is composed of 10 layers and most importantly the photoreceptor layer composed of rod and cones, which is a structure that converted the light into electrical signal as the level of the discs. The feline fundus image shows that in the dorsal region the feline eye has a colored structure called the tapetum, which is thought to increase light exposure of the photoreceptors; RPE; Retinal pigmentary epithelium; Photoreceptor OS/IS; Photoreceptor outer and inners segments, ELM; External limiting membrane, ONL; Outer nuclear layer, OPL; Outer plexiform layer, INL; Inner nuclear layer, IPL; Inner plexiform layer, GCL; Ganglion cell layer, NFL; Nerve fiber layers; ILM; Internal limiting membrane, EZ; ellipsoid zone and IZ; Interdigitation zone.

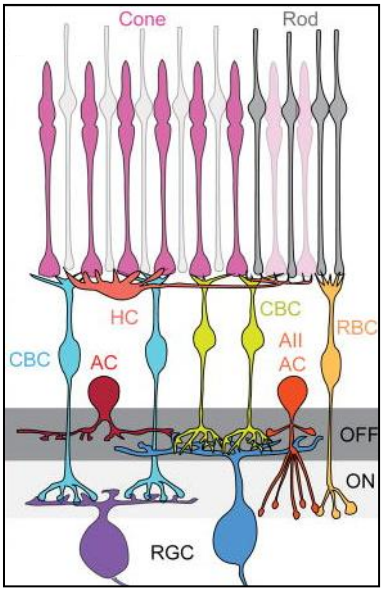

Figure 1.7. Schematic showing major retinal pathways and cells composing the retina (from D'Orazi et *al*., 2014).[11]
Rod and cone photoreceptors detect changes in illumination, with rods functioning at low light levels, and cones at high light levels. Photoreceptor signals are conveyed by bipolar cells to retinal ganglion cells (RGCs). Cone bipolar cells (CBC) that largely contact cone photoreceptors are grouped into two major subclasses. Light increments depolarize ON-bipolar cells and hyperpolarize OFF-bipolar cells. ON and OFF synaptic connections are organized into separate laminae within the IPL. Horizontal cells (HC) and amacrine cells (AC) modulate information flow in the outer and inner retina, respectively. Rod bipolar cells (RBCs) predominantly convey rod input, and contact AII amacrine cells (AII AC) that inhibit transmission from OFF-CBCs.

The development of the retina is called retinogenesis or retinal neurogenesis (Figs. 1.8 and 1.9). This phenomenon results in the formation of the layered retina, which is comprised of three distinct cellular layers. From the exterior of the eye to the inside (side of the vitreous), those cell layers include the outer nuclear layer containing the cell nuclei of the rod and cone photoreceptor cells, the inner nuclear layer composed of the nuclei of the Müller, amacrine, horizontal and bipolar cells and the neuronal layer formed by the nuclei of the ganglion cells. The time for retinogenesis varies depending on the species, but overall they have the same order of cell differentiation as illustrated for the mouse (Figs. 1.8 and 1.9).[12, 13]

The neurosensory retina consists of all retinal layers excluding the retinal pigment epithelium, which is positioned external to the neurosensoryretina. Photoreceptors, which are divided into rods and cones, are specialized cells that are responsible for the conversion of the image focused onto the retina into an electrical message, which is then processed in the rest of the retina and transmitted to the brain (Figs. 1.6 and 1.7). Cones are responsible for higher visual acuity, daytime color vision, whereas rods are highly sensitive allowing for vision at low light levels.

Retinogenesis is controlled by transcription factors and neurotransmitters that determine the fate of retinal progenitors cells and lead to retinal cell differentiation. Retinal progenitor cells undego specific mitosis and migration within the retina to end up differentiating to a specific type of cells and fate. Ganglion cells, horizontal cells, cone photreceptor cells and amacrine cells differentiate first while rod photoreceptor cells, bipolar cells and Müller glail cells differentiate at a later time (Figs. 1.8 and 1.9).

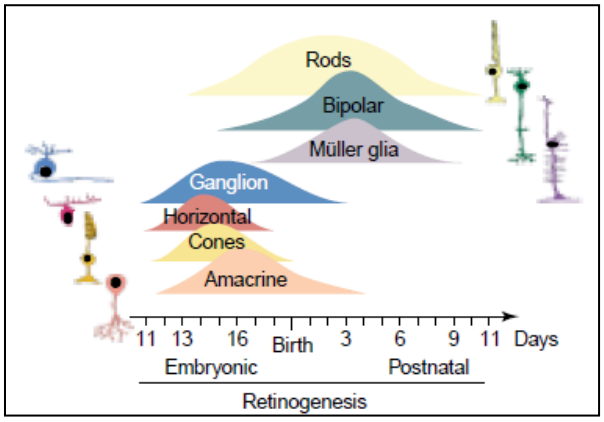

Figure 1.8. Retinal neurogenesis proceeds in a fixed histogenetic order (time scaled from mouse) (from Marquardt et *al.* 2002).[13]

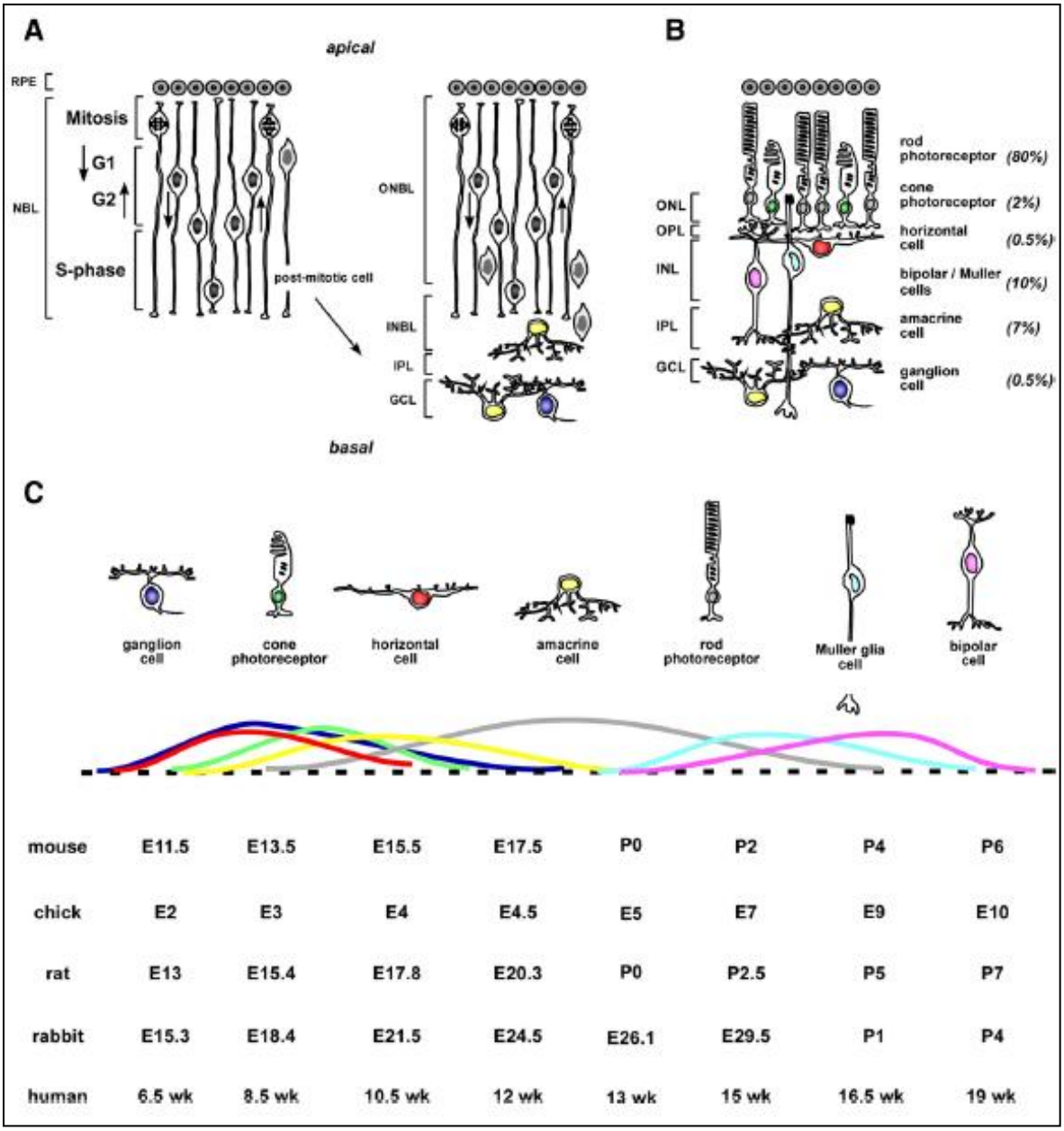

Figure 1.9. Structural organization of the developing and adult vertebrate retina (from Martins et *al.*,2008).[14]

(A) In early retinogenesis, the developing neural retina is composed of undifferentiated dividing cells. These neuroblasts undergo a period of rapid cell division, which allows for the expansion of the retinal progenitor cell pool. As observed throughout most CNS tissue, the nuclei of retinal progenitor cells migrate up and down throughout the depth of the retinal tissue. S-phase occurs at the basal surface, while mitosis occurs at the apical surface, adjacent to the retinal pigmented epithelium (RPE). The nuclei migrate between these two surfaces during G1 and G2 in a process called interkinetic nuclear movement (INM). The extracellular environment undergoes dramatic changes as progenitor cells begin to exit the cell cycle. During neurogenesis the differentiating cells (initially ganglion and amacrine cells) may release a variety of signaling molecules into the environment, which may send feedback to modulate progenitor cell proliferation.

Figure 1.9 (cont'd)
(B) The mature vertebrate retina is mainly comprised of seven cell types (ganglion, amacrine, horizontal and bipolar cells, cone and rod photoreceptors and the Müller glial cell), which are organized into three cell layers. The proportion of the different cell types in the adult retina varies dramatically (more than 100-fold). The generation of the correct proportions of each cell type is crucial for visual function and depends on the appropriate control of proliferation and cell-cycle exit. The approximate proportion of the retinal cell types in the mouse adult retina is shown.
(C) Retinal histogenesis follows an evolutionarily conserved birth order. For clarity, the approximate timing and sequence of neurogenesis of the different retinal cell types during development of the mouse, chick, rat, rabbit and human neural retinas are shown.

1.2.1.3. Specificities of the feline photoreceptor development

Although having similar retinogenesis, the feline retina has its own temporal specificities.

The first wave of cell differentiation during retinogenesis involves 3 cell classes: the ganglion cells, cone photreceptor cells and horizontal cells. The amacrine cells then develop followed by the rod photoreceptor cells, Müller cells then bipolar cells. The known details of the timeline of the cat retina development and maturation are summarized in Fig. 1.10 below.[15]

It should be noted that a spatial/temporal difference in development exists and that a central to peripheral maturation happens during feline retinal retinogenesis and maturation. Indeed the cytogenesis first ceases in the *area centralis* and then in the visual streak (high photoreceptor density areas that will be described in more detail later in the chapter).[16, 17]

Paralleling the retinal cells differentiation, the retinal vasculature also matures from the center to the periphery. The inner vasculature development starts with the spread of mesenchymal cells at E26; then by E48 some coarse capillaires have formed from those spindle cells, and finally the major vessels differentiate and capillaries thinned. Starting at P7-10 and spreading to the periphery, additional vasculature forms from the existing vasculature resulting in vasculature of the area centralis inner layer, the outer layer vasculature and also to the capillaries surrounding the optic papilla (which form at P20).[18]

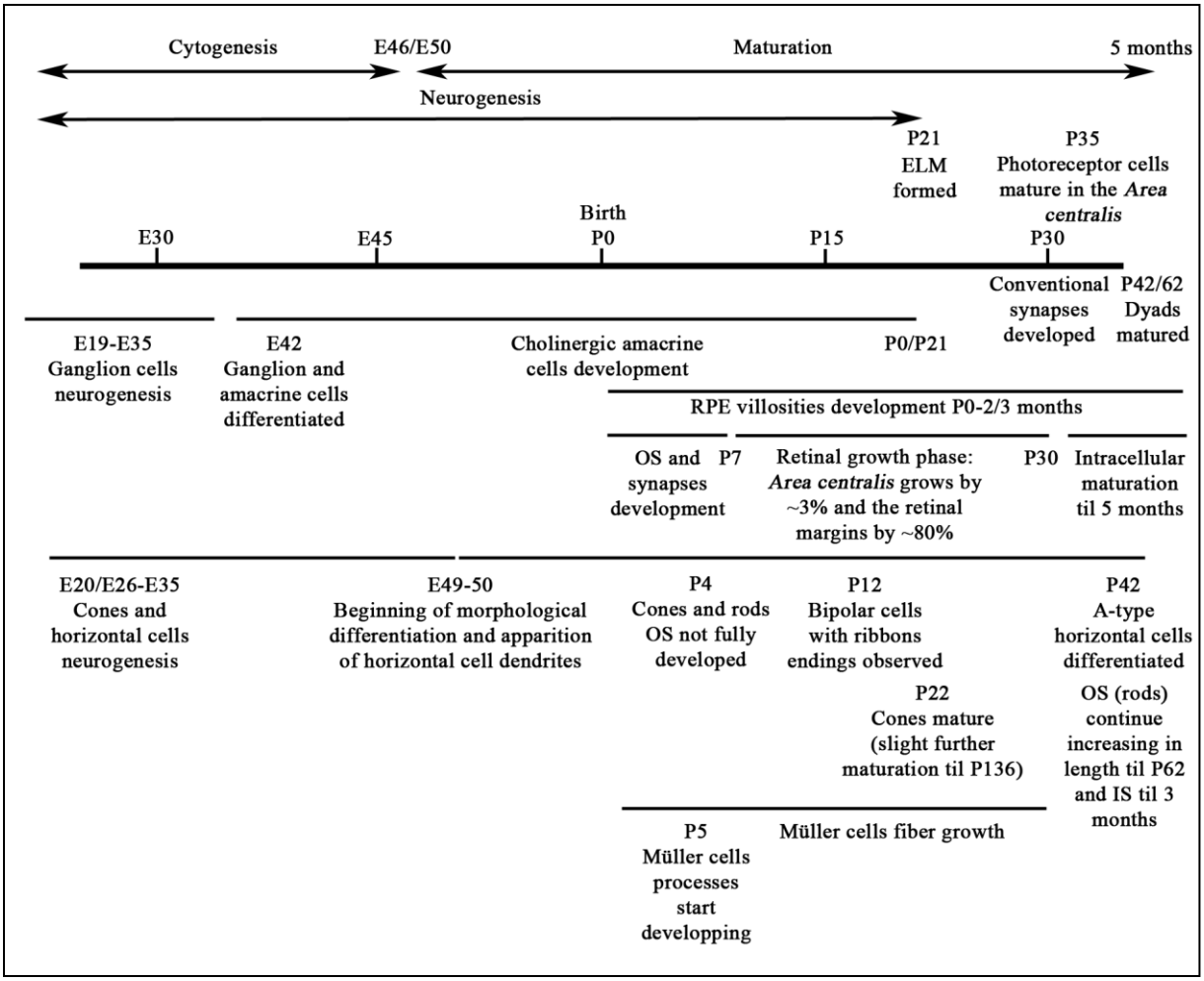

Figure 1.10. Temporal differentiation and maturation of the feline retina. RPE; retinal pigmentary epithelium, ELM; external limiting membrane; OS and IS; outer and inner photoreceptor segments.[15-17, 19-21]

Concomittantly to morphological maturation, the feline retina, similarly to that of other species, undergoes a functional maturation, which can be followed by the electroretinogram (ERG) that assesses the retinal response to a light stimulus. Two types of regular ERG are usually assessed, the dark-adapted or scotopic ERG (where the animal is dark adapted; we allow one hour in our laboratory) and the light-adapted or photopic ERG (where the animal is adapted in a ganzfeld dome to a rod suppressing backgound light of 30 cd/m^2 light for 10 min) (Fig. 1.11, left image). Scotopic ERG are used to assess rod photoreceptor at low light stimulus luminances

while assessing a mixed rod and cone responses at stronger light stimuli. The photopic (light-adapted) ERG is used to assess cone photoreceptor function. Alternating current (AC) ERGs are recorded using three electrodes. A recording electrode which can be an electrode on the cornea (Fig. 1.11, right image) or in some research settings an intraocular electrode may be used. A skin reference electrode is positioned adjacent to the lateral canthus, between the eyes or on the conjunctiva/lid. A ground electrode is usually a skin electrode placed on the forehead, on the occiput or between scapulas. The electrode positioning can be different depending on the laboratory protocol.

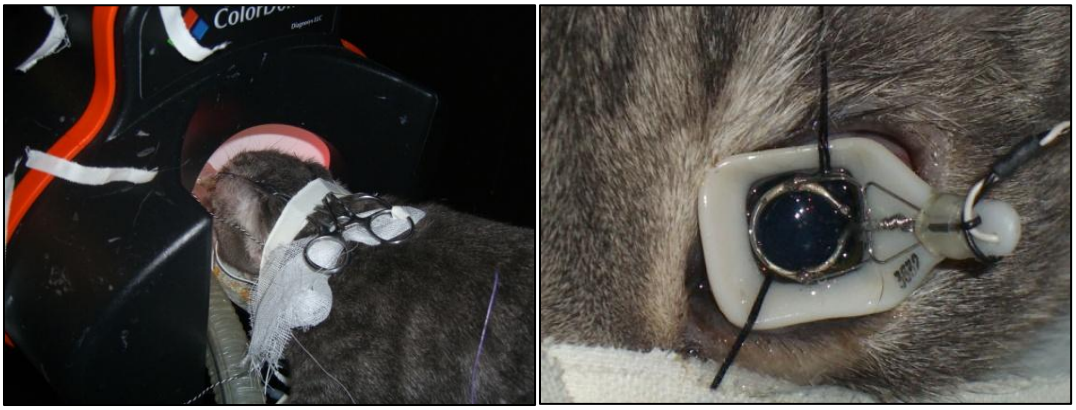

Figure 1.11. Positioning of a cat for ERG. Left image: The image shows a cat with its head in a ganzfeld dome during light adaptation. **Right image:** The image shows the positioning of a corneal Burrian Allen bipolar electrode lens on a cat where the white part is a speculum, which is painted with silver paint that contacts the lids and conjunctiva and acts as the reference electrode and the wire loop on the cornea is the active electrode.

The individual components of the ERG response were first described by Granit in 1933 (Fig. 1.12, corneal recording).[22] In a simplified description, the direct current (DC) ERG response consists of three main components: the a-wave, the b-wave and the c-wave (Fig. 1.12). The a-wave component (representing the leading edge of the PIII wave) is a negative deflection representing the hyperpolarization that the photoreceptors undergo during light stimulation. More

precisely the a-wave results from the elimination of the "dark current" as the photoreceptors hyperpolarize in response to light induced closure of cyclic GMP-gated channels. The b-wave component (predominantly shaped by the P II response) is a positive deflection that results from the depolarization of the ON-bipolar cells. The c-wave is a slower wave due to the summation of the P II and P III waves coming from the retinal pigmentary epithelium cells (RPE). This is present in ERGs recorded under DC conditions but not in the more commonly used AC recording as shown in Fig. 1.13).[23]

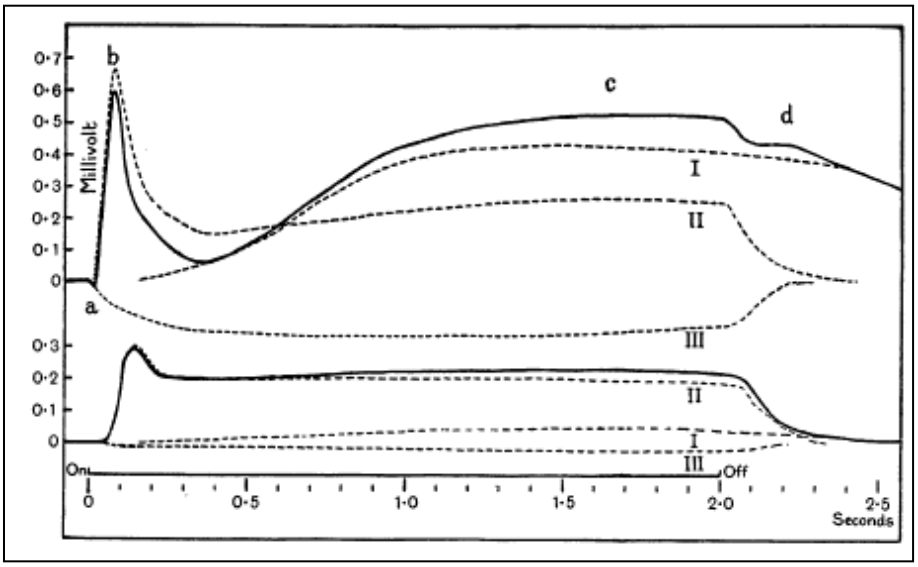

Figure 1.12. Analysis of composite retinal action potential at two intensities from a cat retina (from Granit, 1933).[22] The typical ERG is represented in full trace while the different components P I, P II and P III are represented in dotted tracings. The light stimilus is 2 seconds as shown on the lower scale (On-Off).

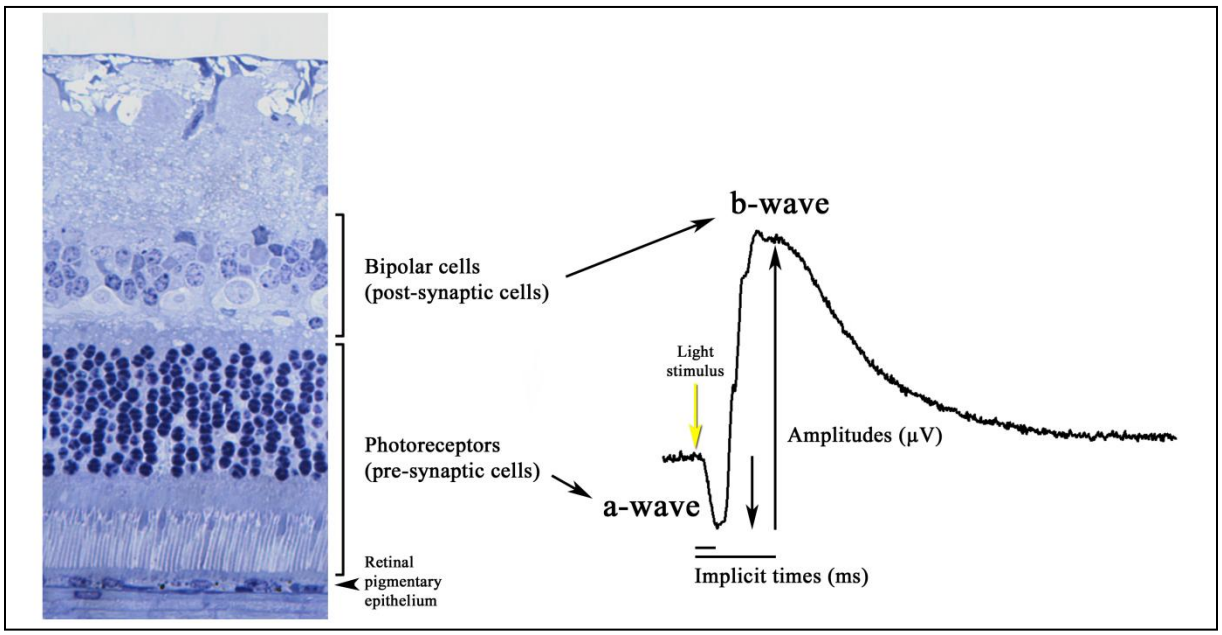

Figure 1.13. Typical feline dark-adapted ERG waveform and its origins. The a-wave predominantly results from the hyperpolarization of the photoreceptor cells while the b-wave originates from the depolarization of the ON-bipolar cells. The amplitude of the a-wave is measured from the baseline to the peak of deflection while the b-wave amplitude is measured from the deflection of the a-wave to the its own positive deflection peak. For both a- and b-waves the implicit times are measured from the light stimulus to their deflection peak.

The feline retina physiological development follows and is related to anatomical differentiation. Scotpic ERG (dark-adapted) of the cat was reported in more detail in 1980's literature and is characterized below.[24]

Functional development of the feline retina as assessed by the ERG can be divided into 3 stages. The first stage is a slow phase during the first few postnatal weeks during which the late receptor potential (slow recovering portion of the PII wave; reflecting the recovery stage to the absorption of light by the disk membranes) and the b-wave first develop.[23] The second stage occurs more rapidly and is characterized by an increase in b-wave amplitudes and the appearance of oscillatory potentials (which are a series of small high frequency wavelets that are present surimpposed to the ascending limb of the b-wave thought to be originated from amacrine cell in the inner retina with a potential ganglion cell component).[23] The last stage is slower and results in

the full maturation of the retina and is correlated to the end of the morphological differentiation of the retina and development of full neuronal connections. Similarly to the different specialized retinal cell types, the different ERG components reach maturation at different ages.

A more precise description of the maturation of the feline ERG follows: At 3 weeks of age, the kitten ERG is not yet mature. At low intensities only there is a late photorecepor potential negative wave, and at higher intensities an a-wave and b-wave can be distinguished but do not have an adultlike waveform shape. By 4 weeks of age, the ERG waveform is adultlike in shape, however, the a-wave is still more prominent than the b-wave, with the b-wave having a lower amplitude and longer implicit time. From 5 weeks and over the following weeks, the b-wave amplitude increases although it is still decreased compared to adulthood at low light stimuli (Fig. 1.14). By 10-12 weeks of age, amplitudes are adultlike. Similarly to the maturation of the ERG amplitudes, the b-wave implicit time shortens with age to reach maturation at approximately 10 weeks of age. On a side note, the oscillatory potentials, a waveform that originates from amacrine cells in the inner retina, are comparable to those of adults by 18 weeks of age.

The photopic (light-adapted) ERG seems to mature differently to that dark-adapted ERG, with some b-wave responses becoming higher in amplitude than adult waveforms and then stabilizing to similar amplitudes to adults by around 14 weeks of age. The impliticit time reaches maturation around 11.5 weeks of age.[25]

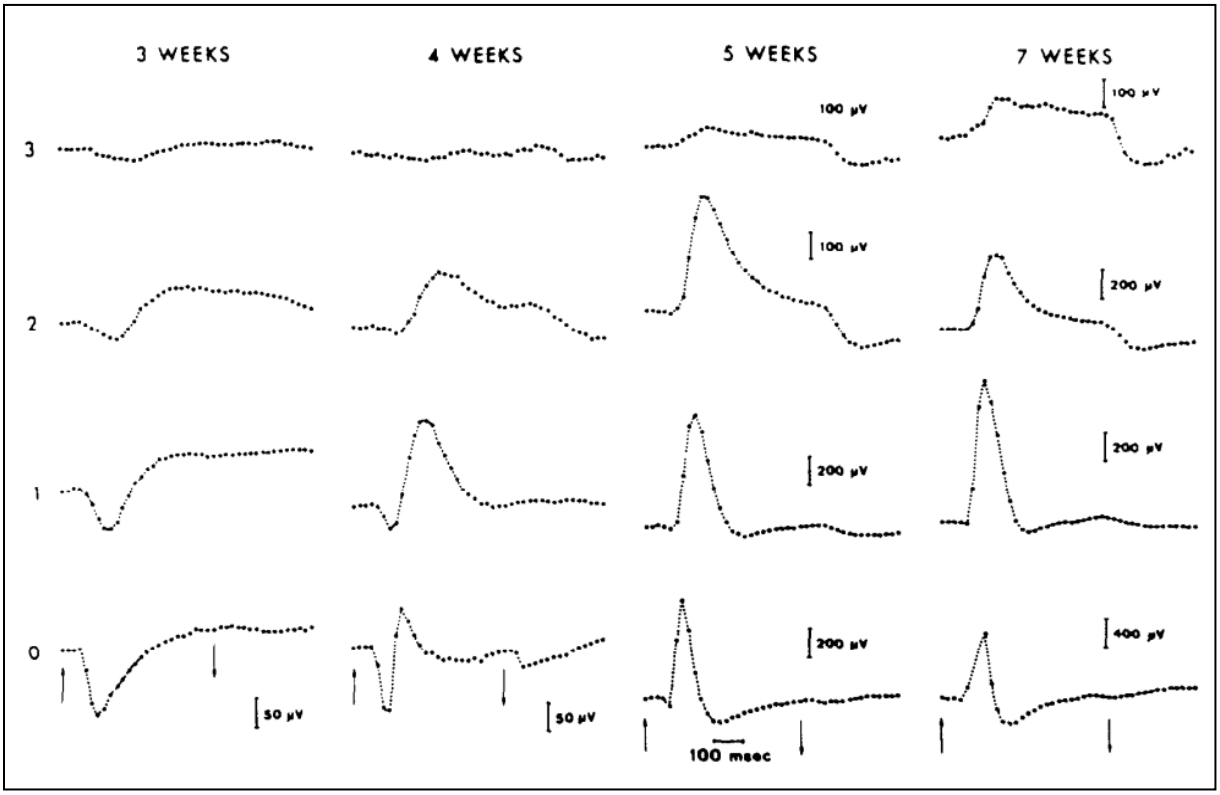

Figure 1.14. Examples of the ERGS recorded from kittens of different ages in response to a long stimulus of light (from Hamasaki et *al*., 1985).[24]
The numbers on the left represent the value of the neutral density filters used to attenuate the full intensity stimulus. At 0, luminance = 1.1 x $l0^4$ cd/m^2. The 50 µV calibration scale for 3 and 4 weeks apply to all intensities. The up arrow shows when the stimulus was turned on, and the down arrow shows when the stimulus was turned off.

1.2.2. Specificities in globe and retinal anatomy in large animal models compared to small animal model and humans

Rodents are small animal models that are commonly used to investigate phenotype, disease mechanisms and test therapies.[26] Yet, although rodents have provided a lot of information on retinal disease mechanisms, they have some important differences from humans in their eye structure and retina i.e. especially in the distribution of their photoreceptors density. The eye of rodents is very small compared to the human eye (Fig. 1.15), and they have a relatively large lens that occupies most of the posterior part of the eye making the development of surgical techniques

more difficult for therapy trials. Also, their retina differs in distribution of cones and rods compared to the human retina (as detailed in the following paragraphs).[27]

Large animal models like the cat and dog have the advantages that they present similarities to humans with comparable eyes' size and anatomy. They possess eyes that have a closer structure to the human eye with similar globe and vitreous chamber sizes (Fig. 1.15).

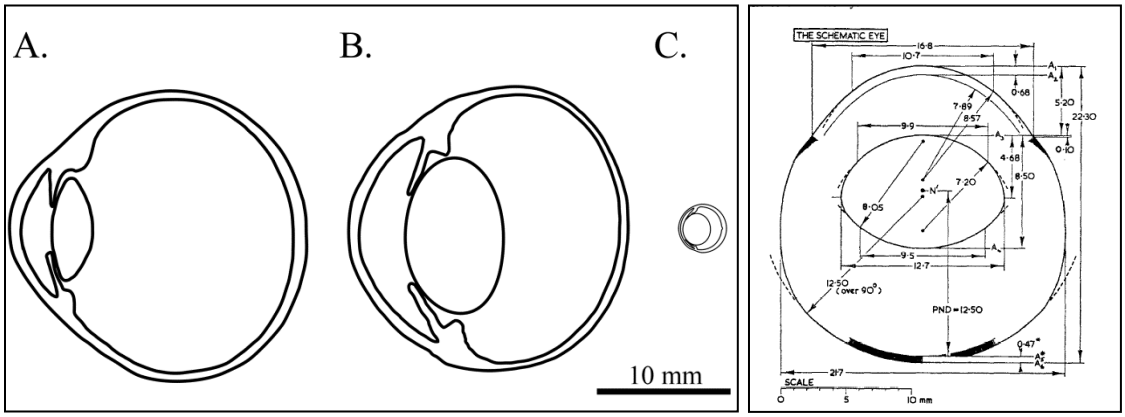

Figure 1.15. Schematic of the human, dog, mouse and cat eye.
Left panel: Human (A-left), dog (B-center) and mouse (C-right) eye schematic (from Petersen-Jones et *al.*, 2012 [27]). **Right panel:** The schematic eye in the cat (from Vakkur et *al.*, 1963).[28] This figure gives the physical dimensions of the feline adult eye.

In general, rods are distributed across the entire retina and represent the majority of photoreceptors in many mammalian species, e.g. 94-97% in human and mouse retinas.[29-33] In contrast, cone ratio, subtypes and distribution (mosaic patterns) vary significantly among mammalian species.[31, 34-36] The human retina contains three cone subtypes: red (long wavelength, or L), green (medium wavelength or M) and blue (short wavelength or S) based on the specific cone opsin expressed.[37, 38] These cones are highly enriched in a central retinal region called the macula with a cone-only center the *fovea*, which is essential for visual acuity.[39, 40] In contrast, rodents like the mouse lack a centralized cone-rich region. The mouse retina contains a dorsal-to-

ventral distribution gradient of M versus S-cone subtypes with some dual expression cones in their central retina (Fig. 1.16).[34] Thus, despite being a commonly utilized model species, which can be genetically well-controlled and have a high cone and rod-density [41], the mouse may not be the best model for human cone development and associated diseases due to its lack of marked regional differences in cone density. In contrast, large animal models such as dogs and cats similarly to humans have marked difference in photoreceptor density and have a central photoreceptor-rich region called the "*area centralis*", which has a high localized cone-density similar to that of the human macula.[32, 42-46]

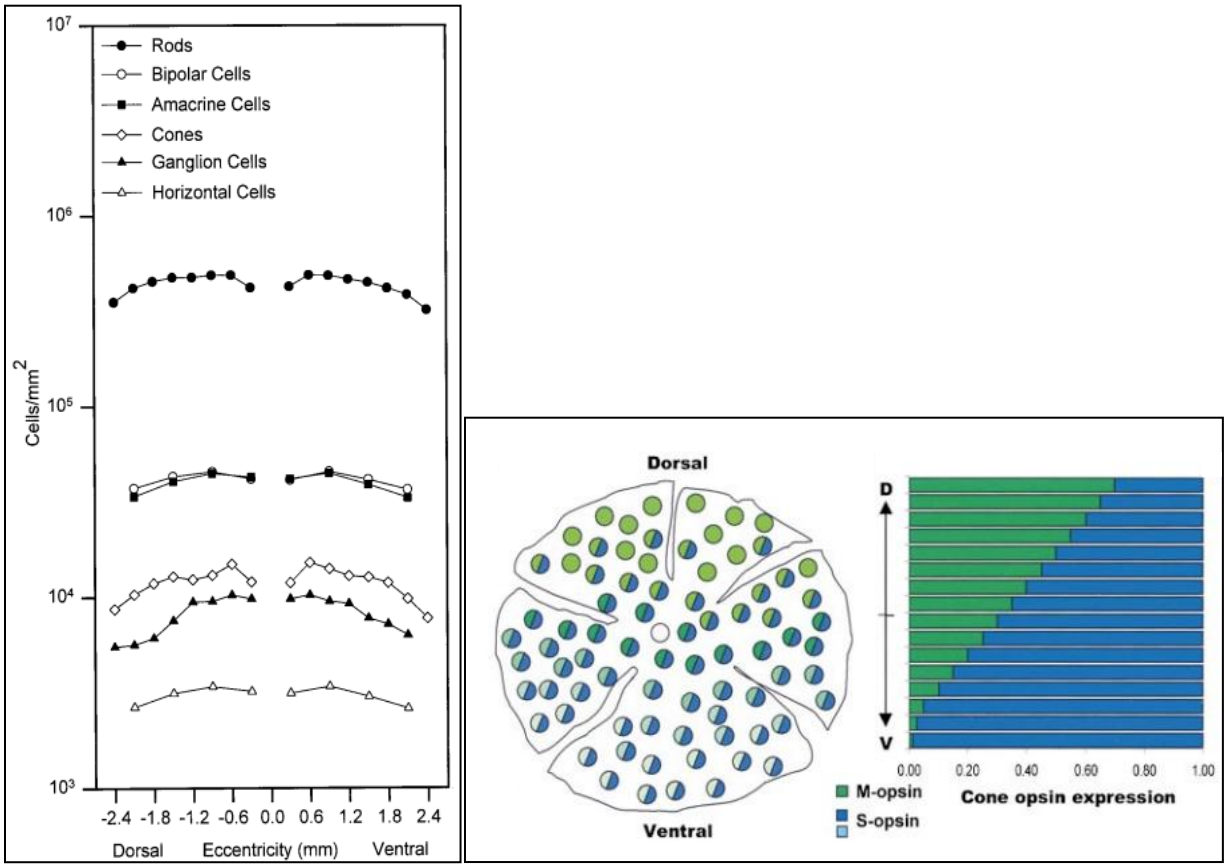

Figure 1.16. Photoreceptor cells distribution in the mouse retina.
Left panel: This figure shows the homogenous distribution of cones and rods dorsally and ventrally and compares their density to other cell types.[31] **Right panel:** This figure shows the distribution of M- and S- cones subtypes in the mice. Dorsally cones only express M-opsin while ventrally they only express S-opsin. Centrally the mouse cones have been shown to express both M- and S-opsins.[34]

As humans have a macula and *fovea*, the feline and canine retina is characterized by a regional difference in photoreceptor density with similar proportions of cone and rod photoreceptors and the presence of a high-density photoreceptor area – the *area centralis* (region dorso-temporal to the optic nerve) and the visual streak (Fig. 1.17).

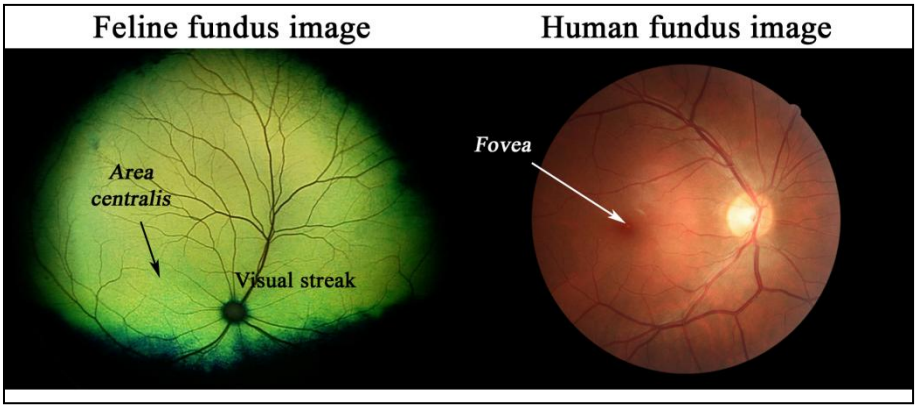

Figure 1.17. Images of a feline and a human right eye fundus.
Left image: The image shows the fundus of an adult cat. The *area centralis* is indicated at the tip of the black arrow and is situated dorso-temporally to the optic nerve. The visual streak is a region situated longitudinally dorsal to the optic nerve going nasally to temporally. **Right image:** The image shows the fundus image of an adult human. The *fovea* is indicated at the tip of the white arrow at the center of the region called macula (darker area surrounding the *fovea*).

The *area centralis* is comparable to the human macula due to its very high cone density. In the cat, as in humans, the majority of photoreceptors are rods, with cones only accounting for ~9-10% of photoreceptors in the *area centralis* and ~5% or less in the peripheral retina.[32, 47] Cats present with only two cone subtypes, red-green (medium-long wavelength, or ML), and blue (short wavelength or S) based on the specific cone opsin expressed.[44] ML cones represent the majority of cones and are highly concentrated in the *area centralis* while the S cones have a higher concentration in the ventro-temporal area of the retina. As previously stated, the *area centralis* contains a high density of cones (and rods) – similar to the human macula (Figs. 1.18

and 1.19). The center of the *area centralis* of the cat is reported to have ~26,000-27,000 cones/mm^2 and 275,000 rods/mm^2 with a peak of 460,000 rods/mm^2 at 10-15° from the region of maximum cone density.[32, 43, 44] The human macula has a *fovea* with maximum cone density of between ~115,000 to ~227,000 cones/mm^2 with a mean of ~164,000 cones/mm^2 and a lack of rods. The area surrounding the fovea has fewer cones and a peak of 160,000 rods/mm^2 at 18° from the fovea.[30, 48-50]

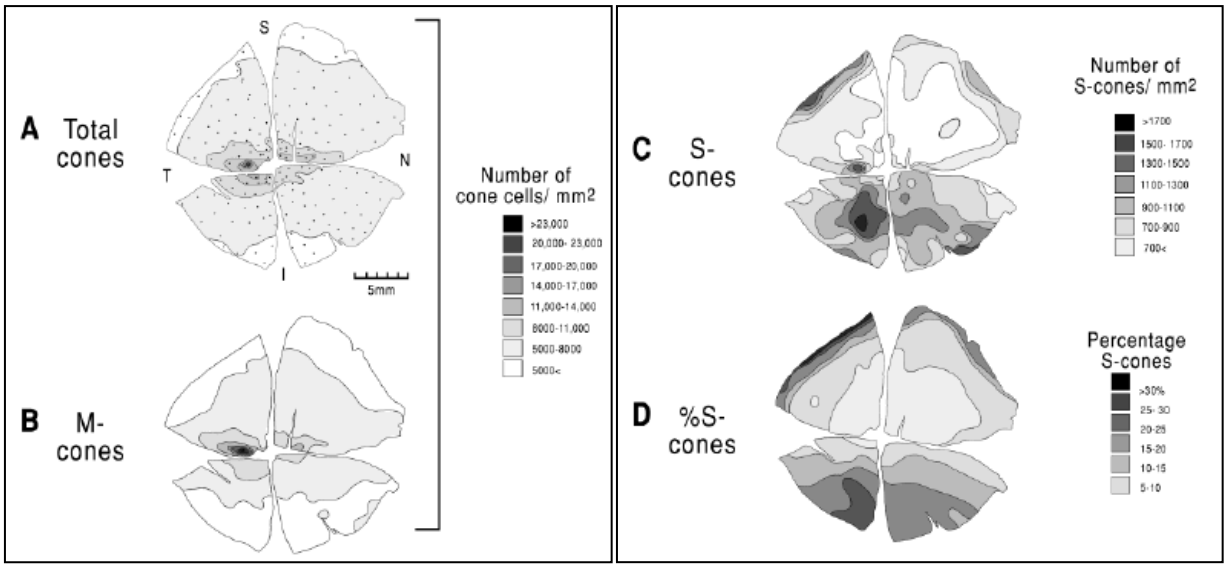

Figure 1.18. Schematic diagrams of cone distributions in a retinal wholemount of normal cat (from Linberg et *al*., 2001).[44]
(A) Total cone density. A sharp peak of just under 28,000 cones/mm^2 was counted at the *area centralis*. Cone densities declined rapidly away from this central region, though more slowly along the horizontal nasotemporal axis wherein a smear of higher density is found. One site at the far inferior periphery had the lowest total cone density of 3,100/mm^2.
(B) Medium wavelength (M)-cone density. Because M-cones predominate in the cat's retina, the isodensity map for M-cones closely parallels that of total cones.
(C) S-cone density. The robust fluorescence of labeled S-cone outer segments facilitated density counts. Peak S-cone densities lie at the far periphery, at the *area centralis* itself, and in the central portions of the inferior hemiretina. Lowest S-cone densities occur in a broad region across the superior retina outside the *area centralis*.
(D) Percent S-cones. A low S-cone percentage is typical for most of the central superior retina, whereas a broad expanse of the inferior hemiretina contains the highest S-cone percentages. S, superior; T, temporal; N, nasal; I, inferior.

The higher density of photoreceptors and in particular cones in the *area centralis* of the cat makes it important as a model for the study of conditions where the degeneration tends to be cone-led. This is an advantage over mouse models where a central region of high photoreceptor packing is not present. Therefore, the cat represents a good model for human retinal diseases as for its photoreceptor distribution compared to the small animal models like the mouse. This characteristic makes such models valuable for understanding human retinal diseases and developing therapeutic approaches, such as adeno-associated virus (*AAV*)-mediated gene therapy.[51-54]

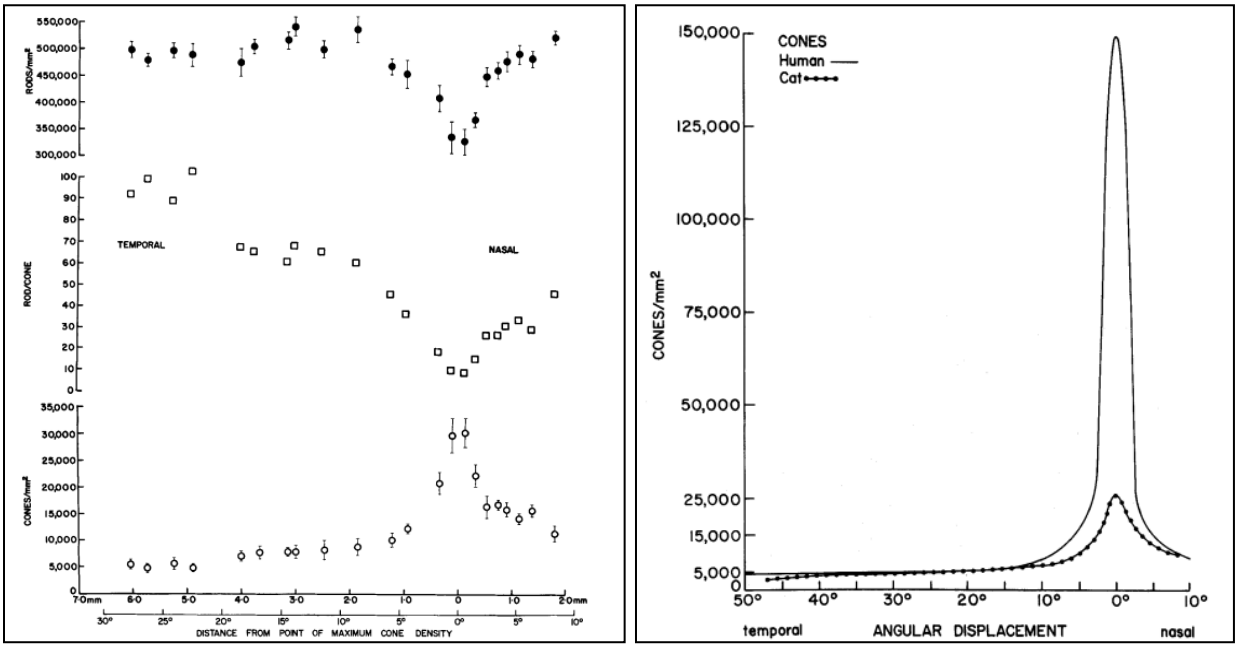

Figure 1.19. Photoreceptor cell densities in the cat and human (from Steinberg et *al.*, 1973)[32]
Left panel: The figure shows the densities of rods and cones in the cat (0 is the position of the *area centralis*). **Right panel:** The figure shows superimposed the cone density in the *area centralis* of a cat and the cone density in the *fovea* of a human.

1.2.3. Cat large animal models in retinal hereditary research

Large animal models of inherited retinal degenerations such as dogs, cats, pigs and even sheep play an important role as models for the comparable conditions in humans. They typically have mutations in the homologous gene.[55-59] Over the last decade, the dog model has proven to be particularly useful because of the spontaneous occurrence of several different forms of inherited retinal degenerations such as retinal dystrophies caused by mutation in the *RPE65*, *PDE6A*, *CNGB1* genes. The different dog models (summarized in Petersen-Jones et al, 2015)[57, 60] have proven valuable in the investigation of disease mechanisms but also in the assessment of promising therapeutic interventions including gene augmentation therapy, drug therapy and optogenetic approaches. More recently the cat has emerged as a source of valuable spontaneous IRD models.[55] This was possible due to the advance in mapping genetic traits in cats.[61, 62] Spontaneous mutations in four different genes that cause early onset IRD in humans, classified most commonly as Leber congential amaurosis, have been identified and studied. Spontaneous mutations in *Cep290, Crx, Aipl1, Kif3b* genes have been described. Those mutations are responsible for LCA like phenotype. The mutations in the *Cep290* gene is known to be a major cause of recessive LCA in humans (about 20%), *Crx* (3%) which results in a variety of typically dominant IRDs, most commonly LCA (see following text), *Aipl1* (4-8%) and *Kif3b* which results in a recessive LCA phenotype.[63-66] Contrary to the other 3 models, the *Cep290* feline models show a slow progressive retinal dystrophy phenotype, while the *Crx* and *Aipl1* show a rapid retinal dystrophy phenotype. The *Kif3b* phenotype is also relatively rapid but a bit slower than the latter two.

1.3. RETINAL DEVELOPMENT AND TRANSCRIPTION FACTORS

Gene expression is most commonly regulated at the transcription level, which is the process of transcribing DNA (deoxyribonucleic acid) to mRNA (messenger ribonucleic acid). The transcription is regulated by the enzyme RNA polymerase, which using the gene's DNA template catalyzes the synthesis of RNA. Associated with proteins the transcription factors control the RNA polymerases function during the initiation. Transcription consists basically of three steps: the initiation step in which the RNA polymerase binds to a specific DNA sequence called the promoter, the elongation i.e. the step where the RNA is synthesized using the DNA as a template, and the termination step in which the RNA polymerase separates from the DNA strand when it recognizes the transcription termination sequence.

Transcription factors [67, 68] are proteins generally acting in multi-subunit protein complexes that lead to a specific expression during development and homeostasis of each gene in different cell types by initiating and regulating gene transcription. Therefore, transcription factors are essential for normal development, dictating individual cell fate and regular cellular functions. Transcription factors can activate or repress the transcription of a gene; they are essential in controlling whether the gene is functional at a given time. They are essential during the cell cycle by determining the genes' activity and also are used by cells to respond to extracellular stimuli and signals from the environment or other cells.

Transcription factors function in the nucleus, where the genomic DNA containing genes is located, and nuclear transport (i.e., import or export) of transcription factors can influence their activity. Another important general mechanism controlling the activity of transcription factors is post-translational modification such as phosphorylation. Finally, in addition to controlling the genes and transcription of other transcription factors, these protein complexes can also control the genes responsible for their own transcription, leading to complex feedback control mechanisms.

Structurally, transcription factors are characterized by the possession of DNA-binding domains. Transcription factors can bind to RNA polymerase in which case they are called basal transcription factors; examples include TFIIA, TFIIB, TFIID/TATA-BOX binding protein (TBP), TFIIE, TFIIF, and TFIIH. Alternatively, they can bind to another transcription factor or cis-acting DNA sequences. More precisely, transcription factors are necessary for the RNA polymerases to recognize sequences to transcribe; they can be activated or repressed by other proteins and can bind to DNA at specific sequences called promoter or enhancers that regulate transcription.

The homeobox genes, which are about 180 base pairs long, encode for transcription factors. They consist of a family of over 200 similar genes directly involved in critical steps during embryonic development such as structural pattern development (i.e. limb formation or front to back axis). The transcribed proteins contain a homedomain, which consists of about 60 amino acids with a helix-turn-helix structure. The homedomain, exclusively found in eukaryotes, has the ability to bind to DNA or RNA specific regulatory target sequences in genes. Most proteins that possess a homedomain are transcription factors and therefore have the ability to control gene expression by binding to promoters or enhancers or regulatory sequences and so induce cascade events necessary for development. This explains why mutations in homeobox genes can have dramatic consequences on development.

Transcription factor genes include retinal transcription factors involved in the eye development like *PAX6* and more specifically in retinal development factors such as *OTX2*, *NR2E3*, *NRL* and the cone-rod homeobox (*CRX*) gene (Fig. 1.20).

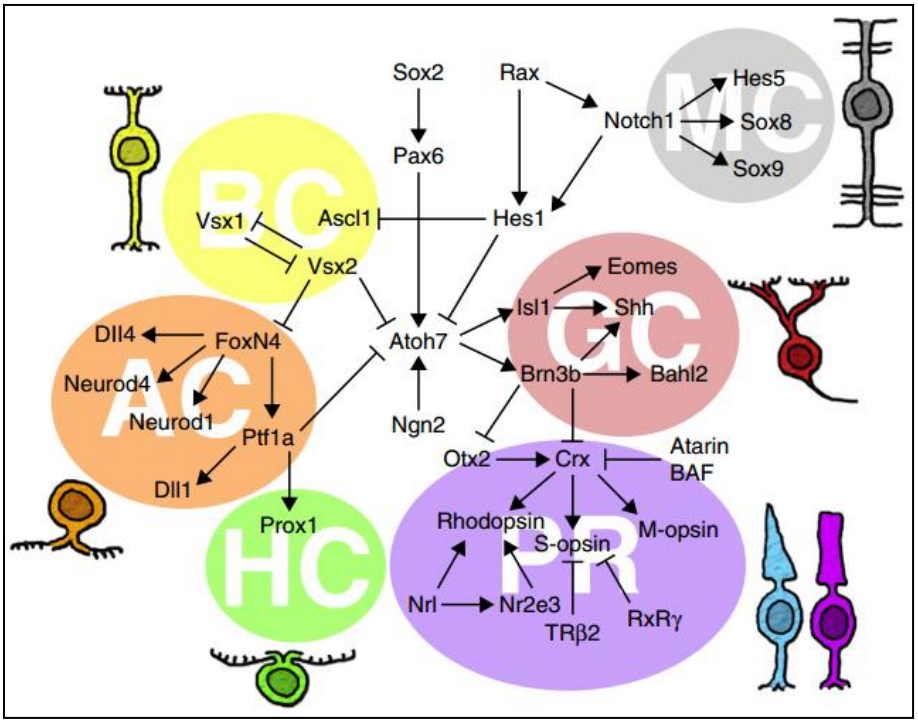

Figure 1.20. The complexity of transcriptional regulation (from Boije et *al.*, 2014).[69]

There are 6 main transcription factors that lead the photoreceptor precursor to form either a rod or a cone: the homeobox protein OTX2, the cone–rod homeobox protein CRX, the neural retina leucine zipper protein NRL, the photoreceptor-specific nuclear receptor NR2E3, the thyroid hormone receptor β2 TRβ2 and the nuclear receptor RORβ (Fig. 1.21).[70-72]

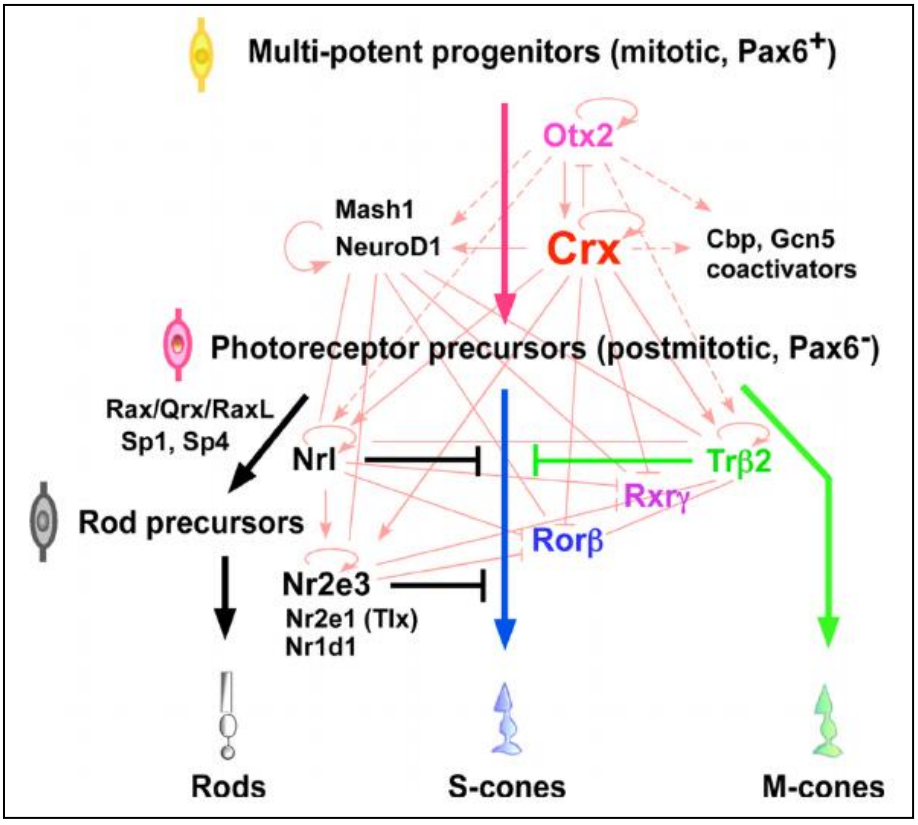

Figure 1.21. Model for transcription factor network regulation of photoreceptor subtype development (from Hennig et al, 2008).[70]

OTX2, the Orthodenticle Homeobox 2 is responsible for the commitment to a photoreceptor fate by being a key regulator of the photoreceptor lineage. It intervenes during final mitosis in retinal progenitors and in early precursors. CRX, the cone-rod homeobox is responsible for the terminal differentiation of photoreceptors. It is also expressed in mature photoreceptor and bipolar cells. CRX is expressed early in post-mitotic photoreceptor precursors and acts downstream of OTX2. CRX is essential for terminal differentiation of rods and cones and is an enhancer for photoreceptor-specific genes expression. NRL, Neural retina-specific leucine zipper protein is responsible for rod photoreceptor fate. NRL interacts with CRX and many other transcription factors and induces the expression of rod-specific genes. NR2E3, the photoreceptor-specific nuclear receptor is a repressor of cone gene expression and with NRL and

CRX, it activates rod genes. RORβ, the orphan nuclear receptor is a transcription factor that is expressed in all cell layers of the neural retina and in the pineal gland. It regulates the development of both cones and rods. In addition to being essential to photoreceptor outer segment formation, RORβ is necessary for the development of inner nuclear and synaptic layers. TRβ2, the thyroid hormone nuclear receptor regulates the development of the M cone and plays a role in the cone opsin retinal patterns.[70, 71, 73]

1.4. *CRX*-LCA INHERITED RETINAL DISEASE

1.4.1. Leber Congenital Amaurosis (LCA)

LCA is an inherited retinal disease with childhood onset, which leads to very severe visual impairment or blindness. It was first described by Theodor Karl Gustav von Leber.[74] LCA is the most severe form of the photoreceptor dystrophies and accounts for ~5% of all inherited retinopathies with a prevalence of about 1 in 30,000 to 81,000 newborns.[75-78] Clinical signs of LCA include wandering nystagmus, delayed and very decreased pupillary light reflexes and absent or severely reduced ERG responses. Additional clinical signs described include fundus changes, keratoconus, cataracts, changes in refraction, sensitivity to light and a behavioral oculodigital sign in young children.[74, 79]

Known genes harboring mutations causing LCA are summarized in Table 1.1 and Figs. 1.22 and 1.23.

Leber congenital amaurosis, autosomal dominant	CRX, IMPDH1, OTX2
Leber congenital amaurosis, autosomal recessive	AIPL1, CABP4, CEP290, CLUAP1, CRB1, CRX, DTHD1, GDF6, GUCY2D, IFT140, IQCB1, KCNJ13, LCA5, LRAT, NMNAT1, PRPH2, RD3, RDH12, RPE65, RPGRIP1, SPATA7, TULP1, MERTK (ALMS, CNGA3, MYO7A, BBS4)

Table 1.1. Identified retinal genes in which mutations can be responsible for LCA.[6, 79, 80]

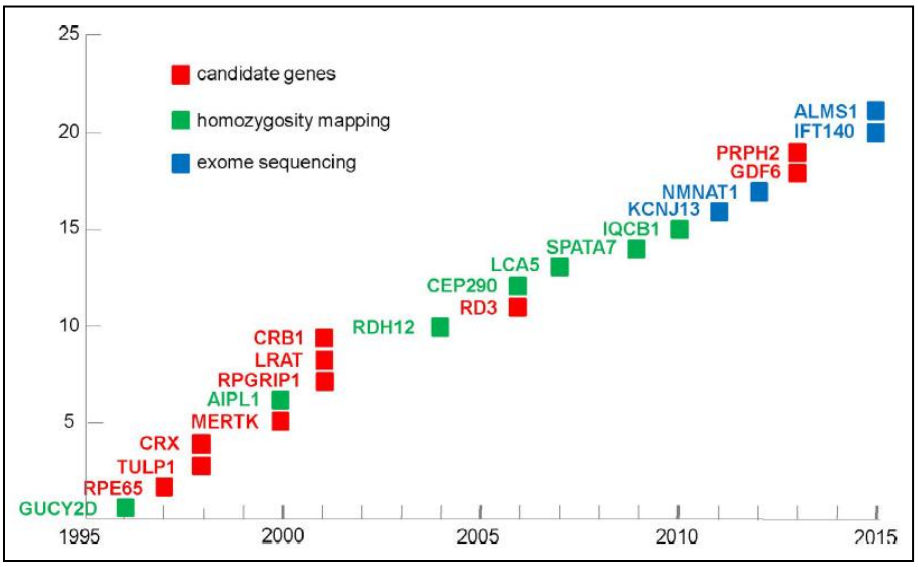

Figure 1.22. Cumulative number of identified LCA genes (from Den Hollander et *al.*, 2016).[80] During the past 20 years, more than 20 genes have been identified for LCA through a candidate gene approach, by homozygosity mapping, or, more recently, using exome sequencing.

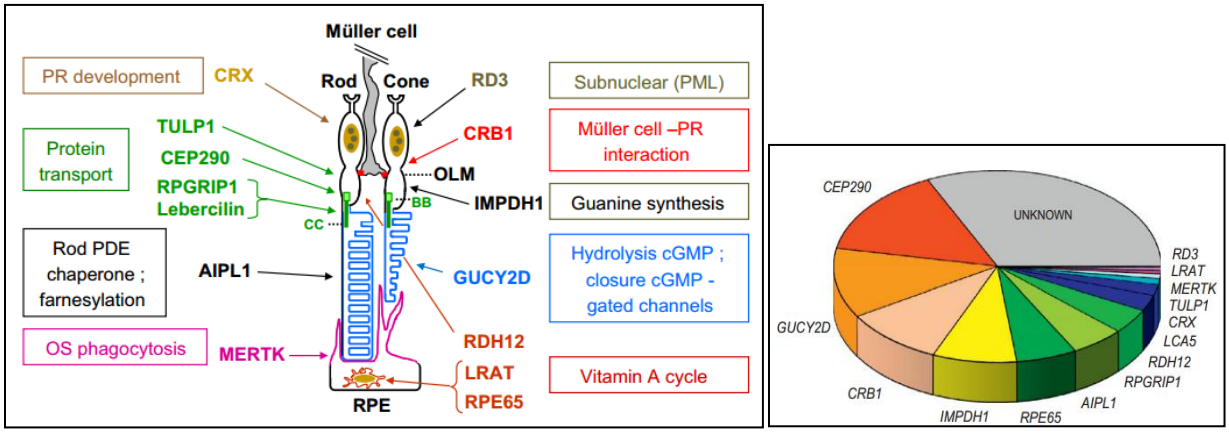

Figure 1.23. Main LCA causing-genes: their spatial expression and their prevalence importance (from Den Hollander et *al.*, 2008).[81]
Left panel: this figure shows the LCA causing-genes can be grouped according to nine different retinal functions. BB, basal body; CC, connecting cilium; OLM, outer limiting membrane; OS, outer segments; PR, photoreceptor. **Right panel:** This figure shows that among LCA causing-genes the *CRX* gene represents only a small prevalence.

1.4.2. CRX transcription factor

CRX encodes an OTX-like homeodomain transcription factor essential for photoreceptor development, maturation and survival.[82-85] It plays a major role at the center of a network of photoreceptor transcription factors controlling the maturation of photoreceptor progenitor cells during retinal development and maintenance of transcription in differentiated photoreceptors.[70, 86]

The *CRX* gene is well-conserved among species. In humans it encodes a 299 amino acid protein, which as with other transcription factors has two characteristic domains: a DNA binding domain (homeodomain) near its N-terminal and a transactivation domain at the C-terminal (Fig. 1.24).[87]

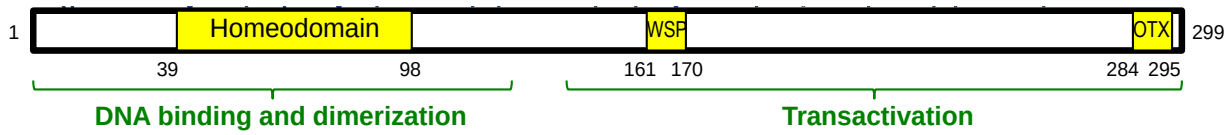

Figure 1.24. CRX transcription factor structure (Courtesy Dr Shiming Chen)**.**[87]

As described above, CRX directly regulates several major genes involved in normal retinal function, including many key components of the phototransduction cascade and the *CRX* gene itself, by binding to the target gene's regulatory elements and interacting with co-factors.[82, 88-91] As being a transcription factor, the wild-type Crx protein is believed even at a very low level to have an impact on the production of other proteins; proteins encoded by a gene containing a binding site for Crx. For example, impairment of the proper transcription rate of *CNGA3* and *KNCV2* genes can have an effect on phototransduction. Similarly, altered production of ABCA4 protein could lead to inefficient visual cycle function (recovery of the photopigment necessary for phototransduction). Crx also has a binding site on the gene encoding for structural proteins such

as PROM1 or for proteins essential for proper transport through the photoreceptor connecting cilium (i.e. RPGRIP1 or AIPL1) (Tables 1.2 and 1.3, Fig. 1.25). In mice, Crx binds to 48 genes within the retinal cells. It binds to promoters for genes encoding for proteins essential in phototransduction (*Cnga3, Cngb3, Gnat2, Opn1mw, Opn1sw, Rho, Grk1, Kcnv2*), the visual cycle (*Abca4*), transport processes within the photoreceptor (*Aipl1, Rpgrip1, Tulp1, Unc119*) and development and formation of the normal structure of the photoreceptor (*Crx, Nrl, Nr2e3, Prom1, Prph2*) (Tables 1.2 and 1.3, Fig. 1.25).[91]

Mouse Gene symbol	Expression (BioGPS)	Disease	Mode
Cnga3	Retina (cones)	Achromatopsia 2	ar
Cngb3	Retina (cones)	Achromatopsia 3	ar
Gnat2	Retina (cones)	Achromatopsia 4	ar
Opn1mw	Retina (cones)	Colorblindness Deutan	X
Opn1sw	Retina (cones)	Colorblindness Tritan	ad
Pde6c	Retina (cones)	Cone Dystrophy 4	ar
Gnat1	Retina (rods)	Congenital Stationary Night Blindness Autosomal Dominant 3	ad
Pde6b	Retina (rods)	Congenital Stationary Night Blindness Autosomal Dominant 2, Retinitis Pigmentosa 40	ar
Rho	Retina (rods)	Retinitis Pigmentosa 4	ad, ar
Grm6	Retina (BP)	Congenital Stationary Night Blindness Type 1B	ar
Cerkl	Retina (RGC)	Retinitis Pigmentosa 26	ar
Rbp4	RPE	RPE Degeneration	ar
Rdh12	RPE	Leber Congenital Amaurosis 13	ar, ad

Table 1.2. Genes which contain a CRX-binding site revealed by ChIP seq that are known to be expressed in specific retinal cells (modified from Corbo et *al.*, 2010)[91] (ar; autosomal recessive, ad; autosonomal dominant, X; X-linked).

Mouse Gene symbol	Expression (BioGPS)	Disease	Mode
Abca4	Retina	Cone-Rod Dystrophy 3, Retinitis Pigmentosa 19, Stargardt Disease 1	ar
Aipl1	Retina	Leber Congenital Amaurosis 4	ar, ad
Cabp4	Retina	Congenital Stationary Night Blindness Type 2B	ar
Cacna1f	Retina	Congenital Stationary Night Blindness Type 2A	X
Cnga1	Retina	Retinitis Pigmentosa 41	ar
Crb1	Retina	Leber Congenital Amaurosis 8, Retinitis Pigmentosa 12	ar
Crx	Retina	Cone-Rod Dystrophy 2, Leber Congenital Amaurosis 7	ar, ad
Elovl4	Retina	Stargardt Disease 3	ad
Fscn2	Retina	Retinitis Pigmentosa 30	ar
Gpr98	Retina	Usher Syndrome Type 2C	ar
Grk1	Retina	Oguchi Disease 2	ar
Guca1a	Retina	Cone Dystrophy 3	ad
Guca1b	Retina	Retinitis Pigmentosa 48	ad
Kcnv2	Retina	Retinal Cone Dystrophy 3B	ar
Lca5	Retina	Leber Congenital Amaurosis 5	ar
Nr2e3	Retina	Retinitis Pigmentosa 37	ar, ad
Nrl	Retina	Retinitis Pigmentosa 27	ad
Nyx	Retina	Congenital Stationary Night Blindness Type 1A	X
Pde6a	Retina	Retinitis Pigmentosa 43	ar
Pitpnm3	Retina	Cone-Rod Dystrophy 5	ad
Prcd	Retina	Retinitis Pigmentosa 36	ar
Prom1	Retina	Macular Dystrophy 2, Stargardt Disease 4, Retinitis Pigmentosa 41	ad, ar
Prph2	Retina	Retinitis Pigmentosa 7	ad/digenic
Rbp3	Retina	Retinitis Pigmentosa	ar
Rd3	Retina	Leber Congenital Amaurosis 12	ar
Rgs9	Retina	Bradyopsia	ar
Rgs9bp	Retina	Bradyopsia	ar
Rom1	Retina	Retinitis Pigmentosa 7	ad/digenic
Rp1	Retina	Retinitis Pigmentosa 1	ar
Rpgrip1	Retina	Leber Congenital Amaurosis 6	ar
Rs1	Retina	X-Linked Retinoschisis	X
Sag	Retina	Retinitis Pigmentosa 47	ar
Trpm1	Retina	Congenital Stationary Night Blindness 1C	ar
Tulp1	Retina	Retinitis Pigmentosa 14	ar
Unc119	Retina	Cone-Rod Dystrophy	ad

Table 1.3. Genes containing a CRX-binding site revealed by ChIP seq that are known to be expressed in the retina (modified from Corbo et *al.*, 2010)[91] (ar; autosomal recessive, ad; autosonomal dominant, X; X-linked).

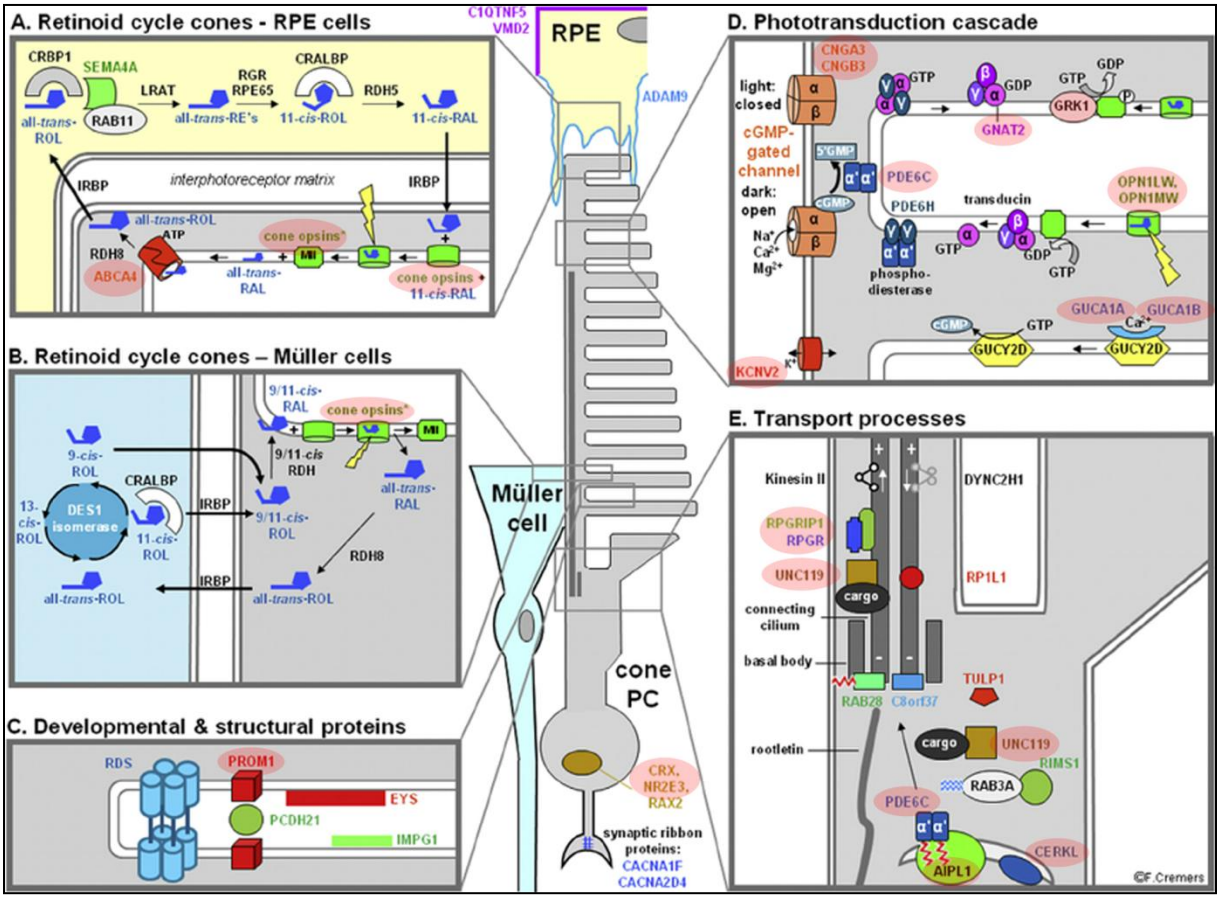

Figure 1.25. Schematic representation of the roles in cones of the proteins that are encoded by genes with a CRX-binding site (modified from Roosing et *al*., 2014).[92]
Proteins which are encoded by genes with a CRX-binding site are indicated by a light red oval shape.

As previously described in detail, CRX is a photoreceptor-specific transcription factor (TF) essential for normal photoreceptor development with a major role in the differentiation of multipotent progenitor cells to photoreceptors precursors then to photoreceptor subtypes, but it also plays an invaluable role in photoreceptor function maintenance and survival. CRX is also expressed in the pineal gland.[70]

The essential role of CRX at an early stage of photoreceptor development and also for maintenance of photoreceptors in the mature retina explains why *CRX* mutations result in a spectrum of retinopathies. They are typically dominantly inherited due to a dominant negative

effect of the mutated protein that is expressed in many instances. The phenotypes vary in severity and are responsible for 4 major phenotypes: Leber congenital amaurosis (LCA) a childhood onset of blindness, cone-rod dystrophy (CoRD), retinitis pigmentosa (RP) and macular dystrophy.[87,93] Mutations in the *CRX* gene have been reported to account for just approximately 2-3% of LCA.[94] LCA caused by CRX mutations is classified as LCA type 7.

1.3. CRX mutation classifications

Recent studies have utilized both spontaneous animal models with *Crx* mutations (2 mouse models) as well as two engineered mouse models of some human *CRX* mutations to understand the mechanisms of how the mutations cause disease and to explain the variation in phenotype severity. Human *CRX* mutations have been classified into four classes based on disease mechanism, more specifically on the mutation type and the functional characteristic of the resulting mutant protein with the existing animal models representing 3 of the classes.[87] Class I and II mutations result from missense mutations in the homeodomain while Class III and IV are frame-shift or nonsense mutations (Fig. 1.26).[87]

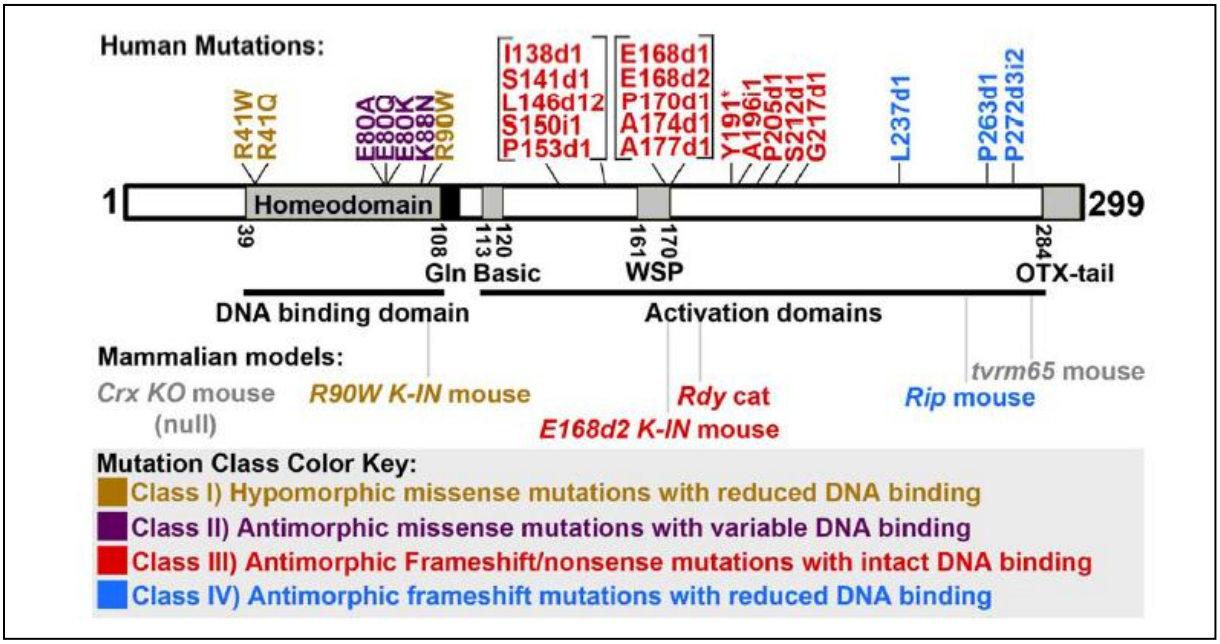

Figure 1.26. Human mutations schematic and animal models mutations (from Tran et *al*. 2014).[87]

Missense mutations in the homeodomain (Classes I and II) lead to milder phenotypes while frameshift or nonsense mutations in the activation domain (Classes III and IV) cause a severe phenotype.[87]

The first two *CRX* mutation classes include missense mutations located in the DNA binding domain. Class I mutations are hypomorphic mutations where the resulting mutant protein has a reduced DNA binding ability but does not interfere with the wild-type protein, while Class II mutations are antimorphic mutations which interfere with wild-type CRX and have variable DNA binding properties. The *R90W* mouse model (*Crx*^{R90W} *knockin*; Arg90Trp substitution mutation in the CRX homeodomain) has been developed as a model of Class I mutations. The mutant protein has decreased binding ability for the *rhodopsin* promoter, which is a well-known target of CRX. The Class I mutations cause later-onset disease; the R90W mouse model has a milder phenotype and the *Crx* knockout mouse when heterozygous shows only a slight delay in

photoreceptor development. Taken together this indicates that the more severe disease phenotypes are not simply the result of haploinsufficiency. In contrast, the predicted Class II mutations have a more severe phenotype predicted to result from interference with the wild-type CRX protein. There are currently no animal models for the Class II mutations.

Class III and IV mutations consist of frameshift and nonsense mutations in the activation domain of the CRX protein and have antimorphic effects. Class III mutations lead to the production of a truncated protein with intact DNA binding abilities while Class IV mutations show reduced DNA binding. The *E168d2* mouse model (Crx^{E168d2} *knockin*; Glu168del2 frameshift mutation in the CRX activation domain) is a model of Class III mutations. The Crx^{Rip} mouse model (spontaneous mouse model; Gly255del1 frameshift mutation in the CRX activation domain) is a model of Class IV mutations, but at present no human equivalent mutations have been reported. Studies of the *R90W* (Class I) and *E168d2* (Class II) mutant mice have shown that the more severe phenotypes result from a dominant negative effect of the expressed mutant transcript causing misregulated gene expression in many pathways critical for photoreceptor structure, function and survival. This is supported by the fact that *E168d2* mouse from which a neomycin resistance cassette had not been excised had a lower expression level of the mutant allele and had a milder phenotype than the model in which the neomycin cassette had been excised. Taken together these findings indicate that the phenotypic variations seems to be related to the molecular structure and binding ability of the CRX mutant protein (Fig. 1.27 and Table 1.4).[87, 95]

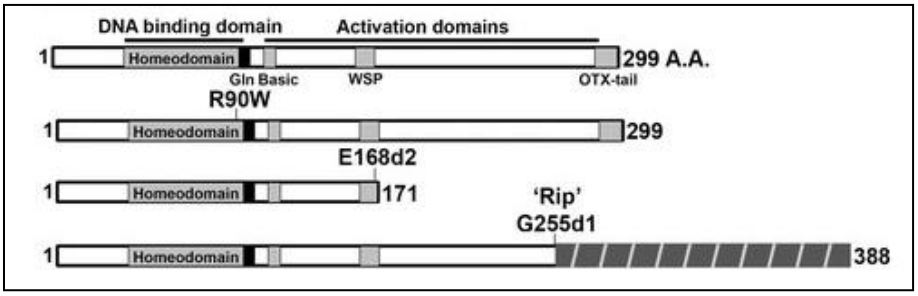

Figure 1.27. Schematic diagram of wild-type (WT) and mutant CRX proteins made by the indicated mouse models (from Ruzycki et *al*., 2015).[87, 96, 97]

The WT CRX protein shown on the top is 299 amino acids (*A.A.*) in length and contains the indicated DNA-binding and transactivation domains (indicated by *bars* above the diagram) and several conserved motifs (marked by *solid grey* and *black boxes*). The substitution mutation *R90W* lies within the homeodomain and reduces DNA-binding. The frameshift mutation *E168d2* results in a C-terminus truncated CRX protein that retains DNA-binding capability but fails to activate transcription, and is, therefore, antimorphic. The frameshift mutation *G255d1* '*Rip*' results in a non-homologous C-terminal extension (*dark grey hashed box*), creating an antimorphic protein that no longer binds DNA.

Mouse	Mutation Class	CRX expression	Rod		Cone		Disease model	Phenotype severity
			Function	Degeneration	Function	Degeneration		
WT	NA	+	++++	Undetectable	++++	Undetectable	NA	NA
R90W$^{/+}$	I	+	++++	Undetectable	++++	Undetectable	CoRD	Mild
E168d2 Neo$^{/+}$	III	+	+++	Undetectable	++	≥ 1year	CoRD	Moderate
E168d2$^{/+}$	III	++	++	1-6 months	+	1 month	LCA	Severe
Rip$^{/+}$	IV	+	-	1-18 months	-	Undetectable	LCA	Very severe
-/-	Null	-	-	1-3 months	-	Undetectable	LCA	Very severe
E168d2/ d2		+++	-	1-3 months	-	Undetectable	LCA	Very severe
R90W/W		+/-	-	1-3 months	-	Undetectable	LCA	Very severe
Rip/Rip		+/-	-	1-9 months	-	Undetectable	LCA	Very severe

Table 1.4. Phenotype summary of heterozygous *Crx* mutant mice (from Tran et *al*., 2014, Roger et *al*., 2014 and Ruzycki et *al*., 2015)[87, 96, 97]

CRX expression is based on quantitative Western blots. Rod and cone function is based on ERG peak amplitudes. Phenotype severity is based on morphological and functional deficits.

The effect of Crx mutations on expression levels of photoreceptor genes has been investigated in some of the mouse models (Figs. 1.28 and 1.29).[95, 96]

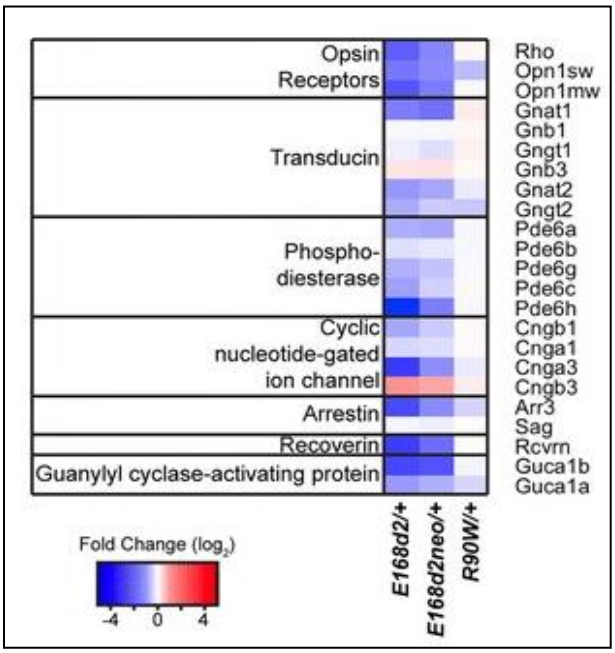

Figure 1.28. Changes in phototransduction photoreceptor-specific gene expression of *Crx* mutant mice retinas photoreceptor-enriched genes involved in phototransduction (changes assessed by RNAseq) (from Ruzycki et *al*., 2015).[96]

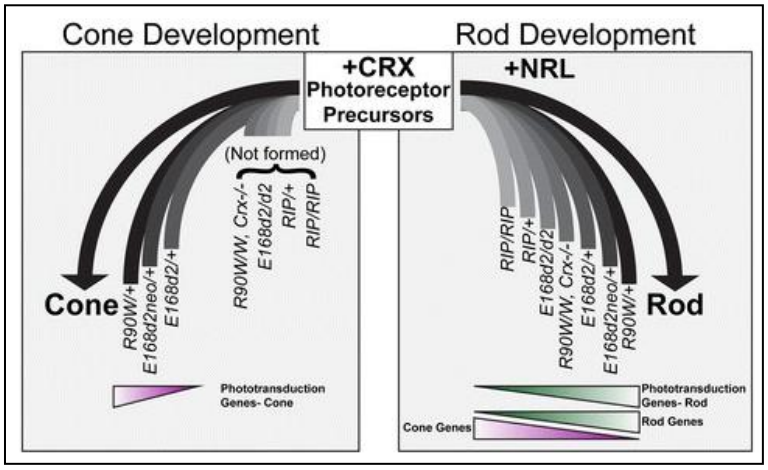

Figure 1.29. Model of how *Crx* mutation-caused gene expression changes affect rod and cone development (from Ruzycki et *al*., 2015).[96]
The **left panel** describes the formation of cones in a subset of the *Crx* mutants and variable levels of those cells' expression of phototransduction genes. The **right panel** shows how development of rods in all models is related to their gene expression changes. It also emphasizes the novel findings that *Crx* mutant rods display a graded phenotype of both the decreased expression of proper rod genes, and the mis-expression of cone genes.

The initial phenotypic description and investigation of mode of inheritance of the *Crx*^{Rdy} mutant cat was published in 1985 by Roger Curtis and Keith Barnett.[98] This was followed by publications that described the condition as an autosomal dominant retinopathy and more specifically a rod-cone dysplasia. These authors gave the mutant mode the name *Rdy* (rod-cone dysplasia) cat. This name has been maintained although the condition was subsequently shown to be a cone-rod dysplasia.

The *Crx*^{Rdy} cat phenotype is also comparable to human and *E168d2* mouse model phenotype with retinal dystrophies caused by similar-type mutations making the *Crx*^{Rdy} cat an excellent model for studying severe human LCA7 (*LCA*^{CRX}) phenotype. Similarly to LCA7 patients and the *E168d2* mouse model with the severe phenotype, studies revealed that the heterozygous *Crx*$^{Rdy/+}$ cats have a severe, early-onset dominant photoreceptors dystrophy with cones being affected more severely. The *Crx*$^{Rdy/+}$ kittens show signs of retinal disease as early as 4-5 weeks of age at which time they have moderate mydriasis and nystagmus. Abnormal pupillary light reflexes (PLR) are noticed as early as 6 weeks of age and changes in fundus appearance first appear as a discoloration in the region of the *area centralis*. With disease progression with age retinal atrophy with superficial retinal vascular attenuation develops. Histologically, the *Crx*$^{Rdy/+}$ kittens show a failure of photoreceptor maturation with photoreceptor degeneration starting in the region of the *area centralis* (macula-like region). Photoreceptors are shortened, with sparse and dystrophic outer segments, which do not develop further with age. Inner photoreceptor segments degeneration as well as retinal thinning and photoreceptor nuclei death develop with disease progression. There is mislocalization of opsins to the inner photoreceptor segments, outer nuclear layer and up to the photoreceptor synapse terminal in the outer plexiform layer. Affected cats also showed a significant increase in glial fibrillary acidic protein (GFAP) expression in Müller cells. Accompanying those cellular and morphologic

changes, the *Crx*$^{Rdy/+}$ kitten has severely reduced visual function with severely decreased dark-adapted electroretinogram (ERG) responses and no cone (light-adapted) ERG responses.[98-102]

Similarly to Class III human *CRX* mutations and the *E168d2* mouse model, in which the mutant protein retains DNA binding and has an antimorphic effect, the *Crx*-mutant cat (*Crx*^{Rdy}) has a mutation in the activation domain and develops a severe dominant retinopathy mimicking human autosomal dominant LCA. The causal mutation is a one base pair deletion (*p.Pro185LysfsTer2 – c.546delC*) in the final exon of the *Crx* gene (which has 4 exons in total). This causes a frameshift mutation resulting in a premature stop codon at residue 186. The position of the stop codon is at an analogous site to several reported human mutations that most frequently result in an LCA phenotype (for a summary, see Table 1.2 in Tran *et al*, 2014 [87] and [75, 103-111]). Because the mutation position is in the last exon, the mRNA is predicted to avoid nonsense mediated decay and to produce a truncated Crx protein (185 amino acids long instead of 299). The truncated protein would be predicted to have an intact DNA binding site but a truncated transactivation site (Figs. 1.30 and 1.31).[112]

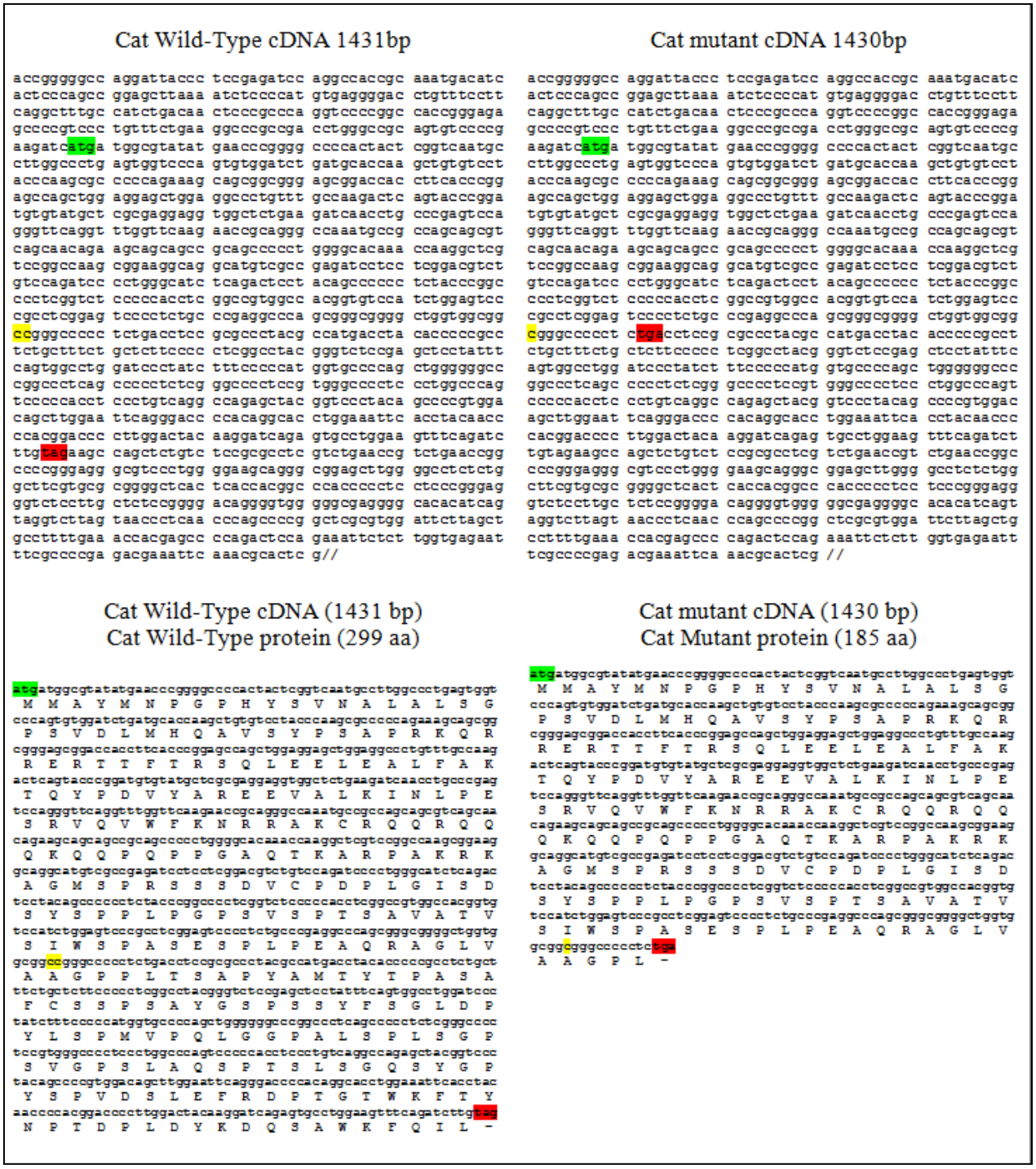

Figure 1.30. Wild-Type and mutant feline cDNA and the predicted protein.
This figure indicates the location of the feline mutation (indicated in *yellow* a deletion of a cytosine) at position 546. This introduces a premature stop codon and therefore encodes a truncated protein. Start codons are indicated in *green* while stop codons are indicated in *red*.

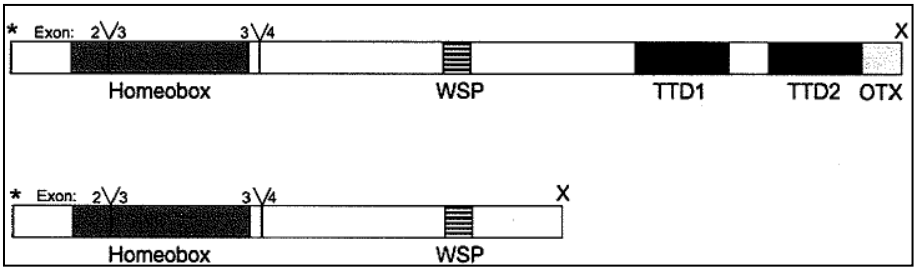

Figure 1.31. Wild-type and mutant *Rdy* Crx feline proteins (from Menotti-Raymond et *al*,. 2010).[112]
Y exon splice junctions, * Start codon , X stop codon, Shaded box homeobox WSP domain, Transcriptional transactivation domains 1 and 2 (TTD1 and TTD2) and OTX tail.

1.5. *CRX*-LCA INHERITED RETINAL DISEASE AND POTENTIAL THERAPIES

1.5.1. The disease phenotype leads to the potential therapy choices

Currently, there are no actual approved treatments for LCA in humans although there are a number of ongoing clinical trials for LCA resulting from *RPE65* mutations.[27, 113] Ongoing therapy testing in rodents exists in LCA caused by mutations in *AIPL1*, *GUCY2* and *CEP290* for example.[114-117] The Crx^{Rdy} cat could therefore be a valuable large animal model to provide new insights into the development of therapies for dominant LCA and for other conditions that have a dominant negative mechanism. Different therapeutic approaches have been developed over the past decade that could be applied to the treatment of LCA.

CRX-LCA retinopathies caused by a dominant negative mechanism present a challenge for treatment compared to recessive diseases. Indeed, recessive diseases result in a simple lack of gene product, which can be treated by gene augmentation. In dominant recessive disease such as *CRX*-LCA retinopathies, due to the over expression of the mutant allele having a negative effect on the wild-type allele, other strategies must be used in order to manipulate the ratio between mutant and WT *Crx* alleles/proteins.

Therefore, prior to loss of photoreceptors potential therapeutic interventions that may be translatable to human patients are those that address the over expression of the mutant *Crx* transcript compared to wild-type *Crx* transcript. These include either knocking down the levels of the mutant transcript, using for example anti-sense oligonucleotides [118-120] or shRNA [121-123], or over expressing the wild-type transcript by gene supplementation using adeno-associated viral vectors [51-54], or a combination of both approaches. Supporting evidence for this approach is provided by the p.E168d2 mouse model where a line of p.E168d2 mice in which a Neo cassette had not been excised (p.E168d2Neo) was investigated. The presence of the Neo cassette reduced expression of the p.E168d2 transcript compared to the wild-type transcript and this line of mice had a milder phenotype than the line where the Neo cassette had been excised and had over expression of the mutant transcript.[95] Also, mice or humans heterozygous for *null* mutations in *CRX* have either a mild phenotype or no phenotype.[83, 85]

1.5.2. Viral vectors for gene supplementation and their potential for therapy

Over the last 15 years viral vectors have been used for gene supplementation (Fig. 1.32). Vectors commonly used in basic science and translational research include those based on adeno-associated virus, adenovirus and lentivirus. Each has their own advantages and disadvantages, and so far the adeno-associated virus has been the most commonly used ocular gene for therapy.

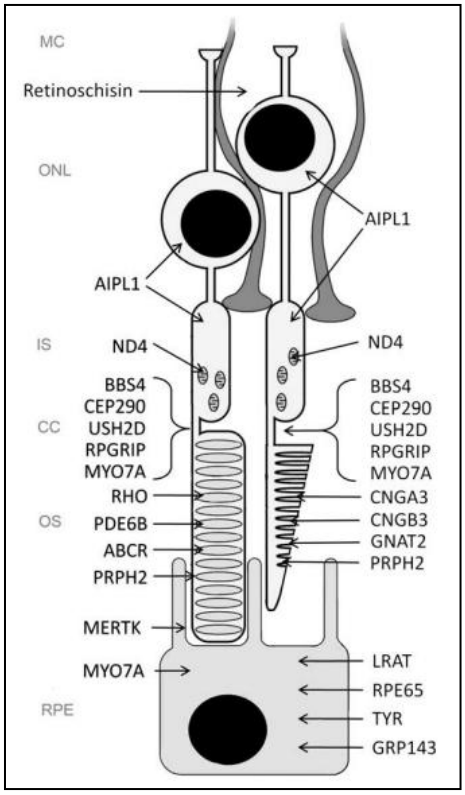

Figure 1.32. Proteins whose genes are candidates for gene supplementation therapy (from Smith et *al*., 2012).[124]
(MC; Müller cells, ONL; outer nuclear layer, IS: inner segment, CC; connecting cilim; OS; outer segment, RPE; retinal pigmentary epithelium.)

1.5.2.1. Viral vectors used for gene therapy

Lentiviruses are enveloped double-stranded RNA virus. They infect non-dividing cells and can integrate themselves into the host cells' genome allowing for long-term transgene expression. They can carry up to ~836 kb of genetic material. Random insertion of Lentiviruses runs the risk of causing tumors (if, for example, they disrupt a tumor suppressor gene or may impair the wild-type gene expression of the host genes). Other disadvantages include variable transgene expression and immune reaction (see review Escors et *al*., 2010 and Sack et *al*., 2009).[125-127]

Adenoviruses are double-stranded DNA viruses that are non-enveloped. They do not integrate, so they carry a very low risk of insertional mutogenesis. They can carry as much as ~36 kb of genetic material. However, disadvantages are frequent off target transduction and induction of immune responses (see review Douglas, 2007, Brunetti-Pierri et *al*., 2017, Sack et *al*., 2009).[127-129]

It is to be noted that all viruses used in gene therapy are foreign to the body cell of the host and therefore can potentially cause an immune reaction. Over the years, tremendous efforts have been made in research to optimize viral vectors to target specific cells with minimal adverse effects such as an adverse immune reaction. Adeno-associated virus vectors have become the vectors of choice for ocular gene therapy and are considered in more detail in the following section.

1.5.2.2. Adeno-associated vectors (AAV)

1.5.2.2.1. Properties of AAV vectors

Adeno-associated viruses are parvoviruses, which are non-replicating, non-enveloped viruses that have an icosahedral protein capsid and contains a single-stranded DNA genome (Fig. 1.33). Their advantages are that they are small in size and can infect both non-dividing and dividing cells. They can induce prolonged expression of the transgene, and certain serotypes can efficiently transduce photoreceptor and retinal pigment epithelial cells. They tend not to be very immunogenic and rarely integrate into the host genome. Their main disadvantage is that they have a relatively low genetic material cargo capacity, typically up to about 4.7 kb (although some techniques suggest up to 8.9 kb may be inserted).[130, 131] This is a significant limitation to their use for gene supplementation in diseases due to mutations in large genes such as *CEP290*, which is important because it is responsible for over 20% of LCA or *ABCA4*, a gene responsible for

Stargardt macular dystrophy. The *CRX* gene described in this dissertation is ~2.9 kb and therefore will fit in an AAV vector (see review Buning et *al*., 2008, Flotte, 2004, Conlon et *al*., 2004, Carter, 2004, Hastie et *al*., 2015).[131-142]

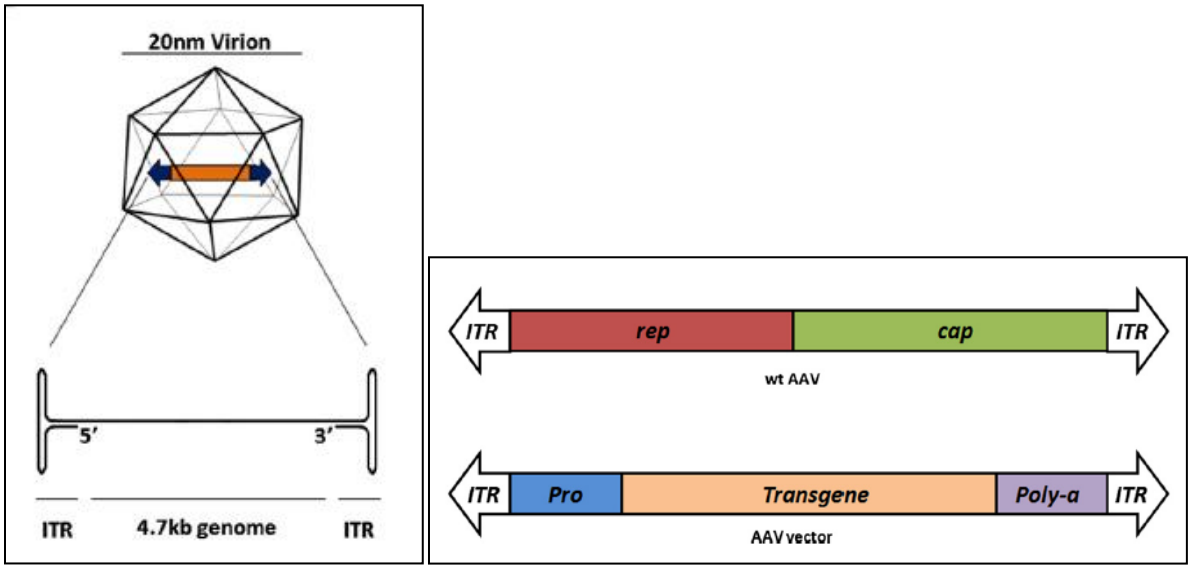

Figure 1.33. Schematic of an AAV vector – its capsid and single stranded DNA (from Lipinski et al., 2013).[143]
The **left panel** shows the icosahedral viral capsid containing a single-stranded DNA AAV genome. The **right panel** represents at the *top* the single stranded DNA of AAV, which is composed by *Rep* (replication) and *Cap* (capsid) genes surrounded by inverted terminal repeats (ITR). For creating a recombinant AAV, the *Rep* and Cap genes of the AAV are replaced by a transgene cassette containing a promoter, a transgene and poly-a tail (*bottom*), which are the regulatory elements required for gene expression.

The AAV genome is composed of 2 genes – open reading frames (ORFs) (*Rep* and *Cap*) and 2 inverted terminal repeats (ITRs) at both ends of the DNA strand flanking both genes that are necessary for the AAV genome multiplication and for packaging the DNA into capsids (Fig. 1.30). The *Rep* gene produces four overlapping transcripts *Rep78*, *Rep68*, *Rep52* and *Rep40* that are essential for viral replication. *Cap* encodes the capsid structural proteins: VP1, VP2 and VP3.[49] Due to its genome simplicity, the AAV genome can be easily modified and used for

development of therapies. Replacing the *Rep* and *Cap* genes allows the creation of a recombinant AAV (rAAV), which can deliver a DNA sequence of interest for gene therapy.[144, 145] The AAV can only replicate in the presence of a helper virus such as herpesvirus, papillomavirus, or adenovirus, which co-infect the host cell.[139, 140]

1.5.2.2.2. Transduction mechanism of action of AAV vectors

The transduction mechanism of action of AAV is summarized below (Fig. 1.34).

1) The first step consists of the recognition by the AAV vectors of the target cells. This happens through binding of the viral capsid proteins to specific membrane surface receptors such as integrins, FGFR-2 and heparin sulfate receptors. This then results in endocytosis of the AAV with the help of co-receptors. This step is an important rate-limiting step.

2) The AAV is then very rapidly internalized by endocytosis in an endosome or lysozome, mainly through the formation of clathrin-coated pits. This endocytosis is thought to be essential for viral trafficking by exposing the viral capsid protein. During this step amino acid residues of the capsid proteins such as tyrosine, serine and threonine can undergo phosphorylation, making the viral particle the target for ubiquitination and subsequent proteasomal degradation within the host cell cytoplasm. This can decrease transduction efficiency. During this "maturation" step the capsid is processed within endosomal compartments of the Golgi apparatus and endoplasmic reticulum to be ready for nuclear entry.

3) After this processing the AAV is then released in to the perinuclear region.

4) The viral vector subsequently enters into the nucleus through a pore complex. It is thought that the VP1 capsid protein is necessary for this entrance.

5) Inside the nucleus, the viral vector undergoes uncoating of the capsid and release of the viral single-stranded DNA genome. This is another rate limiting step for AAV transduction.

6) The AAV genome is then made double-stranded by the host cell machinery.

7) This double-stranded DNA can either be maintained as episomes or integrated into the host genome leading to step 8), transgene expression.[139, 142, 143, 146-151]

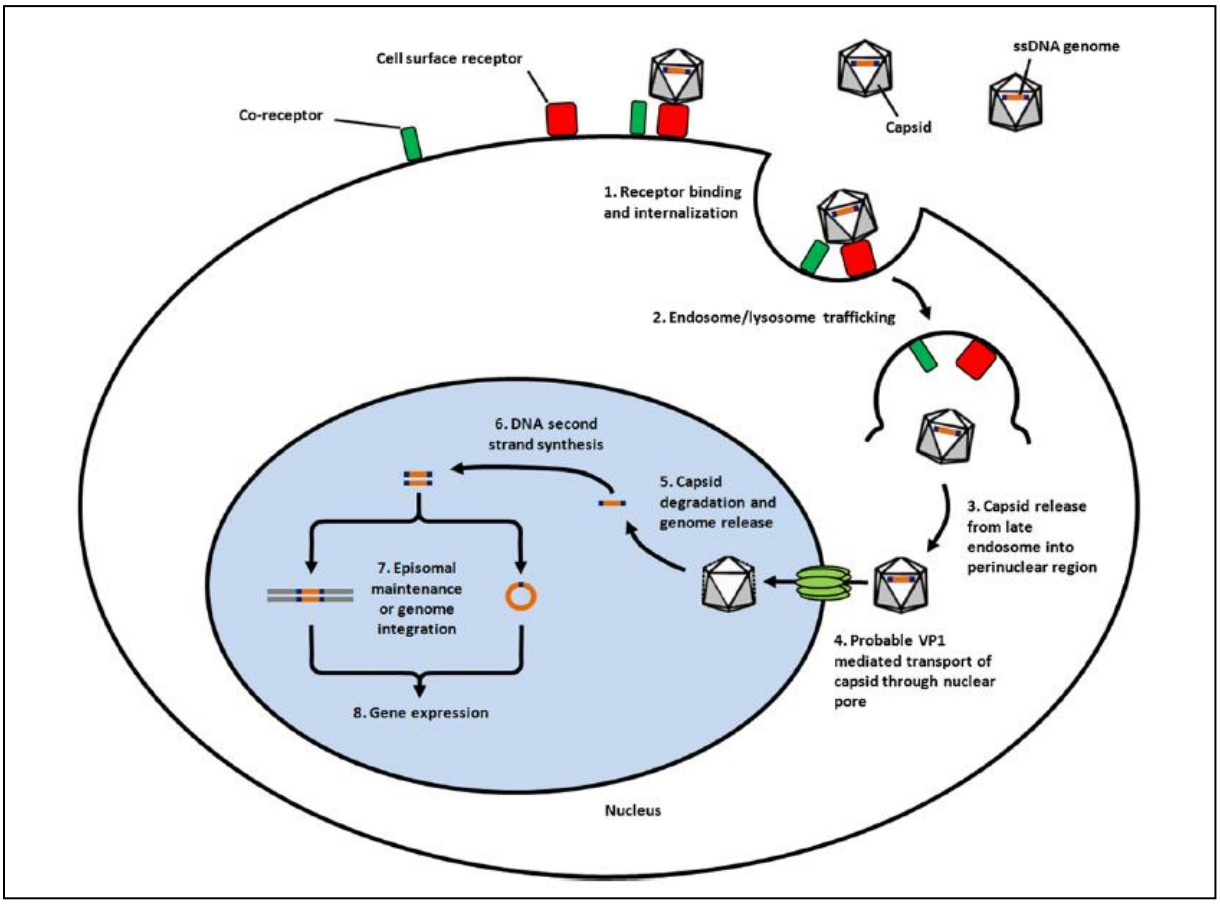

Figure 1.34. AAV vector mechanism of action leading to gene expression from Lipinski et al., 2013).[143]

1.5.2.2.3. Optimization of AAV vectors – recombinant AAV (rAAV) and other modifications

When developing gene therapy, the aim is to use an AAV that will transduce the correct tissue and cell type as well as obtaining the maximum transgene expression with minimal side effects. To achieve these aims, modifications have been made to AAV vectors that have an impact on the efficiency of each step required for AAV transduction.

Over a hundred different AAV serotypes have been identified, and so far twelve different naturally occurring human AAV serotypes (AAV1-12) have been characterized with AAV1-9 having been studied in most detail.[152, 153] The differences between the serotypes result from differences in capsid proteins, and this also accounts for differences in tissue and cell tropism.[142]

The AAV2 serotype has been studied in most detail and is most commonly used for developing therapies. This virus is known to be ubiquitous in the human population with a prevalence of up to 72%.[154]

The isosahedral AAV capsid, which defined the serotype, is composed of 60 capsid protein subtypes of the three viral proteins VP1, VP2 and VP3 in a 1:1:10 ratio.[155-157] Each capsid protein has a specific primary glycosaminoglycan receptor, which is responsible for its tropism.[152] For the purpose of this dissertation, we will not detail here the tropism for tissues other than the retina. For example, AAV1, AAV5 and AAV6 have a N-linked sialic acid glycan receptor associated with other co-receptors. AAV1 has a tropism for retinal-pigmented epithelium. AAV5 has a tropism for photoreceptors, Müller cells and retinal pigmented epithelium. AAV6 has a tropism for amacrine cells, Müller cells, bipolar cells and retinal ganglion cells. AAV2, AAV3 and AAV6 have a heparan sulfate proteoglycan receptor associated with other co-receptors. AAV2 has a tropism for photoreceptors, Müller cells, retinal ganglion

cells and retinal pigmented epithelium. AAV3 has a tropism for photoreceptor and retinal ganglion cells. AAV4 has an O-linked sialic acid receptor and a tropism for amacrine and Müller cells. The receptors of AAV7 and AAV8 are not known. AAV7 has a tropism for photoreceptors and retinal pigmented epithelium. AAV8 has a tropism for photoreceptors, Müller cells, retinal ganglion cells and retinal pigmented epithelium. AAV9 has a N-linked galactose receptor associated to other co-receptors and has a tropism for Müller cells and retinal pigmented epithelium.[139, 158, 159]

As stated previously, recombinant AAV (rAAV) for therapeutic uses are produced by introducing the desired cDNA into the AAV genome by replacing the *Rep* and *Cap* genes (Fig. 1.35). Those rAAV can be optimized to target specific tissue or cells by manipulating the capsid to improve their cell-specific tropism (Fig. 1.36). For such a modification, the backbone genome of the AAV serotype 2 is most commonly used and inserted in the capsid of another AAV serotype (referred to as pseudotyping). If it is inserted into the capsid of the AAV serotype 8, the hybrid vectors are called AAV2/8 (often shortened to AAV8). Capsid serotype is also important during AAV processing in the host cell nucleus and is an additional rate-limiting step, which is dependent on the AAV serotype. For example, the AAV2/2 single-stranded DNA take longer (up to 6 weeks) to be uncoated and released in the host nucleus whereas AAV2/8 vectors are much more rapidly uncoated.

To overcome the rate limiting step of making the transgene double-stranded DNA, one engineering solution has been the development of self-complementary AAV genomes. With this strategy a complementary version of the transgene is packaged in the expression cassette (separated by a mutated termination site). This allows the genome to bind to itself and therefore become double-stranded DNA immediately after release in the host nucleus (Fig. 1.37). This results also in a more robust transgene expression. The main disadvantage is that it increases the

genome size and therefore limits the size of the cDNA of the gene of interest to be delivered.[56, 160-163]

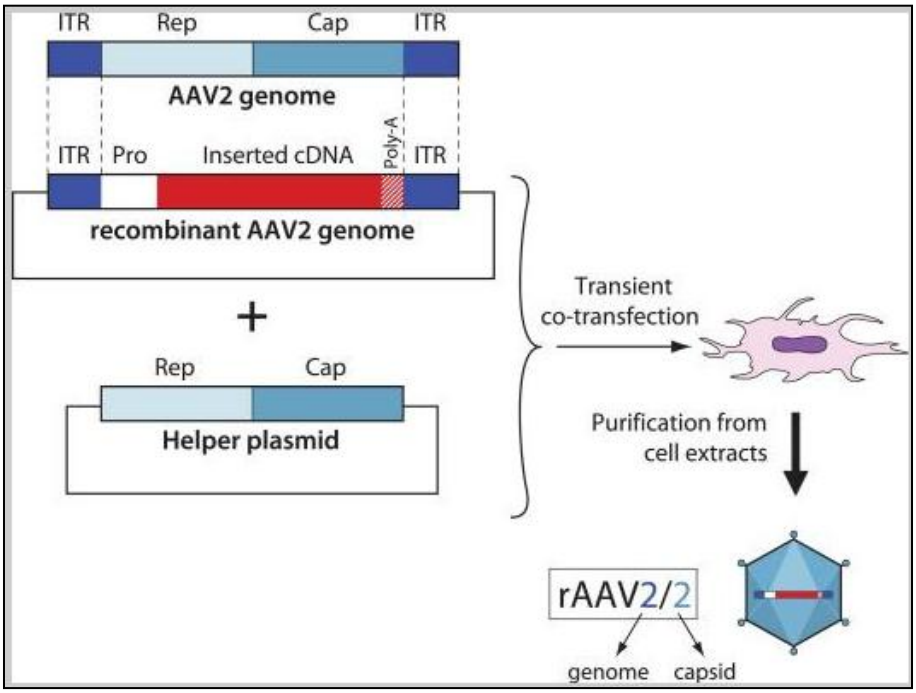

Figure 1.35. Structure and production of a rAAV vector (from Beltran, 2009).[56] The recombinant AAV vector (rAAV) is engineered by removing the *rep* and *cap* genes from the wild-type AAV serotype 2 backbone genome. Those are replaced by a promoter (Pro), the cDNA of a therapeutic gene capped with a poly-adenylation site (PolyA) between the two inverted terminal repeats (ITR). This new genome is then inserted into a plasmid and used with a helper plasmid containing the *rep* and *cap* genes to transfect cells in culture. These cells produce a replication-defective recombinant AAV. In this figure both the genome and the capsid originate from an AAV2 serotype thus generating a rAAV2/2 vector.

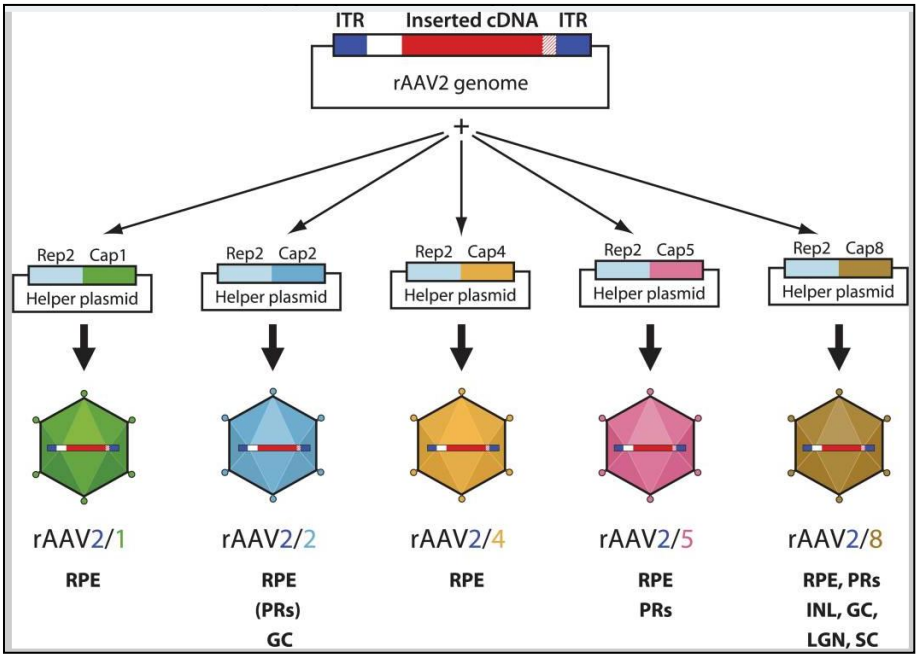

Figure 1.36. Examples of hybrid rAAV and their cell tropism of rAAV in the canine retina. RPE: retinal pigment epithelium; PRs: photoreceptors; INL: inner nuclear layer; GC: ganglion cells; LGN: lateral geniculate nucleus; SC: superior colliculus (from Beltran, 2009).[56]

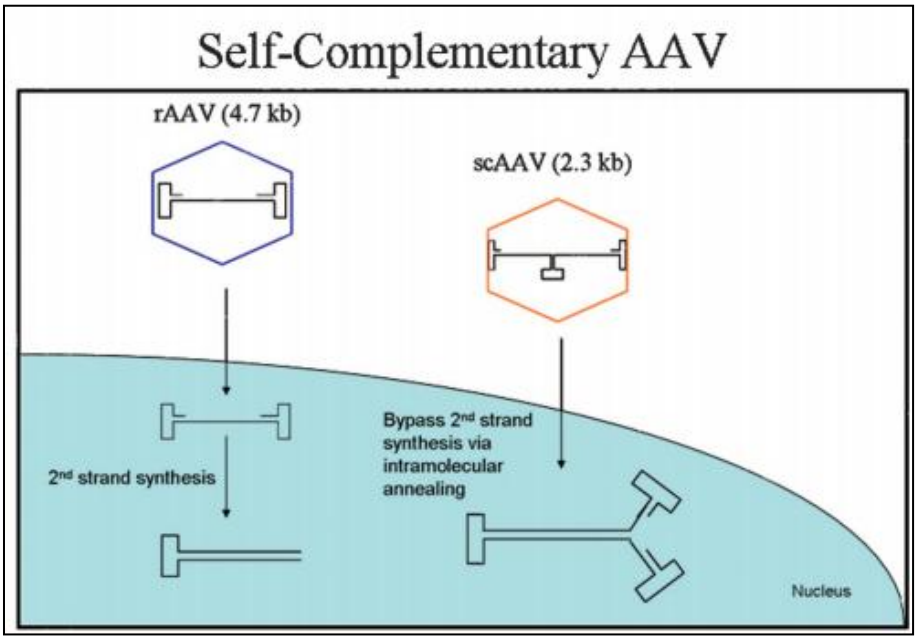

Figure 1.37. Comparison of scAAV and rAAV vectors (from Daya et *al.*, 2008).[163]

Other modifications to improve AAV vectors are the modification of the surface capsid proteins topography and amino-acid composition; this creates hybrid vectors. The parts of the proteins that are modified are the exposed residues (such as tyrosine, serine, threonine, and lysine) that are targets for modification such as phosphorylation that can lead to proteasomal degradation.[91,92] Modifications by mutating those amino acids (producing "mutant capsid AAVs") can help to improve transgene expression efficiency and decrease the potential host immune reaction by avoiding phosphorylation and ubiquitination and therefore degradation by proteosomes that would recognize the viral capsid proteins thorough those residues. This escape from the host defense might also improve the extracellular transport and penetration into the targeted cell.[146, 164-172] Examples of engineered capsid protein mutations are the replacement of a tyrosine by a phenylalanine residue (Y-F) or a threonine by a valine residue (T-V). Mutations can be single (Y733F, replacement of a tyrosine by a phenylalanine residue at the position 733), triple, quadruple…etc. Recent approaches for capsid modification utilize a technique called "directed evolution". This is where mutations of the *Cap* gene are created by error prone PCR, random peptide insertion, or capsid DNA shuffling, to generate a large library of capsid variant vectors. These vectors are then tested for efficiency, to reach a target tissue for example. The target tissue is isolated and the rAAVs within it isolated and perhaps used for subsequent rounds of enrichment to identify capsid variants with the desired characteristic.[52, 138, 173]

At a viral genome level, the use of a specific promoter to drive expression of the transgene can help limit expression of the transgene to the chosen cells. This will limit off-target expression and therefore side-effects (i.e. mOP, hGK1 and PR2.1 promoters).[54, 174, 175]

More recently, advances in AAV engineering have been achieved, such as using a hybrid technique to deliver genes that are too big to fit into the rAAV vector. This technique consists of

using two AAV vectors, each containing separate parts of the cDNA needed. The theory is that they allow recombination of the full transgene cDNA within the host cell and therefore expression of the overlarge cDNA.[176, 177]

1.5.2.2.4. Delivery route of AAV vectors for inherited retinal dystrophy diseases

The two most common AVV delivery routes to treat the retina for inherited retinal dystrophies are intravitreal and subretinal injections (Fig. 1.38).[51] The least invasive is the intravitreal technique, which is suitable for transducing inner retinal cell types. However, for retinal dystrophies, where the RPE or photoreceptors need to be transduced, most rAAVs only inefficiently traverse the retina to reach photoreceptor cells, which are located on the basal side of the retina. Work is progressing to produce vectors that can efficiently target the outer retina from the vitreal cavity.[178-181]

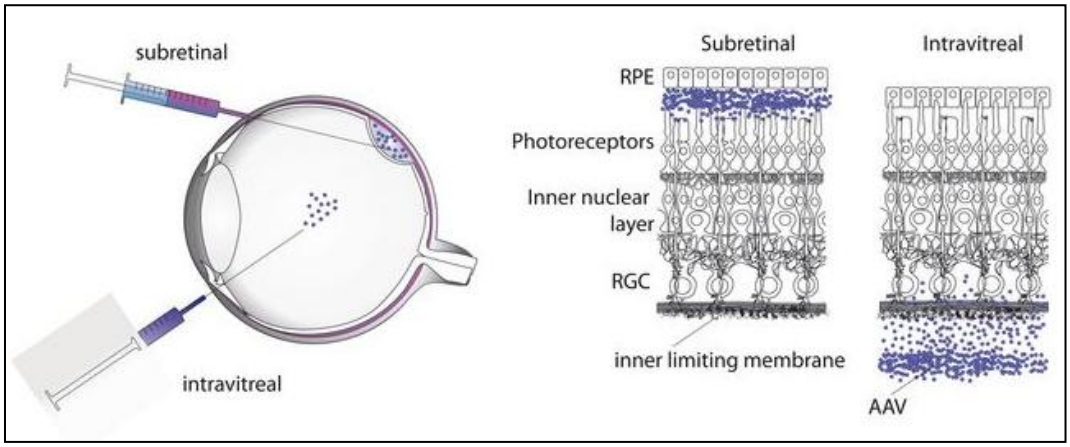

Figure 1.38. Intraocular AAV administration routes from Dalkara (http://www.vision-research.eu/index.php?id=906).[182] Subretinal injection creates a space between the RPE and the photoreceptor and therefore allows delivering of gene therapy vectors directly in proximity of the photoreceptor and RPE cells while the intravitreal injection delivers the AAV vector in the vitreous throughout, which it diffuses to allow treatment of inner retinal cells. RPE: retinal pigment epithelium, RGC: retinal ganglion cells.

For gene therapy targeting photoreceptors (to treat diseases like *CRX*-LCA, *CEP290*-LCA, *AIPL1*-LCA) and retinal pigmentary epithelium (to treat diseases such as *RPE65*-LCA), subretinal delivery of the AAV vector is still required. This technique allows direct supply of the therapeutic genome to the cell targeted. Moreover, a specificity of the subretinal space is that it is an immune-privileged site; therefore, the risk of humoral response towards the AAV vector and its transgene is reduced. However, it is an invasive technique that causes a retinal detachment between the photoreceptor and the RPE. The retina usually reattached within a couple of days, but this could be enough to lead to some cell damage (notably photoreceptor outer segments and apoptosis).[183-190] Another disadvantage of subretinal injection is that effectively only the retina in the region injected is transduced.[191]

Intravitreal injection is less invasive (Fig. 1.38) and potentially could treat the entire retina. One drawback is that immune responses are more likely from intravitreal compared to subretinal administration. Active research is in development to overcome those obstacles; notably using cell-specific promoters as intravitreal injection can easily be done as a routine treatment under local anesthesia without sedation in humans. For instance, investigations have been done in large animal models like the dogs and macaques to look at the effect of vitrectomy. Results are variable; some showed that vitrectomy two weeks prior to intravitreal injection of rAAV can lead to reduction of the transgene transduction and cause vector-immune reaction[179] while others showed that vitrectomy immediately prior to rAAV injection improves transgene tranduction efficiency.[192]

1.5.2.2.5. Immune responses to AAV vectors.

One of the major risks of the use of AAV for gene therapy is the potential immune reaction which increases morbidity. The eye has several advantages; it is an isolated organ and is an immune-privileged site, which is due to the anterior chamber-associated immune deviation (ACAID), a process present in the anterior chamber and the vitreous humor. ACAID is a process by which an immunosuppressive intraocular state is maintained within the eye by specific dendritic cells present in various structure of the eye. If any traumatic or inflammatory events intervene in the eye or its tissues, ACAID can be disrupted and the immunosuppressive state of the eye lost leading to severe inflammation or damage.[193-197]

Both humans and large animal models are naturally exposed to AAV; therefore, systemic circulating neutralizing antibodies (NAb) may be present prior to any rAAV gene therapy injection. This can lead to therapeutic failure and an immune reaction to the injected rAAV. As stated above, the subretinal injection is a technique that has less risk of immune response than the intravitreal injection. It has been shown that repeated subretinal injections can be performed without eliciting any NAb production by humoral response while this is not the case for intravitreal injection.[138, 154, 198-202]

Finally, systemic administration of AAV can lead to cell-mediated responses. Those responses target the protein capsid and the transgene through cytotoxic T lymphocyte reactions. This type of immune reaction can be severe and lead to both the attack of the rAAV but also of the host cells.[203-206]

1.5.3. Potential silencing therapies

There are various existing silencing therapies that include the use of oligonucleotides (ON), which have been developed for a long time and used in clinics.

The different oligonucleotides mechanisms are as follows (Fig. 1.39):

- Binding to Toll-like receptors (TLRs) in the endosome,
- Small interfering RNA (siRNA),
- Micro-RNA (miR) mimic,
- Antagomir, sterically blocking endogenous miR,
- Gapmer AON, inducing RNase H degradation (steric block ONs also exist),
- Aptamer, binding alters protein surface,
- Splice switching ON (SSO),
- Anti-gene ONs,
- ONs directed against nuclear regulatory RNA species, (never yet used in clinics).

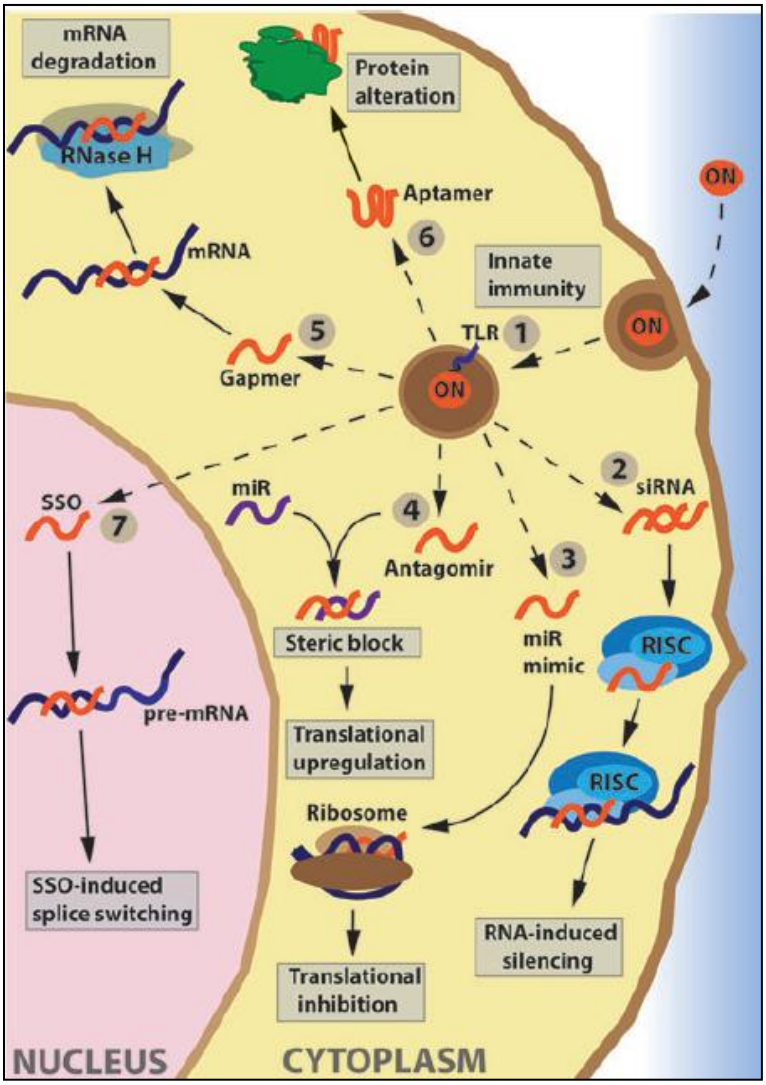

Figure 1.39. Figure showing the currently used oligonucleotide therapeutic approaches (from Lundin et *al*. 2015). The approaches labeled 1 to 7 in the diagram have been used in the clinic.[207]

Others therapies in addition to those described above include pharmacological interventions, CRISPR-Cas9 targeted genome editing, cell transplantation, retinal prosthesis and cortical devices.

All of these therapies could potentially be applied to *CRX*-LCA animal models so long as the phenotype and disease mechanism are well defined and therapies are tested at the correct disease stage and in most appropriate model.

1.6. AIM AND OUTLINE OF THIS THESIS

Based on the findings in the *CRX*^{E168d2} mouse model, we hypothesized that the severe *Crx*$^{Rdy/+}$ feline phenotype would result from a similar mechanism, namely an antimorphic effect associated with over expression of the mutant transcript and that a potential therapeutic approach would be to use an intervention that reduced the mutant-to-wild-type mRNA/protein ratio.

The detailed hypotheses that guided these studies are as follows:

1. Crx$^{Rdy/+}$ cats have a failure of retinal structural and functional maturation associated with reduced expression of specific retinal genes due to expression of the mutant *Crx* transcript, which has a dominant negative effect.

2. Crx$^{Rdy/+}$ cats show severe retinal remodeling that worsens with disease progression, affecting not only the outer retina but also the inner retina and the retinal vasculature.

3. Crx$^{Rdy/Rdy}$ cats have a marked reduction in expression of specific retinal genes resulting in absence or severely decreased retinal function and incomplete photoreceptor maturation with marked morphological abnormalities.

4. Partial rescue of the Crx$^{Rdy/+}$ phenotype will be achievable using gene therapy to either augment the levels of normal *Crx* transcript or to reduce the levels of the mutant transcript or a combination of both approaches.

To test these hypotheses, we aimed to further characterize the phenotype of the *Crx*$^{Rdy/+}$ cat and to also characterize the phenotype of the *Crx*$^{Rdy/Rdy}$ cat by a number of techniques. These included ophthalmic examination and fundus imaging (fundus photography, confocal scanning laser ophthalmoscope and fluorescein angiography) morphological investigations using spectral domain optical coherence tomography and histology, and functional changes by

electroretinography. Retinal gene expression changes were assessed by immunohistochemistry, qRT-PCR and Western blot. Disease mechanisms were further investigated by measuring both expression of the mutant *Crx* transcript and the transactivation activity of the mutant protein. We also investigated treatment strategies to rescue the phenotype of retinopathies due to antimorphic *CRX* mutations.

This current dissertation outline follows detailed aims based on the research-driven hypotheses stated above.

Chapter 1 gives an introduction on animal models for dominant Leber Congenital Amaurosis (LCA) due to *CRX* mutations and introduces the feline model as well as potential therapies.

Chapter 2 tests the hypothesis that the heterozygous *Crx* mutant cat ($Crx^{Rdy/+}$) cat has a failure of retinal structural and functional maturation associated with reduced expression of specific retinal genes due to expression of the mutant *Crx* transcript which has a dominant negative effect. Therefore, the aim of this chapter is to describe a detailed investigation of the phenotype of the $Crx^{Rdy/+}$ cat and the mechanisms underlying the disease.

Chapter 3 investigated the hypothesis that in the late stages of the disease the heterozygous *Crx* mutant cat ($Crx^{Rdy/+}$) presents with severe retinal remodeling throughout all layers of the retina. This chapter aims to give a description of morphologic and metabolic changes undergone by the retina as well as a description of the retinal vasculature changes occurring during the disease progression in $Crx^{Rdy/+}$ cat.

Chapter 4 tests the hypothesis that the homozygous *Crx* mutant (*Crx*$^{Rdy/Rdy}$ cat) will have a marked reduction in expression of specific retinal genes resulting in an absence or severe decrease in retinal function and incomplete photoreceptor maturation with marked morphological abnormalities. This chapter's aim is to detail the phenotype of the *Crx*$^{Rdy/Rdy}$ cat and start unraveling some of the mechanisms underlying the disease pathogenesis.

Chapter 5 initiates work on the hypothesis that partial rescue of the Crx$^{Rdy/+}$ phenotype can be achieved using gene therapy to either augment the levels of normal *Crx* transcript or to reduce the level of the mutant transcript or a combination of both approaches. This chapter gives preliminary results for vision restoration in *Crx*$^{Rdy+/-}$ cat using gene supplementation therapy.

Chapter 6 gives conclusions and future directions.

1.7. CONCLUSION

CRX is an essential transcription factor essential for the development of photoreceptors and their maintenance. Mutations in *CRX* lead severe retinal disease like Leber Congenital Amaurosis. Currently, a few mouse models exist, but only one large animal model is available, the *Crx*^{Rdy} cat. Mouse models have been investigated and their phenotype described; however, the feline model needs further study, and the mechanism underlying the disease needs to be fully elucidated. These models, and in particular the feline model, are highly valuable for the development of therapies for CRX-LCA disease and other dominant negative diseases.

REFERENCES

REFERENCES

1. Organization WH. Visual Impairment and Blindness. Fact Sheet N°282. *WhoInt*; August 2014:Web. 12 June 2017.

2. Ma W, Wei J, Wei Y, et al. Immunogenicity of the capsid precursor and a nine-amino-acid site-directed mutant of the 3C protease of foot-and-mouth disease virus coexpressed by a recombinant goatpox virus. *Arch Virol.* 2014;159:1715-1722.

3. Pacione LR, Szego MJ, Ikeda S, Nishina PM, McInnes RR. Progress toward understanding the genetic and biochemical mechanisms of inherited photoreceptor degenerations. *Annu Rev Neurosci.* 2003;26:657-700.

4. Rattner A, Sun H, Nathans J. Molecular genetics of human retinal disease. *Ann Rev Genet.* 1999;33:89-131.

5. Wright AF, Chakarova CF, Abd El-Aziz MM, Bhattacharya SS. Photoreceptor degeneration: genetic and mechanistic dissection of a complex trait. *Nat Rev Genet.* 2010;11:273-284.

6. Daiger SP, Rossiter BJF, Greenberg J, Christoffels A, Hide W. Data services and software for identifying genes and mutations causing retinal degeneration. *Invest Ophthalmol Vis Sci. (Suppl)* 1998;39:S295.

7. Hejtmancik JF, Nickerson JM. Overview of the Visual System. *Prog Mol Biol Transl Sci.* 2015;134:1-4.

8. Graw J. Eye development. *Curr Top Dev Biol.* 2010;90:343-386.

9. Chow RL, Lang RA. Early eye development in vertebrates. *Annu Rev Cell Dev Biol.* 2001;17:255-296.

10. Heavner W, Pevny L. Eye development and retinogenesis. *Cold Spring Harb Perspect Biol.* 2012;4.

11. D'Orazi FD, Suzuki SC, Wong RO. Neuronal remodeling in retinal circuit assembly, disassembly, and reassembly. *Trends Neurosci.* 2014;37:594-603.

12. Bassett EA, Wallace VA. Cell fate determination in the vertebrate retina. *Trends Neurosci.* 2012;35:565-573.

13. Marquardt T, Gruss P. Generating neuronal diversity in the retina: one for nearly all. *Trends Neurosci.* 2002;25:32-38.

14. Martins RA, Pearson RA. Control of cell proliferation by neurotransmitters in the developing vertebrate retina. *Brain Res.* 2008;1192:37-60.

15. Zimmerman RP, Polley EH, Fortney RL. Cell birthdays and rate of differentiation of ganglion and horizontal cells of the developing cat's retina. *J Comp Neurol.* 1988;274:77-90.

16. Rapaport DH, Stone J. The topography of cytogenesis in the developing retina of the cat. *J Neurosci.* 1983;3:1824-1834.

17. Johns PR, Rusoff AC, Dubin MW. Postnatal neurogenesis in the kitten retina. *J Comp Neurol.* 1979;187:545-555.

18. Chan-Ling TL, Halasz P, Stone J. Development of retinal vasculature in the cat: processes and mechanisms. *Curr Eye Res.*1990;9:459-478.

19. Morrison JD. Morphogenesis of photoreceptor outer segments in the developing kitten retina. *J Anat.* 1983;136:521-533.

20. Mastronarde DN, Thibeault MA, Dubin MW. Non-uniform postnatal growth of the cat retina. *J Comp Neurol.* 1984;228:598-608.

21. Vogel M. *Postnatal development of the cat's retina.* Germany: Springer-Verlag Berlin Heidelberg; 1978:66.

22. Granit R. The components of the retinal action potential in mammals and their relation to the discharge in the optic nerve. *J Physiol.* 1933;77:207-239.

23. Frishman LJ. Origins of the electroretinogram. In: Heckenlively J.R. AGB (ed), *Principles and practice of clinical electrophysiology of vision.* Cambridge, Massachusetts: The MIT press; 2006:139-183.

24. Hamasaki DI, Maguire GW. Physiological development of the kitten's retina: an ERG study. *Vision Res.* 1985;25:1537-1543.

25. Jacobson SG, Ikeda H, Ruddock K. Cone-mediated retinal function in cats during development. *Doc Ophthalmol.* 1987;65:7-14.

26. Veleri S, Lazar CH, Chang B, Sieving PA, Banin E, Swaroop A. Biology and therapy of inherited retinal degenerative disease: insights from mouse models. *Dis Model Mech.* 2015;8:109-129.

27. Petersen-Jones SM, Annear MJ, Bartoe JT, et al. Gene augmentation trials using the Rpe65-deficient dog: contributions towards development and refinement of human clinical trials. *Adv Exp Med Biol.* 2012;723:177-182.

28. Vakkur GJ, Bishop PO. The Schematic Eye in the Cat. *Vision Res.* 1963;61:357-381.

29. Curcio CA, Sloan KR, Kalina RE, Hendrickson AE. Human photoreceptor topography. *J Comp Neurol.* 1990;292:497-523.

30. Østerberg G. Topography of the layer of rods and cones in the human retina. *Acta Ophthalmol.* 1935;13:11-103.

31. Jeon CJ, Strettoi E, Masland RH. The major cell populations of the mouse retina. *J Neurosci.* 1998;18:8936-8946.

32. Steinberg RH, Reid M, Lacy PL. The distribution of rods and cones in the retina of the cat (Felis domesticus). *J Comp Neurol.* 1973;148:229-248.

33. Wikler KC, Williams RW, Rakic P. Photoreceptor mosaic: number and distribution of rods and cones in the rhesus monkey retina. *J Comp Neurol.* 1990;297:499-508.

34. Applebury ML, Antoch MP, Baxter LC, et al. The murine cone photoreceptor: a single cone type expresses both S and M opsins with retinal spatial patterning. *Neuron.* 2000;27:513-523.

35. Bowmaker JK, Dartnall HJ. Visual pigments of rods and cones in a human retina. *J Physiol.* 1980;298:501-511.

36. Bowmaker JK. Evolution of vertebrate visual pigments. *Vision Res.* 2008;48:2022-2041.

37. Yokoyama S. Molecular bases of color vision in vertebrates. *Genes Genet Syst.* 1999;74:189-199.

38. Yokoyama S, Radlwimmer FB. The molecular genetics of red and green color vision in mammals. *Genetics.* 1999;153:919-932.

39. Provis JM, Dubis AM, Maddess T, Carroll J. Adaptation of the central retina for high acuity vision: cones, the fovea and the avascular zone. *Prog Retin Eye Res.* 2013;35:63-81.

40. Rossi EA, Roorda A. The relationship between visual resolution and cone spacing in the human fovea. *Nature Neurosci.* 2010;13:156-157.

41. Volland S, Esteve-Rudd J, Hoo J, Yee C, Williams DS. A comparison of some organizational characteristics of the mouse central retina and the human macula. *PloS one.* 2015;10:e0125631.

42. Beltran WA, Cideciyan AV, Guziewicz KE, et al. Canine retina has a primate fovea-like bouquet of cone photoreceptors which is affected by inherited macular degenerations. *PloS one.* 2014;9:e90390.

43. Bishop PO, Kozak W, Vakkur GJ. Some quantitative aspects of the cat's eye: axis and plane of reference, visual field co-ordinates and optics. *J Physiol.* 1962;163:466-502.

44. Linberg KA, Lewis GP, Shaaw C, Rex TS, Fisher SK. Distribution of S- and M-cones in normal and experimentally detached cat retina. *J Comp Neurol.* 2001;430:343-356.

45. Mowat FM, Petersen-Jones SM, Williamson H, et al. Topographical characterization of cone photoreceptors and the area centralis of the canine retina. *Mol Vis.* 2008;14:2518-2527.

46. Rapaport DH, Stone J. The area centralis of the retina in the cat and other mammals: focal point for function and development of the visual system. *Neuroscience.* 1984;11:289-301.

47. Kemp CM, Faulkner DJ, Jacobson SG. The distribution and kinetics of visual pigments in the cat retina. *Invest Ophthalmol Vis Sci.* 1988;29:1056-1065.

48. Carroll J, Neitz M, Hofer H, Neitz J, Williams DR. Functional photoreceptor loss revealed with adaptive optics: an alternate cause of color blindness. *Proc Natl Acad Sci U S A.* 2004;101:8461-8466.

49. Putnam NM, Hofer HJ, Doble N, Chen L, Carroll J, Williams DR. The locus of fixation and the foveal cone mosaic. *J Vis.* 2005;5:632-639.

50. Li KY, Tiruveedhula P, Roorda A. Intersubject variability of foveal cone photoreceptor density in relation to eye length. *Invest Ophthalmol Vis Sci.* 2010;51:6858-6867.

51. Dalkara D, Sahel JA. Gene therapy for inherited retinal degenerations. *C R Biol.* 2014;337:185-192.

52. Day TP, Byrne LC, Schaffer DV, Flannery JG. Advances in AAV vector development for gene therapy in the retina. *Adv Exp Med Biol.* 2014;801:687-693.

53. Kotterman MA, Schaffer DV. Engineering adeno-associated viruses for clinical gene therapy. *Nat Rev Genet.* 2014;15:445-451.

54. McClements ME, MacLaren RE. Gene therapy for retinal disease. *Transl Res.* 2013;161:241-254.

55. Narfstrom K, Holland Deckman K, Menotti-Raymond M. The domestic cat as a large animal model for characterization of disease and therapeutic intervention in hereditary retinal blindness. *J Ophthalmol.* 2011;2011:906943.

56. Beltran WA. The use of canine models of inherited retinal degeneration to test novel therapeutic approaches. *Vet Ophthalmol.* 2009;12:192-204.

57. Petersen-Jones SM, Komaromy AM. Dog models for blinding inherited retinal dystrophies. *Hum Gene Ther Clin Dev.* 2015;26:15-26.

58. Li ZY, Wong F, Chang JH, et al. Rhodopsin transgenic pigs as a model for human retinitis pigmentosa. *Invest Ophthalmol Vis Sci.* 1998;39:808-819.

59. Banin E, Obolensky A, Ejzenberg A, et al. Gene therapy in a sheep model of CNGA3 achromatopsia. *Invest Ophthalmol Vis Sci.* 2014;55:4566-.

60. Winkler PA, Ekenstedt KJ, Occelli LM, et al. A large animal model for CNGB1 autosomal recessive retinitis pigmentosa. *PloS one.* 2013;8:e72229.

61. Gandolfi B, Alhaddad H. Investigation of inherited diseases in cats: genetic and genomic strategies over three decades. *J Feline Med Surg.* 2015;17:405-415.

62. Montague MJ, Li G, Gandolfi B, et al. Comparative analysis of the domestic cat genome reveals genetic signatures underlying feline biology and domestication. *Proc Natl Acad Sci U S A.* 2014;111:17230-17235.

63. Menotti-Raymond M, David VA, Schaffer AA, et al. Mutation in CEP290 discovered for cat model of human retinal degeneration. *J Hered.* 2007;98:211-220.

64. Menotti-Raymond M, Deckman KH, David V, Myrkalo J, O'Brien SJ, Narfstrom K. Mutation discovered in a feline model of human congenital retinal blinding disease. *Invest Ophthalmol Vis Sci.* 2010;51:2852-2859.

65. Alhaddad H, Gandolfi B, Grahn RA, et al. Genome-wide association and linkage analyses localize a progressive retinal atrophy locus in Persian cats. *Mamm Genome.* 2014;25:354-362.

66. Ofri R, Reilly CM, Maggs DJ, et al. Characterization of an Early-Onset, Autosomal Recessive, Progressive Retinal Degeneration in Bengal Cats. *Invest Ophthalmol Vis Sci.* 2015;56:5299-5308.

67. Spitz F FEE. Transcription factors: from enhancer binding to developmental control. *Nat Rev Genet.* 2012;13:613-626.

68. DS L. Transcription Factors: An Overview. *Int J Biochem Cell Biol.* 1997;29:1305-1312.

69. Boije H, MacDonald RB, Harris WA. Reconciling competence and transcriptional hierarchies with stochasticity in retinal lineages. *Curr Opin Neurobiol.* 2014;27:68-74.

70. Hennig AK, Peng GH, Chen S. Regulation of photoreceptor gene expression by Crx-associated transcription factor network. *Brain Res.* 2008;1192:114-133.

71. Oh EC, Khan N, Novelli E, Khanna H, Strettoi E, Swaroop A. Transformation of cone precursors to functional rod photoreceptors by bZIP transcription factor NRL. *Proc Natl Acad Sci U S A.* 2007;104:1679-1684.

72. Swaroop A, Kim D, Forrest D. Transcriptional regulation of photoreceptor development and homeostasis in the mammalian retina. *Nat Rev Neurosci.* 2010;11:563-576.

73. Beltran WA, Cideciyan AV, Lewin AS, et al. Gene therapy rescues photoreceptor blindness in dogs and paves the way for treating human X-linked retinitis pigmentosa. *Proc Natl Acad Sci U S A.* 2012;109:2132-2137.

74. Leber T. Über retinitis pigmentosa und angeborene Amaurose. *G Graefes Arch Clin Exp Ophthalmol.* 1869;15:1-25.

75. Stone EM. Leber congenital amaurosis - a model for efficient genetic testing of heterogeneous disorders: LXIV Edward Jackson Memorial Lecture. *Am J Ophthalmol.* 2007;144:791-811.

76. Koenekoop RK. An overview of Leber congenital amaurosis: a model to understand human retinal development. *Surv Ophthalmol.* 2004;49:379-398.

77. Alström CH, Olson O. *Heredo-retinopathia congenitalis; monohybrida recessiva autosomalis*. Lund, Sweden: Berlingska Boktryckeriet; 1957:178 p.

78. Schappert-Kimmijser J, Henkes HE, Van Den Bosch J. Amaurosis congenita (Leber). *Arch Ophthalmol.* 1959;61:211-218.

79. Chacon-Camacho OF, Zenteno JC. Review and update on the molecular basis of Leber congenital amaurosis. *World J Clin Cases.* 2015;3:112-124.

80. den Hollander AI. Omics in Ophthalmology: Advances in Genomics and Precision Medicine for Leber Congenital Amaurosis and Age-Related Macular Degeneration. *Invest Ophthalmol Vis Sci.* 2016;57:1378-1387.

81. den Hollander AI, Roepman R, Koenekoop RK, Cremers FP. Leber congenital amaurosis: genes, proteins and disease mechanisms. *Prog Retin Eye Res.* 2008;27:391-419.

82. Chen S, Wang QL, Nie Z, et al. Crx, a novel Otx-like paired-homeodomain protein, binds to and transactivates photoreceptor cell-specific genes. *Neuron.* 1997;19:1017-1030.

83. Furukawa T, Morrow EM, Cepko CL. Crx, a novel otx-like homeobox gene, shows photoreceptor-specific expression and regulates photoreceptor differentiation. *Cell.* 1997;91:531-541.

84. Chau KY, Chen S, Zack DJ, Ono SJ. Functional domains of the cone-rod homeobox (CRX) transcription factor. *J Biol Chem.* 2000;275:37264-37270.

85. Morrow EM, Furukawa T, Raviola E, Cepko CL. Synaptogenesis and outer segment formation are perturbed in the neural retina of Crx mutant mice. *BMC Neurosci.* 2005;6:5.

86. Peng GH, Chen S. Crx activates opsin transcription by recruiting HAT-containing co-activators and promoting histone acetylation. *Hum Mol Genet.* 2007;16:2433-2452.

87. Tran NM, Chen S. Mechanisms of blindness: Animal models provide insight into distinct CRX-associated retinopathies. *Dev Dyn.* 2014;243:1153-1166.

88. Livesey FJ, Furukawa T, Steffen MA, Church GM, Cepko CL. Microarray analysis of the transcriptional network controlled by the photoreceptor homeobox gene Crx. *Curr Biol.* 2000;10:301-310.

89. Hsiau TH, Diaconu C, Myers CA, Lee J, Cepko CL, Corbo JC. The cis-regulatory logic of the mammalian photoreceptor transcriptional network. *PloS one.* 2007;2:e643.

90. Blackshaw S, Fraioli RE, Furukawa T, Cepko CL. Comprehensive analysis of photoreceptor gene expression and the identification of candidate retinal disease genes. *Cell.* 2001;107:579-589.

91. Corbo JC, Lawrence KA, Karlstetter M, et al. CRX ChIP-seq reveals the cis-regulatory architecture of mouse photoreceptors. *Genome Res.* 2010;20:1512-1525.

92. Roosing S, Thiadens AA, Hoyng CB, Klaver CC, den Hollander AI, Cremers FP. Causes and consequences of inherited cone disorders. *Prog Retin Eye Res.* 2014;42:1-26.

93. Hull S, Arno G, Plagnol V, et al. The phenotypic variability of retinal dystrophies associated with mutations in CRX, with report of a novel macular dystrophy phenotype. *Invest Ophthalmol Vis Sci.* 2014;55:6934-6944.

94. Huang L, Xiao X, Li S, et al. CRX variants in cone-rod dystrophy and mutation overview. *Biochem Biophys Res Commun.* 2012;426:498-503.

95. Tran NM, Zhang A, Zhang X, Huecker JB, Hennig AK, Chen S. Mechanistically distinct mouse models for CRX-associated retinopathy. *PLoS Genet.* 2014;10:e1004111.

96. Ruzycki PA, Tran NM, Kefalov VJ, Kolesnikov AV, Chen S. Graded gene expression changes determine phenotype severity in mouse models of CRX-associated retinopathies. *Genome Biol.* 2015;16:171.

97. Roger JE, Hiriyanna A, Gotoh N, et al. OTX2 loss causes rod differentiation defect in CRX-associated congenital blindness. *J Clin Invest.* 2014;124:631-643.

98. Barnett KC, Curtis R. Autosomal dominant progressive retinal atrophy in Abyssinian cats. *J Hered.*1985;76:168-170.

99. Curtis R, Barnett KC, Leon A. An early-onset retinal dystrophy with dominant inheritance in the Abyssinian cat. Clinical and pathological findings. *Invest Ophthalmol Vis Sci.* 1987;28:131-139.

100. Leon A, Curtis R. Autosomal dominant rod-cone dysplasia in the Rdy cat. 1. Light and electron microscopic findings. *Exp Eye Res.* 1990;51:361-381.

101. Leon A, Hussain AA, Curtis R. Autosomal dominant rod-cone dysplasia in the Rdy cat. 2. Electrophysiological findings. *Exp Eye Res.* 1991;53:489-502.

102. Chong NH, Alexander RA, Barnett KC, Bird AC, Luthert PJ. An immunohistochemical study of an autosomal dominant feline rod/cone dysplasia (Rdy cats). *Exp Eye Res.* 1999;68:51-57.

103. Nichols LL, 2nd, Alur RP, Boobalan E, et al. Two novel CRX mutant proteins causing autosomal dominant Leber congenital amaurosis interact differently with NRL. *Hum Mutat.* 2010;31:E1472-1483.

104. Freund CL, Gregory-Evans CY, Furukawa T, et al. Cone-rod dystrophy due to mutation in a novel photoreceptor-specific homeobox gene (CRX) essential for maintenance of the photoreceptor. *Cell.* 1997;91:543-553.

105. Perrault I, Hanein S, Gerber S, et al. Evidence of autosomal dominant Leber congenital amaurosis (LCA) underlain by a CRX heterozygous null allele. *J med Genet.* 2003;40:e90.

106. Zou X, Yao F, Liang X, et al. De novo mutations in the cone-rod homeobox gene associated with leber congenital amaurosis in Chinese patients. *Ophthalmic Genet.* 2015;36:21-26.

107. Wang P, Guo X, Zhang Q. Further evidence of autosomal-dominant Leber congenital amaurosis caused by heterozygous CRX mutation. *Graefes Arch Clin Exp Ophthalmol.* 2007;245:1401-1402.

108. Ziviello C, Simonelli F, Testa F, et al. Molecular genetics of autosomal dominant retinitis pigmentosa (ADRP): a comprehensive study of 43 Italian families. *J Med Genet.* 2005;42:e47.

109. Nakamura M, Ito S, Miyake Y. Novel de novo mutation in CRX gene in a Japanese patient with leber congenital amaurosis. *Am J Ophthalmol.* 2002;134:465-467.

110. Koenekoop RK, Loyer M, Dembinska O, Beneish R. Visual improvement in Leber congenital amaurosis and the CRX genotype. *Ophthalmic Genet.* 2002;23:49-59.

111. Zhang Q, Li S, Guo X, et al. Screening for CRX gene mutations in Chinese patients with Leber congenital amaurosis and mutational phenotype. *Ophthalmic Genet.* 2001;22:89-96.

112. Menotti-Raymond M, Deckman KH, David V, Myrkalo J, O'Brien SJ, Narfström K. Mutation discovered in a feline model of human congenital retinal blinding disease. *Invest Ophthalmol Vis Sci.* 2010;51:2852-2859.

113. Bainbridge JW, Mehat MS, Sundaram V, et al. Long-term effect of gene therapy on Leber's congenital amaurosis. *N Engl J Med.* 2015;372:1887-1897.

114. Ku CA, Chiodo VA, Boye SL, et al. Viral-mediated vision rescue of a novel AIPL1 cone-rod dystrophy model. *Hum Mol Genet.* 2015;24:670-684.

115. Boye SL, Peterson JJ, Choudhury S, et al. Gene Therapy Fully Restores Vision to the All-Cone Nrl(-/-) Gucy2e(-/-) Mouse Model of Leber Congenital Amaurosis-1. *Hum Gene Ther.* 2015;26:575-592.

116. Burnight ER, Wiley LA, Drack AV, et al. CEP290 gene transfer rescues Leber congenital amaurosis cellular phenotype. *Gene Ther.* 2014;21:662-672.

117. Garanto A, Chung DC, Duijkers L, et al. In vitro and in vivo rescue of aberrant splicing in CEP290-associated LCA by antisense oligonucleotide delivery. *Hum Mol Genet.* 2016;25:2552-2563.

118. Ostergaard ME, Southwell AL, Kordasiewicz H, et al. Rational design of antisense oligonucleotides targeting single nucleotide polymorphisms for potent and allele selective suppression of mutant Huntingtin in the CNS. *Nucleic Acids Res.* 2013;41:9634-9650.

119. Bennett CF, Swayze EE. RNA targeting therapeutics: molecular mechanisms of antisense oligonucleotides as a therapeutic platform. *Ann Rev Pharmacol Toxicol.* 2010;50:259-293.

120. Singh J, Kaur H, Kaushik A, Peer S. A Review of Antisense Therapeutic Interventions for Molecular Biological Targets in Various Diseases. *Int J Pharmacol.* 2011;7:294-315.

121. Liao Y, Tang L. Inducible RNAi system and its application in novel therapeutics. *Crit Rev Biotechnol.*2015;1-9.

122. Lambeth LS, Smith CA. Short hairpin RNA-mediated gene silencing. *Methods Mol Biol.* 2013;942:205-232.

123. Rayburn ER, Zhang R. Antisense, RNAi, and gene silencing strategies for therapy: mission possible or impossible? *Drug Discov Today.* 2008;13:513-521.

124. Smith AJ, Bainbridge JW, Ali RR. Gene supplementation therapy for recessive forms of inherited retinal dystrophies. *Gene Ther.* 2012;19:154-161.

125. Nayak S, Herzog RW. Progress and prospects: immune responses to viral vectors. *Gene Ther.* 2010;17:295-304.

126. Escors D, Breckpot K. Lentiviral vectors in gene therapy: their current status and future potential. *Arch Immunol Ther Exp.* 2010;58:107-119.

127. Sack BK, Herzog RW. Evading the immune response upon in vivo gene therapy with viral vectors. *Curr Opin Mol Ther.* 2009;11:493-503.

128. Douglas JT. Adenoviral vectors for gene therapy. *Mol. Biotechnol.* 2007;36:71-80.

129. Brunetti-Pierri N, Ng P. Gene therapy with helper-dependent adenoviral vectors: lessons from studies in large animal models. *Virus genes.* 2017.

130. Allocca M, Doria M, Petrillo M, et al. Serotype-dependent packaging of large genes in adeno-associated viral vectors results in effective gene delivery in mice. *J Clin Invest.* 2008;118:1955-1964.

131. Buning H, Perabo L, Coutelle O, Quadt-Humme S, Hallek M. Recent developments in adeno-associated virus vector technology. *J Gene Med.* 2008;10:717-733.

132. Flotte TR. Gene therapy progress and prospects: recombinant adeno-associated virus (rAAV) vectors. *Gene Ther.* 2004;11:805-810.

133. Conlon TJ, Flotte TR. Recombinant adeno-associated virus vectors for gene therapy. *Expert Opin Biol Ther.* 2004;4:1093-1101.

134. Carter BJ. Adeno-associated virus and the development of adeno-associated virus vectors: a historical perspective. *Mol Ther.* 2004;10:981-989.

135. Hastie E, Samulski RJ. Adeno-associated virus at 50: a golden anniversary of discovery, research, and gene therapy success--a personal perspective. *Hum Gene Ther.* 2015;26:257-265.

136. Tenenbaum L, Lehtonen E, Monahan PE. Evaluation of risks related to the use of adeno-associated virus-based vectors. *Curr Gene Ther.* 2003;3:545-565.

137. Flannery JG, Visel M. Adeno-associated viral vectors for gene therapy of inherited retinal degenerations. *Methods Mol Biol.* 2013;935:351-369.

138. Bartel MA, Weinstein JR, Schaffer DV. Directed evolution of novel adeno-associated viruses for therapeutic gene delivery. *Gene Ther.* 2012;19:694-700.

139. Nonnenmacher M, Weber T. Intracellular transport of recombinant adeno-associated virus vectors. *Gene Ther.* 2012;19:649-658.

140. Surace EM, Auricchio A. Adeno-associated viral vectors for retinal gene transfer. *Prog Retin Eye Res.* 2003;22:705-719.

141. Surace EM, Auricchio A. Versatility of AAV vectors for retinal gene transfer. *Vision Res.* 2008;48:353-359.

142. Schultz BR, Chamberlain JS. Recombinant adeno-associated virus transduction and integration. *Mol Ther.* 2008;16:1189-1199.

143. Lipinski DM, Thake M, MacLaren RE. Clinical applications of retinal gene therapy. *Prog Retin Eye Res.* 2013;32:22-47.

144. Muzyczka N. Use of adeno-associated virus as a general transduction vector for mammalian cells. *Curr Top Microbiol Immunol.* 1992;158:97-129.

145. McLaughlin SK, Collis P, Hermonat PL, Muzyczka N. Adeno-associated virus general transduction vectors: analysis of proviral structures. *J Virol.* 1988;62:1963-1973.

146. Zhong L, Li B, Jayandharan G, et al. Tyrosine-phosphorylation of AAV2 vectors and its consequences on viral intracellular trafficking and transgene expression. *Virology.* 2008;381:194-202.

147. Seisenberger G, Ried MU, Endress T, Buning H, Hallek M, Brauchle C. Real-time single-molecule imaging of the infection pathway of an adeno-associated virus. *Science.* 2001;294:1929-1932.

148. Sonntag F, Bleker S, Leuchs B, Fischer R, Kleinschmidt JA. Adeno-associated virus type 2 capsids with externalized VP1/VP2 trafficking domains are generated prior to passage through the cytoplasm and are maintained until uncoating occurs in the nucleus. *J Virol.* 2006;80:11040-11054.

149. Thomas CE, Storm TA, Huang Z, Kay MA. Rapid uncoating of vector genomes is the key to efficient liver transduction with pseudotyped adeno-associated virus vectors. *J Virol.* 2004;78:3110-3122.

150. Zhong L, Zhao W, Wu J, et al. A dual role of EGFR protein tyrosine kinase signaling in ubiquitination of AAV2 capsids and viral second-strand DNA synthesis. *Mol Ther.* 2007;15:1323-1330.

151. Zhao W, Wu J, Zhong L, Srivastava A. Adeno-associated virus 2-mediated gene transfer: role of a cellular serine/threonine protein phosphatase in augmenting transduction efficiency. *Gene Ther.* 2007;14:545-550.

152. Wu Z, Asokan A, Samulski RJ. Adeno-associated virus serotypes: vector toolkit for human gene therapy. *Mol Ther.* 2006;14:316-327.

153. Schmidt M, Voutetakis A, Afione S, Zheng C, Mandikian D, Chiorini JA. Adeno-associated virus type 12 (AAV12): a novel AAV serotype with sialic acid- and heparan sulfate proteoglycan-independent transduction activity. *J Virol.* 2008;82:1399-1406.

154. Boutin S, Monteilhet V, Veron P, et al. Prevalence of serum IgG and neutralizing factors against adeno-associated virus (AAV) types 1, 2, 5, 6, 8, and 9 in the healthy population: implications for gene therapy using AAV vectors. *Hum Gene Ther.* 2010;21:704-712.

155. Agbandje-McKenna M, Kleinschmidt J. AAV capsid structure and cell interactions. *Methods Mol Biol.* 2011;807:47-92.

156. Becerra SP, Rose JA, Hardy M, Baroudy BM, Anderson CW. Direct mapping of adeno-associated virus capsid proteins B and C: a possible ACG initiation codon. *Proc Natl Acad Sci U S A.* 1985;82:7919-7923.

157. Trempe JP, Carter BJ. Alternate mRNA splicing is required for synthesis of adeno-associated virus VP1 capsid protein. *J Virol.* 1988;62:3356-3363.

158. Lebherz C, Maguire A, Tang W, Bennett J, Wilson JM. Novel AAV serotypes for improved ocular gene transfer. *J Gene Med.* 2008;10:375-382.

159. Hellstrom M, Ruitenberg MJ, Pollett MA, et al. Cellular tropism and transduction properties of seven adeno-associated viral vector serotypes in adult retina after intravitreal injection. *Gene Ther.* 2009;16:521-532.

160. Petersen-Jones SM, Bartoe JT, Fischer AJ, et al. AAV retinal transduction in a large animal model species: comparison of a self-complementary AAV2/5 with a single-stranded AAV2/5 vector. *Mol Vis.* 2009;15:1835-1842.

161. McCarty DM. Self-complementary AAV vectors; advances and applications. *Mol Ther.* 2008;16:1648-1656.

162. Ferrari FK, Samulski T, Shenk T, Samulski RJ. Second-strand synthesis is a rate-limiting step for efficient transduction by recombinant adeno-associated virus vectors. *J Virol.* 1996;70:3227-3234.

163. Daya S, Berns KI. Gene therapy using adeno-associated virus vectors. *Clin Microbiol Rev.* 2008;21:583-593.

164. Gao G, Vandenberghe LH, Alvira MR, et al. Clades of Adeno-associated viruses are widely disseminated in human tissues. *J Virol.* 2004;78:6381-6388.

165. Xie Q, Bu W, Bhatia S, et al. The atomic structure of adeno-associated virus (AAV-2), a vector for human gene therapy. *Proc Natl Acad Sci U S A.* 2002;99:10405-10410.

166. Walters RW, Agbandje-McKenna M, Bowman VD, et al. Structure of adeno-associated virus serotype 5. *J Virol.* 2004;78:3361-3371.

167. Nam HJ, Lane MD, Padron E, et al. Structure of adeno-associated virus serotype 8, a gene therapy vector. *J Virol.* 2007;81:12260-12271.

168. Kern A, Schmidt K, Leder C, et al. Identification of a heparin-binding motif on adeno-associated virus type 2 capsids. *J Virol.* 2003;77:11072-11081.

169. Gabriel N, Hareendran S, Sen D, et al. Bioengineering of AAV2 capsid at specific serine, threonine, or lysine residues improves its transduction efficiency in vitro and in vivo. *Hum Gene Ther Methods.* 2013;24:80-93.

170. Aslanidi GV, Rivers AE, Ortiz L, et al. Optimization of the capsid of recombinant adeno-associated virus 2 (AAV2) vectors: the final threshold? *PloS one.* 2013;8:e59142.

171. Zhong L, Li B, Mah CS, et al. Next generation of adeno-associated virus 2 vectors: point mutations in tyrosines lead to high-efficiency transduction at lower doses. *Proc Natl Acad Sci U S A.* 2008;105:7827-7832.

172. Mowat FM, Gornik KR, Dinculescu A, et al. Tyrosine capsid-mutant AAV vectors for gene delivery to the canine retina from a subretinal or intravitreal approach. *Gene Ther.* 2014;21:96-105.

173. Dalkara D, Byrne LC, Klimczak RR, et al. In vivo-directed evolution of a new adeno-associated virus for therapeutic outer retinal gene delivery from the vitreous. *Sci Transl Med.* 2013;5:189ra176.

174. Martin KR, Klein RL, Quigley HA. Gene delivery to the eye using adeno-associated viral vectors. *Methods.* 2002;28:267-275.

175. Beltran WA, Boye SL, Boye SE, et al. rAAV2/5 gene-targeting to rods:dose-dependent efficiency and complications associated with different promoters. *Gene Ther.* 2010;17:1162-1174.

176. Ghosh A, Yue Y, Lai Y, Duan D. A hybrid vector system expands adeno-associated viral vector packaging capacity in a transgene-independent manner. *Mol Ther.* 2008;16:124-130.

177. Grose WE, Clark KR, Griffin D, et al. Homologous recombination mediates functional recovery of dysferlin deficiency following AAV5 gene transfer. *PloS one.* 2012;7:e39233.

178. Boyd RF, Sledge DG, Boye SL, et al. Photoreceptor-targeted gene delivery using intravitreally administered AAV vectors in dogs. *Gene Ther.* 2016;23:400.

179. Boyd RF, Boye SL, Conlon TJ, et al. Reduced retinal transduction and enhanced transgene-directed immunogenicity with intravitreal delivery of rAAV following posterior vitrectomy in dogs. *Gene Ther.* 2016;23:548-556.

180. Scalabrino ML, Boye SL, Fransen KM, et al. Intravitreal delivery of a novel AAV vector targets ON bipolar cells and restores visual function in a mouse model of complete congenital stationary night blindness. *Hum Mol Genet.*2015;24:6229-6239.

181. Kay CN, Ryals RC, Aslanidi GV, et al. Targeting photoreceptors via intravitreal delivery using novel, capsid-mutated AAV vectors. *PloS one.* 2013;8:e62097.

182. Dalkara D. Deniz Dalkara and her Research Work. Vision Resaerch - European Vision Institute; 2017:Web. 12 June 2017.

183. Bainbridge JW, Smith AJ, Barker SS, et al. Effect of gene therapy on visual function in Leber's congenital amaurosis. *N Engl J Med.* 2008;358:2231-2239.

184. Jacobson SG, Cideciyan AV, Ratnakaram R, et al. Gene therapy for leber congenital amaurosis caused by RPE65 mutations: safety and efficacy in 15 children and adults followed up to 3 years. *Arch Ophthalmol.* 2012;130:9-24.

185. Nork TM, Murphy CJ, Kim CB, et al. Functional and anatomic consequences of subretinal dosing in the cynomolgus macaque. *Arch Ophthalmol.* 2012;130:65-75.

186. Arroyo JG, Yang L, Bula D, Chen DF. Photoreceptor apoptosis in human retinal detachment. *Am J Ophthalmol.* 2005;139:605-610.

187. Lewis GP, Chapin EA, Luna G, Linberg KA, Fisher SK. The fate of Muller's glia following experimental retinal detachment: nuclear migration, cell division, and subretinal glial scar formation. *Mol Vis.* 2010;16:1361-1372.

188. Fisher SK, Lewis GP, Linberg KA, Verardo MR. Cellular remodeling in mammalian retina: results from studies of experimental retinal detachment. *Prog Retin Eye Res.* 2005;24:395-431.

189. Lewis GP, Charteris DG, Sethi CS, Fisher SK. Animal models of retinal detachment and reattachment: identifying cellular events that may affect visual recovery. *Eye (London, England)* 2002;16:375-387.

190. Le Meur G, Weber M, Pereon Y, et al. Postsurgical assessment and long-term safety of recombinant adeno-associated virus-mediated gene transfer into the retinas of dogs and primates. *Arch Ophthalmol.* 2005;123:500-506.

191. Boye SE, Boye SL, Lewin AS, Hauswirth WW. A comprehensive review of retinal gene therapy. *Mol Ther.* 2013;21:509-519.

192. Tshilenge KT, Ameline B, Weber M, et al. Vitrectomy Before Intravitreal Injection of AAV2/2 Vector Promotes Efficient Transduction of Retinal Ganglion Cells in Dogs and Nonhuman Primates. *Hum Gene Ther Methods.* 2016;27:122-134.

193. Streilein JW. Ocular immune privilege: the eye takes a dim but practical view of immunity and inflammation. *J Leukoc Biol.* 2003;74:179-185.

194. Streilein JW. Ocular immune privilege: therapeutic opportunities from an experiment of nature. *Nature reviews Immunology.* 2003;3:879-889.

195. Streilein JW, Masli S, Takeuchi M, Kezuka T. The eye's view of antigen presentation. *Hum Immunol.* 2002;63:435-443.

196. Wenkel H, Streilein JW. Analysis of immune deviation elicited by antigens injected into the subretinal space. *Invest Ophthalmol Vis Sci.* 1998;39:1823-1834.

197. Mochizuki M, Sugita S, Kamoi K. Immunological homeostasis of the eye. *Prog Retin Eye Res.* 2013;33:10-27.

198. Willett K, Bennett J. Immunology of AAV-Mediated Gene Transfer in the Eye. *Front Immunol.* 2013;4:261.

199. Annear MJ, Bartoe JT, Barker SE, et al. Gene therapy in the second eye of RPE65-deficient dogs improves retinal function. *Gene Ther.* 2011;18:53-61.

200. Kotterman MA, Yin L, Strazzeri JM, Flannery JG, Merigan WH, Schaffer DV. Antibody neutralization poses a barrier to intravitreal adeno-associated viral vector gene delivery to non-human primates. *Gene Ther.* 2015;22:116-126.

201. Anand V, Chirmule N, Fersh M, Maguire AM, Bennett J. Additional transduction events after subretinal readministration of recombinant adeno-associated virus. *Hum Gene Ther.* 2000;11:449-457.

202. Li Q, Miller R, Han PY, et al. Intraocular route of AAV2 vector administration defines humoral immune response and therapeutic potential. *Mol Vis.* 2008;14:1760-1769.

203. Gao G, Wang Q, Calcedo R, et al. Adeno-associated virus-mediated gene transfer to nonhuman primate liver can elicit destructive transgene-specific T cell responses. *Hum Gene Ther.* 2009;20:930-942.

204. Vandenberghe LH, Wang L, Somanathan S, et al. Heparin binding directs activation of T cells against adeno-associated virus serotype 2 capsid. *Nat Med.* 2006;12:967-971.

205. Mingozzi F, Anguela XM, Pavani G, et al. Overcoming preexisting humoral immunity to AAV using capsid decoys. *Sci Translat Med.* 2013;5:194ra192.

206. Hareendran S, Balakrishnan B, Sen D, Kumar S, Srivastava A, Jayandharan GR. Adeno-associated virus (AAV) vectors in gene therapy: immune challenges and strategies to circumvent them. *Rev Med Virol.* 2013;23:399-413.

207. Lundin KE, Gissberg O, Smith CI. Oligonucleotide Therapies: The Past and the Present. *Hum Gene Ther.* 2015;26:475-485.

CHAPTER 2

CRX$^{RDY/+}$ CAT: A LARGE ANIMAL MODEL FOR *CRX*-ASSOCIATED LEBER CONGENITAL AMAUROSIS

Occelli LM, Tran NM, Narfström K, Chen S, Petersen-Jones SM.

Crx^{Rdy} Cat: A Large Animal Model for *CRX*-Associated Leber Congenital Amaurosis.

Invest Ophthalmol Vis Sci. 2016; 57: 3780-3792. DOI:10.1167/iovs.16-19444, PMID: 27427859

2.1. ABSTRACT

PURPOSE. Mutations in the retinal transcription factor cone-rod homeobox (*CRX*) gene result in severe dominant retinopathies. A large animal model, the *Rdy* cat, carrying a spontaneous frameshift mutation in *Crx*, was reported previously. The present study aimed to further understand pathogenesis in this model by thoroughly characterizing the *Rdy* retina. **METHODS.** Structural and functional changes were found in a comparison between the retinas of $Crx^{Rdy/+}$ kittens and those of wild-type littermates and were determined at various ages by fundus examination, electroretinography (ERG), optical coherence tomography and histologic analyses. RNA and protein expression changes of Crx and key target genes were analyzed using quantitative reverse transcriptase-PCR, Western blot and immunohistochemistry. Transcription activity of the mutant Crx was measured by a dual-luciferase transactivation assay. **RESULTS.** $Crx^{Rdy/+}$ kittens had no recordable cone ERGs. Rod responses were delayed in development and markedly reduced at young ages and lost by 20 weeks. Photoreceptor outer segment development was incomplete and was followed by progressive outer retinal thinning starting in the cone-rich *area centralis*. Expression of cone and rod Crx target genes was significantly down-regulated. The mutant *Crx* allele was overexpressed, leading to high levels of the mutant protein lacking transactivation activity. **CONCLUSIONS.** The Crx^{Rdy} mutation exerts a dominant negative effect on wild-type *Crx* by overexpressing mutant protein. These findings, consistent with those of studies in a mouse model, support a conserved pathogenic mechanism for *CRX* frameshift mutations. The similarities between the feline eye and to the human eye with the presence of a central region of high cone density makes the $Crx^{Rdy/+}$ cat a valuable model for preclinical testing of therapies for dominant *CRX* diseases.

.

2.2. INTRODUCTION

Inherited retinal degenerations result in a range of different phenotypes and can be caused by mutations in a multitude of different genes (currently mutations in 240 different genes that cause inherited retinal degenerations are listed. RetNet[1] ; https://sph.uth.edu/retnet; available in the public domain). Mutations in one of these genes, the cone-rod homeobox (*CRX*) gene, cause a spectrum of retinopathies that vary in severity and age of onset. These *CRX*-linked retinopathies are mostly dominantly inherited. Among them, Leber congenital amaurosis (LCA) is the most severe, leading to vision loss starting in childhood. The less severe forms have a later onset and can cause a variety of phenotypes including cone-rod dystrophy, retinitis pigmentosa and an adult-onset macular dystrophy.[2, 3] CRX is an OTX-like homeodomain transcription factor expressed in both rod and cone photoreceptors and is essential for their development, maturation, and continued survival.[4-7] CRX interacts with subtype-specific transcription factors to control rod-versus-cone specification during development and directly regulates many genes essential for normal retinal function, including key components of the phototransduction cascade and the *CRX* gene itself.[8, 9] CRX binds to regulatory sequences of target genes and interacts with cofactors to influence transcription levels.[6, 10-13] It has a homeodomain near the N terminus that mediates DNA binding[6, 14] and two transactivation domains in the C-terminal portion for activating target gene transcription.[14]

Disease-causing *CRX* mutations can be grouped into four classes based on the mutation type and the functional characteristic of the resulting mutant protein.[3] Among them, Class III mutations consist of frameshift and nonsense mutations causing truncations of the protein affecting the transactivation domains. The C-terminal truncated forms of CRX maintain DNA binding but lack transcriptional activation function and thus have an antimorphic effect.[2, 3, 15, 16] All identified Class III mutations are linked to autosomal dominant LCA or early onset severe

cone-rod dystrophy. To understand the pathogenesis of the Class III mutations, a knock-in mouse model, *Crx-E168d2* has been generated.[15] The 2 bp deletion at the E168 codon (Glu168del2) is equivalent to a human *CRX*-LCA mutation.[15, 17] The heterozygous *E168d2* mouse develops severe retinopathy, similar to *CRX*-LCA, and has been used to complete a detailed investigation of the disease mechanism.[15] This investigation revealed that the mutant allele is overexpressed and interferes with the function of the wild-type (WT) allele. Although we have learned a great deal from this mouse model, it has certain limitations. First, the mouse retina differs from the human retina in photoreceptor distribution, particularly in the cone mosaic patterns.[18-22] Humans have a *macula,* a central retinal region of higher photoreceptor density, in particularly of cones, including a central cone-only *foveola*. This *macula* region is responsible for high-acuity color vision. The lack of an equivalent retinal region in the mouse is especially problematic for a disease primarily affecting cones at early stages. Second, it is unclear if the pathogenic mechanisms learned from this singular animal model are conserved among mammalian species, including humans.

To overcome the above limitations, we carried out an in-depth characterization of a feline model, the rod-cone dysplasia (*Rdy*) cat, which has a dominantly inherited, severe retinal dystrophy[23-27] due to a 1 bp deletion in *Crx* (*p.Pro185LysfsTer2*).[28] The frameshift mutation leads to a premature stop codon at the 185th residue with loss of the last 114 amino acids, eliminating the region of Crx that is presumed to mediate transactivation. Several human *CRX* retinopathies, most frequently classified as LCA, are due to frameshift mutations causing a stop codon at the same position (see Table 2 in Tran *et al.*[3]) (Appendix A - Fig. 2.S1).[29-38] The *Rdy* cat is a valuable model for *CRX-LCA* because cats have an *area centralis,* a region of higher photoreceptor density enriched with cones, which has strong similarities to human *macula*.[39-41] Although the phenotype of the heterozygous *Rdy* cat ($Crx^{Rdy/+}$) has been partially characterized[23-

[26], the dynamics of disease progression and underlying molecular changes have not been investigated. The current study addresses this knowledge gap by providing a detailed investigation of the progression of functional, cellular and molecular phenotypes of the $Crx^{Rdy/+}$cat. The mutant cat shows incomplete photoreceptor maturation with cones more severely affected than rods, followed by a progressive cone-led photoreceptor degeneration, starting in the cone-rich *area centralis*. This phenotype is more accurately classified as an early onset, severe cone-rod dystrophy (rather than a rod-cone dystrophy as originally described) that mimics *CRX*-LCA. Similar to the *E168d2* mouse model, the $Crx^{Rdy/+}$cat retina undergoes significant biochemical and molecular changes before and during disease progression. More strikingly, the mutant *Crx* allele produces much more mRNA and protein than the WT allele, supporting across-species conservation of the cellular and molecular mechanisms underlying Class III *CRX* mutation-mediated blinding disease. The $Crx^{Rdy/+}$cat provides an excellent large animal model of *CRX*-LCA and will be invaluable for the preclinical testing of treatment strategies.

2.3. MATERIALS AND METHODS

2.3.1. Ethics statement

All procedures were performed in accordance with the ARVO statement for the Use of Animals in Ophthalmic and Vision Research and approved by the Michigan State University Institutional Animal Care and Use Committee.

2.3.2. Animals

Purpose-bred Crx^{Rdy} cats maintained as a colony at Michigan State University were used in this study. They were housed under 12L:12D cycles and fed a commercial feline dry diet

(Purina One Smartblend and Purina kitten chow; Nestlé Purina, St Louis, MO. USA). Animals ranging from 4 weeks to one year of age were studied.

2.3.3. Ophthalmic examination and fundus imaging

Full ophthalmic examinations included indirect ophthalmoscopy, fundus photography (Ret-Cam II, Clarity Medical Systems, Inc., Pleasanton, CA, USA) and imaging with confocal scanning laser ophthalmoscopy (Spectralis OCT+HRA; Heidelberg Engineering Inc., Heidelberg, Germany).

2.3.4. Electroretinography (ERG)

The kittens were dark-adapted for 1 hour and pupils were dilated with tropicamide ophthalmic solution, UPS 1% (Falcon Pharmaceuticals Ltd., Fort Worth, TX, USA). Anesthesia was induced, and following intubation, maintained with isoflurane (IsoFlo; Abbott Laboratories, North Chicago, IL, USA). A Burian-Allen bipolar electrode contact lens (Burian-Allen ERG electrode; Hansen Ophthalmic Development Lab, Coralville, IA, USA) was used, and a platinum needle skin electrode placed over the occiput as used for grounding (Grass Technologies, Warwick, RI, USA). ERGs were recorded using an Espion E^2 Electrophysiology system with ColorDome Ganzfeld (Diagnosys LLC, Lowell, MA, USA). A dark-adapted luminance-response series (-4.5 to 1.4 log cd.s/m²), followed by light adaptation (10 minutes expose to a 30 cd/m² white light), and a light-adapted series (-2.4 to 1.4 log cd.s/m²) and 33 Hz cone flicker (-0.4 log cd.s/m²) were recorded. ERG a- and b-wave amplitudes and implicit times were measured in a standard fashion.

The leading edge of the rod a-wave was fitted to the Birch and Hood[42] version of the Lamb and Pugh rod phototransduction model using the following equation:

$$R(I,t) = \{1 - \exp[-I \cdot S \cdot (t - t_d)^2]\} \cdot R_{max} \quad for\ t > td$$

The amplitude *R* is a function of the retinal luminance, *I*, and time, *t*, after the flash, and *td* is a brief delay. *S* is a sensitivity factor, and R_{max} is the maximum amplitude of the response.

The first limb of the dark-adapted b-wave luminance-amplitude plot was fitted to the Naka-Rushton equation to derive values for retinal sensitivity (*K* is a semisaturation constant, the luminance, *L*, that induces a response amplitude of ½ R_{max}).[43]

$$R/R_{max} = L^n/(L^n + K^n)$$

where R_{max} represents the maximum response amplitude of the first limb of the b-wave luminance-response plot, the *K* is a semi-saturation constant, considered a measurement of retinal sensitivity, and *n* is a factor of the slope of the plot at the position of *K*, suggested to indicate retinal homogeneity.

2.3.5. Retinal morphology

2.3.5.1. *In vivo* Spectral Domain-Optical Coherence Tomography (SD-OCT)

SD-OCT imaging (Heidelberg Engineering) was used to capture single scan line and volume scan images from the central retinal to include the *area centralis* and from the four retinal quadrants (4 optic nerve head distances from the edge of the optic nerve head superiorly, inferiorly, nasally and temporally as illustrated in Appendix B - Fig. 2.S2). Thicknesses of the total retinal and outer nuclear layer (ONL) and receptor+ (including layers between retinal pigmentary epithelium and outer plexiform layer[44]) and inner retina layers between the inner nuclear layer and the internal limiting membrane were measured using the Heidelberg Eye Explorer (HEYEX) software.

2.3.5.2. Immunohistochemistry (IHC)

After cats were euthanized, their eyes were removed and immersed in 4% paraformaldehyde (Electron Microscope Sciences, Hatfield, PA, USA) in phosphate-buffered saline (PBS, Sigma-Aldrich Corp., Saint Louis, MO, USA) on ice for 2 to 3.25 hours. They were then processed for immunohistochemistry and imaged as previously described[45] (Appendix H - Table 2.S1 lists the antibodies used).

2.3.5.3. Plastic embedded sections

Eyes were fixed in 3% glutaraldehyde, 2% paraformaldehyde (Electron Microscope Sciences) in 0.1 M PBS pH 7.4 (Sigma-Aldrich Corp.) on ice for 1 hour, then hemisectioned, and the posterior eyecups were placed in the same fixative overnight. Following rinsing in 0.1 M sodium cacodylate buffer samples from the dorsal, central and ventral retinal regions were dissected, embedded in 2% agarose gel, 0.1 M sodium cacodylate buffer then embedded in resin (SPURR;, Low Viscosity, Embedding Kit, Electron Microscopy Sciences).[46] Five hundred-nanometers sections were stained with Epoxy Tissue Stain (Electron Microscope Sciences).

2.3.6. Quantitative Reverse Transcriptase-Polymerase Chain Reaction (qRT-PCR)

Two retinal regions (central and peripheral) from 2-week-old kittens were dissected (Appendix C - Fig. 2.S3A); in older animals samples were collected from five areas (superior far-periphery, superior mid-periphery, central (*area centralis*), inferior mid-periphery, inferior far-periphery (Appendix C - Fig. 2.S3B)). Samples were flash frozen and stored at -80°C until RNA extraction. RNA extraction, cDNA synthesis, and qRT-PCR reaction were performed as previously described.[15] Levels of *arrestin3* (*Arr3*, specific to cones), *rhodopsin* (*Rho*, specific to rods), and total *Crx* (WT and mutant) mRNA were measured and normalized to *Tubulin alpha-*

1B chain (*Tuba1b*) and *Glyceraldehyde-3-phosphate dehydrogenase* (*GAPDH*) (for primers sequence, see Appendix H - Table 2.S2).

Due to the difficulty of establishing a qRT-PCR assay to differentially amplify mutant and WT *Crx* cDNA a PCR restriction enzyme assay was developed to estimate the mutant-to-WT *Crx* mRNA ratio. Total combined *Crx* cDNA was amplified (forward primer 5'-cgtggccacggtgcccatct-3' reverse primer 5'-tccaggccactgaaatagga-3') followed by *Hpa II* digestion (BioLabs, Inc., Ipswich, MA, USA). The mutant *Crx* amplicon (189 bp) is not cut by *Hpa II*, whereas the WT is (112 and 78 bp products). Following electrophoresis on 2% agarose gel, the bands were imaged and quantified, and the mutant amplicon-to-WT amplicon ratio of calculated (Image Lab 5.2.1. Bio-Rad Laboratories; Hercules, CA, USA). A control using known WT-to-mutant *Crx* PCR product ratios generated from plasmid-cloned WT and mutant feline *Crx* was included to verify the accuracy of the technique.

2.3.7. Western blot assay

Retina remaining after samples for qRT-PCR were dissected was flash frozen in liquid nitrogen and stored at -80°. Protein extraction from nuclear versus cytoplasmic fractions and Western blot assay was performed as previously described.[15] Monoclonal mouse anti-β-actin antibody (Sigma-Aldrich Corp.) and polyclonal rabbit anti-CRX 119b1[15] at 1:1000 were used to probe the membranes. Secondary antibodies were goat anti-mouse IRDye 680LT and goat anti-rabbit IRDye 800CW (LI-COR Biosciences, Lincoln, NE, USA) respectively. Fluorescence was detected using the Odyssey Infrared Imager (LI-COR Biosciences) and quantified using ImageJ software[47] (http://imagej.nih.gov/ij/; provided in the public domain by the National Institutes of Health, Bethesda, MD, USA).

2.3.8. Dual-Luciferase assay

Dual-luciferase assays were performed as previously described.[15] HEK293 cells (catalog ATCC CRL-11268; American Type Culture Collection, Manassas, VA, USA) were cultured in Dulbecco minimum essential media (Gilco, Life technologies, Carlsbad, CA, USA) with 10% fetal bovine serum and penicillin/streptomycin (100 U/mL, Gibco, Life technologies). Cells at 60% confluence were transfected with 2 µg of *mCrx-Luc* reporter, which carries 500 bp of the mouse *Crx* promoter driving firefly luciferase in the *pGL3* vector (Promega Corp., Madison, WI, USA) and 100 ng *pcDNA3.1hisc*, 100 ng of *pCAGIG-feline Crx WT* or 100 ng of *pCAGIG-feline* Crx^{Rdy}, using $CaCl_2$ (0.25 M) and boric acid-buffered saline (1x), pH 6.75 as previously described.[15] Cells were harvested 48 hours post transfection, and dual-luciferase assays run.

2.3.9. Statistical analysis

Statistical analysis of ERG, SD-OCT, cDNA levels, Western blots, and fluorescence levels data differences were tested for normality (Shapiro-Wilk test for normality). Normally distributed data was analyzed by unpaired 2-tailed Student's T-test (significance level set at $P < 0.05$), nonparametric data by a Mann-Whitney rank sum test (SigmaPlot 12.0; Systat Software, Inc., San Jose, CA, USA).

Statistical analysis of mRNA levels (using qRT-PCR) was carried out using a 2-way repeat measure ANOVA (Holm-Sidak parametric method and Shapiro-Wilk normality test) (SigmaPlot 12.0; Systat Software).

2.4. RESULTS

2.4.1. *Crx*$^{Rdy/+}$ kittens have markedly reduced retinal function

To examine the progression of functional changes in *Crx*$^{Rdy/+}$ kittens, ERGs were recorded at multiple time points from 4 to 20 weeks of age (n = 4-8) and compared with those of WT littermate controls (n = 3-7). Light-adapted ERGs could not be recorded from *Crx*$^{Rdy/+}$ kittens at any time point. Small dark-adapted responses were recordable and showed that the *Crx*$^{Rdy/+}$ kittens had severely reduced retinal function (Figs. 2.1 and 2.2). At 4 weeks, a very low amplitude negative waveform typical of a scotopic threshold response (STR) was recordable from *Crx*$^{Rdy/+}$ kittens, whereas the waveform of WT kittens was similar in shape to that of adult cats (data not shown). By 6 weeks of age the *Crx*$^{Rdy/+}$ kittens had very small a- and b-wave responses. Interestingly, responses continued to develop through 10 weeks of age, although they were very reduced compared to the WT (the WT kitten ERGs had peak amplitudes at 12 weeks of age). After peaking at 10 weeks of age, responses progressively declined until the ERG was unrecordable at approximately 20 weeks of age (Figs. 2.1A and 2.2C). At peak retinal function (10 weeks of age), the a-wave of *Crx*$^{Rdy/+}$ kittens had a similar threshold to that of WT kittens, although the relatively prominent STR made precise identification of the a-wave threshold difficult (Figs. 2.1A and 2.2A). However, compared to the peak WT controls, the peak mean maximum a-wave amplitude was significantly reduced and delayed, at only ~30% of the mean control amplitude (P = 0.002) and with a mean implicit time approximately 2.5 to 4.5 times longer, depending on the stimulus strength (P < 0.001 to 0.003) (Figs. 2.1A, 2.1B, 2.2B and 2.2C). Although the a-wave of the *Crx*$^{Rdy/+}$ kitten was very reduced it was still possible to fit the leading edge of the response at 10 weeks of age to the Birch and Hood model to assess rod phototransduction. This showed a significant decrease in R_{max} in the *Crx*$^{Rdy/+}$ kittens compared to that in WT kittens (-23.86 ± 10.34 compared to -64.76 ± 25.87 µV, respectively; P = 0.003). The

sensitivity log *S* of the response was also significantly decreased in the $Crx^{Rdy/+}$ kittens (0.54 ± 0.23 compared to 1.27 ± 0.12 log scot $td^{-1}.sec^{-3}$ (scotopic torland-seconds) in WT kittens, $P < 0.001$) (Fig. 2.1B).

The b-wave of the $Crx^{Rdy/+}$ kitten was even more severely decreased in amplitude than the a-wave and was also delayed. At 10 weeks of age, compared to that in WT controls, the b-wave response threshold was elevated by about 1.5 to 2 log units, and the mean maximum amplitude was only ~20% that of controls ($P < 0.001$), and implicit times were 2 to 3 times longer ($P < 0.001$ to 0.071) (Figs. 2.1A and 2.2). Naka-Rushton fittings were performed in $Crx^{Rdy/+}$ kittens (n = 7) and WT control kittens (n = 6) at 10 weeks of age to derive values for the R_{max}, the semi-saturation constant *K* and *n* the slope factor. All three factors were significantly different between $Crx^{Rdy/+}$ kittens and WT controls. The mean R_{max} was much lower in $Crx^{Rdy/+}$ kittens (20.1 ± 14.7 compared with 169.3 ± 52.5 µV in controls, $P = 0.001$), indicating reduced retinal function. The mean of the factor *n* was increased, suggesting a reduction in the homogeneity of the retinal response (2.3 ± 1.98 compared to 0.91 ± 0.08, respectively, $P = 0.035$). Finally the mean luminance required to induce a response of $½R_{max}$ was significantly increased (0.027 ± 0.013 compared to 0.008 ± 0.003 $cd.s/m^2$, respectively, $P = 0.033$) indicating decreased retinal sensitivity. This ~0.5 log unit increase in stimulus luminance required to induce a response of $½R_{max}$ was less than the increase in response threshold for the dark-adapted b-wave (1.5 to 2 log units) (Fig. 2.1C).

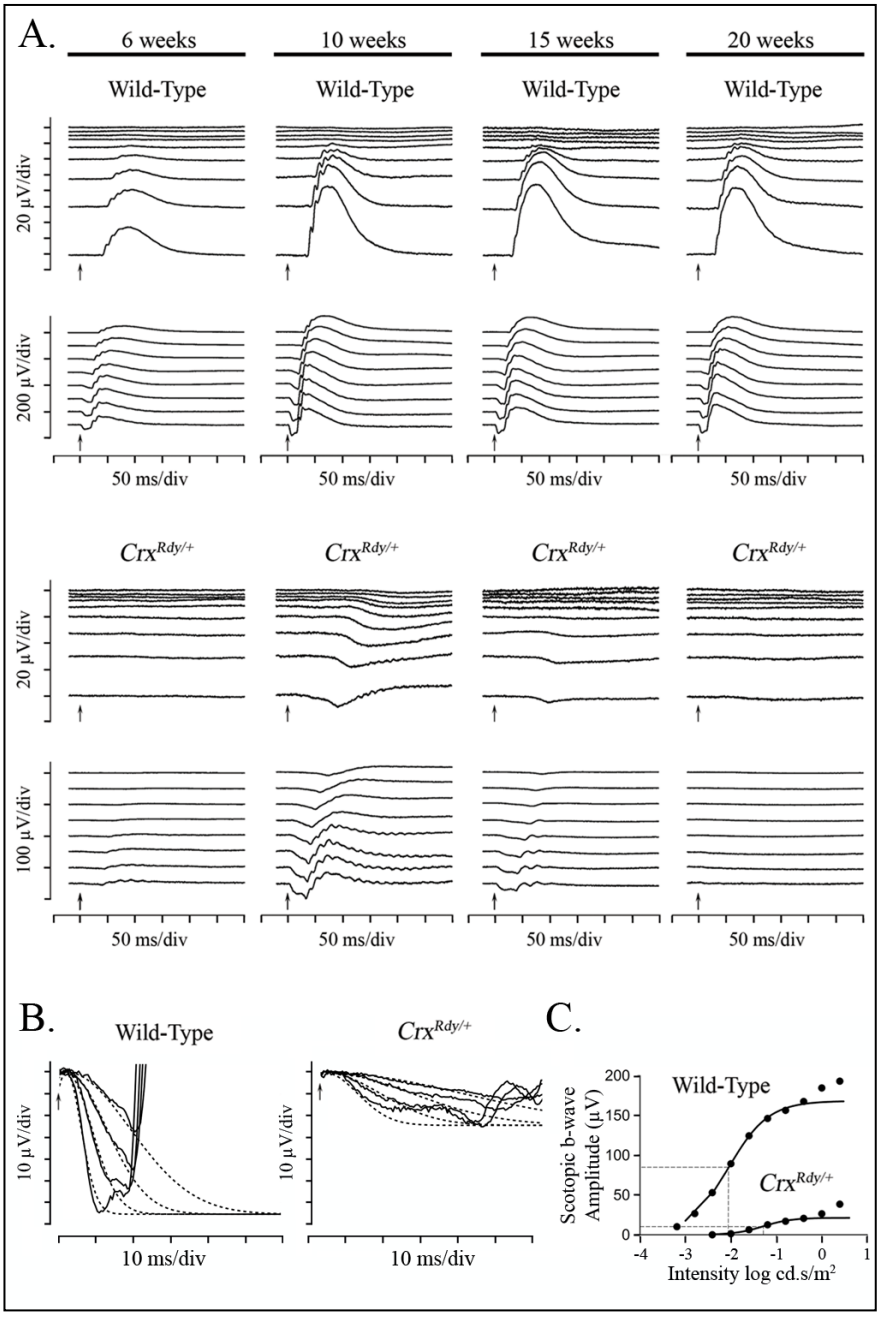

Figure 2.1. Dark-adapted luminance series ERG from *Crx*$^{Rdy/+}$ and WT kittens, a-wave modeling and b-wave Naka-Ruston fitting.

(A) Representative dark-adapted luminance series ERG from *Crx*$^{Rdy/+}$ and WT kittens at 6, 10, 15 and 20 weeks of age. Flash stimuli ranged from -4.5 (*top*) to 1.4 (*bottom*) log cd.s/m². The *Crx*$^{Rdy/+}$ kitten has very reduced (note the scale difference) and delayed a- and b-waves. Oscillatory potentials were present on the b-wave of the *Crx*$^{Rdy/+}$ kitten ERG. Note the relatively large STR in the *Crx*$^{Rdy/+}$ kitten, which remains prominent to higher flash luminances than normal; the developing a-wave becoming superimposed on it. A- and b-wave thresholds occurred at similar flash luminances in contrast to those of the WT, where b-wave threshold occurs at a much lower stimulus strength than a-wave threshold.

Figure 2.1. (cont'd)

(B) Modeling of the leading edge of the rod-isolated ERG a-wave of a representative *Crx*$^{Rdy/+}$ and WT kitten at 10 weeks of age.

The raw a-waves (*solid lines*) and fitted curves (*dashed lines*) for four flash stimuli ranging 0 to 1.4 log cd.s/m². Note the *Crx*$^{Rdy/+}$ kitten rod photoreceptor R_{max} (maximum receptor response) is much lower than that of the WT kitten.

(C) Naka-Rushton fitting of the first limb of the dark-adapted b-wave luminance-response plot of a representative *Crx*$^{Rdy/+}$ and WT kitten at 10 weeks of age.

The raw b-waves data values are shown by *round symbols* and the Naka-Rushton fit by *solid lines*. $½R_{max}$ of each waveform is represented by the *horizontal dashed lines*, and the luminance required to elicit a response of $½R_{max}$ (the semisaturation constant K) is indicated by the *vertical dashed lines*. Note the semisaturation constant K of *Crx*$^{Rdy/+}$ kitten is elevated by approximately 0.8 log units compared to the WT and the R_{max} (maximum amplitude of the first limb of the b-wave luminance amplitude plot) is very reduced.

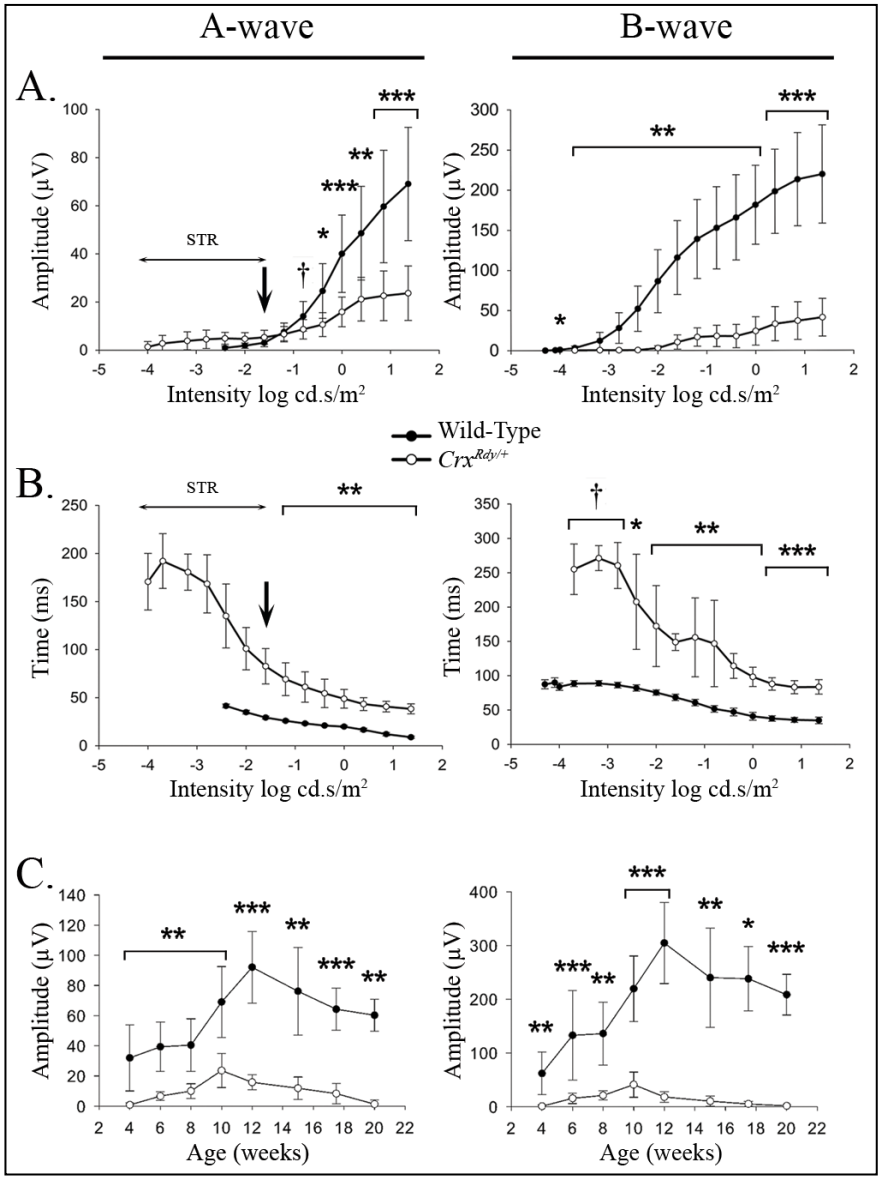

Figure 2.2. A-wave and b-wave amplitude and implicit time plotted relative to flash luminance (A-B) and maximal recorded amplitude plotted relative to age (C).
(A) Dark-adapted a- and b-wave luminance-response plots from 10-week-old WT and *Crx*$^{Rdy/+}$ kittens (the age at which maximum amplitudes were recordable from the *Crx*$^{Rdy/+}$ kittens). Note the *Crx*$^{Rdy/+}$ kittens had markedly reduced a- and b-wave amplitudes. The a-wave threshold was masked by the STR in the *Crx*$^{Rdy/+}$ kittens (see Fig. 2.1A). Therefore, the negative component of the waveform at intensities lower than that indicated by the *arrow* in the figure consisted of the STR then with increasing intensities a combination of STR and a-wave. At intensities greater than -1.6 log cd.s/m^2 the a-wave was clearly discernible. The b-wave threshold was elevated by ~2 log units in *Crx*$^{Rdy/+}$ kittens.
(B) Dark-adapted STR, a- and b-wave luminance-implicit time plots from 10-week-old WT and *Crx*$^{Rdy/+}$ kittens. Note the increased implicit times for the *Crx*$^{Rdy/+}$ kittens for both a- and b-waves. The implicit times (*left plot*) at intensities below that indicated by the *arrow* represent that of the STR.

Figure 2.2. (cont'd)
(C) A-wave and b-wave maximum amplitudes-age plots. The increase in ERG waveforms reflects retinal maturation. Peak amplitudes were recorded at 10 weeks of age for the *Crx*$^{Rdy/+}$ kitten compare to 12 weeks of age for WT kittens. By 20 weeks of age the *Crx*$^{Rdy/+}$ ERG was almost extinguished. $^{\dagger}P \leq 0.1$,$*P < 0.05$, $**P < 0.01$ and $***P < 0.001$ (n = 3 to 8).

2.4.2. *Crx*$^{Rdy/+}$ kittens have a progressive photoreceptor degeneration starting in the *area centralis*

To determine how photoreceptor degeneration evolved in *Crx*$^{Rdy/+}$ kittens, *in vivo* ophthalmic imaging was performed at multiple time points from 6 weeks to 1 year of age. Ophthalmoscopic examination revealed tapetal hyperreflectivity in *Crx*$^{Rdy/+}$ kittens (an indication of retinal thinning) in the *area centralis* from 7 weeks of age. Generalized tapetal hyperreflectivity and superficial retinal blood vessel attenuation was apparent from as early as 20 weeks of age (Fig. 2.3).

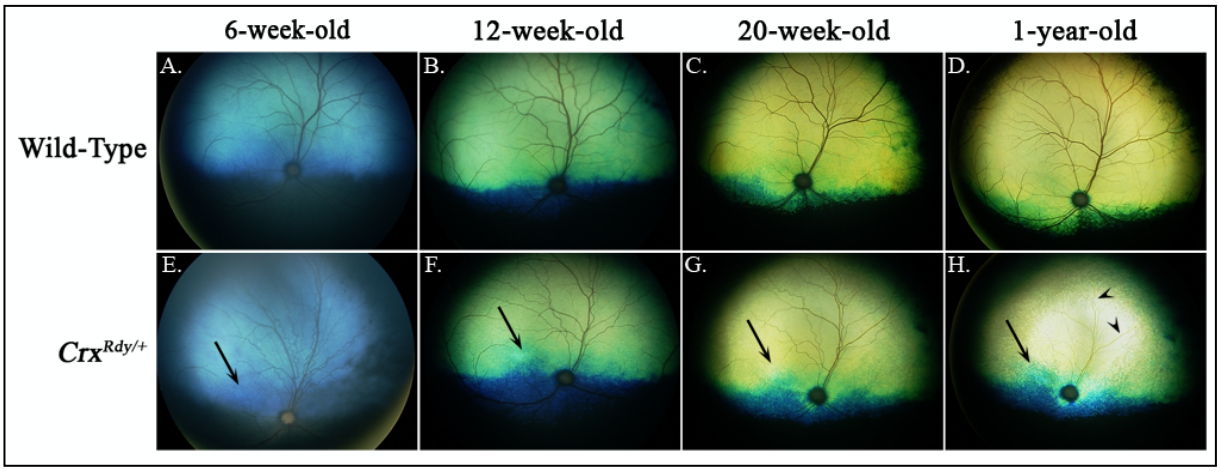

Figure 2.3. Color fundus photographs showing progression of fundus changes in *Crx*$^{Rdy/+}$ kittens from 6 weeks of age to 1 year of age (**(E-H)** right eye shown) compared to WT **(A-D)**. The *Crx*$^{Rdy/+}$ kitten developed tapetal hyperreflectivity (indicative of retinal thinning) in the *area centralis* (high photoreceptor density – region indicated by the (*arrows*)) as first seen in the image at 12 weeks of age. Hyperreflectivity of the entire tapetal fundus was discernible from 20 weeks of age and had progressed by one year of age. Superficial retinal blood vessel attenuation developed (**(H)** remaining very attenuated superficial retinal blood vessels are indicated by arrowheads).

Retinal SD-OCT cross-sectional images were recorded from 4 to 26 weeks of age (n = 3-8 for $Crx^{Rdy/+}$ kittens and n = 2-8 for WT littermate controls). The first abnormality detected in the $Crx^{Rdy/+}$ kittens was a halt in the maturation of the zone on the SD-OCT image that corresponds to the photoreceptor inner and outer segments (IS/OS). This was followed by a progressive thinning of the outer retinal layers starting in the *area centralis* (Fig. 2.4 and Appendix D - Fig. 2.S4). The SD-OCT image of layers representing inner and outer segments was thinner than in controls, and the bands that comprise the interdigitation zone and ellipsoid zone[48] could not be discerned in the $Crx^{Rdy/+}$ kittens. In WT kittens, these zones became clearly visible as the retina matured (typically they could easily be seen by 6 weeks of age (Fig. 2.4A, top panel)). In the $Crx^{Rdy/+}$ kittens, there was further progressive thinning of the IS/OS until it disappeared as the entire outer retina progressively thinned (Fig. 2.4A, lower panel). The lamination of the rest of the retina on SD-OCT imaging initially appeared normal, and at 4 weeks of age, $Crx^{Rdy/+}$ and WT kittens had comparable ONL thickness in the *area centralis* (Fig. 2.4B). Thereafter a progressive outer retinal thinning occurred starting in the *area centralis* and eventually spreading to involve the peripheral retina (the heat map in Fig. 2.4C illustrates the more severe retinal thinning in the *area centralis*). Despite developing some retinal function, by 6 weeks of age, the ONL was significantly thinned in the region of the *area centralis* (Figs. 2.4A and 2.4B) and by 12 weeks of age, it was reduced to ~25% the thickness of that in the WT kitten ($P < 0.001$), (Figs. 2.4A and 2.4B). The REC+ layer (which approximates the entire length of the photoreceptors, i.e., synaptic termini, cell bodies, and IS/OS) was reduced by ~50% by 12 weeks of age ($P < 0.001$) (Figs. 2.4A and 2.4B). The thinning of the outer retinal layers progressed, and by 26 weeks of age, the ONL in the *area centralis* was no longer discernible (Figs. 2.4A and 2.4B). As the outer retina thinned, the inner retina initially thickened, such that by 12 weeks the inner retina of the $Crx^{Rdy/+}$ kittens was ~30% greater than that of controls in the *area centralis*

region ($P < 0.001$), whereas due to the severe thinning of the outer retina the total retinal thickness had decreased to ~80% of normal ($P < 0.001$) (Figs. 2.4B and 2.4C). Similar retinal changes developed in the four retinal quadrants between 10 and 20 weeks of age (Appendix D - Fig. 2.S4).

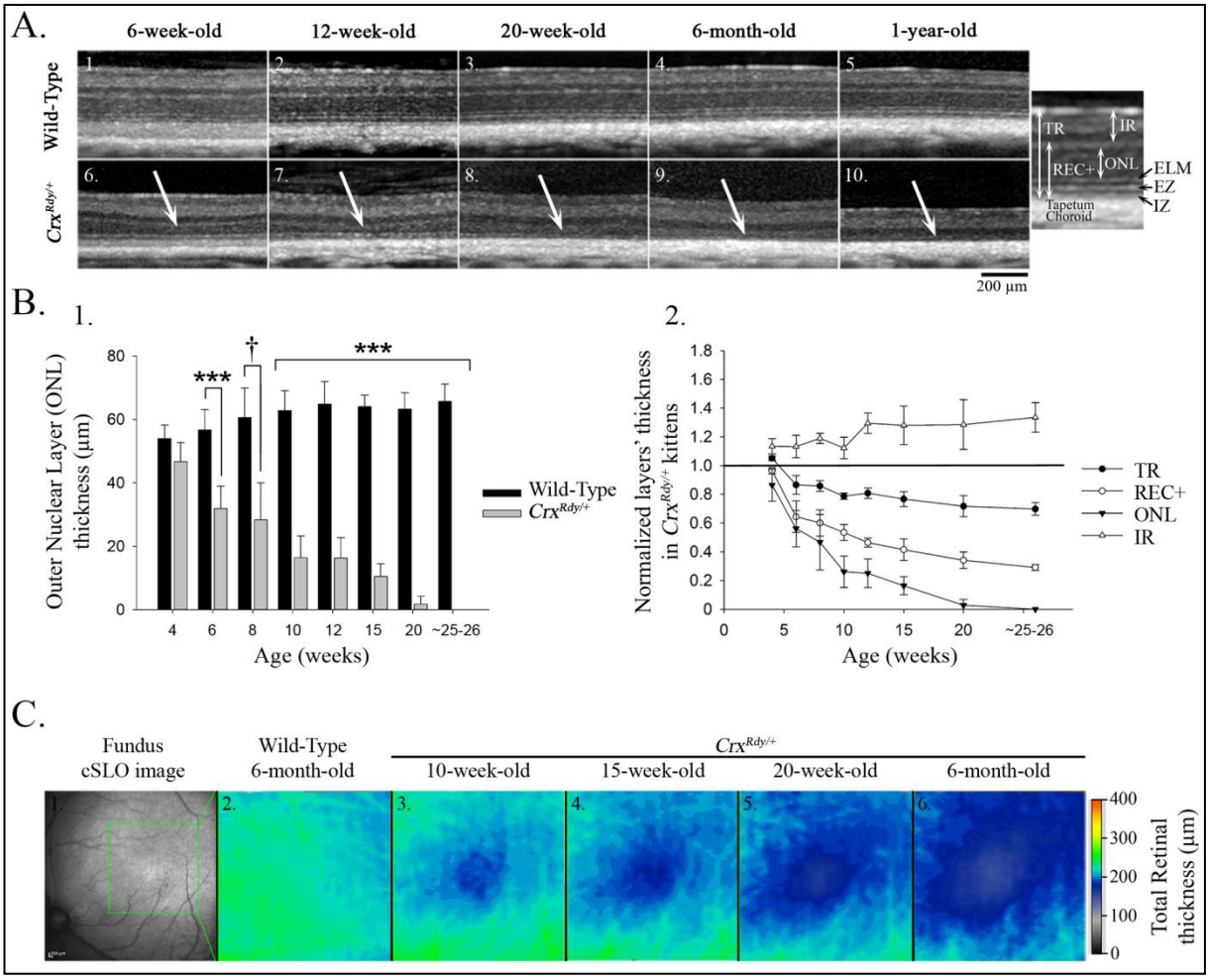

Figure 2.4. Spectral Domain – Optical Coherence Tomography (SD-OCT) *in vivo* retinal morphology analysis.
(A) SD-OCT cross-section views of the retina in the region of the *area centralis* of representative WT (1-5) and *Crx*$^{Rdy/+}$ (6-10) cats at the following ages: 6, 12, and 20 weeks, 6 months and 1year of age. The *white arrows* indicate the outer nuclear layer (ONL) which progressively thinned in the *area centralis* region of *Crx*$^{Rdy/+}$ cats. Note, specific features of the SD-OCT image including photoreceptor ellipsoid zone (EZ) and interdigitation zone (IZ) boundaries were not discernible in the *Crx*$^{Rdy/+}$ kittens. The magnified image of an OCT image of a WT retina on the right indicates the layers that were measured.

Figure 2.4. (cont'd)
TR, total retina; REC+, receptor plus, which includes all layers from the interdigitation zone to the outer plexiform layer (OPL), representing the entire photoreceptor cell length; ONL, outer nuclear layer; IR, inner retina, including all layers from inner nuclear layer to the external limiting membrane.

(B) Thickness of retinal layers in the *area centralis*.

1. ONL thickness in *area centralis* of $Crx^{Rdy/+}$ and WT kittens at 4, 6, 8, 10, 12, 15, and 20 weeks and 6 months of age. Significant ONL thinning was apparent at 6 weeks of age with a decrease ~50% normal thickness between 7 to 10 weeks of age in $Crx^{Rdy/+}$ kittens. By 6 months of age the ONL was no longer apparent. $^{\dagger}P \leq 0.1$; $^{***}P < 0.001$ (n = 2-8).

2. TR, REC+, ONL and IR layer thicknesses in the *area centralis* of $Crx^{Rdy/+}$ kittens normalized to controls at 4, 6, 8, 10, 12, 15, and 20 weeks and 6 months of age.
ONL, REC+, and TR thicknesses were decreased in $Crx^{Rdy/+}$ kittens from 6 weeks of age. In contrast, the IR became significantly thicker in $Crx^{Rdy/+}$ kittens compared to that of WT kittens. Those differences were statistically significant from 10-weeks of age ($P < 0.001$ for ONL, REC+, and TR; $P = 0.008$ for IR).

(C) Total retinal thickness map in the *area centralis*. The region of the *area centralis* indicated on the confocal scanning laser ophthalmoscope image (1) is represented as a color heat map (the optic nerve head is on the *left lower*). Warmer colors represent thicker retina, whereas cooler colors are thinner retina. Althought the WT kittens had a relatively homogenous retinal thickness in this region at 6 months of age (2), the $Crx^{Rdy/+}$ kittens showed a progressive thinning the center of the *area centralis*, with severe thinning by 6 months of age (3-6). The color map also demonstrates that in both WT and $Crx^{Rdy/+}$ kittens, the retina is thicker in the region of retinal vessels and thinner towards the periphery (*top left*).

Examination of plastic embedded semi-thin sections revealed that the maturation of the shape of $Crx^{Rdy/+}$ photoreceptor nuclei appeared delayed; at 6 weeks of age, they still had a spindle shape typical of the immature photoreceptor, whereas in WT kittens, they had gained a mature, round shape by this age (Fig. 2.5). Also at this age mislocalized photoreceptor nuclei could be seen in the subretinal space in the central region of the $Crx^{Rdy/+}$ kittens (Figs. 2.5 and 2.6). These mislocalized photoreceptor nuclei were positive for ML-opsin (medium/long wavelength-opsin) immunolabeling (Fig. 2.6). Compared to the well-developed WT photoreceptor OS, those of $Crx^{Rdy/+}$ kittens were much shorter and were disorganized. Those defects worsened with age, and by 20 weeks, OS were no longer apparent (Figs. 2.5 and 2.6).

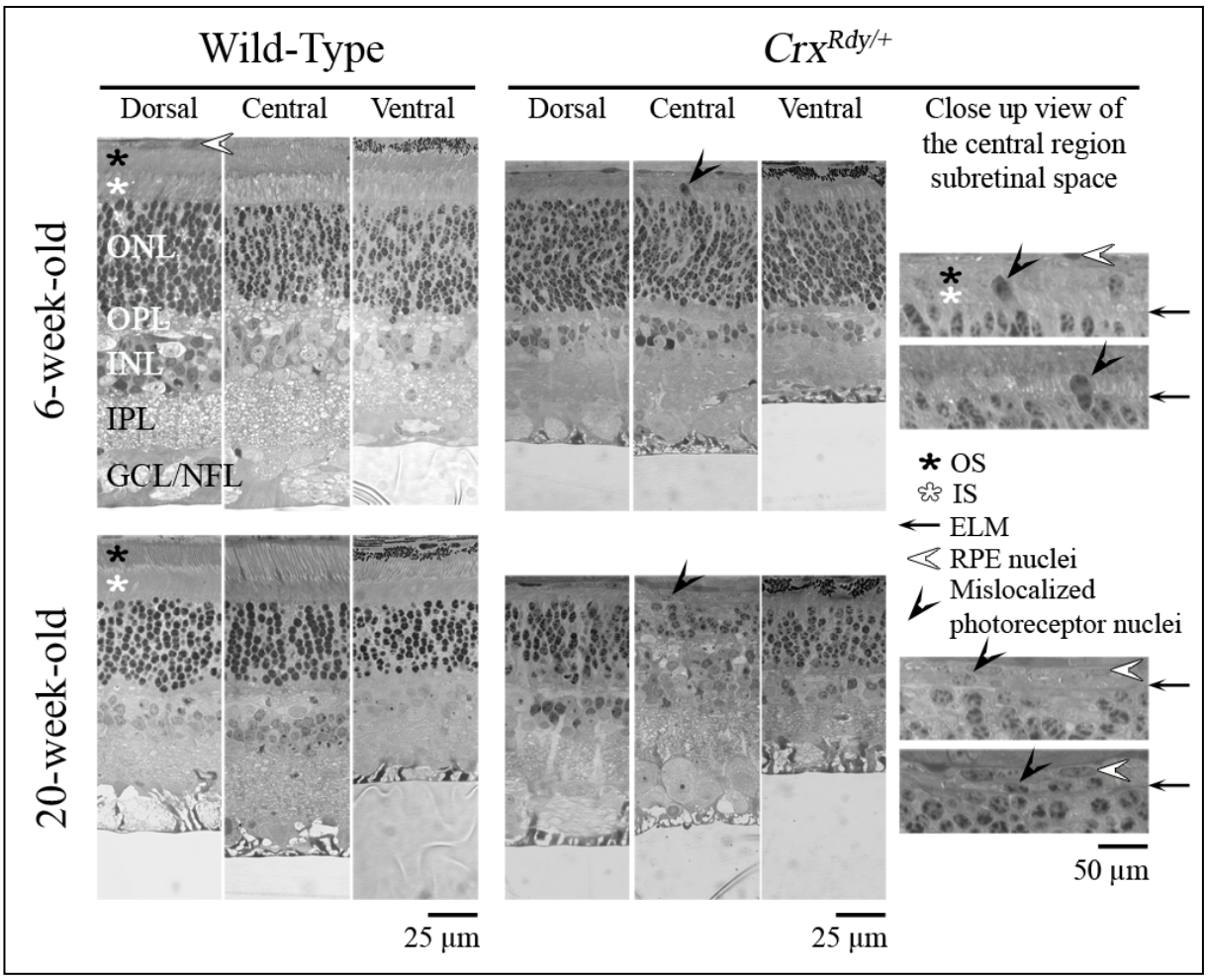

Figure 2.5. Representative plastic sections of retina from central, dorsal and ventral regions in WT and *Crx*$^{Rdy/+}$ kittens at 6 and 20 weeks of age.

Note that mislocalized photoreceptor nuclei ((*black arrowheads*) see magnified views) were present in the subretinal space or bulging through the ELM of the central region of the *Crx*$^{Rdy/+}$ retina at both ages. OS, photoreceptor outer segment; IS, photoreceptor inner segment; ONL, Outer Nuclear Layer; OPL, Outer Plexiform Layer; INL, Inner Nuclear Layer; IPL, Inner Plexiform Layer; GCL/NFL, Ganglion Cell Layer/Nerve Fiber Layer; *white star*, photoreceptor IS; *black star*, photoreceptor OS; *black arrow*, External Limiting Membrane (ELM); *white arrowhead*, Retinal Pigmentary Epithelium (RPE) nuclei.

To further investigate rod versus cone subcellular structural changes, immunolabeling of key photoreceptor structural and phototransduction proteins was performed on frozen retinal sections (Fig. 2.6, Appendix E - Fig. 2.S5 and Appendix H - Table 2.S1). At 2 weeks of age, *Crx*$^{Rdy/+}$ kittens had minimal human cone arrestin (hCAR) signals (hCAR labels both cone types) compared to the WT kittens (Fig. 2.6). By 6 weeks of age, a reduced number of hCAR-labeled cones (compared to those in WT controls) were detectable, but they had very short, stunted OS as well as shorter IS. At 12 weeks of age, although cones in the WT retina appeared mature, *Crx*$^{Rdy/+}$ retinas showed a severe loss of cones, and the remaining cones had severely shortened OS/IS. By 20 weeks of age, there were very few remaining cones. Short wavelength cones were more severely affected than medium/long wavelength cones. At 2 weeks of age S-opsin (short wavelength-opsin) labeling of a few cone cell bodies and OPL synaptic terminals could be seen in some animals, but no S-opsin immunolabeling was detected at 6, 12 and 20 weeks of age (Appendix E - Fig. 2.S5). Apart from the few S-opsin positive cones at 2 weeks of age, the remaining cones were ML-opsin positive (Fig. 2.6). Occasional stunted ML-opsin labeled OS were present, but most labeling was of the stunted IS, cell bodies, and synaptic terminals, indicative of mislocalization (in WT controls, ML-opsin only labeled the OS) (Fig. 2.6 and Appendix E - Fig. 2.S5).

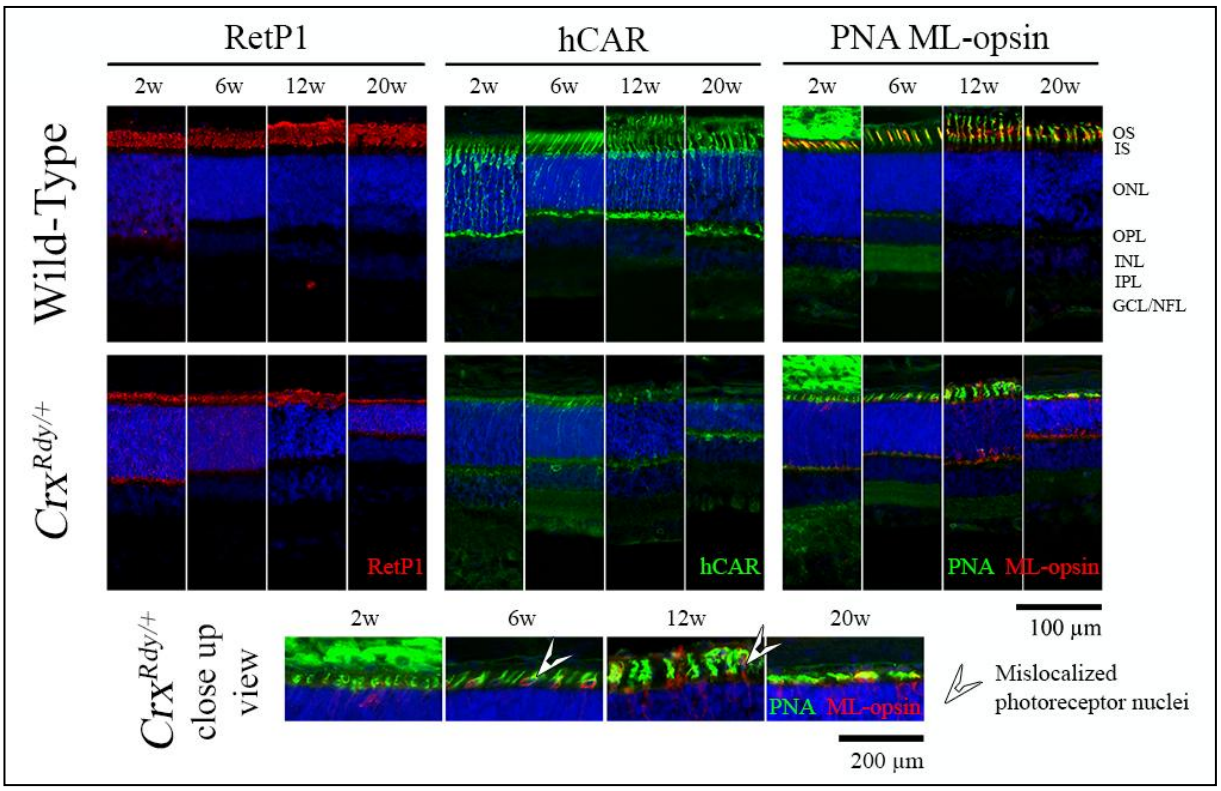

Figure 2.6. Immunohistochemistry using rod and cone markers.
Frozen sections from the dorso-temporal retinal region of *Crx*$^{Rdy/+}$ kittens and WT controls at the indicated ages were immunostained with rhodopsin (RetP1), cone arrestin (hCAR) and medium/long wavelength-opsin (ML-opsin) along with the pan cone marker peanut agglutinin (PNA). The higher magnification views of *Crx*$^{Rdy/+}$ sections (*bottom* row) show mislocalization of ML-opsin to the inner segments, cell bodies and pedicles of the cones *(white arrowheads*). photoreceptor outer segment; ONL, Outer Nuclear Layer; OPL, Outer Plexiform Layer; INL, Inner Nuclear Layer; IPL, Inner Plexiform Layer; GCL/NFL, Ganglion Cell Layer/Nerve Fiber Layer; *white arrowhead*, mislocalized photoreceptor nuclei.

Crx$^{Rdy/+}$ retinas had reduced labeling for rod opsin (RetP1, Fig. 2.6). Rod OS did start to develop, but this was halted prior to maturation and was followed by a progressive degeneration such that by 20 weeks of age they were markedly atrophied in all retinal regions. Parallel with the failure of rod maturation, mislocalization of rod opsin to the inner segments, cell body and synaptic terminal occurred and was present at all ages tested.

Immunolabeling for rod bipolar cells (using an anti-PKCalpha antibody) showed apparently normal numbers of rod bipolar cells at the ages examined, but their dendrites were retracted from an early age (Appendix E - Fig. 2.S5).

Immunolabeling for glial fibrillary acidic protein (GFAP) was markedly increased by 12 weeks of age, indicative of extensive Müller cell activation (Appendix E - Fig. 2.S5).[49-51]

2.4.3. *Crx*$^{Rdy/+}$ retinas had markedly reduced levels of cone and rod transcripts

To decipher the molecular changes underlying *Crx*$^{Rdy/+}$ retinal pathology, we investigated mRNA levels of selected CRX target genes; cone arrestin (*arrestin3* (*Arr3*)), rhodopsin (*Rho*, specific to rods), and total *Crx* (mutant plus WT) (Fig. 2.7 and Appendix I - Table 2.S2) in retinal subregions (Appendix C - Fig. 2.S3). For all retinal regions at the four ages tested (2, 6, 12 and 20 weeks of age) mRNA levels for *Arr3* and *Rho* in the *Crx*$^{Rdy/+}$ kittens were significantly decreased. *Arr3* was more dramatically decreased (between 93 and 99%) than *Rho* (between 31 and 81%). There were no consistent differences in the mRNA levels between the different retinal regions tested. In contrast, *Crx* mRNA was overexpressed in the *Crx*$^{Rdy/+}$ kittens when compared to WT controls (between 9 and 185%). For the average of all retinal regions, the difference was significant at 6 and 20 weeks of age (P = 0.037 and 0.038, respectively) (Fig. 2.7A); however these differences did not achieve statistical significance for every retinal region tested at each age. More importantly, when allele-specific expression levels for the mutant versus WT allele were assessed, a significantly higher level of mutant *Crx* transcript than WT *Crx* transcript was detected (P < 0.001) (Figs. 2.7B and 2.7C) with a ratio of 7.4 ± 0.4 times the amount of mutant transcript to WT transcript at 6 weeks of age.

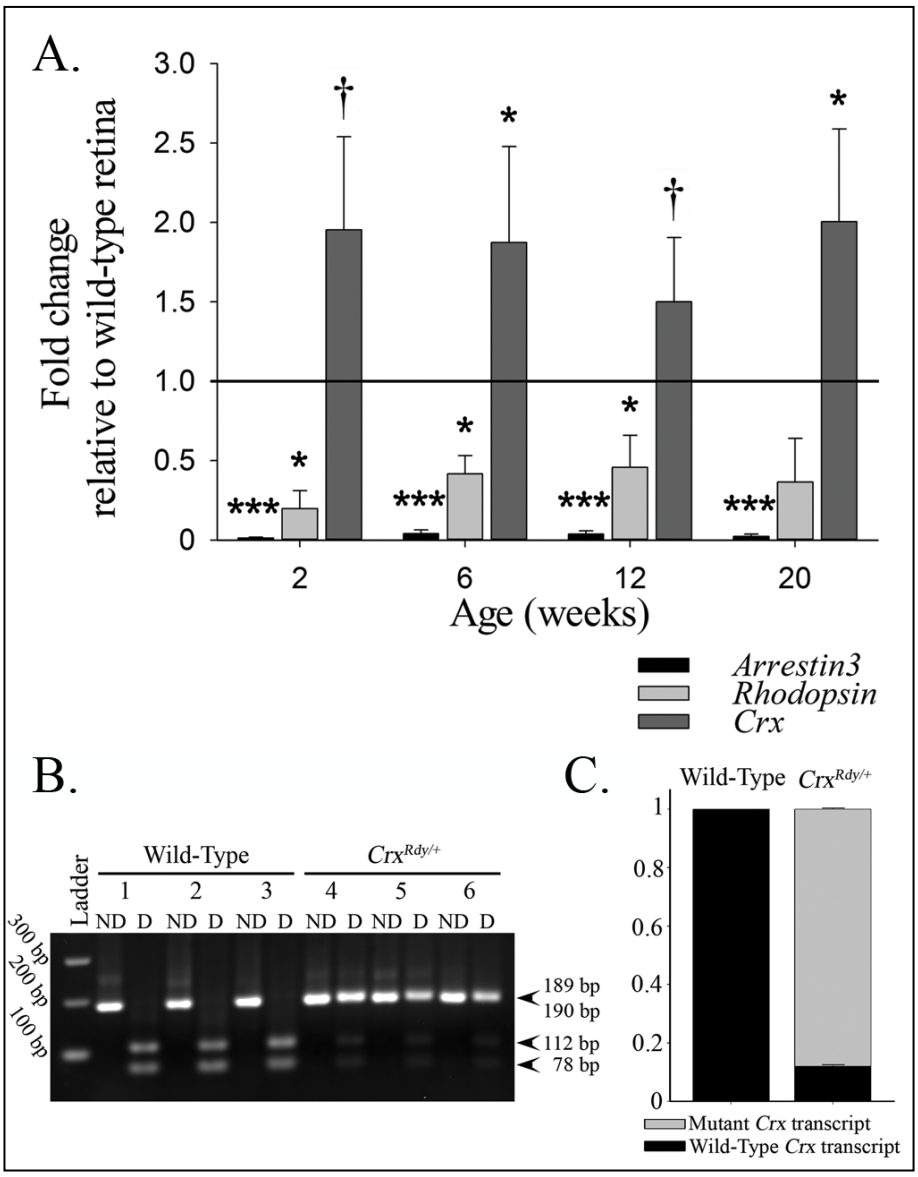

Figure 2.7. Changes of mRNA expression in *Crx*$^{Rdy/+}$ retinas.
(A) qRT-PCR overall (average of the areas assessed) mRNA expression levels of *arrestin3* (*Arr3 = Cone* arrestin), *rhodopsin* (*Rho*) and *Crx* in *Crx*$^{Rdy/+}$ retina at 2, 6, 12 and 20 weeks of age relative to levels in WT retinas.
The *Crx*$^{Rdy/+}$ kitten retinas had significantly decreased levels of cone and rod opsin mRNA. In contrast, the expression of total *Crx* was significantly increased. P-values comparing the mean *Crx*$^{Rdy/+}$ and WT expression levels are $^{\dagger}P \leq 0.1$,$^{*}P < 0.05$, $^{**}P < 0.01$, and $^{***}P < 0.001$ (n = 3).
(B, C) PCR restriction enzyme digest was used to compare the levels of mutant mRNA compared to those of WT mRNA by using cDNA from 6-week-old *Crx*$^{Rdy/+}$ and WT retinas.
(B) Agarose gel of PCR nondigested (ND) and digested (D) products digested with *HpaII*, which digests the amplicon from WT cDNA. Note the presence of both the mutant *Crx* transcript (189 bp of length) and the WT *Crx* transcript (digested in to products of 78 and 112 bp) in the *Crx*$^{Rdy/+}$ kitten retina (kittens 4, 5 and 6). The WT kitten retina contains only WT *Crx* transcript (completely digested in kittens 1, 2 and 3).

Figure 2.7. (cont'd)
(C) Wild-type-to-mutant *Crx* transcripts level ratios in wild-type and *Crx*$^{Rdy/+}$ kittens. Densitometry measurements of the bands in the agarose gel (**(B)** mutant 189 bp and sum of WT transcript digested products 78 and 112 bp) from the *Crx*$^{Rdy/+}$ kitten retinas were assessed. In 6-week-old *Crx*$^{Rdy/+}$ kitten, the mutant-to-WT *Crx* transcript ratio was ~7.4:1. (mutant transcript representing 88% of the total transcript; $P < 0.001$). As expected in WT kittens, the WT transcript represents 100% of the total *Crx* mRNA.

This allele specific overexpression of the mutant product was confirmed by Western blot assays (Fig. 2.8). The mutant Crx protein was at higher levels than the WT Crx protein in the *Crx*$^{Rdy/+}$ retinas at each time point (Fig. 2.8B). The mutant protein was able to enter the nucleus as indicated by the results of Western blot of separated retinal nuclear and cytoplasmic fractions (Appendix F - Fig. 2.S6). As anticipated for a heterozygous animal, the amount of WT Crx protein was lower in the *Crx*$^{Rdy/+}$ kittens than in WT and the difference was significant at 12 and 20 weeks of age ($P < 0.01$) (Fig. 2.8B). Because of the overproduction of the truncated mutant protein, the level of the combined Crx proteins was markedly higher in the *Crx*$^{Rdy/+}$ kittens compared to WT kittens at 2, 6 and 12 weeks of age but not at 20 weeks of age (an age at which photoreceptor degeneration was well established).

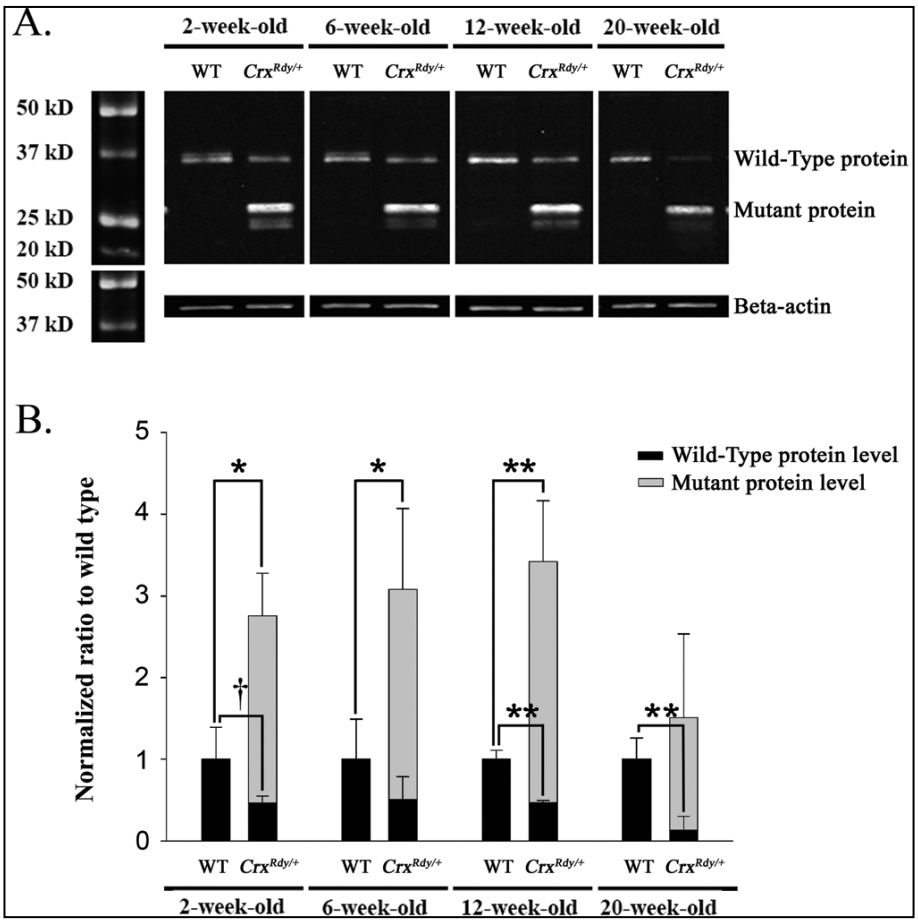

Figure 2.8. Western blot analysis for Crx nuclear protein.
(A) Western blot for nuclear Crx protein (immunolabeled with antibody 119b1). The amount of Crx protein present in retinal nuclear extract was investigated by Western blot from kittens at 2, 6, 12, and 20 weeks of age. Note the presence in the $Crx^{Rdy/+}$ kitten's retina of the truncated mutant Crx protein, which persisted to the 20 week-old time point, whereas the amount of WT protein had decreased by 20 weeks of age. Beta-actin was used as protein loading control.
(B) Normal and mutant protein levels in $Crx^{Rdy/+}$ and wild-type kittens.
Crx protein levels were normalized to beta-actin levels, and the $Crx^{Rdy/+}$ kitten protein levels shown normalized to the Crx levels in the WT retinas. The level of normal protein was lower in the $Crx^{Rdy/+}$ kitten retina than in the WT kittens at each age. Note high levels of the truncated mutant Crx protein compared to the amount of normal protein in $Crx^{Rdy/+}$ kitten retina and therefore the overall higher total Crx protein levels (normal plus mutant) in $Crx^{Rdy/+}$ kitten retina compared to WT kitten retina. $^{\dagger}P \leq 0.1$; $*P < 0.05$; $**P < 0.01$ (n = 2 to 4; statistical analysis was applied only when $n \geq 3$ for both WT and $Crx^{Rdy/+}$ kitten retina sample).

2.4.4. Effect of the *Rdy* mutation on Crx's transcription regulatory activity

To determine whether the *Rdy* mutation altered Crx function, we measured the ability of recombinant Crx proteins to activate the target gene promoter *Crx,* driving a luciferase reporter in HEK293 cells. This dual-luciferase reporter assay revealed that the mutant Crx protein failed to activate the *Crx* promoter ($P = 0.729$) while the WT protein led to significant activation ($P < 0.001$) (Appendix G - Fig. 2.S7), confirming that this class III *Crx* mutation eliminated transactivation function.

2.5. DISCUSSION

This study expanded on previous studies showing that the $Crx^{Rdy/+}$ cat has a severe, early onset, dominantly inherited, retinal degeneration.[24-27] Similar to other Class III *CRX* mutation models, overexpression of the mutant transcript occurs and most likely exerts a dominant negative effect. These findings support previous studies in mouse models that suggest a therapeutic approach by which early intervention to increase the normal-to-mutant CRX transcript ratios could lessen the disease severity in *CRX*-LCA patients.[3, 15] The $Crx^{Rdy/+}$ cat enables characterization of the early changes that occur in retinal regions of high cone density, which model the environment within the human *macula*. Such investigations are not possible in mouse models because mice lack the retinal regional differences in photoreceptor distribution and density of the human retina. The cat will be invaluable for preclinical testing of therapies to rescue photoreceptors in this region that is so critical for human visual function.

2.5.1. The *Crx*$^{Rdy/+}$ kitten provides a model for human *CRX*- LCA phenotype

Crx$^{Rdy/+}$ kittens show incomplete maturation of photoreceptors associated with reduced expression of photoreceptor transcripts and followed by progressive photoreceptor degeneration. Despite the importance of CRX as a transcription factor, the retina in the *Crx*$^{Rdy/+}$ kitten develops relatively normal stratification (Figs. 2.4, 2.5, 2.6 and Appendix E - Fig. 2.S5). Cone nuclei do become aligned to form a single layer in the outer most row of the ONL, similar to the WT kittens, although from an early stage some become mislocalized to the subretinal space, particularly in the *area centralis*. In the *p.E168d2* mouse model of Class III *CRX* mutations, retinal stratification also develops normally, but in contrast to the cat model, more extensive mislocalization of cone nuclei to the inner portions of the ONL occurs.[15] The photoreceptor nuclei in the *Crx*$^{Rdy/+}$ kittens retain an immature oval shape because they are delayed in attaining the adult circular appearance in retinal sections, reflecting the incomplete photoreceptor maturation (Figs. 2.5, 2.6 and Appendix E - Fig. 2.S5). Similarly, only partial development of inner and outer segments occurs. Cones are more severely affected than rods, with cone function not being recordable by ERG at any age and photoreceptor degeneration developing most rapidly in the *area centralis*, the region of highest cone density.[39,41] Expression of the cone proteins investigated (cone arrestin by qRT-PCR and IHC, and cone opsins by IHC) was much reduced, more so than that of rod opsin (qRT-PCR and IHC). S-opsin positive cones were only detectable in some kittens at 2 weeks of age and at no other ages, showing the most severe effects were on the S-cones. The ML-cones remained present for longer but only developed very stunted outer segments which did not show expression of ML-opsin. The reduced amounts of ML-opsin present were mislocalized to other parts of the cell (Fig. 2.6 and Appendix E - Fig. 2.S5).

Rod photoreceptors showed evidence of maturing further than cones. Although outer segments were stunted there was rod opsin present, although expression levels were much

reduced. Rod function was recordable by ERG and showed evidence of maturation to 10 weeks of age prior to a rapid decline thereafter (Figs. 2.1A and 2.2C). Leon et al.[26] had previously performed a detailed electrophysiological study on the *Rdy* cat but needed to use intravitreal recording, or to perform testing on *ex-vivo* retinal pieces, to reliably record responses and overcome background electrical noise present when using corneal electrodes. In the current study it was possible to record very small ERGs using corneal contact lens electrodes without resorting to invasive methods. This probably reflects improvements in recording techniques rather than a drift in phenotype over the ~25 years since the study by Leon et al.[26] Similar to that study, a negative waveform ERG waveform was recorded to lower stimuli strengths in our study. The shape and timing of this waveform are in keeping with it representing an inner retinal component of the ERG present close to response threshold, the STR.[52] A-and b-wave components of the ERG developed later in age than in WT cats reflecting the delay and only partial nature of rod photoreceptor maturation. They were much reduced in amplitude and showed delayed timing. Modeling of the leading edge of the rod a-wave showed a significant decrease in maximum amplitude response R_{max} and sensitivity log S (Fig. 2.1B). This reflects the reduced rod outer segment length and low rod opsin levels in the affected cats. In the normal dark-adapted cat ERG the b-wave appears with increasing strength of stimuli initially superimposed on the STR and as its amplitude increases obscures it. In the $Crx^{Rdy/+}$ cat the appearance of the b-wave with increasing stimulus strength was more severely delayed than that of the a-wave meaning the a-wave became superimposed on the STR prior to the development of the b-wave. These findings of a more severe delay and suppression of the b-wave compared to the a-wave may reflect an altered maturation of rod bipolar cells which are the origin of the rod ERG b-wave.[53] *CRX* is expressed in developing bipolar cells,[54] so it is conceivable that impaired bipolar cell maturation may be a cause for the more severe changes in the b-wave than the a-wave. An electron

microscopy study of *Rdy* cats previously reported an early reduction in the number of rod spherules and cone pedicles,[25] and synaptophysin (a synaptic vesicle protein) immunolabeling was reported to be reduced in another study.[27] PKCalpha immunolabeling of rod bipolar cells in this study did not reveal an alteration in numbers of labeled cells early in the disease process although an early retraction of dendrites was noted. Inner retinal components of the ERG such as the STR and oscillatory potentials which would require bipolar cell signal transmission were present and relatively prominent in the very small ERG responses from the $Crx^{Rdy/+}$ kittens.

Naka-Rushton fitting of the rod b-wave luminance-amplitude plots showed very reduced values for the receptor response and also for retinal sensitivity (Fig. 2.1C). There was an increase in the *n* value, which is a component reflective of the slope of the plot at the point of ½ R_{max} and has been suggested to reflect a less homogeneous retinal response[55] and may reflect the regional variation in the rapidity of photoreceptor degeneration.

Of the nine reported human disease causing *CRX* frameshift mutations that result in a transcript shortened to 185 residues (as in the Crx^{Rdy} cat) (Appendix A - Fig. 2.S1), eight were reported to result in an LCA phenotype.[29-38] ERG results were reported from patients representing seven of the nine mutations (Appendix A - Fig. 2.S1) (Table 2.2 in Tran *et al.*[3]). ERGs were not recordable from infants when tested for three of the mutations.[29, 34, 36, 56] When tested in older children and adults the ERG was also reported to be nonrecordable,[32, 35, 37, 38] with the exception of one patient reported by Koenekoop *et al.*[36] who had a *p.A177d1* mutation. This patient had a nonrecordable ERG at 8 months of age, then as a child had some improvement in vision and a recordable cone ERG when tested at both 10 and 11 years of age. This is the only instance in the literature where improvement in visual function was noted in a *CRX*-LCA patient. It seems likely that this was due to some degree of delayed retinal maturation occurring prior to photoreceptor degeneration. Development of the small ERG responses in the Crx^{Rdy} cat are

delayed and there is some evidence of rod maturation but unlike the human patient, cone function was not recordable and cones deteriorated prior to rods.

Following the halting of photoreceptor development in the *Crx*$^{Rdy/+}$ kitten, a rapid cone-led loss in photoreceptors occurs, resulting in outer retinal thinning starting in the *area centralis* (Fig. 2.4). With disease progression, outer retinal thinning in the more peripheral retinal regions also developed (Appendix D - Fig. 2.S4). The initial thickening of the inner retina detected on SD-OCT imaging, may be due to neuronal remodeling and glial activation as commonly seen in models of retinal degeneration[57] (Appendix E - Fig. 2.S5).

2.5.2. Molecular mechanism underlying *Crx*^{Rdy} phenotype and implications in therapy development

The *Crx*^{Rdy} mutation results in a premature stop codon in the transactivation domain of *Crx*[28], the mutant transcript escapes nonsense-mediated decay and as shown in this study is overexpressed (Fig. 2.7). Studies of other Class III *CRX* mutations have also shown that there is mutant allele overexpression (human *CRX*-LCA *p.I138d1* mutation, truncation at codon 185, and the *p.E168d2* knock-in mouse model, truncation at codon 171).[15, 16, 29] The elevation of *Crx*^{Rdy} transcript levels may be the result of increased synthesis or decreased degradation of the mutant mRNA. Class III mutation-introduced premature stop codons could enhance RNA stability of the mutant allele over its WT counterpart. A feedback regulatory mechanism to decrease *Crx* transcripts when overexpressed could attribute to the reduction of WT *Crx* transcripts, while mutant allele transcripts are resistant to this regulation. Further studies are required to ascertain the precise mechanism involved. In the *Crx*$^{Rdy/+}$ kitten the mutant transcript and protein remained at elevated levels even when photoreceptor degeneration was well established and the levels of expression of the WT allele were very reduced (Figs. 2. and 2.8). This continued overexpression

of mutant *Crx* despite photoreceptor loss has not been previously demonstrated in similar models. Similar to findings in the *p.E168d2* knock-in mouse model, the truncated feline Crx^{Rdy} protein fails to activate its own promoter *in vitro* (Appendix G - Fig. 2.S7) thus showing across-species conservation of the cellular and molecular mechanisms underlying Class III *CRX* mutations.

Prior to loss of photoreceptors potential therapeutic interventions that address the overexpression of the mutant *Crx* transcript may be translatable to human patients. These include either knocking down the levels of the mutant transcript using, for example, anti-sense oligonucleotides,[58-60] or shRNA,[61-63] or overexpressing the WT transcript by gene supplementation using adeno-associated viral vectors,[64-67] or a combination of both approaches. Supporting evidence for this approach is provided by a line of *E168d2* mice where a Neo cassette was not excised (*E168d2*neo) resulting in lowered expression of the truncated Crx protein and a much milder phenotype than in the line of *E168d2* mice where the Neo cassette had been excised.[15] Also, mice or humans heterozygous for *null* mutations in *CRX* have either a mild phenotype or no phenotype indicating that severe phenotypes are not the result of simple haploinsufficiency and supporting the hypothesis of a dominant negative effect of the mutant protein.[5, 7]

To summarize, the $Crx^{Rdy/+}$ cat provides a large animal model for the severe dominant *CRX* mutations associated with overexpression of a mutant transcript with an antimorphic effect resulting in a LCA phenotype. The *area centralis* is affected earliest and degenerates prior to the peripheral retina. Presence of the *area centralis* allows the assessment of therapeutic interventions aiming to rescue function in this critical retinal region meaning the Crx^{Rdy} cat has a valuable advantage over mouse models. The slow inner retinal degeneration in the face of photoreceptor loss and complete blindness will also make this an excellent model for testing

optogenetic approaches to provide visual function by expression of light-sensitive proteins in bipolar or ganglion cells.

2.6. ACKNOWLEDGEMENTS

The authors would like to thank Dr Cheryl Craft for the donation of the hCAR antibody, Nate Pasmanter for his help with analyzing the ERG a-wave leading edges, and Hui Wang for constructing feline Crx expression vectors.

Supported by National Institutes of Health Grants EY012543 and EY025272-01A1 (SC), EY002687 (P30 Core Grant) (Washington University Department of Ophthalmology and Visual Sciences [WU-DOVS]), EY013360 (T32 Predoctoral Training Grant) (WU), unrestricted funds from Research to Prevent Blindness (WUDOVS), Foundation Fighting Blindness (SC), Hope for Vision (SC), George H. Bird and ‘‘Casper’’ Endowment for Feline Initiatives (LMO and SMPJ), Michigan State University Center for Feline Health and Well-Being (LMO and SMPJ), and Myers-Dunlap Endowment (SMPJ).

APPENDICES

APPENDIX A – Figure 2.S1

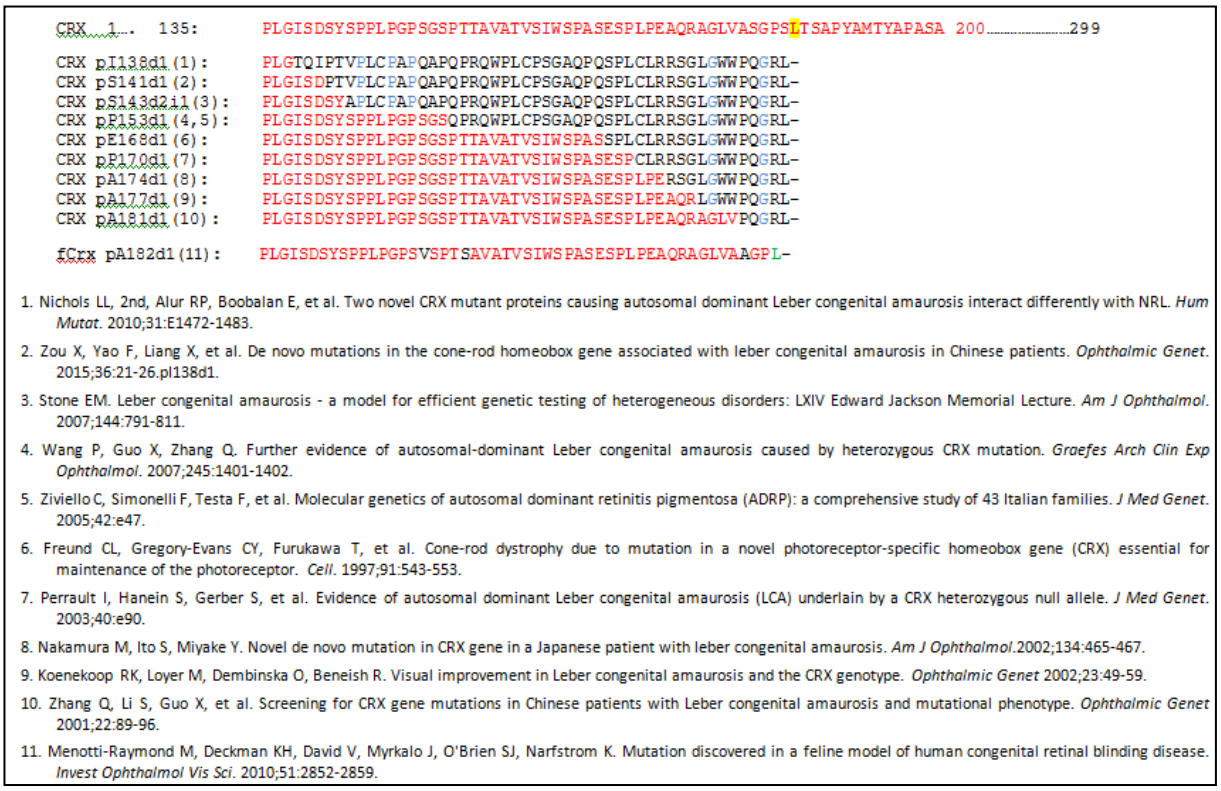

1. Nichols LL, 2nd, Alur RP, Boobalan E, et al. Two novel CRX mutant proteins causing autosomal dominant Leber congenital amaurosis interact differently with NRL. *Hum Mutat*. 2010;31:E1472-1483.

2. Zou X, Yao F, Liang X, et al. De novo mutations in the cone-rod homeobox gene associated with leber congenital amaurosis in Chinese patients. *Ophthalmic Genet*. 2015;36:21-26.pI138d1.

3. Stone EM. Leber congenital amaurosis - a model for efficient genetic testing of heterogeneous disorders: LXIV Edward Jackson Memorial Lecture. *Am J Ophthalmol*. 2007;144:791-811.

4. Wang P, Guo X, Zhang Q. Further evidence of autosomal-dominant Leber congenital amaurosis caused by heterozygous CRX mutation. *Graefes Arch Clin Exp Ophthalmol*. 2007;245:1401-1402.

5. Ziviello C, Simonelli F, Testa F, et al. Molecular genetics of autosomal dominant retinitis pigmentosa (ADRP): a comprehensive study of 43 Italian families. *J Med Genet*. 2005;42:e47.

6. Freund CL, Gregory-Evans CY, Furukawa T, et al. Cone-rod dystrophy due to mutation in a novel photoreceptor-specific homeobox gene (CRX) essential for maintenance of the photoreceptor. *Cell*. 1997;91:543-553.

7. Perrault I, Hanein S, Gerber S, et al. Evidence of autosomal dominant Leber congenital amaurosis (LCA) underlain by a CRX heterozygous null allele. *J Med Genet*. 2003;40:e90.

8. Nakamura M, Ito S, Miyake Y. Novel de novo mutation in CRX gene in a Japanese patient with leber congenital amaurosis. *Am J Ophthalmol*.2002;134:465-467.

9. Koenekoop RK, Loyer M, Dembinska O, Beneish R. Visual improvement in Leber congenital amaurosis and the CRX genotype. *Ophthalmic Genet* 2002;23:49-59.

10. Zhang Q, Li S, Guo X, et al. Screening for CRX gene mutations in Chinese patients with Leber congenital amaurosis and mutational phenotype. *Ophthalmic Genet* 2001;22:89-96.

11. Menotti-Raymond M, Deckman KH, David V, Myrkalo J, O'Brien SJ, Narfstrom K. Mutation discovered in a feline model of human congenital retinal blinding disease. *Invest Ophthalmol Vis Sci*. 2010;51:2852-2859.

Figure 2.S1. List of the *CRX* human mutations leading to the production of a premature stop codon at amino acid 185 compared to the human wild-type and feline mutant sequence.

APPENDIX B – Figure 2.S2

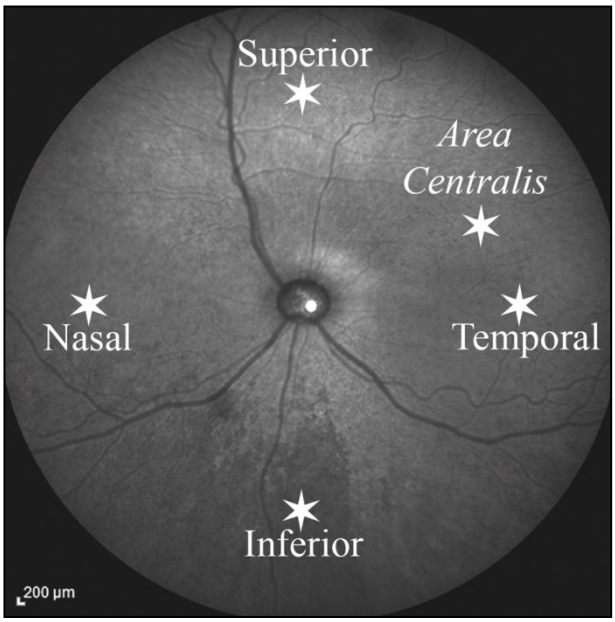

Figure 2.S2. Retinal regions imaged by SD-OCT. Cross sectional retinal images were captured for measurement of retinal layer thicknesses at the following regions (as indicated on the fundus image by an asterisk): the *area centralis*; 4 optic nerve diameters from the optic nerve edge superiorly, inferiorly, temporally and nasally.

APPENDIX C – Figure 2.S3

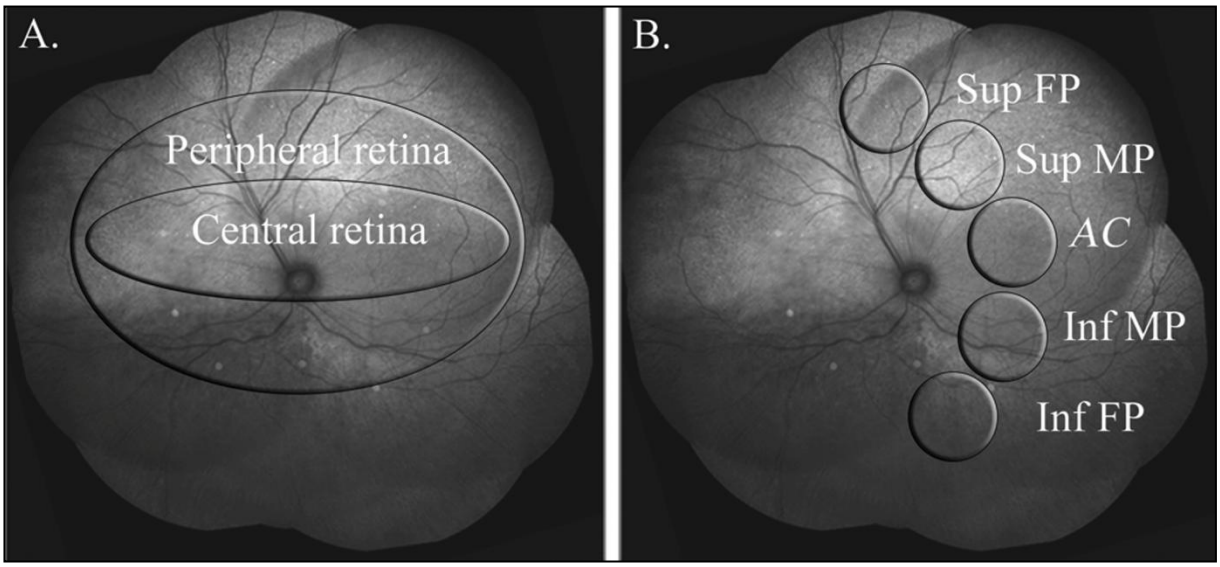

Figure 2.S3. Sites of retinal sampling for qRT-PCR. A. For the 2-week-old kittens, due to the small globe size, retina was collected from two regions as indicated (central and peripheral retinal regions). **B.** In the 6, 12 and 20 weeks of age kittens retinal biopsies were collected from the indicated five regions (*area centralis* – *AC*; inferior mid-peripheral – Inf MP; inferior far-peripheral – Inf FP; superior mid-peripheral – Sup MP; and superior far-periphery – Sup FP).

APPENDIX D – Figure 2.S4

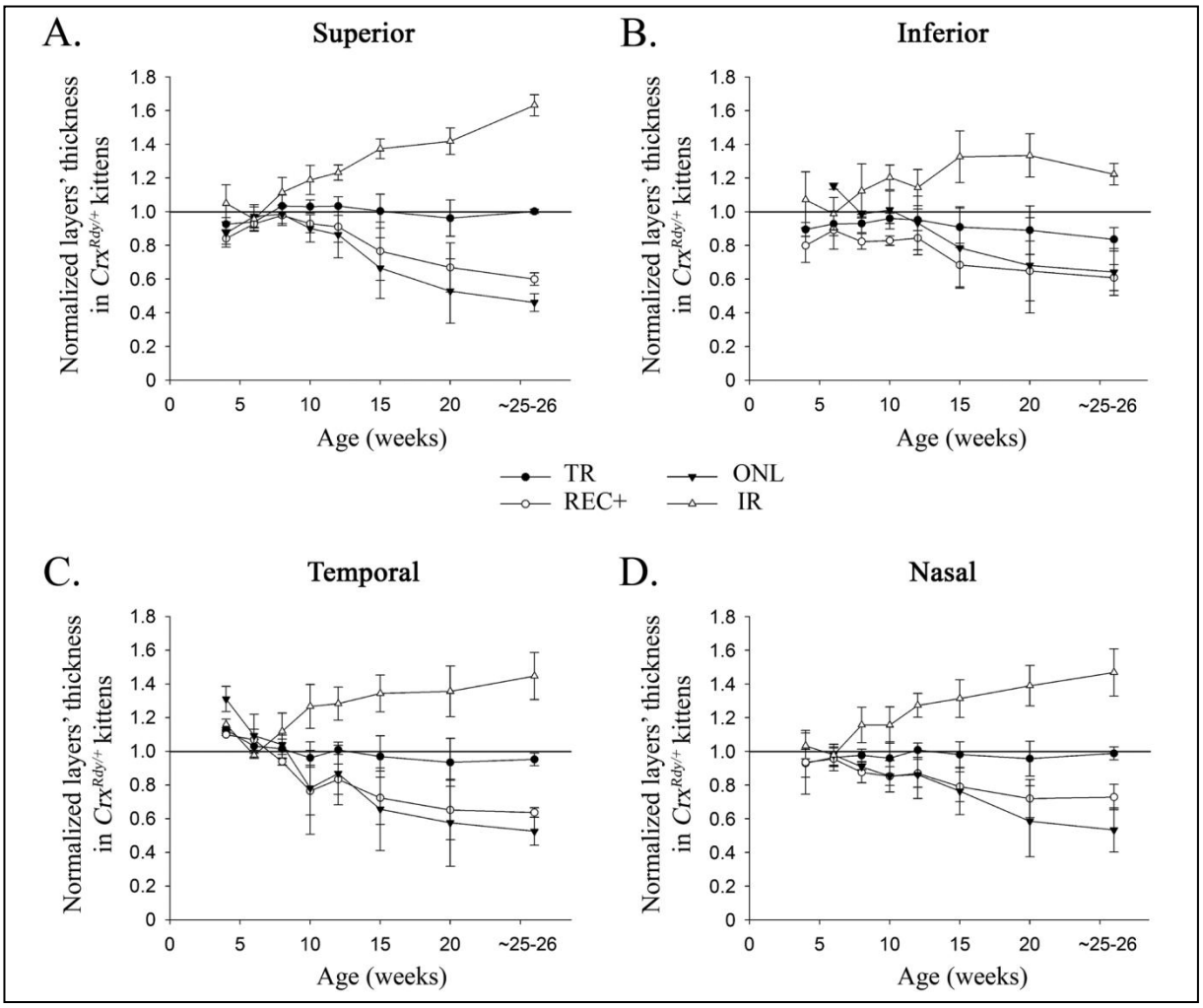

Figure 2.S4. TR, REC+, ONL and IR layer thicknesses on SD-OCT images, four optic nerve distance from the optic nerve rim itself **A. Superiorly, B. Inferiorly, C. Temporally and D. Nasally** of *Crx*$^{Rdy/+}$ kittens normalized to control WT kittens at 4, 6, 8, 10, 12, 15, 20 weeks-old and 6 months of age.

The ONL and REC+ thicknesses showed thinning with age in *Crx*$^{Rdy/+}$ kittens compared to WT. TR was not significant thinned until 6 months of age inferiorly. Conversely, the IR became thicker in *Crx*$^{Rdy/+}$ kittens compared to the wild-type kittens in all regions from 10 weeks of age.

APPENDIX E – Figure 2.S5

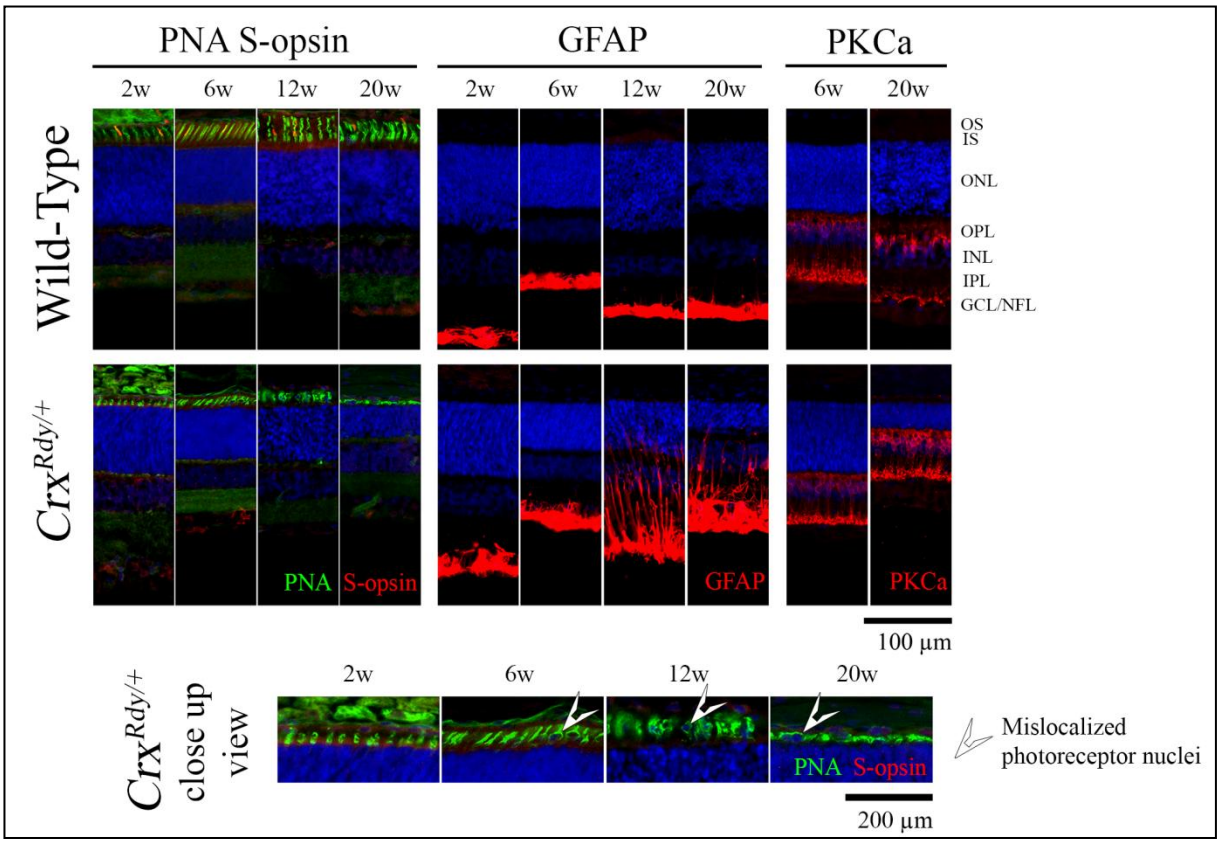

Figure 2.S5. Immunolabeling of the retina for S cones and inner retinal cells.
Frozen sections of central retinal labeled with PNA combined with S-opsin, and with GFAP, and PKCalpha.
The *Crx*$^{Rdy/+}$ retina showed a lack of S-opsin staining cells. Cone nuclei (PNA positive) became mislocalized to the subretinal space but did not stain for S-opsin (indicated by *white arrowheads* in the bottom panel – high magnification view). There was marked Müller cell activation as indicated by GFAP upregulation at 12 and 20 weeks of age. Rod bipolar cells were labeled by PKCalpha and showed dendrite retraction in the *Crx*$^{Rdy/+}$ retina.
Key: OS= Photoreceptor Outer segment, IS= Photoreceptor Inner segment, ONL= Outer Nuclear Layer, OPL= Outer Plexiform Layer, INL= Inner Nuclear Layer, IPL= Inner Plexiform Layer, GCL/NFL= Ganglion Cell Layer/Nerve Fiber Layer; *White arrowhead*= Mislocalized photoreceptor nuclei.

APPENDIX F – Figure 2.S6

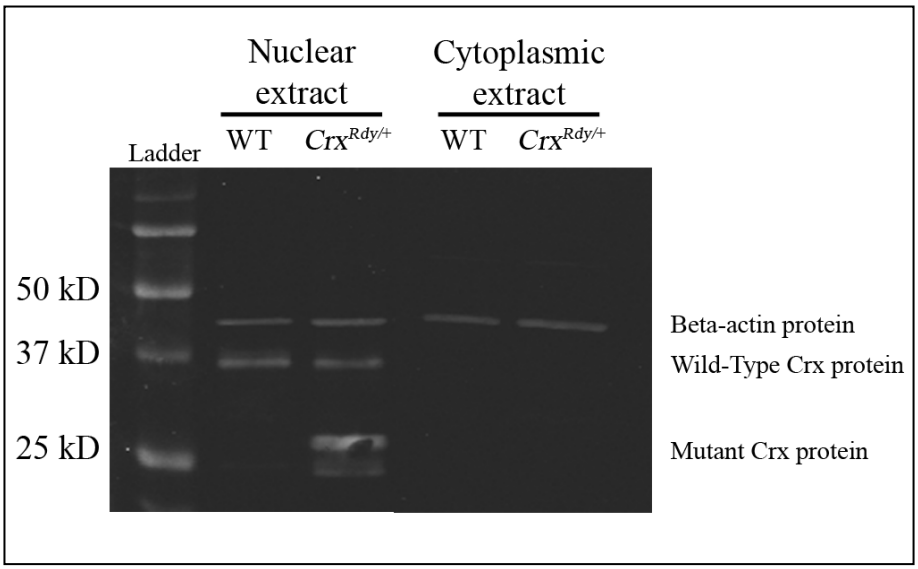

Figure 2.S6. Western blot for Crx protein in retinal nuclear and cytoplasmic extracts from 2 week old kittens.
Note that the truncated mutant Crx protein was exclusively detected in the nuclear extract from the *Crx*$^{Rdy/+}$ kitten and was at a higher level than the wild-type protein (immunolabeled with anti-Crx antibody 119b1).
Beta-actin was used as protein loading control.

APPENDIX G – Figure 2.S7

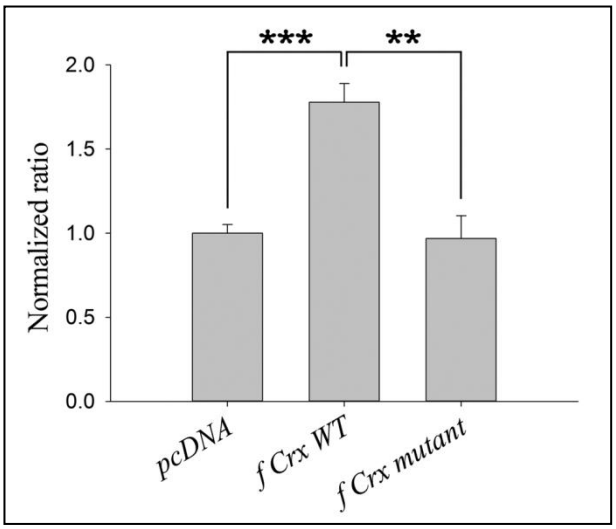

Figure 2.S7. Dual-Luciferase assays for CRX transactivation activity on mouse *Crx-Luc* reporter.

Crx auto-activation ability of WT or mutant Crx protein on its own promoter *Crx* (containing 2 binding sites within 500 bp upstream region of the mouse *Crx* gene) was tested using HEK293 cells transfected by plasmids containing the 500 bp mouse *Crx* promoter-luciferase reporter (*mCrx-Luc*) and the indicated Crx protein expression vector. Comparing to *pcDNA3.1hisc control*, only *pCAGIG-feline Crx WT* significantly activated the *mCrx-Luc* reporter. *pCAGIG-feline* Crx^{Rdy} *mutant* did not show any transactivation compared to the control vector.

P-values indicate as followed: $^{**}P<0.01$ and $^{***}P<0.001$.

APPENDIX H – Table 2.S1.

Antibody – Source	Type	Primary Dilution	Secondary Antibody – Source	Secondary Dilution
hCAR (Human cone arrestin) Dr. Cheryl Craft; LUMIJ, University of Southern California, Los Angeles, CA, USA	Polyclonal rabbit	1:10,000	Alexa Fluor 488 Goat anti-rabbit IgG Life technologies, Carlsbad, CA, USA	1:500
PNA (Biotinylated Peanut Agglutinin) Vector Labs Inc., Burlin-game, CA, USA	Biotinylated Lectin	1:500	Alexa Fluor 488 Streptavadin Life technologies, Carlsbad, CA, USA	1:500
ML-opsin (Anti-Opsin, Red/Green; Medium/ Long wavelength cone opsin) Millipore Corp., Billerica, MA, USA	Polyclonal rabbit	1:1,000	Alexa Fluor 568 or 594 Goat anti-rabbit IgG Life technologies, Carlsbad, CA, USA	1:500
S-opsin (Anti-Opsin, Blue; Short wavelength cone opsin) Millipore Corp., Billerica, MA, USA	Polyclonal rabbit	1:1,000	Alexa Fluor 568 or 594 Goat anti-rabbit IgG Life technologies, Carlsbad, CA, USA	1:500
RetP1 (Rhodopsin Ab-1) Thermo Scientific, Rockford, IL, USA	Monoclonal mouse	1:2	Alexa Fluor 594 Rabbit anti-mouse IgG Life technologies, Carlsbad, CA, USA	1:500
GFAP (Anti-Glial Fibrillary Acidic Protein) Cell Signaling Technology Inc., Danvers, MA, USA	Monoclonal mouse	1:300	Alexa Fluor 594 Rabbit anti-mouse IgG Life technologies, Carlsbad, CA, USA	1:500
PKCa (Protein Kinase C-alpha) BD Biosciences, San Jose, CA, USA	Monoclonal mouse	1:500	Alexa Fluor 594 Rabbit anti-mouse IgG Life technologies, Carlsbad, CA, USA	1:500

Table 2.S1. List of antibodies used for IHC – their origins and dilutions

APPENDIX I – Table 2.S2.

Primer name	Forward primer	Reverse primer	Amplicon size (bp)	Annealing temperature (°C)
Crx Total	5' AAGACTCAGTACCCGGATGTGTA 3'	5' GGGGCTGTAGGAGTCTGAGAT 3'	223	60
Arr3	5' CGTTGTCCTGTATTCCCTAGAC 3'	5' GCTAGAGGCCAGATTAGTATCAC 3'	190	60
Rho	5' GGTGCCCTACGCCAGCGTG 3'	5' CAGTGGGTTCTTGCCACAG 3'	190	60
Tuba1b	5' GCTCTATTGCCTGGAACACG 3'	5' CATCTTCCTTGCCCGTGATG 3'	230	60
GAPDH	5' GGTCTTCACCACCATGGAGA 3'	5' TGGACTGTGGTCATGAGTCC 3'	237	60

Table 2.S2. Primer sequences for qRT-PCR assays

REFERENCES

REFERENCES

1. Daiger SP, Rossiter BJF, Greenberg J, Christoffels A, Hide W. Data services and software for identifying genes and mutations causing retinal degeneration. *Invest Ophthalmol Vis Sci*. 1998;39:S295.

2. Hull S, Arno G, Plagnol V, et al. The phenotypic variability of retinal dystrophies associated with mutations in CRX, with report of a novel macular dystrophy phenotype. *Invest Ophthalmol Vis Sci*. 2014;55:6934-6944.

3. Tran NM, Chen S. Mechanisms of blindness: animal models provide insight into distinct CRX-associated retinopathies. *Dev Dyn*. 2014;243:1153-1166.

4. Chau KY, Chen S, Zack DJ, Ono SJ. Functional domains of the cone-rod homeobox (CRX) transcription factor. *J Biol Chem*. 2000;275:37264-37270.

5. Morrow EM, Furukawa T, Raviola E, Cepko CL. Synaptogenesis and outer segment formation are perturbed in the neural retina of Crx mutant mice. *BMC Neurosci*. 2005;6:5.

6. Chen S, Wang QL, Nie Z, et al. Crx, a novel Otx-like paired-homeodomain protein, binds to and transactivates photoreceptor cell-specific genes. *Neuron*. 1997;19:1017-1030.

7. Furukawa T, Morrow EM, Cepko CL. Crx, a novel otx-like homeobox gene, shows photoreceptor-specific expression and regulates photoreceptor differentiation. *Cell*. 1997;91:531-541.

8. Hennig AK, Peng GH, Chen S. Regulation of photoreceptor gene expression by Crx-associated transcription factor network. *Brain Res*. 2008;1192:114-133.

9. Peng GH, Chen S. Crx activates opsin transcription by recruiting HAT-containing co-activators and promoting histone acetylation. *Hum Mol Genet*. 2007;16:2433-2452.

10. Corbo JC, Lawrence KA, Karlstetter M, et al. CRX ChIP-seq reveals the cis-regulatory architecture of mouse photoreceptors. *Genome Res*. 2010;20:1512-1525.

11. Livesey FJ, Furukawa T, Steffen MA, Church GM, Cepko CL. Microarray analysis of the transcriptional network controlled by the photoreceptor homeobox gene Crx. *Curr Biol*. 2000;10:301-310.

12. Blackshaw S, Fraioli RE, Furukawa T, Cepko CL. Comprehensive analysis of photoreceptor gene expression and the identification of candidate retinal disease genes. *Cell*. 2001;107:579-589.

13. Hsiau TH, Diaconu C, Myers CA, Lee J, Cepko CL, Corbo JC. The cis-regulatory logic of the mammalian photoreceptor transcriptional network. *PLoS One*. 2007;2:e643.

14. Chen S, Wang QL, Xu S, et al. Functional analysis of cone-rod homeobox (CRX) mutations associated with retinal dystrophy. *Hum Mol Genet*. 2002;11:873-884.

15. Tran NM, Zhang A, Zhang X, Huecker JB, Hennig AK, Chen S. Mechanistically distinct mouse models for CRX-associated retinopathy. *PLoS Genet*. 2014;10:e1004111.

16. Terrell D, Xie B, Workman M, et al. OTX2 and CRX rescue overlapping and photoreceptor-specific functions in the Drosophila eye. *Dev Dyn*. 2012;241:215-228.

17. Freund CL, Wang QL, Chen S, et al. De novo mutations in the CRX homeobox gene associated with Leber congenital amaurosis. *Nat Genet*. 1998;18:311-312.

18. Applebury ML, Antoch MP, Baxter LC, et al. The murine cone photoreceptor: a single cone type expresses both S and M opsins with retinal spatial patterning. *Neuron*. 2000;27:513-523.

19. Provis JM, Dubis AM, Maddess T, Carroll J. Adaptation of the central retina for high acuity vision: cones, the fovea and the avascular zone. *Prog Retin Eye Res*. 2013;35:63-81.

20. Rossi EA, Roorda A. The relationship between visual resolution and cone spacing in the human fovea. *Nat Neurosci*. 2010;13:156-157.

21. Volland S, Esteve-Rudd J, Hoo J, Yee C, Williams DS. A comparison of some organizational characteristics of the mouse central retina and the human macula. *PLoS One*. 2015;10:e0125631.

22. Jeon CJ, Strettoi E, Masland RH. The major cell populations of the mouse retina. *J Neurosci*. 1998;18:8936-8946.

23. Barnett KC, Curtis R. Autosomal dominant progressive retinal atrophy in the Abyssinian cat. *J Hered*. 1985;76:168-170.

24. Curtis R, Barnett KC, Leon A. An early-onset retinal dystrophy with dominant inheritance in the Abyssinian cat. Clinical and pathological findings. *Invest Ophthalmol Vis Sci*. 1987;28:131-139.

25. Leon A, Curtis R. Autosomal dominant rod-cone dysplasia in the Rdy cat. 1. Light and electron microscopic findings. *Exp Eye Res*. 1990;51:361-381.

26. Leon A, Hussain AA, Curtis R. Autosomal dominant rod-cone dysplasia in the Rdy cat. 2. Electrophysiological findings. *Exp Eye Res*. 1991;53:489-502.

27. Chong NH, Alexander RA, Barnett KC, Bird AC, Luthert PJ. An immunohistochemical study of an autosomal dominant feline rod/cone dysplasia (Rdy cats). *Exp Eye Res*. 1999;68:51-57.

28. Menotti-Raymond M, Deckman KH, David V, Myrkalo J, O'Brien SJ, Narfstrom K. Mutation discovered in a feline model of human congenital retinal blinding disease. *Invest Ophthalmol Vis Sci*. 2010;51:2852-2859.

29. Nichols LL II, Alur RP, Boobalan E, et al. Two novel CRX mutant proteins causing autosomal dominant Leber congenital amaurosis interact differently with NRL. *Hum Mutat.* 2010;31:E1472-E1483.

30. Stone EM. Leber congenital amaurosis - a model for efficient genetic testing of heterogeneous disorders: LXIV Edward Jackson Memorial Lecture. *Am J Ophthalmol.* 2007;144:791-811.

31. Wang P, Guo X, Zhang Q. Further evidence of autosomal-dominant Leber congenital amaurosis caused by heterozygous CRX mutation. *Graefes Arch Clin Exp Ophthalmol*. 2007;245:1401-1402.

32. Ziviello C, Simonelli F, Testa F, et al. Molecular genetics of autosomal dominant retinitis pigmentosa (ADRP): a comprehensive study of 43 Italian families. *J Med Genet*. 2005;42:e47.

33. Freund CL, Gregory-Evans CY, Furukawa T, et al. Cone-rod dystrophy due to mutation in a novel photoreceptor-specific homeobox gene (CRX) essential for maintenance of the photoreceptor. *Cell*. 1997;91:543-553.

34. Perrault I, Hanein S, Gerber S, et al. Evidence of autosomal dominant Leber congenital amaurosis (LCA) underlain by a CRX heterozygous null allele. *J Med Genet*. 2003;40:e90.

35. Nakamura M, Ito S, Miyake Y. Novel de novo mutation in CRX gene in a Japanese patient with Leber congenital amaurosis. *Am J Ophthalmol*.2002;134:465-467.

36. Koenekoop RK, Loyer M, Dembinska O, Beneish R. Visual improvement in Leber congenital amaurosis and the CRX genotype. *Ophthalmic Genet.* 2002;23:49-59.

37. Zhang Q, Li S, Guo X, et al. Screening for CRX gene mutations in Chinese patients with Leber congenital amaurosis and mutational phenotype. *Ophthalmic Genet* 2001;22:89-96.

38. Zou X, Yao F, Liang X, et al. De novo mutations in the cone-rod homeobox gene associated with Leber congenital amaurosis in Chinese patients. *Ophthalmic Genet.* 2015;36:21-26.

39. Steinberg RH, Reid M, Lacy PL. The distribution of rods and cones in the retina of the cat (*Felis domesticus*). *J Comp Neurol*. 1973;148:229-248.

40. Rapaport DH, Stone J. The area centralis of the retina in the cat and other mammals: focal point for function and development of the visual system. *Neuroscience*. 1984;11:289-301.

41. Linberg KA, Lewis GP, Shaaw C, Rex TS, Fisher SK. Distribution of S- and M-cones in normal and experimentally detached cat retina. *J Comp Neurol*. 2001;430:343-356.

42. Hood DC, Birch DG. Light adaptation of human rod receptors: the leading edge of the human a-wave and models of rod receptor activity. *Vision Res*. 1993;33:1605-1618.

43. Evans LS, Peachey NS, Marchese AL. Comparison of three methods of estimating the parameters of the Naka-Rushton equation. *Doc Ophthalmol*. 1993;84:19-30.

44. Hood DC, Lin CE, Lazow MA, Locke KG, Zhang X, Birch DG. Thickness of receptor and post-receptor retinal layers in patients with retinitis pigmentosa measured with frequency-domain optical coherence tomography. *Invest Ophthalmol Vis Sci*. 2009;50:2328-2336.

45. Mowat FM, Gornik KR, Dinculescu A, et al. Tyrosine capsid-mutant AAV vectors for gene delivery to the canine retina from a subretinal or intravitreal approach. *Gene Ther*. 2014;21:96-105.

46. Spurr AR. A low-viscosity epoxy resin embedding medium for electron microscopy. *J Ultrastruct Res*. 1969;26:31-43.

47. Schneider CA, Rasband WS, Eliceiri KWNIH. Image to ImageJ: 25 years of image analysis. *Nat Methods*. 2012;9:671-675.

48. Staurenghi G, Sadda S, Chakravarthy U, Spaide RF; International Nomenclature for Optical Coherence Tomography Panel. Proposed lexicon for anatomic landmarks in normal posterior segment spectral-domain optical coherence tomography: the IN·OCT consensus. *Ophthalmology*. 2014;121:1572-1578.

49. Ekstrom P, Sanyal S, Narfström K, Chader GJ, van Veen T. Accumulation of glial fibrillary acidic protein in Müller radial glia during retinal degeneration. *Invest Ophthalmol Vis Sci*. 1988;29:1363-1371.

50. Linberg KA, Fariss RN, Heckenlively JR, Farber DB, Fisher SK. Morphological characterization of the retinal degeneration in three strains of mice carrying the rd-3 mutation. *Vis Neurosci*. 2005;22:721-734.

51. Sarthy PV, Fu M. Transcriptional activation of an intermediate filament protein gene in mice with retinal dystrophy. *DNA* 1989;8:437-446.

52. Sieving PA, Frishman LJ, Steinberg RH. Scotopic threshold response of proximal retina in cat. *J Neurophysiol*. 1986;56:1049-1061.

53. Stockton RA, Slaughter MM. B-wave of the electroretinogram. A reflection of ON bipolar cell activity. *J Gen Physiol*. 1989;93:101-122.

54. Glubrecht DD, Kim JH, Russell L, Bamforth JS, Godbout R. Differential CRX and OTX2 expression in human retina and retinoblastoma. *J Neurochem*. 2009;111:250-263.

55. Massof RW, Wu L, Finkelstein D, Perry C, Starr SJ, Johnson MA. Properties of electroretinographic intensity-response functions in retinitis pigmentosa. *Doc Ophthalmol*. 1984;57:279-296.

56. Koenekoop RK. An overview of Leber congenital amaurosis: a model to understand human retinal development. *Surv Ophthalmol*. 2004;49:379-398.

57. Zhao TT, Tian CY, Yin ZQ. Activation of Müller cells occurs during retinal degeneration in RCS rats. *Adv Exp Med Biol*. 2010;664:575-583.

58. Ostergaard ME, Southwell AL, Kordasiewicz H, et al. Rational design of antisense oligonucleotides targeting single nucleotide polymorphisms for potent and allele selective suppression of mutant Huntingtin in the CNS. *Nucleic Acids Res*. 2013;41:9634-9650.

59. Bennett CF, Swayze EE. RNA targeting therapeutics: molecular mechanisms of antisense oligonucleotides as a therapeutic platform. *Annu Rev Pharmacol Toxicol*. 2010;50:259-293.

60. Singh J, Kaur H, Kaushik A, Peer S. A review of antisense therapeutic interventions for molecular biological targets in various diseases. *Int J Pharmacol*. 2011;7:294-315.

61. Liao Y, Tang L. Inducible RNAi system and its application in novel therapeutics. *Crit Rev Biotech*. 2016;36:630-638.

62. Lambeth LS, Smith CA. Short hairpin RNA-mediated gene silencing. *Methods Mol Biol*. 2013;942:205-232.

63. Rayburn ER, Zhang R. Antisense, RNAi, and gene silencing strategies for therapy: mission possible or impossible? *Drug Discov Today*. 2008;13:513-521.

64. Day TP, Byrne LC, Schaffer DV, Flannery JG. Advances in AAV vector development for gene therapy in the retina. *Adv Exp Med Biol*. 2014;801:687-693.

65. McClements ME, MacLaren RE. Gene therapy for retinal disease. *Trans Res*. 2013;161:241-254.

66. Kotterman MA, Schaffer DV. Engineering adeno-associated viruses for clinical gene therapy. *Nat Rev Genet*. 2014;15:445-451.

67. Dalkara D, Sahel JA. Gene therapy for inherited retinal degenerations. *C R Biol*. 2014;337:185-192.

CHAPTER 3

METABOLIC CHANGES AND RETINAL REMODELING IN HETEROZYGOUS *CRX* MUTANT CATS ($CRX^{RDY/+}$)

3.1. ABSTRACT

PURPOSE. CRX is a transcription factor essential for normal photoreceptor development and survival. The Crx^{Rdy} cat has a spontaneous mutation in *Crx*. Early disease stages in heterozygous cats ($Crx^{Rdy/+}$) mimic severe Leber's congenital amaurosis. This study investigated the timing and extent of retinal remodeling during retinal degeneration. This will help optimizing the best time for therapies such as retinal prosthesis or optogenetics before retinal rewiring and glial scar formation becomes too extensive. **METHODS.** $Crx^{Rdy/+}$ cats from 6 weeks to 10 years of age were investigated. *In vivo* structural changes of retinas were analyzed by fundus examination, confocal scanning laser ophthalmoscopy, spectral domain optical coherence tomography and fluorescein angiography. Post-mortem, structural changes were characterized by histologic analyses including immunohistochemistry, regular thin histologic sections and immunocytochemistry for computational molecular phenotyping for macromolecules and small molecules. **RESULTS.** As early as 12 weeks of age, the retina of the $Crx^{Rdy/+}$ cats showed some glial reaction to photoreceptor death followed by formation of a glial seal, rewiring and inner nuclear layer cell migration with disease progression as well as changes in inner retina thickness. There was preservation of inner retinal cells such as bipolar, amacrine and horizontal cells in early adulthood. Additionally, marked retinal and retinal pigmentary epithelium atrophy developed in the *area centralis*. With further progression, microneuroma formation, severe retinal thinning and more severe remodeling occured. The superficial retinal vasculature was attenuated with eventually a lack of peripheral fundus perfusion and development of arterio-venous shunts. **CONCLUSIONS.** This study indicates that retinal degeneration in the $Crx^{Rdy/+}$ cat retina follows the 3 phases that have been described for retinal remodeling. These findings suggest that therapy dependent on targeting inner retinal cells may be useful in young adults with preserved inner retinas prior to advanced stages of retinal remodeling and neuronal cell loss.

3.2. INTRODUCTION

Cone-rod homeobox (*CRX*) is an *OTX*-like homeobox gene encoding a transcription factor essential for normal photoreceptor development, function and homeostasis.[1, 2] *CRX* mutations result in a spectrum of dominant retinopathies ranging from Leber congenital amaurosis (LCA) to cone–rod dystrophy (CoRD), retinitis pigmentosa (RP) and macular degeneration (MD).[3, 4] The Crx^{Rdy} cat has a spontaneous frameshift mutation in *Crx* (single nucleotide deletion in exon 4) leading to a premature stop codon and therefore the production of a truncated mutant Crx protein.[5] This type of mutation is an example of a Class III *CRX* mutation in which accumulation of mutant CRX protein with a functional DNA binding domain but disrupted or missing transactivation occurs and has a dominant negative action.[6] The heterozygous *Crx* mutant cat ($Crx^{Rdy/+}$) develops an autosomal dominant cone-rod dystrophy characterized by very early dysfunction and degeneration of photoreceptors, thus mimicking the severe Leber congenital amaurosis phenotype.[7-10] A detailed phenotypic description of the early disease stages of the $Crx^{Rdy/+}$ cat has been reported in chapter 2. Affected animals have a halted development of photoreceptors followed by a progressive retinal degeneration.[10] The retinal changes that develop later in the disease process have not been reported.

A feature of Class III *CRX* mutations is accumulation of the mutant protein by a mechanism that is not yet fully understood. The presence of increased amounts of mutant transcript and mutant protein with a dominant negative effect makes development of potential therapeutic approaches challenging. Similar to other dominant retinopathies an approach to reduce the level of mutant transcript may be necessary, unlike the situation in many recessive conditions where a gene augmentation approach is appropriate. Furthermore the rapid loss of photoreceptors may dictate that alternative approaches such as optogenetics, retinal prosthesis, transplantation of cells or retinal sheets may be needed once patients have lost their

photoreceptors. Such approaches rely on the retaining inner retinal structure and retinal vasculature for them to be feasible. Investigation of later disease stages are important to provide information on the retinal status following photoreceptor loss which is the stage that will need to be treated. Studies of animal models have already revealed the extensive and progressive retinal remodeling that occurs as photoreceptors die. Understanding of this very dynamic process will aid in development of novel treatments to be performed on patients with late stage disease. Animal models such as the *Crx*$^{Rdy/+}$ cat show potential for developing these treatment modalities.

Immunohistochemistry can provide some information about changes in specific retinal cell types but over the last 15 years, the use of amino acid retinal signatures has been developed and used to investigate retinal remodeling resulting from inherited and acquired retinal diseases.[11-14] Amino acid retinal signatures have also been described in normal and detached cat retinas.[15, 16] Fourteen separable biochemical theme classes have been identified: photoreceptor, bipolar and ganglion cells characterized by specific glutamate signature, amacrine cells by glycine and gamma-aminobutyric acid (GABA) signature, horizontal cells by GABA signature, Müller cells by taurine-glutamine signature and retinal pigmentary epithelium (RPE) cells by an aspartate-glutamate-taurine-glutamine signature. The rest of the cells which fill the neuronal space, present with glutamate, GABA, or glycine signatures.

Three phases have been described during retinal remodeling in hereditary retinal degenerations (retinitis pigmentosa and rod/cone dystrophies).[13, 17, 18] Phases are classified as follow: during the initial Phase 0-1, down regulation of glutamate receptor expression occurs in rod bipolar cells dendrites; during Phase 1-2, rod and cone photoreceptors undergo stress which leads to their death, concurrently dendritic modules are lost; during the last stage Phase 3, sprouting and formation of new axonal modules develop and generalized retinal remodeling

occurs. In models in which cones die later than rods, some bipolar cell dendrites sprout and make contact with different targets.

The purpose of this study was to investigate the timing and extent of retinal remodeling during retinal degeneration in the *Crx*$^{Rdy/+}$ cat. This information will be important for assessing the stages of remodeling that may be amenable to therapies such as retinal prosthesis or optogenetics. For translational therapies it will be important to know at which stages of retinal remodeling that such interventions may be of benefit.

3.3. MATERIALS AND METHODS

3.3.1. Ethics Statement

All procedures were performed in accordance with the ARVO statement for the Use of Animals in Ophthalmic and Vision Research and approved by the Michigan State University Institutional Animal Care and Use Committee.

3.3.2. Animals

Heterozygous mutant *Crx*$^{Rdy/+}$ cats and wild-type (WT) control cats maintained within a colony at Michigan State University housed under a 12L:12D cycles, were studied. They received commercial feline dry diet (Purina One Smartblend and Purina Kitten Chow, Nestlé Purina, St Louis, MO. USA). Cats were studied during retinal maturation and adulthood from 6 weeks to 10 years of age.

A table of the number of animals/samples from each experiment is available in Appendix M – Table 3.S1.

3.3.3. Ophthalmic examination and fundus imaging

In vivo ophthalmic fundus and retinal changes in the heterozygous $Crx^{Rdy/+}$ cats was investigated by ophthalmic examination, fundus photography (Ret-Cam II, Clarity Medical Systems, Inc., Pleasanton, CA, USA) and confocal scanning laser ophthalmoscopy (cSLO) including autofluorescence imaging (AF) and spectral domain – optical coherence tomography (SD-OCT) (Spectralis OCT+HRA, Heidelberg Engineering Inc., Heidelberg, Germany) as previously described.[10]

To assess retinal vasculature, fluorescein angiography (FA) was performed injecting 20 mg/kg of 10% sodium fluorescein (Fluorescite 10%, Alcon Laboratories Inc, Fort Worth, Texas, USA) in the left cephalic vein. One-minute movies then images at regular intervals were recorded with confocal scanning laser ophthalmoscopy (cSLO) and a 55° wide field lens. Anesthesia, pupil dilation and globe positioning were performed as described chapter 2 for ERG and SD-OCT.[10]

3.3.4. Retinal morphology and vasculature evaluation

3.3.4.1. *In vivo* Spectral Domain-Optical Coherence Tomography (SD-OCT)

Retinal morphology was assessed in $Crx^{Rdy/+}$ and wild-type control kittens from 4 weeks to 10.25 years of age were included (animals from 4 weeks to 26 weeks of age from chapter 2 were included in the analysis).

Anesthesia, pupil dilation and globe positioning were performed as described for ERG and SD-OCT in chapter 2.[10] cSLO retinal images were captured. Then spectral-domain optical coherence tomography (SD-OCT) imaging was performed to obtain detailed retinal cross section images (Spectralis OCT+HRA, Heidelberg Engineering Inc., Heidelberg, Germany). SD-OCT single scan line and volume scan images were recorded from the center of the *area centralis* and in the four retinal quadrants (at 4 optic nerve head distances from the edge of the optic nerve head

superiorly, inferiorly, nasally and temporally as illustrated in chapter 2. Total thickness, Receptor+ (REC+; including layers between retinal pigmentary epithelium and outer plexiform layer included)[19], inner nuclear layer (INL), ganglion cell complex (GCC; including the inner plexiform layer (IPL) and the ganglion cell layer (GCL)) and inner retina (IR; layers between inner nuclear layer and internal limiting membrane) thickness were measured (Fig. 3.1) using the Heidelberg Eye Explorer (HEYEX) software.

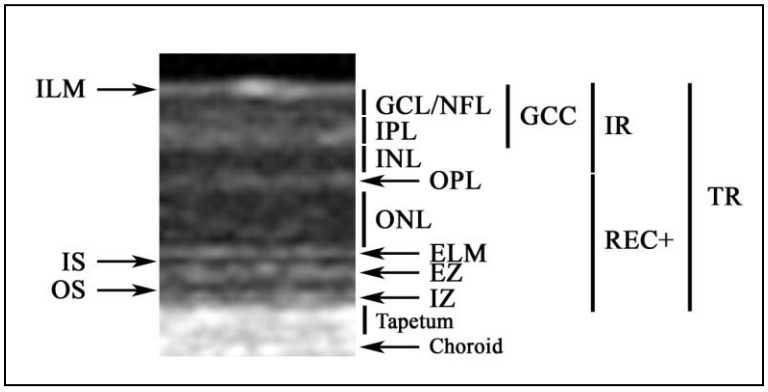

Figure 3.1. Representative SD-OCT high resolution cross-section image of a normal cat showing the different layers that can be viewed. In the present study, measurements of TR, REC+, IR, ONL, INL and GCC were performed.
TR; Total retina, REC+; Receptor+, IR; Inner retina, ONL; Outer nuclear layer, INL; Inner nuclear layer, GCC; Ganglion cell complex, NFL; Nerve fiber layer, ILM; Inner limiting membrane, ELM; external limiting membrane, EZ; Ellipsoid zone, IZ; Interdigitation zone, IS/OS; photoreceptor inner and outer segments.
The REC+ includes layers from IZ to OPL. The GCC includes the IPL and GCL/NFL layers. IR includes the INL and GCC.

3.3.4.2. Post-mortem retinal and vascular morphology and remodeling investigation

Retinal and vascular morphology and remodeling were investigated using immunohistochemistry (IHC), regular plastic histologic thin sections and immunocytochemistry for computational molecular phenotyping (CMP).

3.3.4.2.1. Immunohistochemistry (IHC)

IHC was performed on frozen sections from eyes at different ages to evaluate retinal changes and remodeling with disease progression. After euthanasia, eyes were processed as previously described.[10, 20] The antibodies used are listed in Appendix N – Table 3.S2.

Retinas from four cats (three *Crx*$^{Rdy/+}$ and one WT cats) were flatmounted to evaluate retinal vasculature changes. Eyes were fixed for 3.25 hours similarly as for regular IHC. After eyecup dissection and an additional 30 minutes fixation, the eyecups were rinsed 2 times for 10 minutes in 1M phosphate-buffered saline pH 7.4 (PBS; Sigma-Aldrich Corp., St. Louis, MO, USA). The retinas were dissected and blocked with 10% horse serum (Sigma-Aldrich Corp.) and 0.3% Triton X-100 (Sigma-Aldrich Corp.) in PBS for 2 hours at room temperature. Primary antibodies; Isolectin GS-IB4 Alexa Fluor 488 conjugate at a 1:1,000 dilution (Life technologies, Carlsbad, CA, USA) and Collagen Type IV at a 1:200 dilution (Millipore Corp. Billerica, MA, USA) were applied and flatmounts incubated for 4 days at 4°C. Retinas were then rinsed 3 times for 20 minutes in 0.3% Triton X-100. Secondary antibody (Alexa Fluor 546 goat anti-rabbit IgG, Life technologies, Carlsbad, CA, USA) at a 1:1,000 dilution were applied and the flatmounts incubated for 24 hours at 4°C. After 3 washes for 5 minutes with PBS the retina were flatmounted on slides.

3.3.4.2.2. Regular plastic embedded histologic thin sections

Eyes were fixed in 2.5% glutaraldehyde (Glutaraldehyde, Alfa Aesar, Heysham, England), 1% formaldehyde (Formal-Fixx, Thermo Shandon Ltd., Runcorn, UK) in 0.2 M PBS pH 7.4 (Sigma-Aldrich Corp.), 0.1% magnesium sulfate ($MgSO_4$; Sigma-Aldrich Corp.) and 3% sucrose on ice for 1 hour. The eyes were then hemisectioned, the vitreous removed and the posterior eyecups placed in the same fixative until processed as described in chapter 2.[10] Retinal samples were collected from 5 different regions (Appendix J – Fig. 3.S1.) and epoxy-embedded: *area centralis* (AC), superior mid- and far-periphery (SupMP, SupFP), and inferior mid- and far-periphery (InfMP, InfFP) to investigate regional differences. ONL, INL and GCC cells were counted on 3 different 1 µm sections for each time point (same area/same animal) and on a 100 µm width for each area.

3.3.4.2.3. Immunocytochemistry for computational molecular phenotyping for macromolecules and small molecules (CMP)

The same eyes as previously fixed in mixed aldehyde buffer for regular histologic sections were used. Retinas were collected from 5 different areas of the fundus (Appendix J – material Fig. 3.S1) and epoxy-embedded: *area centralis* (AC), superior mid- and far-periphery (SupMP, SupFP) and inferior mid- and far- periphery (InfMP, InfFP) to investigate regional differences. 200 nm serial retinal sections were assessed.

Retinal remodeling was then evaluated by computational molecular phenotyping (CMP) then evaluate as previously described.[21] Retinal samples were processed for immunocytochemistry for CMP for macromolecules and small molecules (CMP) including GABA (yy), glycine (G), L-glutamate (E), taurine (TT), L-glutamine (Q), glutathione red ox (J), L-aspartate (D), L-arginine (R), red-green opsin (RGO), rhodopsin (1D4), cellular retinaldehyde binding protein (CRALBP), and glutamine synthetase (GS) (for the antibodies list and dilution

refer to Jones et *al.*, 2016 [22]). CMP were visualized with secondary antibodies conjugated to 1.4 nm gold, followed by silver intensification as previously described[21]. Images were captured and processed [23]. Molecular signals were visualized on images as rgb maps using red, green, and blue for example respectively TQE: Taurine red, L-Glutamine green, L-Glutamate E blue, YGE: GABA γ red, glycine G green, glutamate E blue.

3.3.5. Statistical analysis

A mixed effect model using R studio was used to analyze the data for SD-OCT and measurements as data was evaluated over time. The equation below was used.[24]

$$Y_i = \sum_{i=0}^{n} \beta \mathrm{X} + \alpha_i + \varepsilon_i$$

where *ß* is the parameter vector. X is the independent variable matrix, α_i is the cat level residual, and the $\mathcal{E}_i$ is the individual observation level residual.

No statistical analysis was performed for the cell nuclei counting as only a n number of 1 was available for most of the ages and there was a lack of age-matched WT controls.

3.4. RESULTS

3.4.1. *Crx*$^{Rdy/+}$ cats present with severe retinal degeneration starting and more pronounced in the *area centralis*

Fundus and retinal changes were investigated during retinal maturation and adulthood in the *Crx*$^{Rdy/+}$ cat and compare to age matched WT controls. As early as 7 weeks of age, tapetal hyperreflectivity was present in the *area centralis*, and then in the rest of the fundus by 20 weeks of age in the *Crx*$^{Rdy/+}$ cat (Fig. 3.2). By 6.5 years of age some affected cats had developed a bluish appearing lesion in the *area centralis*. This progressed such that in the older cats the lesion appeared dark in color. On fundus autofluorescence (FAF) cSLO, the lesion showed a decrease in FAF in the region of the *area centralis* which extended along the visual streak and with disease progression could worsen to be a more severe lesion with a complete lack FAF in the *area centralis* (Fig. 3.2). Vasculature attenuation was noticeable as early as 20-weeks of age and obvious by 9-months of age as seen on color and cSLO fundus images and became advanced with disease progression (Fig. 3.2). Vasculature changes were further investigated by fluorescein angiography and IHC (detailed further, Fig. 3.8). Morphological changes were investigated *in vivo* by high resolution cross-section SD-OCT images in the *area centralis* and the four quadrant regions. SD-OCT images showed a lack discernible ellipsoid and interdigitation zones from as early as 4 weeks of age, earliest age imaged (Fig. 3.2.).

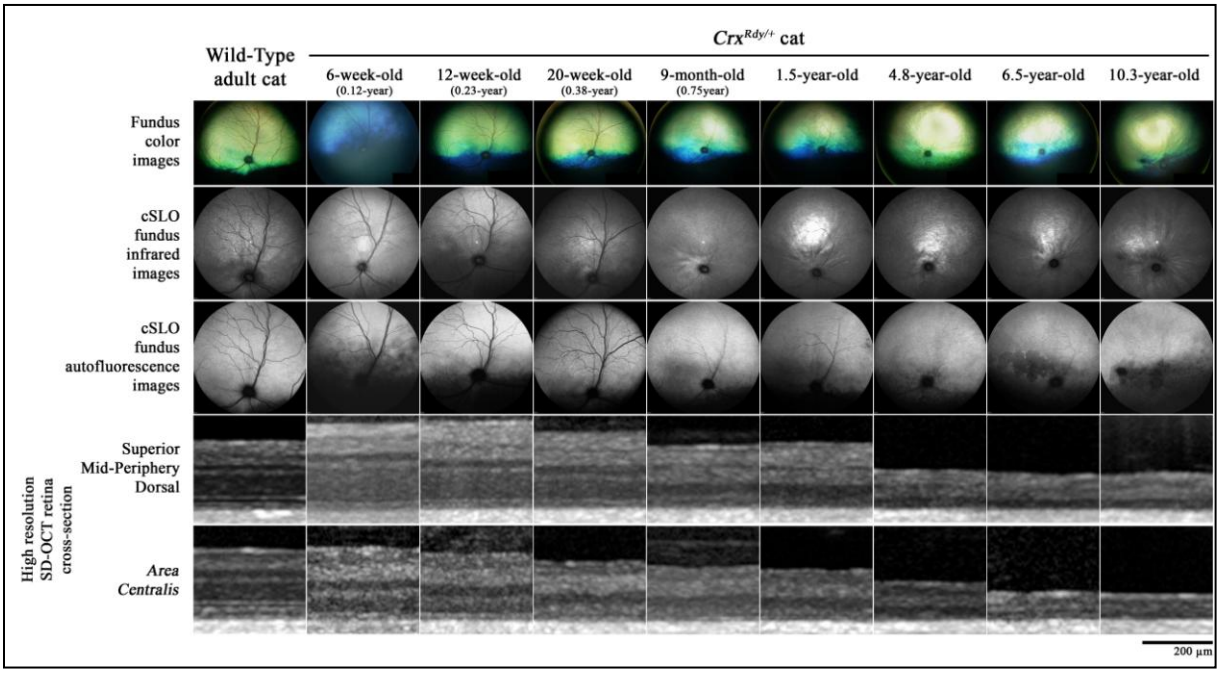

Figure 3.2. Fundus changes and morphological changes in the $Crx^{Rdy/+}$ cat at different ages.
Color fundus images. Vasculature attenuation was noticeable as early as 20-weeks of age and obvious by 9-months of age. Fundus hyperreflectivity was noticeable in the region of the *area centralis* at 12-weeks of age (in this panel) then became more generalized by 20-weeks of age. Color fundus images also showed that by at 6.5 and 10.3-years of age a lesion in the region of the *area centralis* had developed.
Infrared cSLO fundus images. Those images demonstrate the vascular attenuation that occured with the disease progression and was very obvious after 20-weeks of age.
Autofluorescence cSLO fundus images. Similarly to the color and infrared cSLO images, images illustrate the vascular attenuation. They also show the presence of a lesion seen as a decrease in fundus autofluorescence in the region of the *area centralis* and extending along the visual streak in the 6.5- and 10-years of age affected cats. The 10.3-years of age affected cat showed a more severe lesion with a complete lack of fundus autofluorescence in the *area centralis*.
High resolution cross-section SD-OCT images of the dorsal (Sup Mid-Periphery) and *area centralis* regions. SD-OCT images showed a lack discernible ellipsoid and interdigitation zones from as early as 6-weeks of age. They showed initially a thinning of the outer retina with apparent absence of the outer nuclear layer from 9-months of age. The inner retina initially thickened then thinned in the late stages disease progression. The disease progression started earlier the *area centralis* (as early as 6 weeks of age).

Measurements of the different outer and inner retina layers and total retina showed significant changes in thicknesses in all regions of the retina of the *Crx*$^{Rdy/+}$ cat during the disease progression (Fig. 3.3 and Appendix K – Fig. 3.2). The changes were similar in all regions but more marked in the *area centralis*. As shown in chapter 2, the Receptor+ (REC+) and the outer nuclear layer (ONL) layer, which is part of the REC+, show severe thinning from an early age (as early as 6 weeks of age in the *area centralis* and 10/12 weeks of age in the other regions). For example, the thickness of the REC+ layer was 29.0 ± 8.2 µm in the *area centralis* of the *Crx*$^{Rdy/+}$ cat at 1 year of age compared to 125.3 ± 9.3 µm in WT controls. The total retina (TR) underwent also severe thinning but not until after 26 weeks of age. At 1 year of age, the TR thickness in the dorsal region of the *Crx*$^{Rdy/+}$ cat was 161.5 ± 15.0 µm compared to 197.9 ± 3.7 µm in the WT cat. The inner retina (IR) as well as the individual layers it includes (inner nuclear layer; INL, ganglion cell complex; GCC) became thickened after 20 to 26 weeks of age and this peaked at around 1 year of age. After 2 years of age the IR thinned as part of the severe generalized retinal degeneration (Fig. 3.3 and Appendix K – Fig. 3.2). For example at 1 year of age, the IR thickness in the dorsal region of the *Crx*$^{Rdy/+}$ cat was 132.1 ± 12.78 µm (while being 107.8 ± 7.9 µ at 10 weeks of age) compared to 78.7 ± 2.1 µm in the WT cat.

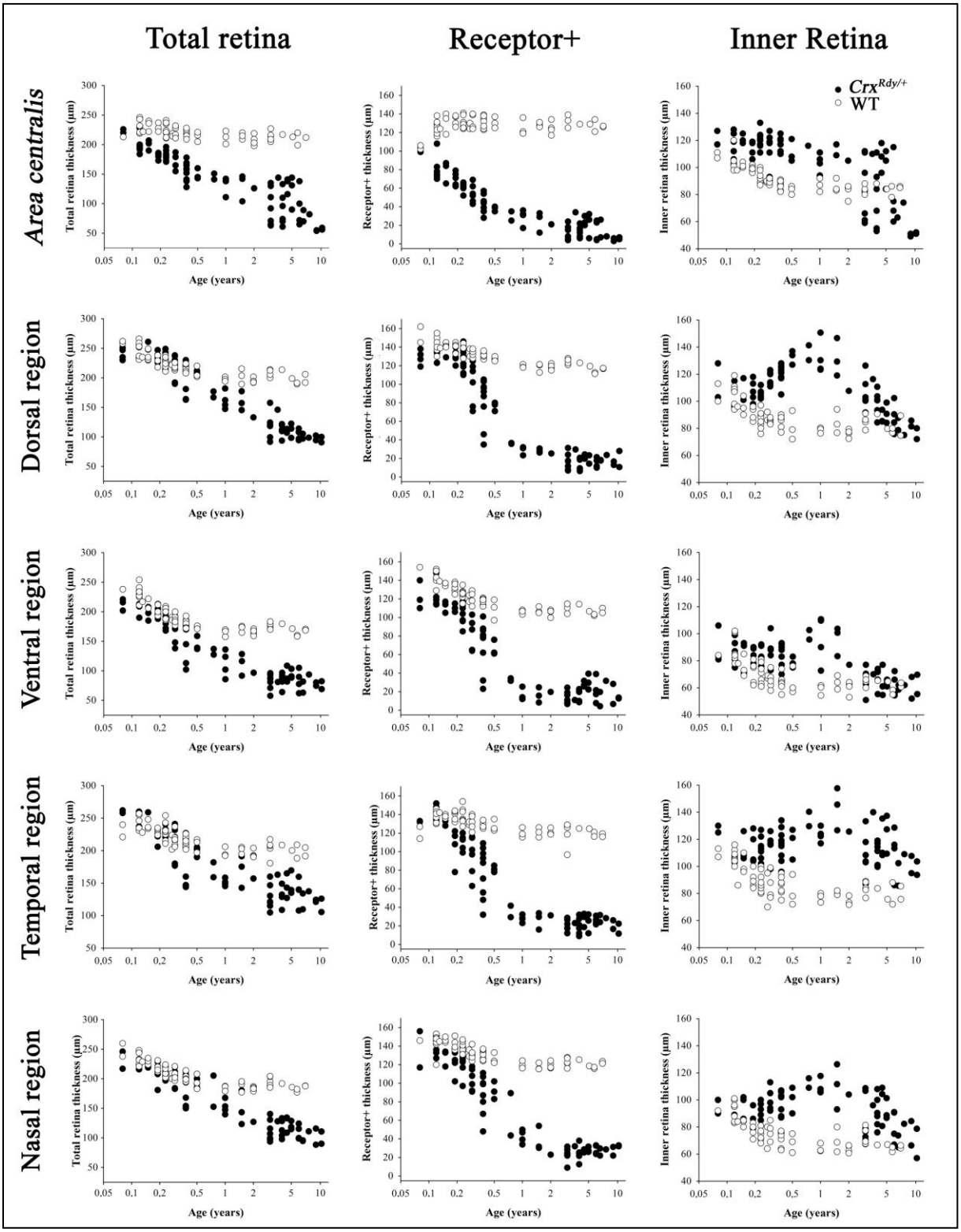

Figure 3.3. Total retina (TR), Receptor+ (REC+) and Inner retina (IR) thicknesses scatter plots from *Crx*$^{Rdy/+}$ and WT control cats from 4 weeks to 10.25 years of age.

Figure 3.3 (cont'd)
Measures were made on SD-OCT images from the *area centralis* region and from four optic nerve distance from the optic nerve rim itself dorsally, ventrally, temporally and nasally.
The TR and REC+ showed some severe thinning such that it became undiscernible with disease progression in the $Crx^{Rdy/+}$ cats. Interestingly, in the WT animals in all retinal areas except the *area centralis* the REC+, TR and REC+ thinned during the first year of age after which thickness remained similar for the duration of the study.
In the $Crx^{Rdy/+}$ the IR thickened in all regions (except for the GCC layer in the *area centralis*) with a peak around 1 to 2 years of age then thinned with the disease progression.

In order to further evaluation the changes in retinal cellular layers, we evaluated the number of cell nuclei of each layer in each retinal region during the disease progression. There was a severe loss of ONL nuclei during the first 6 months of life. The INL did not have major changes. This was not proven statistically due to the n number of only one individual for most of the time points assessed. (Fig. 3.4 and Appendix L – Fig. 3.3B). For example, in the *area centralis* there was a decrease of ONL nuclei from 129 ± 7.2 at 6 weeks of age to 44.7 ± 6.0 at 9 months of age (over a 100 µm width). While it decreased from 270 ± 9.5 to 34 ± 2.6 in the dorsal Sup MP region.

As in he SD-OCT characteristics described above, for all regions there was a severe thinning of the retina could be seen in the $Crx^{Rdy/+}$ cat by 20 weeks of age. Abnormal photoreceptor IS/OS were seen as early as 6 weeks of age and by 20 weeks of age only stunted IS are seen. More extensive remodeling is seen from as early as 9 months of age where the different layers of nuclei start to show severe disorganization. The changes observed and layer thinning is more rapid in the *area centralis* region. It is to be noted that ganglion cells are well preserved during the disease progression. (Figs. 3.4A and 3.4C).

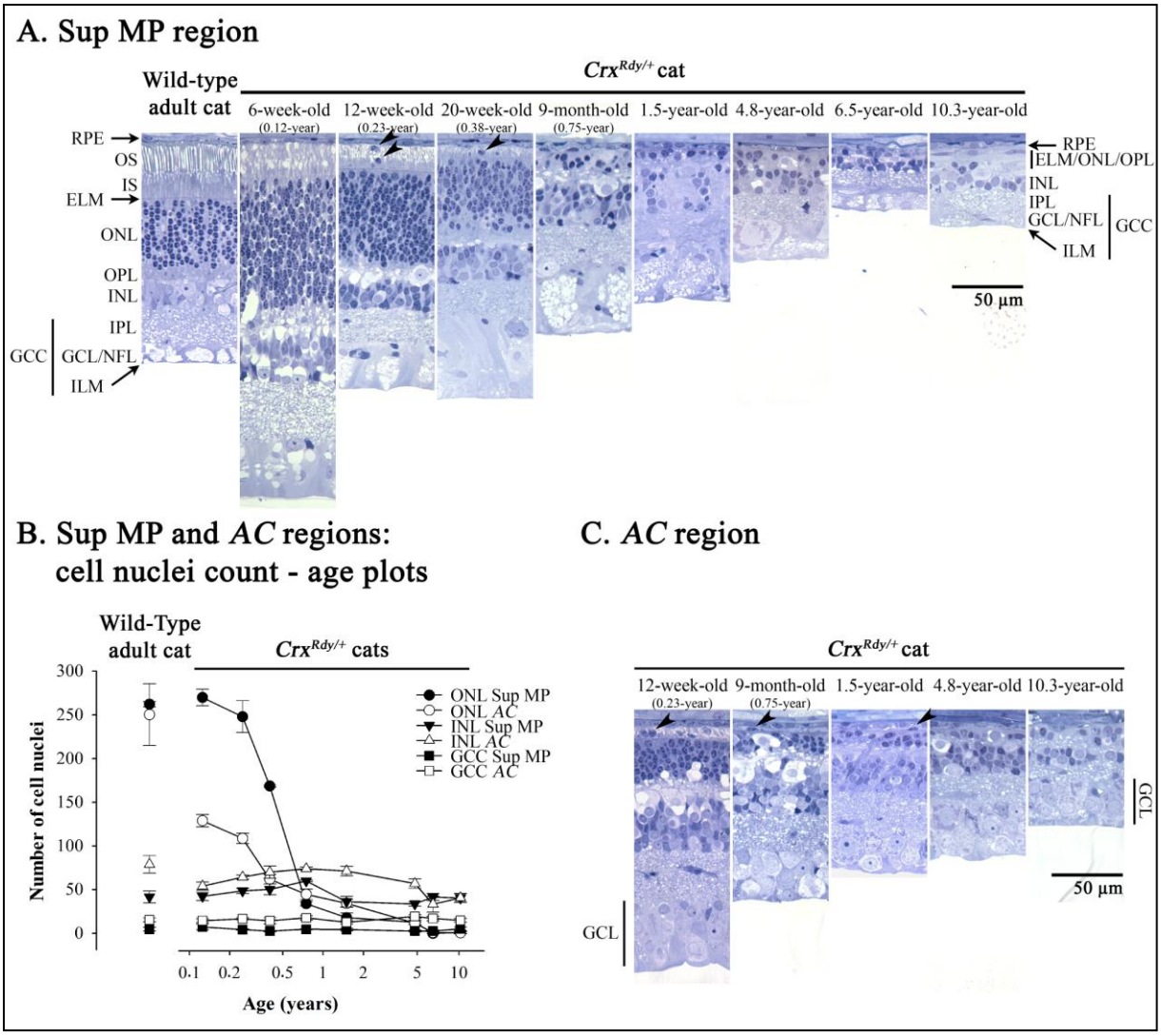

Figure 3.4. Histologic images from plastic sections from (A) the Superior Mid-Periphery (Sup MP) and (C) the *area centralis* regions and (B) their nuclei cell counts.

(A) Semithin histological sections from the SupMP periphery. With age, a severe thinning of the retina could be seen in the *Crx*$^{Rdy/+}$ cat by 20 weeks of age. Abnormal photoreceptor IS/OS were seen as early as 6 weeks of age and by 20 weeks of age only stunted IS are seen. In early age some ectopic nuclei are seen in the subretinal space (indicated by *black arrowheads*). More extensive remodeling is seen as early as 9 months of age where the different layers of nuclei start to show severe disorganization.

(B) Cell nuclei count of the ONL, INL and GCC in the Sup MP and *area centralis* regions (number of cell nuclei per 100 µm retinal section). Severe loss of nuclei was seen in both regions. The *area centralis* has a less number from the earliest age tested (6 weeks of age) then WT.

(C) Semithin histological sections from the *area centralis* region. The changes observed and layer thinning is more rapid than in (A). It is to be noted that ganglion cells are well preserved during the disease progression.

3.4.2. *Crx*$^{Rdy/+}$ cat retinas undergo marked retinal remodeling

To more precisely investigate the retinal changes, further histology, immunohistochemistry (IHC) and computational molecular phenotyping (CMP) were performed. They allowed characterization of the molecular and metabolic of the retinal remodeling during maturation and adulthood in the *Crx*$^{Rdy/+}$ cat.

As on SD-OCT and histology, IHC and thin sections for CMP showed a significant retinal thinning over time with the outer nuclear layer (ONL) being the first to thin then at a later stage the inner retina also thinned. On IHC, as reported in chapter 2[10], cone human arrestin (hCAR) labeling was not present after 12 weeks of age. Labeling with a S-cone opsin antibody was never detectable. ML-cones detectable by IHC showed opsin mislocalization to the photoreceptor inner segments and cell bodies (Fig. 3.5). Rods photoreceptors were identified by both IHC and CMP and similarly to ML-cones developed some rhodopsin mislocalization to the inner segments (IS) and cell bodies from as early as 6 weeks of age. Immunolabeling for rhodopsin was not detected in older animals (Figs. 3.5 and 3.6). IHC did show some ML-opsin labeling mislocalization to the inner segment and ONL which disappear with the disease. CMP did not detect it. Some migration of rod bipolar cells to the ONL was detected and there was extensive Müller cell activation (Fig. 3.5B). Glutamate and aspartate CMP labeling was present in most cells except Müller cells which showed an increased activation with development of glial seals and columns (Fig. 3.6). There was migration of inner retinal cells towards both the outer retina and the ganglion cell layer as demonstrated by CMP GABA labeling of the horizontal cells, bipolar and amacrine cells and calbindin and PKCα IHC labeling. Taurine labeling showed the loss of inner-outer photoreceptor segments and that most cells remaining had an inner retinal origin. CRALBP labeling was decreased from an early age. Interestingly, labeling with NeuN, a marker for neuronal cells, was increased in the *Crx*$^{Rdy/+}$ cat.

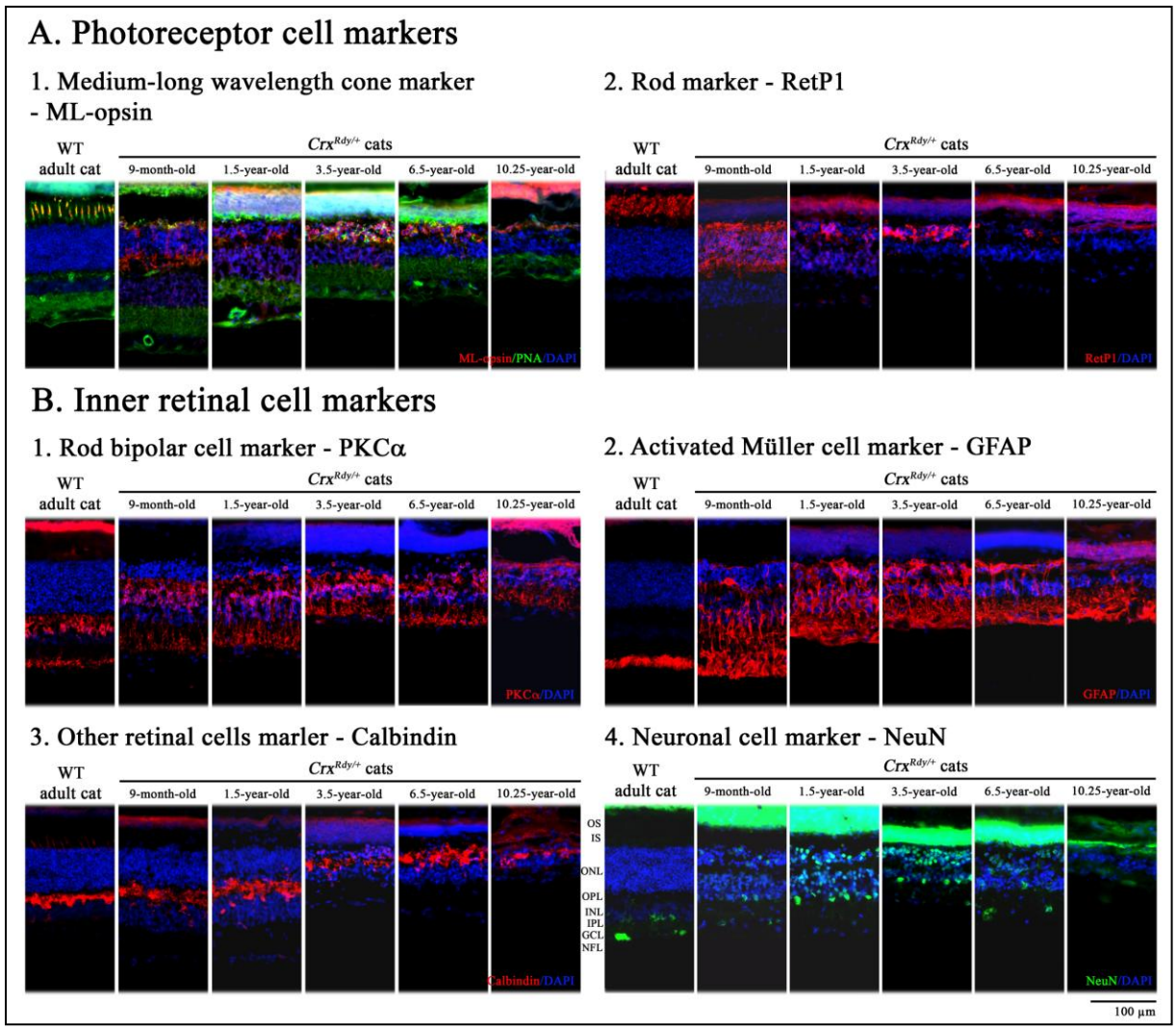

Figure 3.5. Immunohistochemisty during disease progression in the *Crx*$^{Rdy/+}$ cat.
(A) Photorceptor cell markers. 1. ML-opsin was mislocalized to the ONL initially and then not detectable (only background is detectable). 2. Rhodopsin was similarly mislocalized to the ONL and was detectable in the ONL up to 6.5 year of age.
(B) Inner retinal cell markers. 1. Rod bipolar cells were present in the *Crx*$^{Rdy/+}$ cat until later in disease progression. However, with disease progression some of their nuclei migrate to the outer retina starting at 1.5 years of age. Age at which, it is noticed that their dendrites are retracted and quasi absent. **2. Müller cells** are highly activated and from an early age they invaded the ONL towards the subretinal space. **3. Calbindin labeling** of the inner retinal cells showed some moderate changes in normal staining sign of remodeling. Contrarily of that in the WT control (very faint), no staining of cone photoreceptor was noted. **4. NeuN labeling** showed some abnormal localization to the ONL and a more prominent labeling of the INL nuclei than normal.

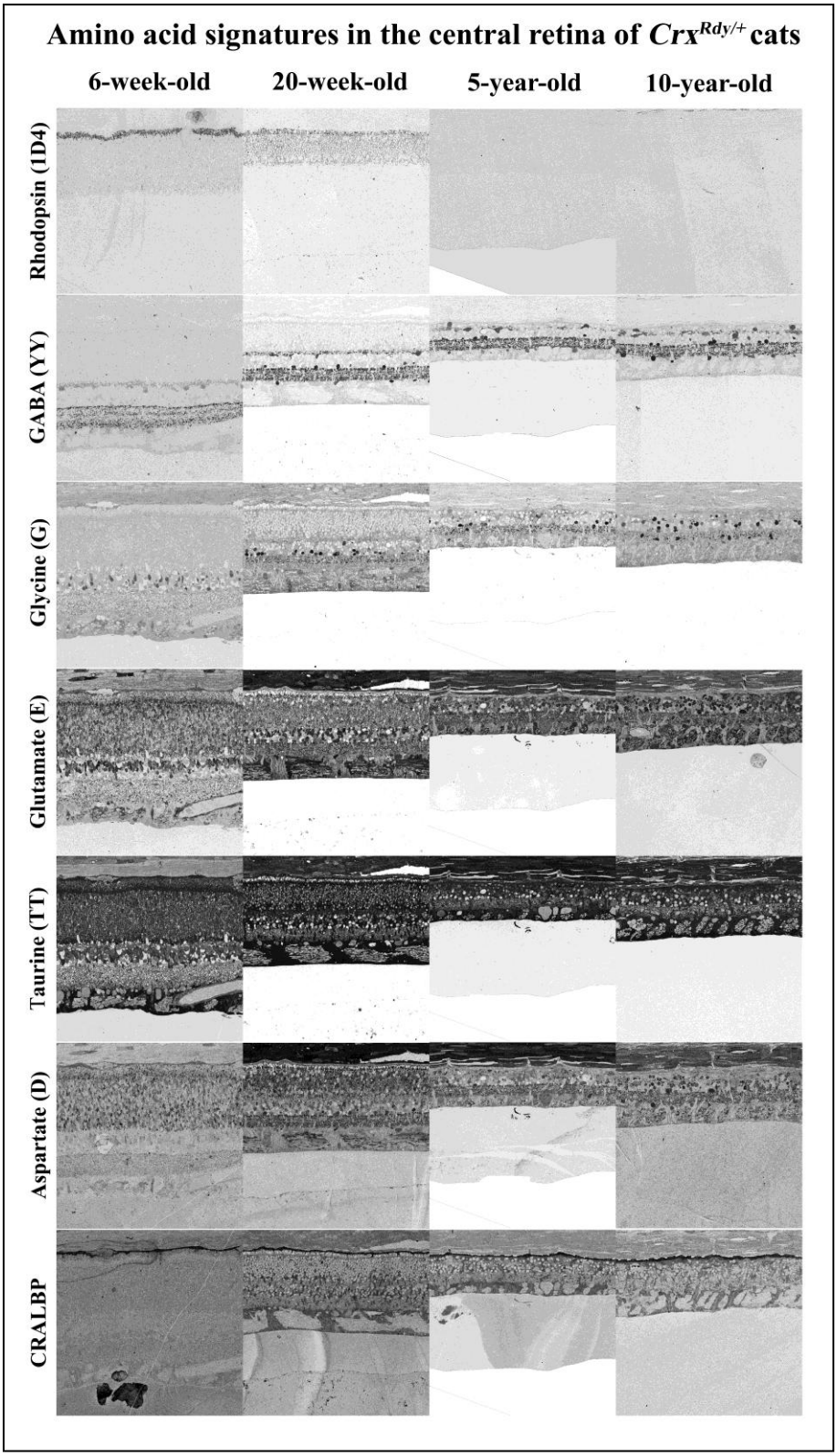

Figure 3.6. Retinal amino acid signatures in a 6-week, 20-week, 5-year and 10-year-old *Crx*$^{Rdy/+}$ cats. Serial 200 nm sections in the superior mid-periphery (SupMP; central retina).

Figure 3.6 (cont'd)
There was significant retinal thinning over time, with some individual variation at later ages. The outer nuclear layer was the first to thin then the inner retina. **Rhodopsin** labeling decreased with age and became extensively mislocalized to the photoreceptor inner segments and rod somas, then disappeared at ~5 years of age. **GABA** labeling the horizontal cells, bipolar and amacrine cells showed migration of inner retinal cells towards the outer retina and the ganglion cell layer. **Glutamate** and **aspartate** labeling was present in most cells except Müller cells which showed an increased activation with development of glial seals and columns. **Taurine** labeling showed the loss of inner-outer photoreceptor segments and that most cells remaining had an inner retinal origin. **CRALBP** labeling was decreased from an early age.

TQE and YGE mapping on thin sections as well as examination of semithin histologic sections showed major remodeling with migration of inner retina cells into the outer retina through some migration column. Remodeling of inner retinal cells led to formation of microneuroma forming abnormal connection between cells. Retinal pigmentary epithelium atrophy is also noticeable on many sections (Fig. 3.7).

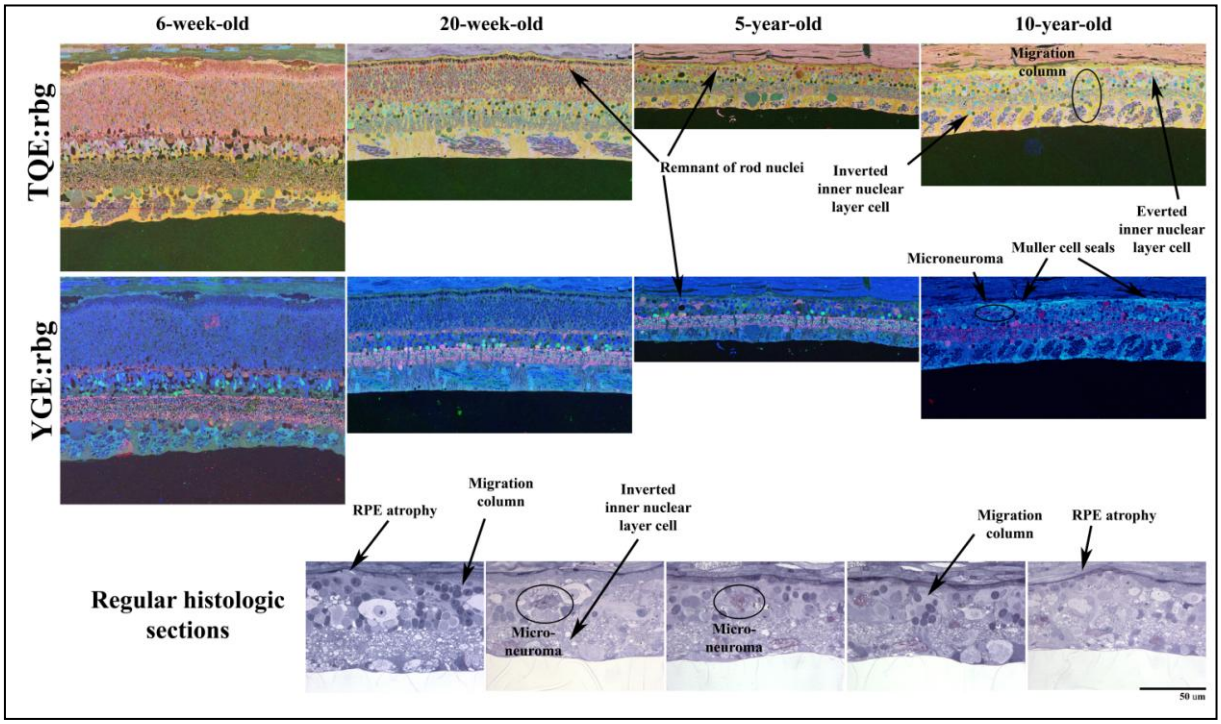

Figure 3.7. TQE and YGE CMP mapping and semithin histologic sections in the *Crx*$^{Rdy/+}$ cat at different ages in the superior mid-periphery area (central retina) and 1 µm histologic semithin sections epoxy-stained from in a dorso-central retinal samples (from 5- and 10-year-old animals).

Figure 3.7 (cont'd)
This figure displays the different stages of degeneration and remodeling with loss of photoreceptor outer and inner segments then death followed by Müller cell activation then hypertrophy. With disease progression, migration columns appeared, inverted and everted inner nuclear cells as well as microneuromas and RPE atrophy.

3.4.3. *Crx*$^{Rdy/+}$ cat retinas undergo marked retinal vasculature remodeling

To further investigate the vascular changes seen on fundus imaging, fluorescein angiography was performed and IHC flatmounts prepared. As age increased, the retina became increasing thin seen by an increase of tapetal hyperreflectivity (Fig. 3.8A). Fundus images showed a loss in retinal vasculature definition as early as 26 weeks of age and severe vascular attenuation was present by one year of age. As indicated previously, fundus images also showed hyporeflective changes in the *area centralis*.

Fluorescein angiography showed a severe loss of peripheral vessels, which worsened with disease progression. Disappearance of the peripheral and ventral vasculature was seen first. Additionally, an interesting feature was noted; some arterio-venous shunts developed in the peripheral *Crx*$^{Rdy/+}$ cat fundus. These became more prominent with age. These appeared as vascular loops and were most readily detected at the periphery of the remaining vasculature (Fig. 3.8A). Investigation of the remaining vasculature was performed in 3 adult cats (3.5, 4.7 and 6.5 years of age) by flatmounting and immunolabeling their retina (Fig. 3.8B). The same features were seen as with the fluorescein angiography imaging. Isolectin GS-B4, a marker of perfused vessels[25, 26] (green), labeled the same pattern of vessels as seen on fluorescein angiography (see respectively Figs. 3.8A and 3.8B). Collagen IV, a marker of the vascular basement membrane[27], labeled all vessels present regardless of whether they were patent. All the vessels in the *Crx*$^{Rdy/+}$ cat were labeled by the Collagen IV antibody, although only the central vessels were perfused (as

seen labeling by isolectin GS-B4) and the shunts between patent vessels were also labeled. Additionally on close views, it was noted that the vessels from the *Crx*$^{Rdy/+}$ cat became more tortuous.

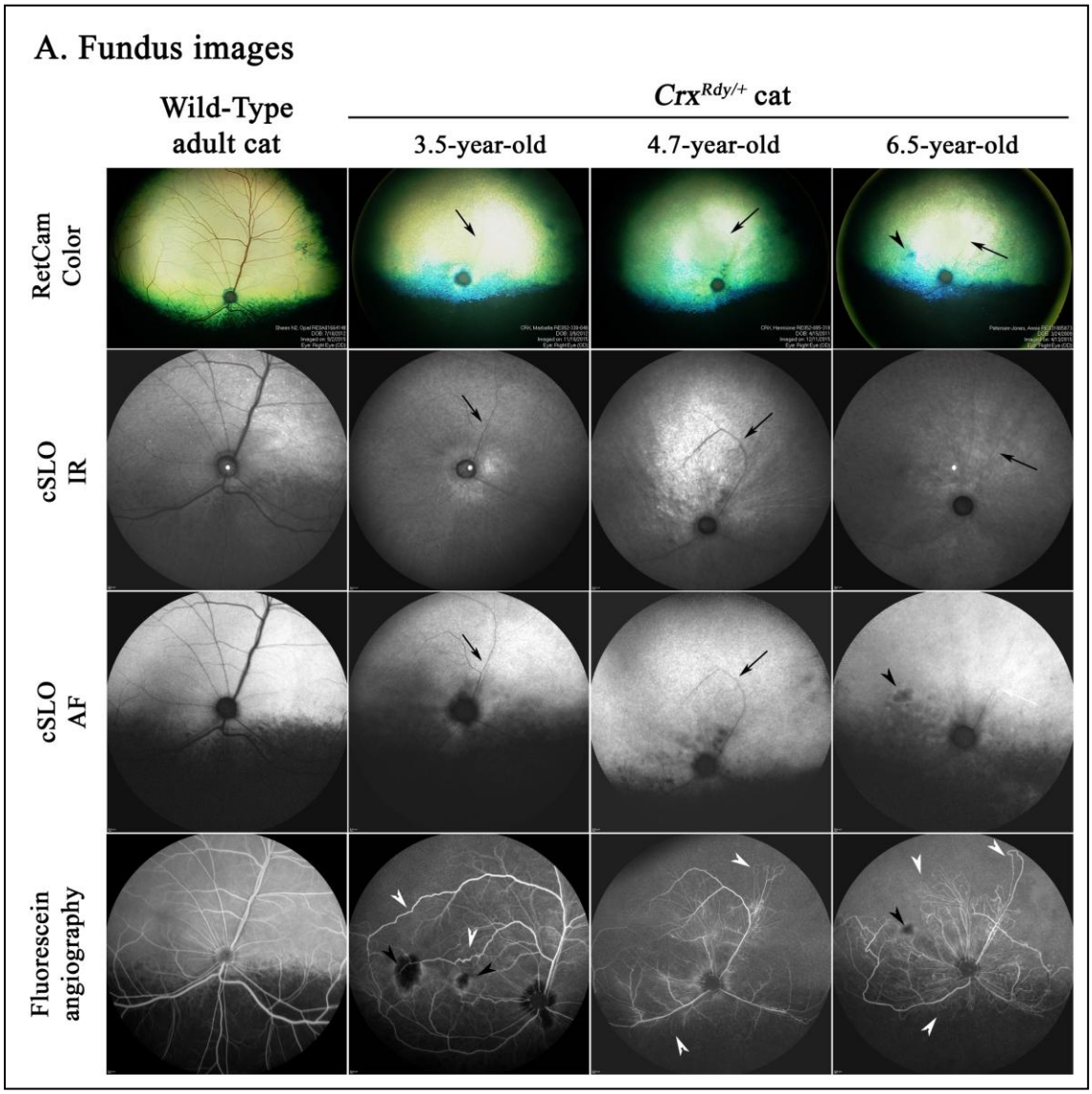

Figure 3.8. Retinal vascular remodeling in the *Crx*$^{Rdy/+}$ cat.
(A) Fundus images showing the generalized tapetal hyperflectivity on color images. On all images thinning of the vasculature is seen (indicated by the *black arrows*). In both the 3.5- and 6.5-year-old an *area centralis* lesion is seen (indicated by the *black arrowheads*). On fluorescein angiography this lesion has a lack of fluorescence. On fluorescein angiography, generalized retinal vasculature atrophy is noted especially in the periphery and ventrally. Arterio-venous shunts are present especially at the edges of the vasculature. These shunts can be tortuous. (IR; infrared, AF, autofluorescence)

Figure 3.8 (cont'd)

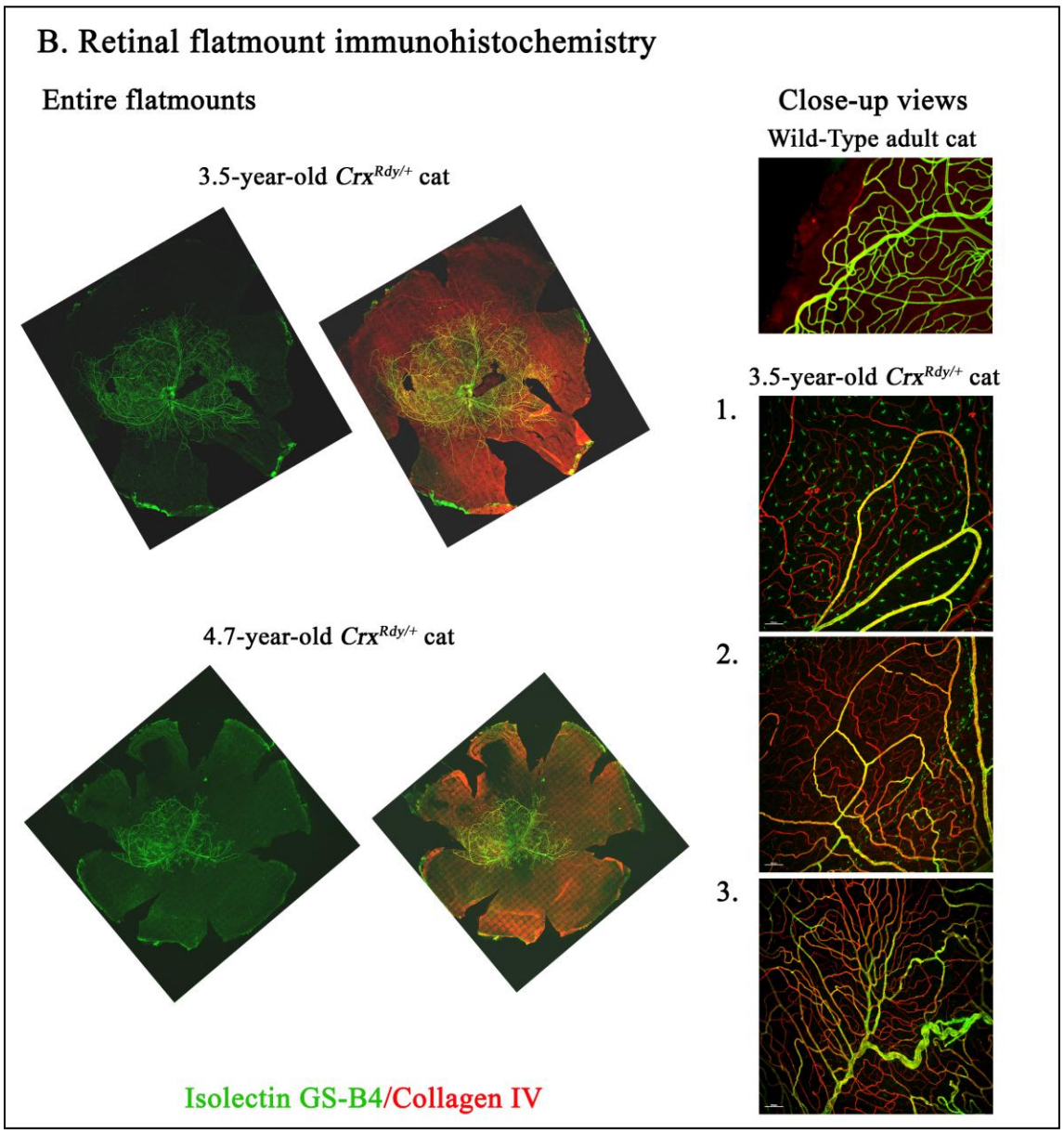

(B) Retinal flatmounts. Perfused vessels on the center of the retina as seen on fluorescein angiography are also detected by labeling with isolectin GS-B4 which also labeled microglia (green stars on close-up views)[28]. In the peripheral retina, vessels were present but not patent as detected by anti-collagen IV antibody. Compared to the WT retina, we noticed arterio-venous shunts (1, 2 and 3)and disappearance of small secondary vessels. Some of the remaining functional vessels had a tortuous appearance pattern (2 and 3).

3.4.4. *Crx*$^{Rdy/+}$ cat present with severe *area centralis* retinal pigmentary epithelium degeneration

Additional to the generalized retinal remodeling, a focal lesion was detected on both color and autofluorescence fundus imaging (Fig. 3.2). This could also be seen during fluorescein angiography (Fig. 3.8A) as a dark lesion lacking fluorescence in the early filling phase followed by some secondary fluorescence in the later phases. As described above, the lesion seems to initially be characterized by a slight sometimes bluish fundus color changes then a darker lesion in the region of the *area centralis* (extending along the visual streak in one cat). On FAF, the lesion is seen as a loss of AF then a complete absence of AF. When further investigating it, it was found to correspond to a loss of retinal pigmentary epithelium (RPE) on both SD-OCT high resolution cross sectional imaging and on IHC (Fig. 3.9). Analysis of the SD-OCT as well as histologic and IHC sections within the area of degeneration some islands of remaining RPE cells are present and some hypertrophy can be present in those areas and at the edge of the lesion (Fig. 3.9 shows hyperfluorescent spots of fluorescein angiography (A), thicker RPE and REC+ on color thicknesses map B1 and SD-OCT (B2) and seen on histologic (B3) and IHC (B4) sections).

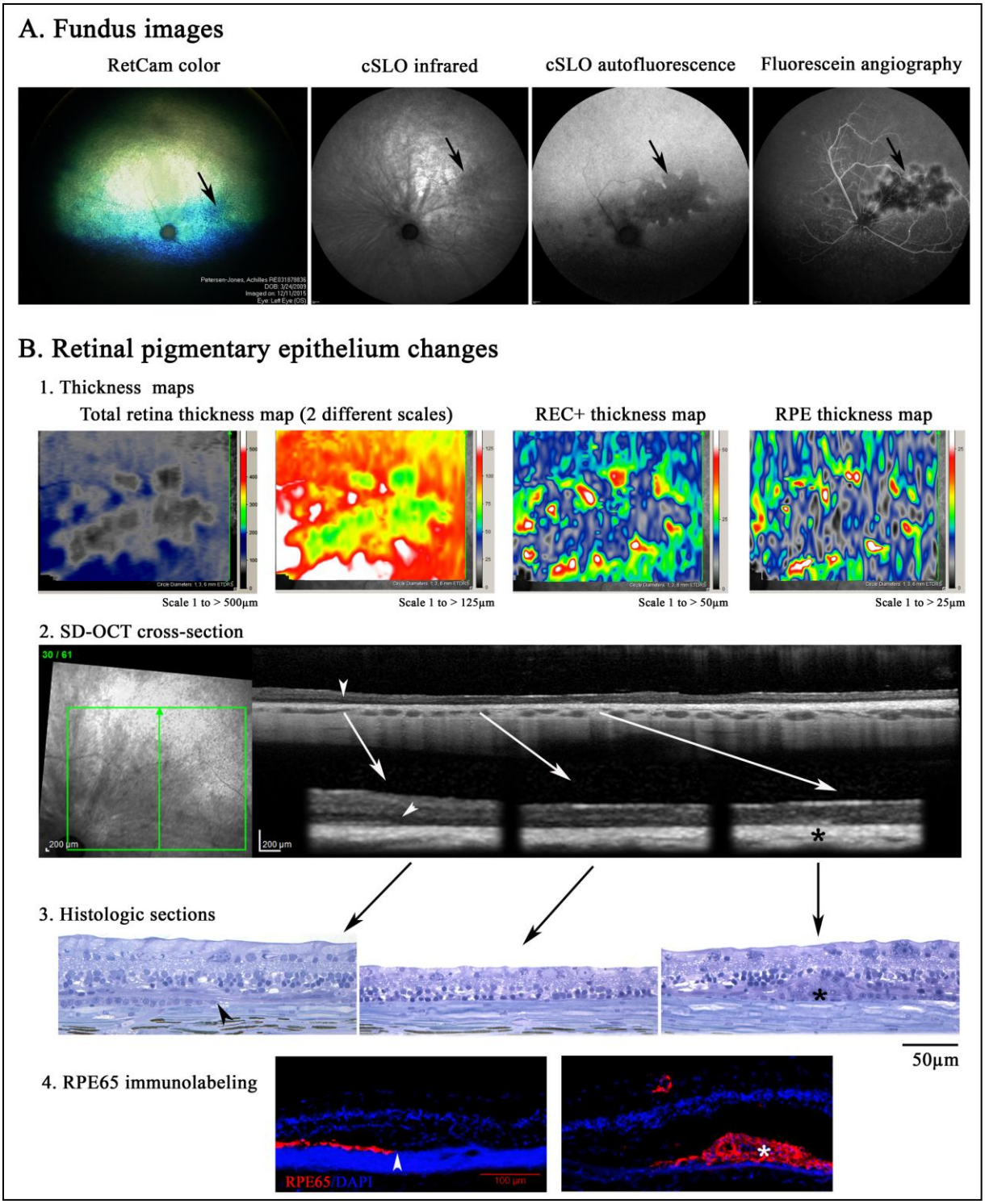

Figure 3.9. *Area centralis* lesion in a 6.5-year-old *Crx*$^{Rdy/+}$ cat.
(A) Fundus images indicating the lesion in the *area centralis* (black arrows). The lesion has has a bluish appearance on the color fundus images, darker appearance on IR cSLO and shows some loss of autofluorescence on FAF. Fluorescein angiography shows some lack of fluorescence in the region of the *area centralis* and its surroundings.

Figure 3.9 (cont'd)
(B) Retinal epithelium pigmentary changes.
1. Thickness maps in the area of the lesion show some full thickness thinning but also of the REC+. Interesting the RPE layer is thinned but some thinned spots (green to red color are seen in the edges of the lesion. Those corresponded on retinal cross sections (**2**) to an RPE thickening (right panel), seen as RPE cells proliferation on histologic and immunolabeled sections (**2**,**3,4**: *black* and *white stars*). The center of the lesion is thin and has a lack of RPE layer (central panels; **3,4**). The region where the integrity of the RPE stops can be seen on SD-OCT, histologic section and IHC (*white* and *black arrows*; left panels; **2,3,4**)

3.4.5. Other findings in individual *Crx*$^{Rdy/+}$ cats

Additionally to the lesions described above, individual cats presented with the following lesions. Very old cats presented some retinal holes in their ventral retina due to the extreme degeneration. This could be seen either by fundus examination (fundus images) or SD-OCT retinal cross-section (Fig. 3.10). However in some areas cells accumulations of cells could be detected on SD-OCT and CMP histology. Small areas of retinal detachments could be seen next to the *area centralis* degeneration in SD-OCT imaging. One cat presented with retinoschisis in its ventral non-tapetal retinal region (Fig. 3.10)

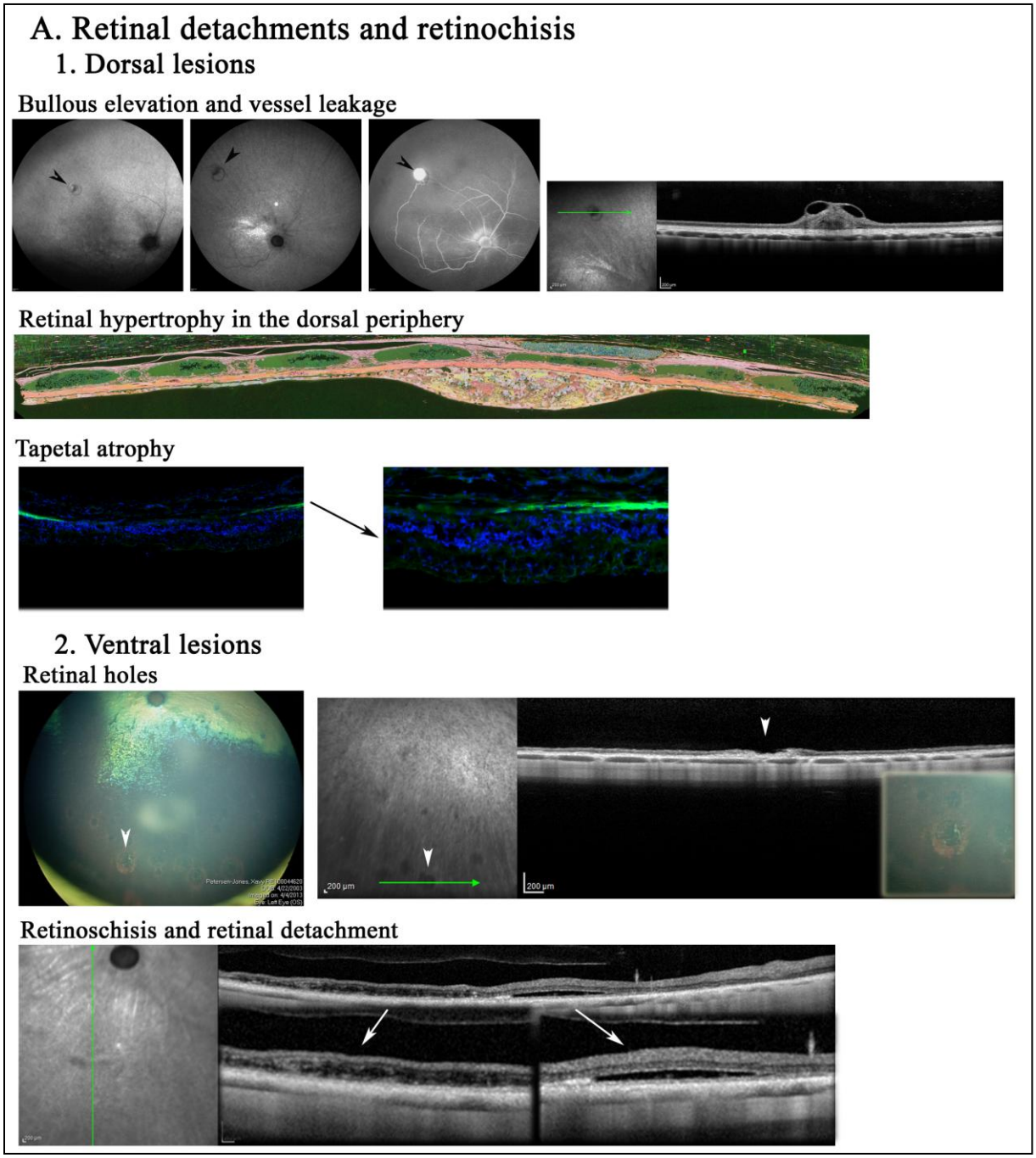

Figure 3.10. Additional lesions observed in the *Crx*$^{Rdy/+}$ cat.
(A) Dorsal lesions were seen as bullous elevation of the retina (*black arrowheads*) with internal limiting membrane detachments. Some retinal hypertrophy was noticed in the far dorsal periphery and some tapetal atrophy was randomly found (seen as a lack of tapetal autofluorescence on IHC).
(B) Ventral lesions included presence of retinal holes (*white arrowheads*) in very advanced degeneration cases and one cat presented with bilateral retinoschisis (*white arrow* left panel) and retinal detachments (*white arrow* right panel).

3.5. DISCUSSION

This study expands on previous studies showing that the *Crx*$^{Rdy/+}$ cat has a severe, early onset, dominantly inherited, retinal degeneration.[7-10, 29] No functional evaluation was performed in this study as no ERG responses have been detectable after 20 weeks of age in the *Crx*$^{Rdy/+}$ cat.[9, 10]

The *Crx*$^{Rdy/+}$ cat showed a severe retinal degeneration involving first the outer retina layer which thinned. Due to a compensatory remodeling mechanism, the total retina thickness is initially preserved until 6 months of age after which it also decreased. Concomitantly extensive remodeling developed. The *Crx*$^{Rdy/+}$ cat showed similar remodeling as previously described in other inherited retinal dystrophies. Retinal degeneration and remodeling in the cone-rod dystrophy *CRX*-LCA feline model follows the 3 previously described phases of retinal remodeling.[13, 17, 18] In this model, cones degenerate first followed by rods then the rest of the retina which is in contrast to typical retinitis pigmentosa in humans in which the peripheral retina progresses into phases 1-3 before the central retina and fovea does. During the first phase, the photoreceptors undergo stress and in the case of the *Crx*$^{Rdy/+}$ cat incomplete development then death and degeneration with the start of second phase of remodeling. During the second phase, the Müller cell are activated and lead to formation of glia seals accompanied by hypertrophy and extension of horizontal cell neurites and bipolar cell dendrite retraction. During the third phase, the neuronal retina remodels. During that phase, the glial seal becomes fibrotic and Müller cell hypertrophic. Neuronal cells start dying and microneuromas start to form. This worsens at the end of the remodeling. In the *Crx*$^{Rdy/+}$ cat, the first phase occurs during the first few weeks of age. The second phase is also rapid; occurring over the first months of age. By 1.5-years of age, the inner retina is severely affected and by 5-years of age severe neuronal remodeling has developed.

.

Further immunohistochemistry and molecular investigations to precise the remodeling mechanism with synapses labeling for example would help to further characterize the changes. It would also be of value to further investigate changes in melanopsin expressing ganglion cells both functionally by chromatic pupillometry and also morphologically by IHC.[30, 31] The NeuN labeling showed good preservation of ganglion cells until very late in the disease progression therefore investigating ganglion cells as potential target for optogenetic treatment would be of value.

During advanced stages of the disease the *Crx*$^{Rdy/+}$ cat develops a severe lesion in the *area centralis* region characterized by retinal pigmentary epithelium degeneration. The lesion was shown to be caused by a loss of the RPE cells starting from the edge of the lesion. Some islands of RPE hypertrophy were also seen. This lesion is similar to a lesion in humans with macular degeneration and further supports the fact that the cat is a comparable model to the human form of the disease. The mechanism of RPE degeneration in the macula-like region of the *Crx*$^{Rdy/+}$ cat warrants further investigation to determine the underlying causal factors and molecular mechanism. Also we need to investigate if it is a consequence of the dominant negative effect of the *Crx* mutant allele or due to the retinal degeneration and its molecular consequences.[32] The possibility that the *Crx*$^{Rdy/+}$ cat be a good model for RPE atrophy mechanistic studies in inherited disease or age macular degeneration is of importance.[33, 34]

Interestingly, the *Crx*$^{Rdy/+}$ cat presents severe vascular thinning with vascular remodeling leading to arterio-venous shunt formation. As with many models of retinal inherited dystrophies[35, 36], the *Crx*$^{Rdy/+}$ cat develops severe attenuation of retinal vasculature and loss of patent vasculature in the peripheral and ventral retina. Yet, the *Crx*$^{Rdy/+}$ cat present a very specific characteristic which have rarely been described in inherited disease[37, 38]. During the vascular degeneration, the retina vessels remained but were not perfused. The remaining vessels

developed some arterio-venous shunts and in some older animals the vessels became more tortuous. During fluorescein angiography the arterio-venous shunting could be seen as a direct communication between an artery and a vein without blood flow through a capillary bed. More investigation on the molecular mechanism underlying the arterio-venous shunt formation is necessary. The *Crx*$^{Rdy/+}$ cat could be an interesting model for vascular changes in human inherited disease but also for branch vein occlusion, retinal detachments or surgery induced vascular shunts.

This study showed that retinal degeneration in the *Crx*$^{Rdy/+}$ cat retina follows the 3 proposed phases of retinal remodeling. As early as 12 weeks of age, some glial reaction to photoreceptor death was observed followed by formation of a glial seal, rewiring and inner nuclear layer cell migration. Finally, microneuroma formation, severe retinal thinning and remodeling developed. Paralleling those characteristic, the RPE degeneration in the macula-like region of the cat and some vascular remodeling occurs quite early in the disease progression. These findings emphasize the importance of testing therapies like optogenetics or retinal transplant well before 1.5-years of age to ensure healthy neuronal environment at the time of treatment. Adding to the previous description of the *Crx*^{Rdy} phenotype (chapter 2) these findings provide baseline information for planned therapeutic interventions and evaluation. The *Crx*^{Rdy} cat is a valuable large animal model for studying the severe forms of Leber congential amaurosis due to *CRX* mutations but also retinal pigmentary atrophy and vascular arterio-venous shunts

3.6. ACKNOWLEDGEMENTS

The authors would like to thank Dr Bryan Jones for its help with CMP processing and analysis, Dr Alicia Withrow for her help with semithin sections, Hope Morrison for her help with thin sectioning and CMP processing, Dr Melinda Frame for her help with the flatmount images capture, Wenjuan Ma from MSU CSTAT for her help with statistical analysis, Dr Cheryl Craft for the donation of the hCAR antibody, Dr Debra Thompson for the donation of RPE65 antibody, Taylor Chamber for help with SD-OCT and cell counting measurements and Janice Querubin for help with animal anesthesia.

Supported by National Institutes Health Grants EY02576 (BWJ), EY015128 (BWJ), EY014800(BWJ), EY024234(BWJ), unrestricted funds from Research to Prevent Blindness (BWJ), Myers Dunlap Endowment (SMPJ), George H. Bird and "Casper" Endowment for Feline Initiatives (LMO and SMPJ), MSU Center for Feline Health and Well Being (LMO and SMPJ).

APPENDICES

APPENDIX J – Figure 3.S1

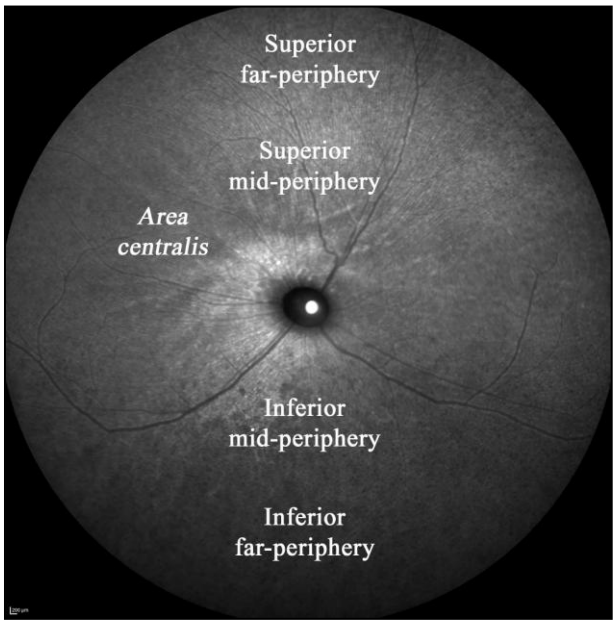

Figure 3.S1. Fundus areas sampled from 5 retinal areas were collected: *area centralis*, mid- and far-superior as well as mid and far-inferior regions.

APPENDIX K – Figure 3.S2

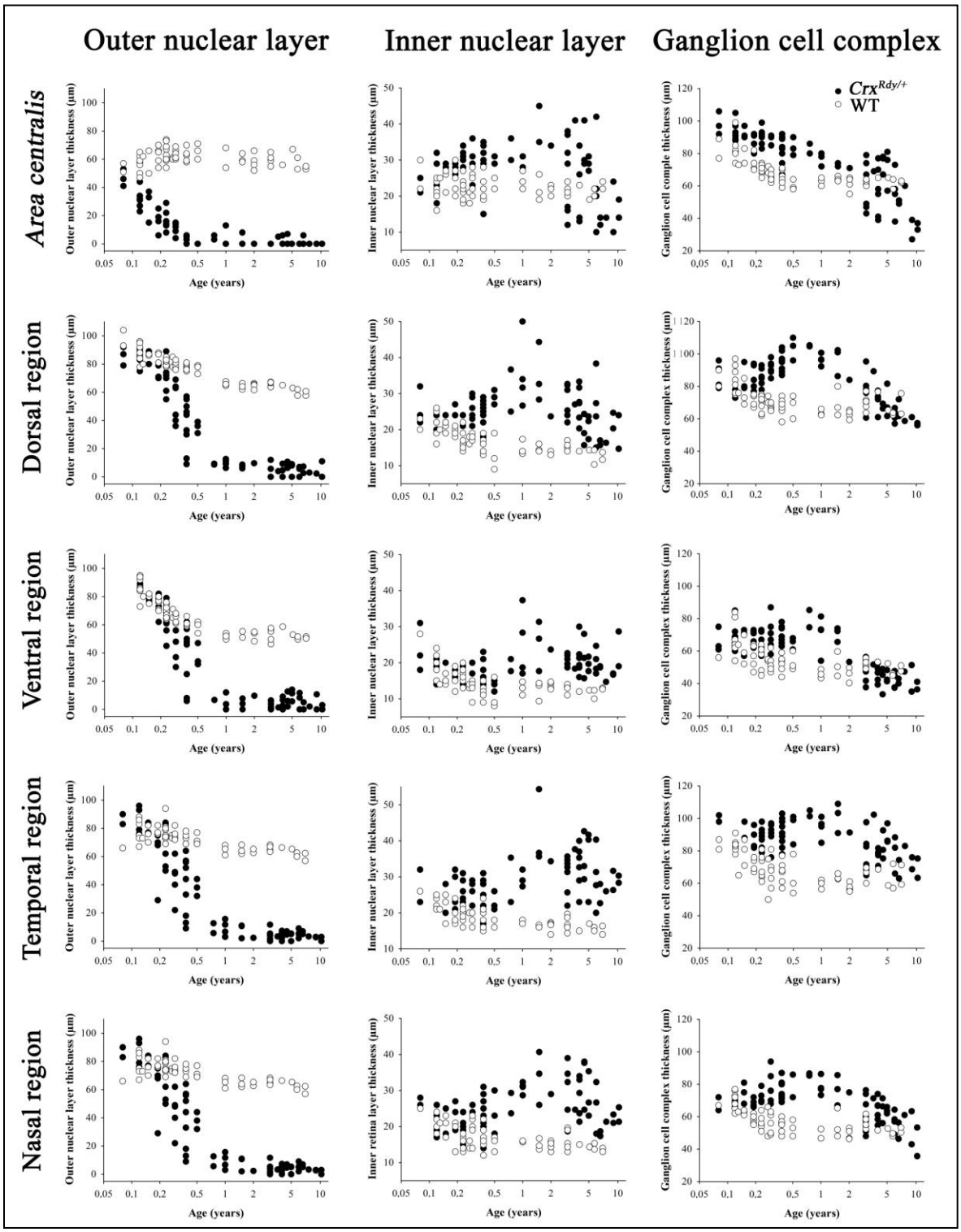

Figure 3.S2. Outer nuclear layer (ONL), inner nucler layer (INL) and ganglion cell complex (GCC) layer thicknesses scatter plots from *Crx*$^{Rdy/+}$ and WT control cats from 4 weeks to 10.25 years of age.

Figure 3.S2 (cont'd)
Measures were made on SD-OCT images from the *area centralis* region and from four optic nerve distance from the optic nerve rim itself dorsally, ventrally, temporally and nasally.
The ONL showed some severe thinning to be quasi inexistent with disease progression in the $Crx^{Rdy/+}$ cats. Interestingly, except in the *area centralis* the ONL in the WT controls thinned during maturation and then stabilized after a year of age.
The INL and GCC layers thickened in all regions (except for the GCC layer in the *area centralis*) with a peak around 0.5 to 2 years of age then thinned with the disease progression.

APPENDIX L – Figure 3.S3

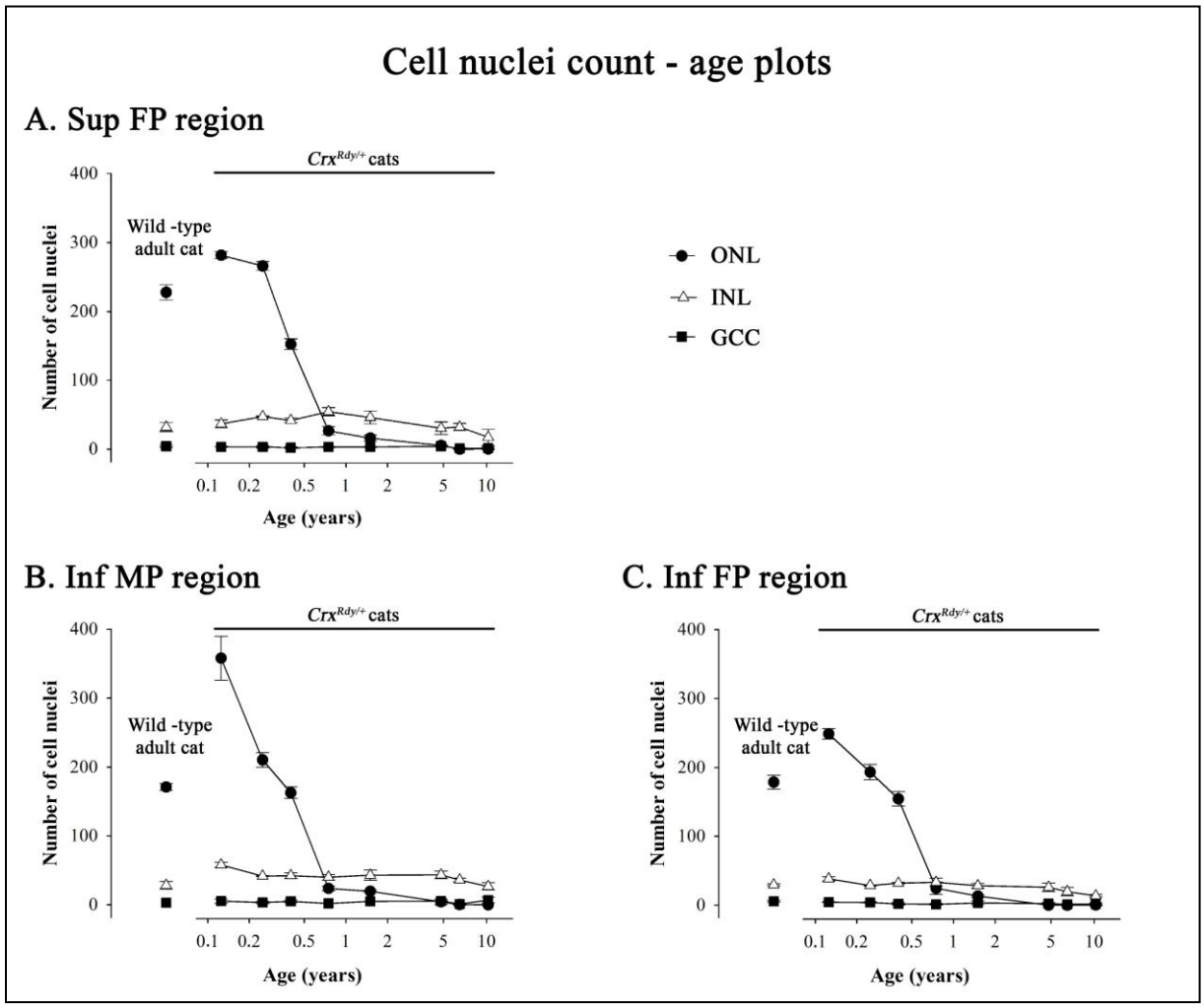

Figure 3.S3. Cell nuclei count of the ONL, INL and GCC from (A) the Superior Far-Periphery (Sup FP), (B) Inferior Mid-Periphery and (C) Inferior Far-Periphery.
In all regions, a severe ONL loss of nuclei is seen between 6 weeks and 9 months of age to be more subtle at a later age. Sight increase in INL number was seen in the SupFP.

APPENDIX M – Table 3.S1.

Age (years)	Age (weeks)	SD-OCT	SD-OCT WT	CMP Cell counting	Fluorescein angiography	IHC	Retinal flatmount
0.08	4	4	2				
0.12	6	6	7	1		3	
0.13	7		1				
0.15	8	3	3				
0.19	10	5	5				
0.23	12	8	8	1		4	
0.27	14		2				
0.29	15	6	5				
0.34	17.5					5	
0.38	20	9	7	1			
0.5	26	3	3				
0.58							
0.75		2		1		1	
1		4	3				
1.5		3	3	1	1	2	
2		1	4				
3		7	5		1		
3.5		1			1	1	1
4		6	1		1		
4.5		3		1	2	2	1
5		3	1		1	1	
6		4	2		3		
6.5		2		1	1	2	1
7			2				
7.5		1					
9		2					
10.25		2		2		1	
Total different animals							
		28	**27**	**9 + 1 WT**	**8 + 6 WT**	**22**	**3 + 1 WT**

Table 3.S1. Experimental numbers of *Crx*$^{Rdy/+}$ cats
Ages for adult SD-OCT, fluorescein angiography, IHC and flatmounts where approximate.

APPENDIX N – Table 3.S2.

Antibody – Source	Type	Primary Dilution	Secondary Antibody – Source	Secondary Dilution
hCAR (Human cone arrestin) Dr. Cheryl Craft; LUMIJ, University of Southern California, Los Angeles, CA, USA	Polyclonal rabbit	1:10,000	Alexa Fluor 488 Goat anti-rabbit IgG Life technologies, Carlsbad, CA, USA	1:500
PNA (Biotinylated Peanut Agglutinin) Vector Labs Inc., Burlin-game, CA, USA	Biotinylated Lectin	1:500	Alexa Fluor 488 Streptavadin Life technologies, Carlsbad, CA, USA	1:500
ML-opsin (Anti-Opsin, Red/Green; Medium/ Long wavelength cone opsin) Millipore Corp., Billerica, MA, USA	Polyclonal rabbit	1:1,000	Alexa Fluor 568 or 594 Goat anti-rabbit IgG Life technologies, Carlsbad, CA, USA	1:500
S-opsin (Anti-Opsin, Blue; Short wavelength cone opsin) Millipore Corp., Billerica, MA, USA	Polyclonal rabbit	1:1,000	Alexa Fluor 568 or 594 Goat anti-rabbit IgG Life technologies, Carlsbad, CA, USA	1:500
RetP1 (Rhodopsin Ab-1) Thermo Scientific, Rockford, IL, USA	Monoclonal mouse	1:2	Alexa Fluor 594 Goat anti-mouse IgG Life technologies, Carlsbad, CA, USA	1:500
GFAP (Anti-Glial Fibrillary Acidic Protein) Cell Signaling Technology Inc., Danvers, MA, USA	Monoclonal mouse	1:300	Alexa Fluor 594 Rabbit anti-mouse IgG Life technologies, Carlsbad, CA, USA	1:500
PKCa (Protein Kinase C-alpha) BD Biosciences, San Jose, CA, USA	Monoclonal mouse	1:500	Alexa Fluor 594 Goat anti-mouse IgG Life technologies, Carlsbad, CA, USA	1:500
Calbindin Swant, Marly, Switzerland	Monoclonal mouse	1:500	Alexa Fluor 568 Goat anti-mouse IgG Life technologies, Carlsbad, CA, USA	1:500
NeuN (Neuron-Specific Nuclear Protein) Millipore Corp., Billerica, MA, USA	Monoclonal mouse	1:2,000	Alexa Fluor 488 Goat anti-mouse IgG Life technologies, Carlsbad, CA, USA	1:500
RPE65 (Retinal pigmentary epithelium-specific 65kDA protein) Dr. Debra Thompson; Kellogg eye center, University of Michigan, Ann Arbor, MI, USA	Monoclonal mouse	1:500	Alexa Fluor 568 Goat anti-mouse IgG Life technologies, Carlsbad, CA, USA	1:500

Table 3.S2. List of antibodies used for IHC – their origins and dilutions

REFERENCES

REFERENCES

1. Hennig AK, Peng GH, Chen S. Regulation of photoreceptor gene expression by Crx-associated transcription factor network. *Brain Res.* 2008;1192:114-133.

2. Furukawa T, Morrow EM, Cepko CL. Crx, a novel otx-like homeobox gene, shows photoreceptor-specific expression and regulates photoreceptor differentiation. *Cell.* 1997;91:531-541.

3. Sohocki MM, Sullivan LS, Mintz-Hittner HA, et al. A range of clinical phenotypes associated with mutations in CRX, a photoreceptor transcription-factor gene. *Am J Hum Genet.* 1998;63:1307-1315.

4. Hull S, Arno G, Plagnol V, et al. The phenotypic variability of retinal dystrophies associated with mutations in CRX, with report of a novel macular dystrophy phenotype. *Invest Ophthalmol Vis Sci.* 2014;55:6934-6944.

5. Menotti-Raymond M, Deckman KH, David V, Myrkalo J, O'Brien SJ, Narfström K. Mutation discovered in a feline model of human congenital retinal blinding disease. *Invest Ophthalmol Vis Sci.* 2010;51:2852-2859.

6. Tran NM, Chen SM. Mechanisms of Blindness: Animal Models Provide Insight Into Distinct CRX-Associated Retinopathies. *Dev Dyn.* 2014;243:1153-1166.

7. Curtis R, Barnett KC, Leon A. An early-onset retinal dystrophy with dominant inheritance in the Abyssinian cat. Clinical and pathological findings. *Invest Ophthalmol Vis Sci.* 1987;28:131-139.

8. Leon A, Curtis R. Autosomal dominant rod-cone dysplasia in the Rdy cat. 1. Light and electron microscopic findings. *Exp Eye Res.* 1990;51:361-381.

9. Leon A, Hussain AA, Curtis R. Autosomal dominant rod-cone dysplasia in the Rdy cat. 2. Electrophysiological findings. *Exp Eye Res.* 1991;53:489-502.

10. Occelli LM, Tran NM, Narfstrom K, Chen S, Petersen-Jones SM. CrxRdy Cat: A Large Animal Model for CRX-Associated Leber Congenital Amaurosis. *Invest Ophthalmol Vis Sci.* 2016;57:3780-3792.

11. Marc RE, Jones BW, Watt CB, Strettoi E. Neural remodeling in retinal degeneration. *Prog Retin Eye Res.* 2003;22:607-655.

12. Marc RE, Jones BW. Retinal remodeling in inherited photoreceptor degenerations. *Mol Neurobiol.* 2003;28:139-147.

13. Jones BW, Watt CB, Frederick JM, et al. Retinal remodeling triggered by photoreceptor degenerations. *J Comp Neurol.* 2003;464:1-16.

14. Jones BW, Marc RE. Retinal remodeling during retinal degeneration. *Exp Eye Res* 2005;81:123-137.

15. Marc RE, Murry RF, Fisher SK, Linberg KA, Lewis GP, Kalloniatis M. Amino acid signatures in the normal cat retina. *Invest Ophthalmol Vis Sci.* 1998;39:1685-1693.

16. Marc RE, Murry RF, Fisher SK, Linberg KA, Lewis GP. Amino acid signatures in the detached cat retina. *Invest Ophthalmol Vis Sci.* 1998;39:1694-1702.

17. Jones BW, Pfeiffer RL, Ferrell WD, Watt CB, Marmor M, Marc RE. Retinal remodeling in human retinitis pigmentosa. *Exp Eye Res.* 2016;150:149-165.

18. Jones BW, Kondo M, Terasaki H, Lin Y, McCall M, Marc RE. Retinal remodeling. *Jpn J Ophthalmol.* 2012;56:289-306.

19. Hood DC, Lin CE, Lazow MA, Locke KG, Zhang X, Birch DG. Thickness of receptor and post-receptor retinal layers in patients with retinitis pigmentosa measured with frequency-domain optical coherence tomography. *Invest Ophthalmol Vis Sci.* 2009;50:2328-2336.

20. Mowat FM, Gornik KR, Dinculescu A, et al. Tyrosine capsid-mutant AAV vectors for gene delivery to the canine retina from a subretinal or intravitreal approach. *Gene Ther.* 2014;21:96-105.

21. Marc RE, Murry RF, Basinger SF. Pattern recognition of amino acid signatures in retinal neurons. *J Neurosci.* 1995;15:5106-5129.

22. Jones BW, Pfeiffer RL, Ferrell WD, Watt CB, Tucker J, Marc RE. Retinal Remodeling and Metabolic Alterations in Human AMD. *Front Cell Neurosci.* 2016;10:103.

23. Marc RE, Jones BW. Molecular phenotyping of retinal ganglion cells. *J Neurosci.* 2002;22:413-427.

24. RStudio Team (2015). RStudio: Integrated Development for R. RStudio I, Boston, MA URL http://www.rstudio.com/.

25. Ernst C, Christie BR. Isolectin-IB 4 as a vascular stain for the study of adult neurogenesis. *J Neurosci Methods.* 2006;150:138-142.

26. Walchli T, Mateos JM, Weinman O, et al. Quantitative assessment of angiogenesis, perfused blood vessels and endothelial tip cells in the postnatal mouse brain. *Nat Protoc.* 2015;10:53-74.

27. Kalluri R. Basement membranes: structure, assembly and role in tumour angiogenesis. *Nat Rev Cancer.* 2003;3:422-433.

28. Lehnardt S, Massillon L, Follett P, et al. Activation of innate immunity in the CNS triggers neurodegeneration through a Toll-like receptor 4-dependent pathway. *Proc Natl Acad Sci U S A.* 2003;100:8514-8519.

29. Chong NH, Alexander RA, Barnett KC, Bird AC, Luthert PJ. An immunohistochemical study of an autosomal dominant feline rod/cone dysplasia (Rdy cats). *Exp Eye Res.* 1999;68:51-57.

30. Yeh CY, Koehl KL, Harman CD, et al. Assessment of Rod, Cone, and Intrinsically Photosensitive Retinal Ganglion Cell Contributions to the Canine Chromatic Pupillary Response. *Invest Ophthalmol Vis Sci.* 2017;58:65-78.

31. Athanasiou D, Aguila M, Bevilacqua D, Novoselov SS, Parfitt DA, Cheetham ME. The cell stress machinery and retinal degeneration. *FEBS Lett.* 2013;587:2008-2017.

32. Veleri S, Lazar CH, Chang B, Sieving PA, Banin E, Swaroop A. Biology and therapy of inherited retinal degenerative disease: insights from mouse models. *Dis Model Mech.* 2015;8:109-129.

33. Green WR. Histopathology of age-related macular degeneration. *Mol Vis.* 1999;5:27.

34. Ramkumar HL, Zhang J, Chan CC. Retinal ultrastructure of murine models of dry age-related macular degeneration (AMD). *Prog Retin Eye Res.* 2010;29:169-190.

35. Blanks JC, Johnson LV. Vascular atrophy in the retinal degenerative rd mouse. *The J Comp Neurol.* 1986;254:543-553.

36. Winkler PA, Ekenstedt KJ, Occelli LM, et al. A large animal model for CNGB1 autosomal recessive retinitis pigmentosa. *PloS one.* 2013;8:e72229.

37. Abu el-Asrar AM, Kahtani ES, Tabbara KF. Retinal arteriovenous communication in retinitis pigmentosa with Refsum's disease-like findings. *Doc Ophthalmol.* 1995;89:313-320.

38. Mansour AM, Walsh JB, Henkind P. Arteriovenous anastomoses of the retina. *Ophthalmology* 1987;94:35-40.

CHAPTER 4

PHENOTYPIC CHARACTERIZATION OF CATS HOMOZYGOUS FOR A FRAMESHIFT MUTATION IN *CRX* (*CRX*$^{RDY/RDY}$)

4.1. ABSTRACT

PURPOSE. CRX is a transcription factor essential for normal photoreceptor development and survival. The *Rdy* cat has a spontaneous frameshift mutation in *Crx*. This type of mutation is similar to Class III C*RX* mutations that result in accumulation of mutant CRX protein, which has a dominant negative action. The heterozygous cat ($Crx^{Rdy/+}$) has early dysfunction and degeneration of photoreceptors mimicking the severe Leber congenital amaurosis phenotype. This study investigated the phenotype of the homozygous cat ($Crx^{Rdy/Rdy}$). **METHODS.** Functional and structural characteristics of the retina and the globe of the $Crx^{Rdy/Rdy}$ cats were investigated at various ages by ophthalmic examination, combined A-and B-mode ultrasound (US), intraocular pressure (IOP), refraction, electroretinography (ERG), spectral domain optical coherence tomography (SD-OCT) and histology. Molecular changes were assessed by quantitative reverse transcriptase-PCR (qRT-PCR, Western blot (WB) and immunohistochemistry (IHC). **RESULTS.** $Crx^{Rdy/Rdy}$ cats lacked vision and showed an absence of menace response and dazzle reflex. They also had a very decreased pupillary light reflex. Unlike the $Crx^{Rdy/+}$ cats, the $Crx^{Rdy/Rdy}$ cats did not exhibit nystagmus. The globe length was significantly greater than that of wild-type and $Crx^{Rdy/+}$ kittens, showing severe posterior segment myopia with no IOP increase when investigated at adulthood. Scotopic and photopic ERG responses were absent at all ages tested. $Crx^{Rdy/Rdy}$ cats developed tapetal hyperreflectivity detectable as early as 12 weeks of age, but there was no obvious retinal vasculature attenuation with disease progression. The features that represent the photoreceptor inner/outer segments (IS/OS) were not discernible on SD-OCT images from an early age. Histological examination showed that only very small photoreceptor inner segments formed; outer segments were never identified. Although the other retinal layers appeared relatively normal at 2 weeks of age, retinal stratification became increasingly abnormal with age. QRT-PCR in 2-week-old kittens revealed a

marked decrease in cone and rod opsin mRNA levels while that of *Crx* was elevated and the expression level of other transcription factors was also changed. WB revealed that the amount of mutant Crx present was greater than that of normal Crx protein in wild-type control retinas. **CONCLUSIONS.** The retina of the $Crx^{Rdy/Rdy}$ cat failed to fully mature resulting in congenital blindness. Also, abnormal globe growth with myopia occurred. Although relatively normal retinal stratification had developed at a very early age, lack of normal development of photoreceptor IS/OS was noted, and retinal layers became disorganized with disease progression. This was accompanied by decreased expression of rod and cone opsins and absence of photoreceptor function. The phenotype of the $Crx^{Rdy/Rdy}$ differs considerably from that of the $Crx^{Rdy/+}$ cat.

4.2. INTRODUCTION

Cone-rod homeobox (*CRX*) is an *OTX*-like homeobox gene encoding a transcription factor essential for normal photoreceptor development, function and survival.[1-3] Indeed, numerous genes necessary for the retinal functions such as genes coding for proteins involved in phototransduction or the visual cycle have a binding site for CRX in their promoter, and CRX also has a binding site on its own promoter.[4-9] In humans, *CRX* mutations result in a spectrum of typically dominant retinopathies with variable severity ranging from Leber congenital amaurosis (LCA7) to cone–rod dystrophy, retinitis pigmentosa and macular degeneration.[10, 11] LCA is the most severe form. LCA represents approximately 5% of all human inherited retinopathies with a prevalence of 1 in 30,000 to 81,000 newborns.[12, 13] *CRX* mutations accounts for approximately 2.35% of the cases of LCA.[14]

Mice models for CRX-retinopathies have been well described even though the precise mechanisms underlying the diseases need to be further elucidated (see review Tran et al., 2014).[9, 15] Among the available CRX-retinopathy models one large animal model exists: the Crx^{Rdy} cat. This cat model has a spontaneous frameshift mutation in *Crx* (single nucleotide deletion in exon 4 leading a truncated protein of 185 amino acids compared to 299 residues in the wild-type protein).[16] The position of the introduced premature stop codon is at an analogous site to several reported human mutations that most frequently result in an LCA phenotype and are classified as Class III *CRX* mutations. Those mutations are believed to be associated with an accumulation of mutant CRX protein which has a dominant negative action.[9, 15, 17, 18] The heterozygous cat ($Crx^{Rdy/+}$) has been described previously and presents with an LCA phenotype characterized by an early dysfunction and degeneration of photoreceptors. [16, 19, 20] There is over expression of the mutant *Crx* allele resulting in a higher level of Crx protein compared to wild-type cat's retina,

which has a dominant negative effect [17] and is similar to the phenotype of the Class III *E168d2* heterozygous mouse model.[15, 17]

Among the mice models for CRX-retinopathies, the phenotype of homozygous animals has been well described in the literature.[3, 9, 21-23] The Class III *E168d2/d2* homozygous mouse model has a similar yet more severe phenotype to the Class III *E168d2* heterozygous mouse. The *E168d2* homozygous mouse undergoes rapid photoreceptor degeneration, with absence of photoreceptor outer segments (OS) development and rapid loss of outer nuclear layer (onl) thickness. This mouse model lacked vision and did not have any recordable electroretinographic responses at any time point. The *E168d2/d2* homozygous mouse also has a more marked decrease in expression of certain retinal genes compared to the *E168d2* heterozygous mouse. These include cone arrestin, and cone and rod opsin.[9]

Based on the studies in the $Crx^{Rdy/+}$ cats and the homozygous *E168d2* mouse, we hypothesized that the phenotype of the homozygous cat will have a more severe phenotype than that of the heterozygote, with no photoreceptor development and a total absence of normal *Crx* mRNA/protein, but normal development of other cell types. We expect even higher levels of mutant Crx mRNA and protein. Even though there is a very low incidence of humans homozygous for *CRX* mutations, the study of the homozygous cat and its comparison with the mice models may give a valuable insight into the dominant negative mutation mechanism or help to guide therapeutic interventions. The purpose of this study was to investigate the functional, morphological and molecular phenotype of the Class III *Crx* mutant homozygous cat ($Crx^{Rdy/Rdy}$).

4.3. MATERIALS AND METHODS

4.3.1. Ethics statement

All procedures were performed in accordance with the ARVO statement for the Use of Animals in Ophthalmic and Vision Research and approved by the Michigan State University Institutional Animal Care and Use Committee.

4.3.2. Animals

A colony of *Crx*^{Rdy} cats maintained at Michigan State University was used for this study and bred to obtain homozygote affected (*Crx*$^{Rdy/Rdy}$), heterozygote affected (*Crx*$^{Rdy/+}$) kittens and wild-type (WT) control cats. Animals were housed under 12D:12L cycles during breeding and 14D:10L the rest of the time. They were fed a commercial feline dry diet (Purina One Smartblend and Purina Kitten Chow; Nestlé Purina, St Louis, MO. USA). Animals studied ranged from 4 weeks to 6 years of age. For n numbers used in the different experiments, please refer to Appendices X, Y, and Z – Tables 4.S1, 4.S2 and 4.S3.

4.3.3. Ophthalmic examination and fundus imaging

At each time point assessed, kittens underwent a full ophthalmic examination including indirect ophthalmoscopy and capture of digital wide-field color fundus images (Ret-Cam II, Clarity Medical Systems, Inc., Pleasanton, CA, USA). Fundus images were also captured using a confocal scanning laser ophthalmoscope (cSLO) (Spectralis OCT+HRA, Heidelberg Engineering Inc., Heidelberg, Germany). (This was performed under anesthesia after each Spectral domain-optical coherence tomography (SD-OCT) examination: see below).

In vivo fluorescein angiography imaged with a confocal scanning laser ophthalmoscope (cSLO) was performed in a few animals. Retinal vasculature was assessed in *Crx*$^{Rdy/Rdy}$ kittens

and compared with *Crx*$^{Rdy/+}$ kittens and WT controls from chapter 3. Anesthesia, pupil dilation and globe positioning were performed as described in chapter 2 for ERG and SD-OCT.[17] Firstly cSLO retinal images were captured with both 875 nm and 488 nm lasers. Fluorescein angiography imaging was then performed by injecting 20 mg/kg of 10% sodium fluorescein (Fluorescite 10%, Alcon Laboratories Inc, Fort Worth, Texas, USA) as a bolus through a 20G catheter in the left cephalic vein followed by a 2mL bolus of Ringer Lactate. The timer was started at the beginning of injection. One-minute movies then images at regular intervals were recorded using cSLO with a 55° wide field angled lens.

4.3.4. Measurement of globe length

Axial globe length was measured using a combined A- and B-mode ultrasound (A/B Scan System 835, Humphrey, Dublin, CA, USA) under anesthesia (after SD-OCT in some of the animals). Initially, only the axial globe length was measured, but in later studies the cornea-anterior segment width, lens width and posterior segment depth were also measured. Measurements in millimeters (mm) were taken from the best A scan and B scan combined on the same images (Fig. 4.1A).

4.3.5. Intraocular pressure (IOP)

Intraocular pressure was assessed in few *Crx*$^{Rdy/Rdy}$ and wild-type control adults (older than 6 months of age) using a TonoVet (Icare Finland Oy, Helsinki, Finland). Due to the feline species having a tendency to be fractious, only animals of a temperament that allowed them to be assessed without tight restraint and without being stressed were included. Measurements were done within a week between 8.10-9.30 am. Each animal was assessed two to three times during that week. During each session, the IOP was measured 3 times for each eye.

4.3.6. Refractive error

Refractive error was assessed in few *Crx*$^{Rdy/Rdy}$, *Crx*$^{Rdy/+}$ and WT control adult cats (older than 6 months of age) using a retinoscopy and standard refractive bars. It was noted that due to the blindness in the *Crx*$^{Rdy/Rdy}$ and *Crx*$^{Rdy/+}$ cats, the pupil dilation and absence of focusing made measurements challenging.

4.3.7. Electroretinography (ERG)

Electroretinography was performed on *Crx*$^{Rdy/Rdy}$ kittens as described in chapter 2.[17] Scotopic and photopic ERGs were recorded in animals from 4 to 20 weeks of age and compared to those from wild-type and heterozygous animals (chapter 2).

4.3.8. Retinal morphology and vasculature

4.3.8.1. *In vivo* Spectral Domain-Optical Coherence Tomography

Retinal morphology was assessed by SD-OCT in *Crx*$^{Rdy/Rdy}$ kittens, *Crx*$^{Rdy/+}$ kittens and wild-type control kittens from 4 weeks to 5 years of age.

Anesthesia, pupil dilation and globe positioning were performed as described for ERG and SD-OCT in chapter 2. cSLO retinal images were captured. Then, spectral-domain optical coherence tomography (SD-OCT) imaging was performed to obtain detailed retinal cross section images (Spectralis OCT+HRA, Heidelberg Engineering Inc., Heidelberg, Germany). SD-OCT single scan line and volume scan images were recorded from the center of the *area centralis* and in the four retinal quadrants (at 4 optic nerve head diameter distances from the edge of the optic nerve head superiorly, inferiorly, nasally and temporally as illustrated in Appendix O – Fig. 4.S1). Total retinal thickness, Receptor+ (REC+; including layers between retinal pigmentary epithelium and outer plexiform layer included)[24], inner nuclear layer (INL), ganglion cell

complex (GCC; including the inner plexiform layer (IPL) and the ganglion cell layer (GCL)) and inner retina (IR; layers between inner nuclear layer and internal limiting membrane) thickness were measured using the Heidelberg Eye Explorer (HEYEX) software.

4.3.8.2. Immunohistochemistry (IHC)

After humane euthanasia, eyes from *Crx*$^{Rdy/Rdy}$ and wild-type kittens were collected (at 2, 6, 12 and 20 weeks, and 2 and 3.5 years of age). They were processed as described in chapter 2.[17] They were then processed for immunolabeling and imaged.[17, 25] The antibodies used are listed in Appendix a – Table 4.S4.

4.3.8.3. Plastic embedded sections

Eyes were processed for plastic histologic sections and imaged as described in chapter 2.[17] Samples from the dorsal, central, nasal, temporal and *area centralis* regions were obtained by using a biopsy punch of 3 to 3.5 mm diameter Appendix O – Fig. 4.S1.

4.3.9. Quantitative Reverse Transcriptase-Polymerase Chain Reaction (qRT-PCR)

As described in chapter 2, immediately following euthanasia and globe removal, the neurosensory retina was dissected from 2-week-old *Crx*$^{Rdy/Rdy}$, *Crx*$^{Rdy/+}$ and wild-type kittens. Two areas (central and peripheral areas) were dissected (Appendix P – Fig. 4.S2). Retinal samples were flash frozen in liquid nitrogen and stored at -80°C until RNA extraction. RNA extraction, cDNA synthesis and qRT-PCR reaction were performed as previously described.[9] RNA quality was assessed, and only samples with an RNA integrity number RIN > 7.0 were used to evaluate gene expression changes.

Levels of *arrestin3* (*Arr3*, specific to cones), *medium-long wavelength opsin* (*MOP*, specific to cones), *short wavelength opsin* (*SO*, specific to cones), *rhodopsin* (*Rho*, specific to rods), total *Crx* (WT and mutant), *homeobox protein* (*Otx2*), *neural retina leucine zipper protein* (*Nrl*), *photoreceptor-specific nuclear receptor* (*Nr2e3*), *thyroid hormone receptor β2* (*Trβ2*) and the *nuclear receptor* (*Rorβ*) mRNA were measured and normalized to *Tubulin alpha-1B chain* (*Tuba1b*) and *Glyceraldehyde-3-phosphate dehydrogenase* (*GAPDH*) (for primers sequence, see Appendix b – Table 4.S5). mRNA expression levels of retinal transcription profiles of $Crx^{Rdy/Rdy}$ and $Crx^{Rdy/+}$ kittens were compared to control wild-type kittens.

4.3.10. Western blot assay

As described in chapter 2, following sampling of the retina for qRT-PCR the remaining retina was flash frozen in liquid nitrogen, then protein extraction and western blot assay were performed.[9, 17] Monoclonal mouse anti-β-actin antibody (Sigma-Aldrich, Saint Louis, MO, USA) and polyclonal rabbit anti-CRX 119b1 at 1:1000 dilution were used to probe the membranes. Secondary antibodies goat anti-mouse IRDye 680LT and goat anti-rabbit IRDye 800CW (LI-COR Biosciences, Lincoln, NE, USA) respectively were used. Fluorescence was detected using the Odyssey Infrared Imager (LI-COR Biosciences, Lincoln, NE, USA). Quantification was performed using Image J (http://imagej.nih.gov/ij/; provided in the public domain by the National Institutes of Health, Bethesda, MD, USA).[26]

4.3.11. Statistical analysis

Statistical analysis of IOP, refraction, cDNA level and Western blot fluorescence level data differences were tested for normality (Shapiro-Wilk test for normality). Normally distributed data was analyzed by unpaired 2-tailed Student's T-test (significance level set at $P < 0.05$), nonparametric data by a Mann-Whitney rank sum test (SigmaPlot 12.0; Systat Software, Inc., San Jose, CA, USA). Student's T-test was performed when comparing only two groups. A mixed effect model using R studio was used to analyze the data for globe length and SD-OCT measurements; SD-OCT measurements as data was evaluated over time. This was also used to analyze the effect of other factors on IOP and refraction (age) using the equation below.[27]

$$Y_i = \sum_{i=0}^{n} \beta \mathrm{X} + \alpha_i + \varepsilon_i$$

Where ß is the parameter vector, X is the independent variable matrix, α_i is the cat level residual, and the $\mathcal{E}_i$ is the individual observation level residual.

4.4. RESULTS

4.4.1. *Crx*$^{Rdy/Rdy}$ cats have an increased globe length and a myopic refractive error

Analysis of the *Crx*$^{Rdy/Rdy}$ cat axial globe length showed a significant increase compared to heterozygous *Crx*$^{Rdy/+}$ and to control WT cats (Fig. 4.1) ($P < 0.002$ and $= 0.003$, respectively). For example, at one year of year the *Crx*$^{Rdy/Rdy}$, *Crx*$^{Rdy/+}$ and WT cats had an axial globe length of respectively 23.1 ± 0.4, 19.5 ± 0.3 and 20.1 ± 0.4 mm. This difference was obvious on US, and in the enucleated eye (Figs. 4.1A and 4.1B). Measurement analysis (Fig. 4.1C) confirmed that finding. Statistical analysis showed that the eye (left or right), or sex had no effect and that the differences in axial length increased with age. A difference in axial globe length was also present between *Crx*$^{Rdy/+}$ and WT cats ($P = 0.02$), with WT having a slightly longer globe. It is to be noted that the *Crx*$^{Rdy/Rdy}$ group included measurements from 55 males (M) and 13 females (F) (each time point considered independently), the WT group included measurements in 94 M and 54 F and the *Crx*$^{Rdy/+}$ group in 44 M and 106 F. It is possible that the difference between the *Crx*$^{Rdy/+}$ and the WT group was due to high number of females that were of smaller size compared to the males. For example, at 3 years of age female and male *Crx*$^{Rdy/+}$ cats had a mean axial globe length of 20.4 ± 0.13 and 21.50 ± 0.34 mm respectively, a difference which was statistically significant ($P \leq 0.001$).

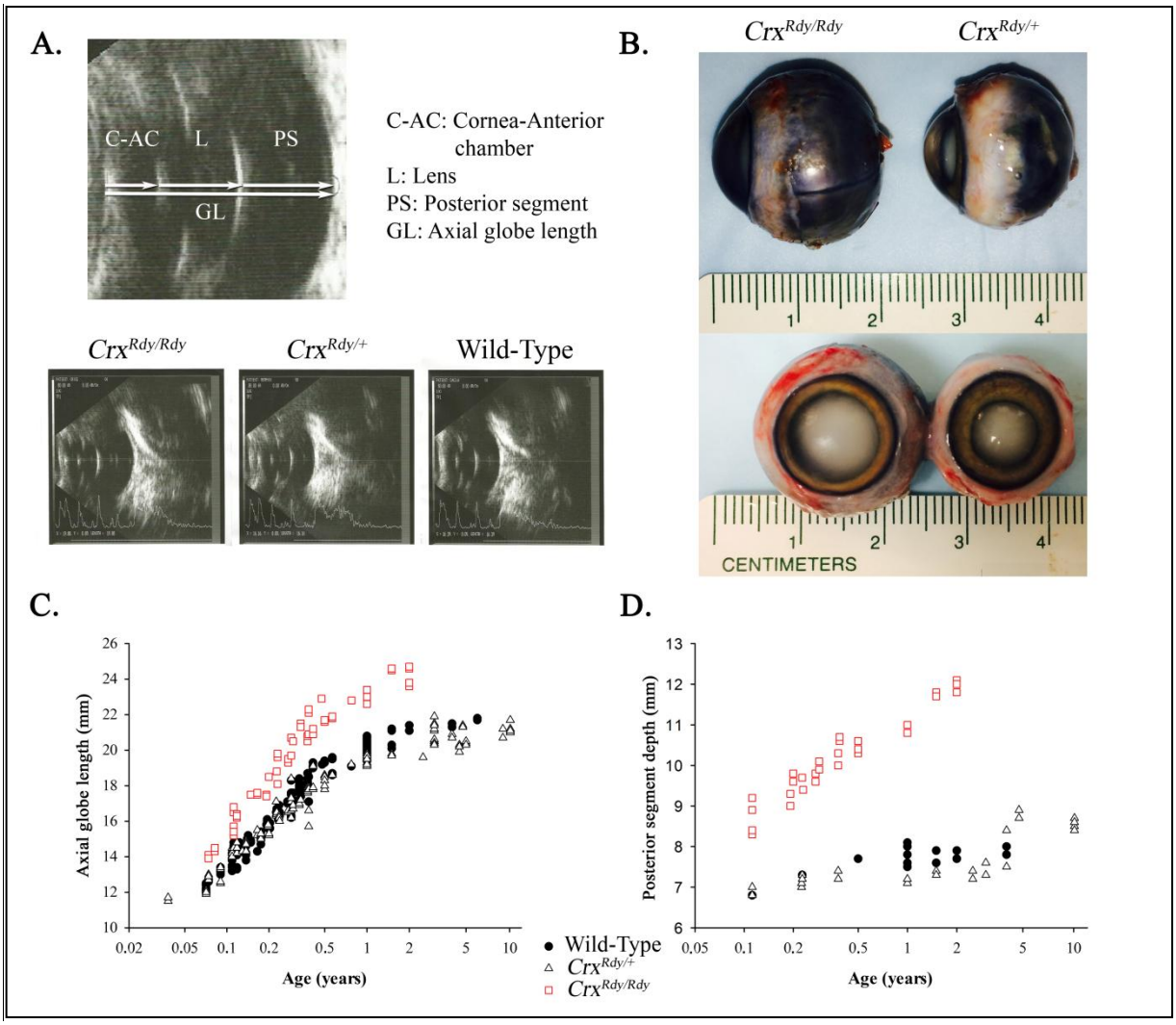

Figure 4.1. Globe lengths.
(A) Combined A- and B-Mode ocular ultrasound images. The images show the different measurements taken. C-AC: Cornea-Anterior chamber width, L: lens width, PS: posterior segment depth and GL: axial globe length. Representative ultrasound images of the globe from a *Crx*$^{Rdy/Rdy}$, a *Crx*$^{Rdy/+}$ and a WT 12-week-old cat show the enlarged globe of the *Crx*$^{Rdy/Rdy}$ due to an enlarged posterior segment.
(**B) Enucleated fixed eyes from a 12-week-old *Crx*$^{Rdy/Rdy}$ and *Crx*$^{Rdy/+}$ cats.** These pictures show an enlarged globe with a deeper posterior segment in the *Crx*$^{Rdy/Rdy}$ cat.
(**C) Scatter plot of the axial globe length versus the age.** A significant difference can be seen between the axial globe length of the *Crx*$^{Rdy/Rdy}$ cat compared to that of the *Crx*$^{Rdy/+}$ and WT cats at all ages tested.
(**D) Scatter plot of the posterior segment depth versus the age.** A significant difference can be seen between the posterior segment depth of the *Crx*$^{Rdy/Rdy}$ cat compared to that of the *Crx*$^{Rdy/+}$ and WT cats at all ages tested.

To investigate the anatomical origin of the increase in axial globe length, cornea-anterior segment width, lens width and posterior segment depth measures were analyzed and showed a significant increase in posterior segment depth in $Crx^{Rdy/Rdy}$ cats compared to $Crx^{Rdy/+}$ and to control WT cats ($P < 0.0001$) (Fig. 4.1D and Appendix Q – Fig. 4.S3). No difference was found overall between $Crx^{Rdy/+}$ and WT cats ($P = 0.250$) although an effect of the sex between $Crx^{Rdy/+}$ and WT groups (more male in WT group) was found ($P = 0.006$). For example, at one year of age the $Crx^{Rdy/Rdy}$, $Crx^{Rdy/+}$ and WT cats had a posterior segment depth of respectively 10.9 ± 0.1, 7.1 ± 0.1 and 7.8 ± 0.3 mm. For the axial globe length and the posterior segment depth, the older the animals were the greater the differences. No significant difference was found in cornea-anterior chamber widths, yet an effect of the sex between $Crx^{Rdy/+}$ and WT groups (more male in WT group) was found ($P = 0.007$). Similarly, no significant difference was found in cornea-anterior chamber widths; the effect of the sex between $Crx^{Rdy/+}$ and WT groups (more male in WT group) was significant ($P = 0.011$) (Appendix Q – Fig. 4.S3).

Due to the increase in posterior segment depth, investigation of the possibility for increase in intraocular pressure and changes in refractive error were performed. There were no differences in IOPs between $Crx^{Rdy/Rdy}$ and WT cats (16.0 ± 1.8 and 15.4 ± 1.6 mmHg, respectively $P = 0.577$) in the animals investigated (Fig. 4.2A). However, a statistically marked significant difference was found in refractive state. The $Crx^{Rdy/Rdy}$ cats had a very myopic refractive error of a mean of -14 ± 1.1 D compared to -0.9 ± 0.4 D in the WT cats ($P = 0.004$, Ttest) (Fig. 4.2B). A refractive error was also present in the $Crx^{Rdy/+}$ cats with an average of -2.7 ± 0.8 D ($P < 0.001$ compared to $Crx^{Rdy/Rdy}$ cats and $P = 0.002$ compared to WT cats, Ttest). When analyzed with a mixed effect model, age had a significant influence in the difference between the $Crx^{Rdy/+}$ cats and both the $Crx^{Rdy/Rdy}$ and WT cats ($P = 0.003$). The eye (left or right) did not have an effect on the difference between groups nor did it have an effect on refraction or IOP.

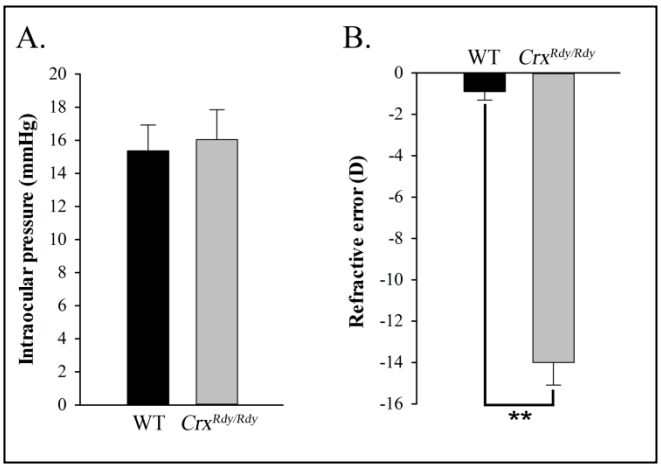

Figure 4.2. (A) Intraocular pressure (IOP). There was no significant difference in IOP between the *Crx*$^{Rdy/Rdy}$ and WT cats. **(B) Refractive error.** Severe myopia was found in the *Crx*$^{Rdy/Rdy}$ cats with a mean -14 D of compared to -0.9 D in the WT cats. $^{**}P < 0.01$

4.4.2. *Crx*$^{Rdy/Rdy}$ kittens lack retinal function

At all ages examined, the *Crx*$^{Rdy/Rdy}$ cats had an absence of menace response and dazzle reflex (although this could be hard to assess due to the animals moving and blinking) and decreased pupillary light reflexes. Nystagmus was not noted at any age. To more precisely assess retinal functional, ERGs were recorded at multiple time points from 4 to 20 weeks of age.[17] *Crx*$^{Rdy/Rdy}$ kittens did not have any recordable ERG responses at any age tested for either scotopic or photopic ERG (Fig. 4.3). Therefore no statistical analysis was performed.

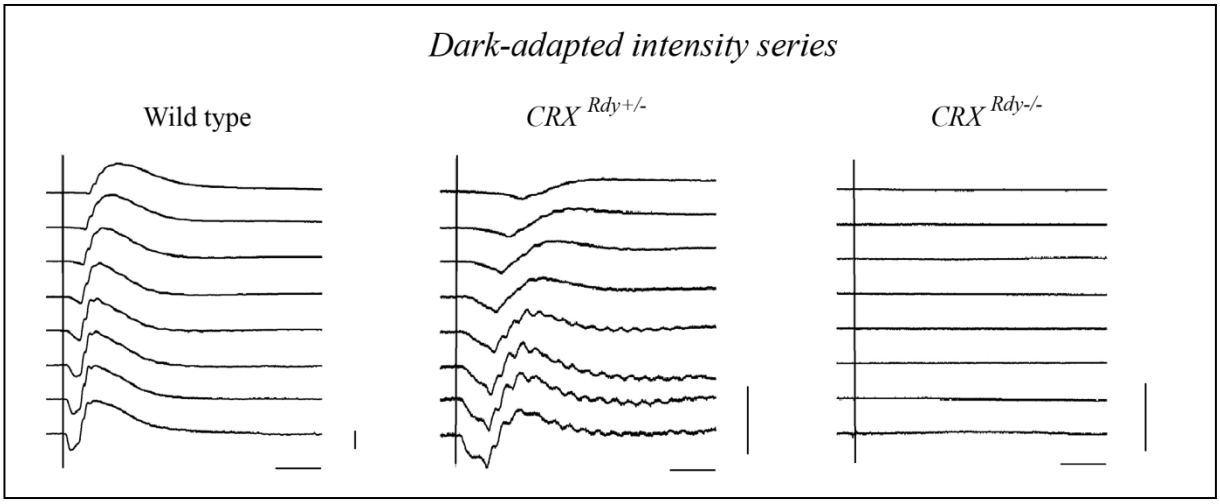

Figure 4.3. Dark-adapted intensity series ERGs from WT, *Crx*$^{Rdy+/-}$ and *Crx*$^{Rdy/Rdy}$ kittens at 10-weeks of age (age of peak maturation of the ERG in the *Crx*$^{Rdy/+}$ cat). The *Crx*$^{Rdy/+}$ kitten waveforms are very reduced in amplitude (note the scale differences between the sets of tracings) and have increased implicit times. There was no recordable ERG from the *Crx*$^{Rdy/Rdy}$ kitten. Responses to stimulation from top to bottom of -1.6, -1.2, -0.8, -0.4, 0.0, 0.4, 0.9, and 1.4 log cdS/m². (Scale bars: vertical 100 µV; horizontal 50 ms).

4.4.3. *Crx*$^{Rdy/Rdy}$ kittens have changes in fundus reflectivity and tapetal thinning, but superficial retinal vasculature persists into adulthood

To determine the progression of retinal degeneration in *Crx*$^{Rdy/Rdy}$ kittens, *in vivo* ophthalmic imaging was performed at multiple time points from 4 weeks to 5 years of age. Ophthalmoscopic examination revealed that there were some changes in tapetal reflectivity as early as 6 to 8 weeks of age (when the tapetum develops). Discernible tapetal hyperreflectivity (indicative of retinal thinning) was visible as early as 12 weeks of age (Fig. 4.4). The appearance of the tapetum and tapetal reflectivity in *Crx*$^{Rdy/Rdy}$ kittens was never normal with a generalized abnormally appearing "sheen" to it when compared to WT cats. Interestingly, all animals developed a specific lesion with the choroidal vessels starting to become apparent at an early age, and some increased cSLO autofluorescence was visible paralleling choroidal vessels as early as

12-15 weeks of age (Fig. 4.4B). This worsened with age and seemed to correlate with the SD-OCT imaging, with severe thinning of the *tapetum lucidum* but also choroidal thinning.

The generalized tapetal reflectivity changes were not so severe as in the $Crx^{Rdy/+}$ cats where marked hyperreflectivity developed (Fig. 4.4). In the $Crx^{Rdy/Rdy}$ kittens superficial retinal vasculature is preserved up to at least 5 years (oldest animal examined). In contrast in the $Crx^{Rdy/+}$ cats by this age vessels were markedly attenuated, arteriovenous shunts had developed, and there was a mild leakage of fluorescein apparent a few minutes after injection of fluorescein. (Fig. 4.4B).

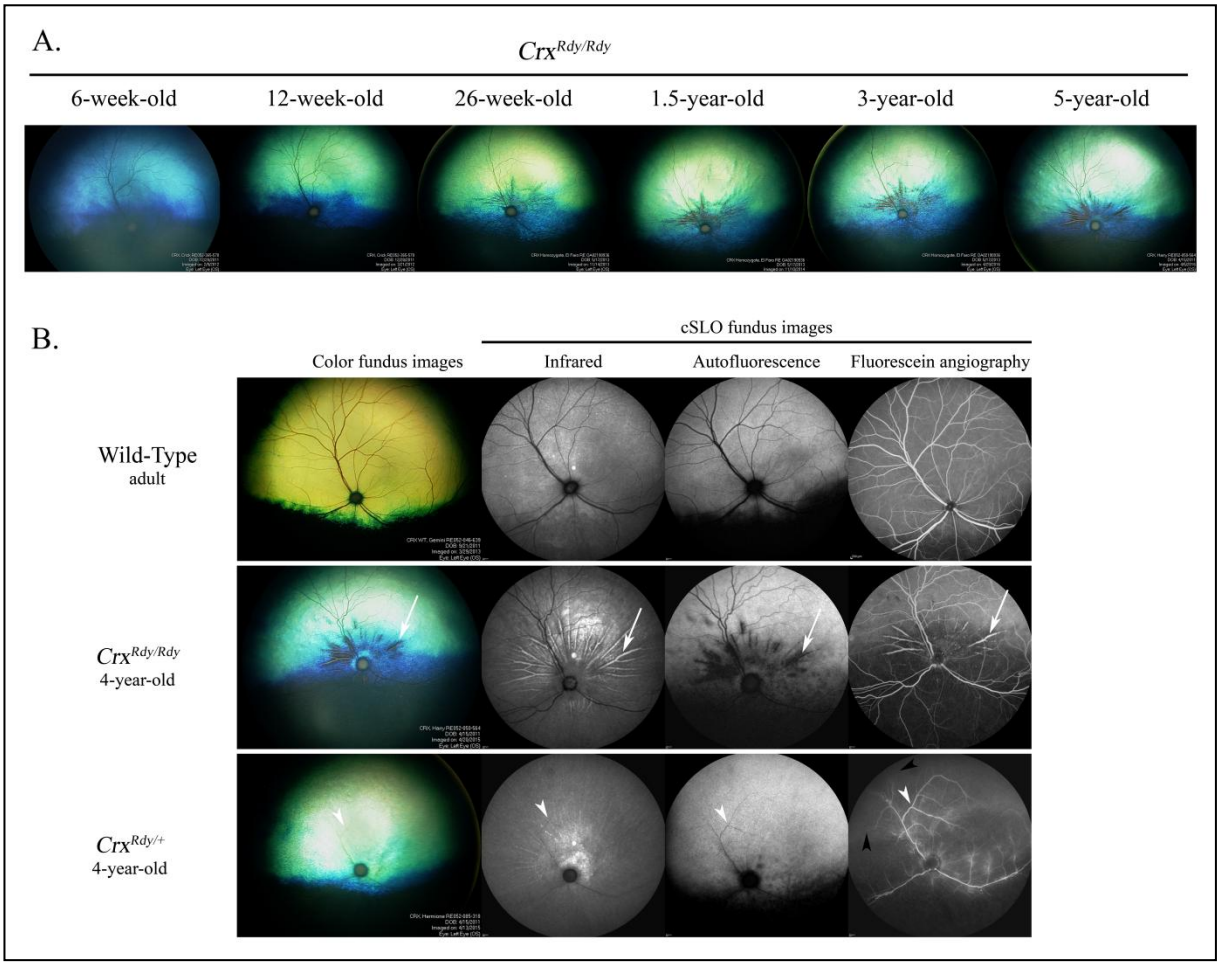

Figure 4.4. Fundus images during development and adulthood.

Figure 4.4 (cont'd)
(A) Fundus color images showing tapetal hyperreflectivity (a sign of retinal thinning) as early as 12 weeks of age, while the retinal vasculature is relatively well preserved even though thinned during advanced disease stages. At 26 weeks of age, extreme thinning of the tapetum can be seen, which allows the choroidal vessels to be seen (shown by the white arrows in (B).
(B) Fundus color and cSLO images from WT adult cat, 4-year-old $Crx^{Rdy/Rdy}$ and $Crx^{Rdy/+}$ cats. Infrared (IR, 875nm), Autofluorescence (AF, 488nm) and Fluorescein angiography (FA, 488nm) images showing the preservation of the retinal vasculature despite disease progression. Arrows indicate an area of tapetal thinning exposing the choroidal vasculature (dark streak on AF and hyperfluorescent streak on FA: white arrows). Note the difference compared to the $Crx^{Rdy/+}$ cat in which the retinal vessels are very thinned (white arrow head and show some arterio-venous shunts: black arrow heads).

4.4.4. The $Crx^{Rdy/Rdy}$ cat lacks development of photoreceptor inner and outer segments, and despite extensive retinal remodeling has preservation of total retinal thickness

Retinal SD-OCT cross-sectional images were captured from $Crx^{Rdy/Rdy}$ animals between 4 weeks and 5 years of age. SD-OCT zones representing photoreceptor inner/outer segments (IS/OS) could not be detected at any age from $Crx^{Rdy/Rdy}$ animals (Fig. 4.5A). These included the ellipsoid zone and differentiation of the interdigitation zone and external limiting membrane.[28] Due primarily to the absence of IS/OS the overall retinal thickness was thinner than in age-matched $Crx^{Rdy/+}$ and WT cats. The rest of the retinal layers appeared to have developed normally and were clearly discernible. Interestingly, at an early age (4 and 6 weeks of age) the ONL appeared to be bilayered; this corresponded on IHC and histology to two ONL cell nuclei populations: the outer portion consisted of elongated nuclei elongated while the nuclei in the inner portion were circular (Fig. 4.7 and Appendix V – Fig. 4.S8). With disease progressive the clear demarcation of retinal layers was lost as remodeling occurred, and it became harder to recognize them and therefore to measure them. We noted that there was some degree of individual variation. Interestingly, the retina did not thin so severely with age as in the $Crx^{Rdy/+}$ cats. The retina seems to initially thin and then become thicker (Figs. 4.5A and 4.5B). While the

total retinal thickness (TR) of the *Crx*$^{Rdy/Rdy}$ cat was similar to the WT cat in most regions, the REC+ was thinner than in the WT cat while the inner retinal layers (IR) became thicker as also occurs in the *Crx*$^{Rdy/+}$ cat. In the *Crx*$^{Rdy/Rdy}$ cat, overall all layers had a tendency to thicken with age, yet the *area centralis* was thinner. (Fig. 4.6 and Appendix R – Fig. 4.S4). This overall thickness preservation indicates that there is photoreceptor nuclei/cell degeneration and inner retinal proliferation (Fig. 4.7). To summarize, there is an initial reduction in TR thickness followed by an increase, which is mainly due to IR thickening (INL and GCC maintained and thickening) while the REC+, even if initially thinner than that of *Crx*$^{Rdy/+}$ and WT cats (due to the lack of photoreceptor IS/OS), is maintained or only mildly thinned (Appendix S, T and U – FigS. 4.S5, 4.S6 and 4.S7).

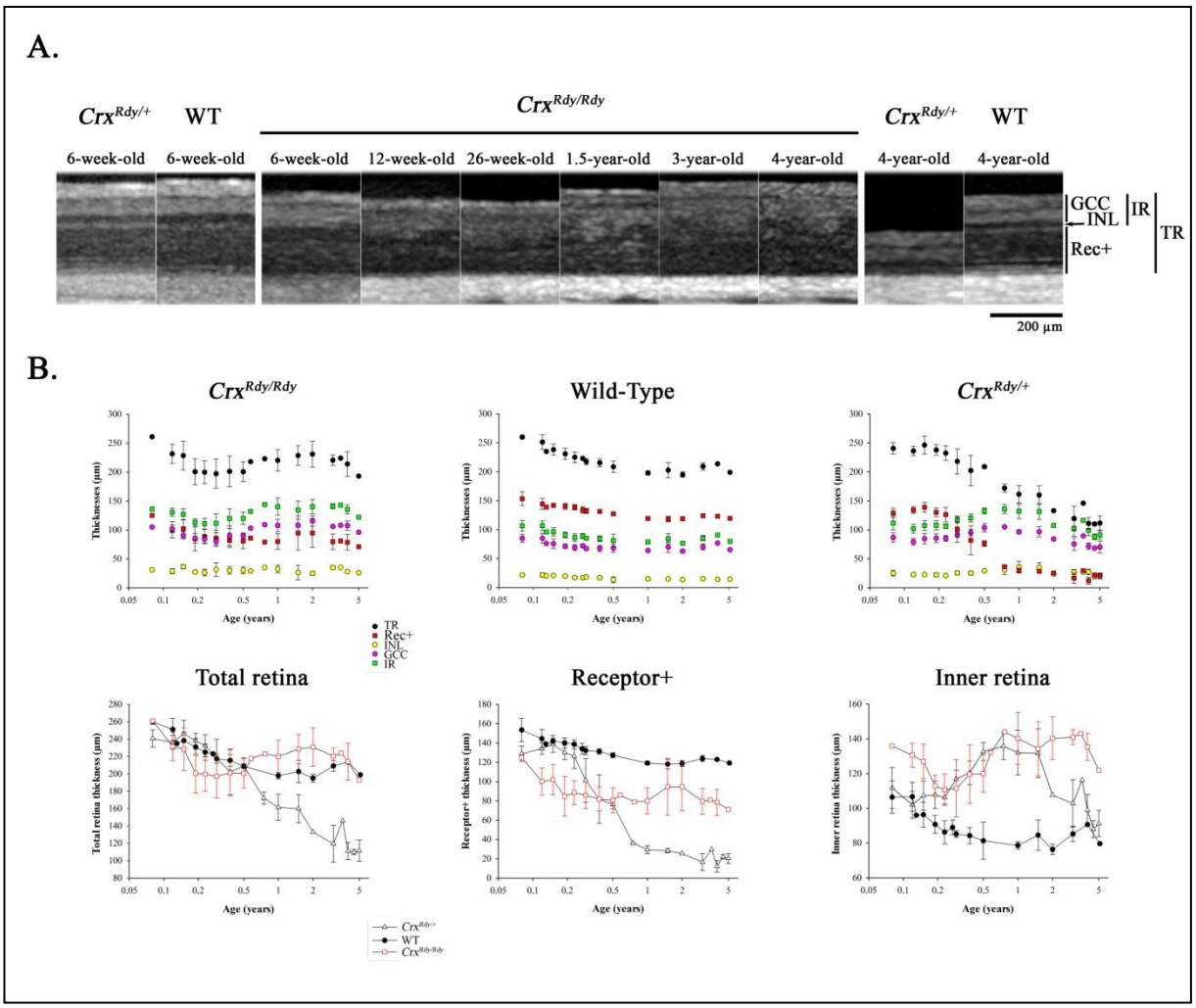

Figure 4.5. Spectral Domain – Optical Coherence Tomography (SD-OCT) *in vivo* retinal morphology analysis of the dorsal retina.

(A) SD-OCT cross-section images of the retina in the region dorsal to the optic disc. Showingrepresentative *Crx*$^{Rdy/Rdy}$ animals at 6, 12 and 26 weeks, 1.5, 3 and 4 years of age. As comparison, cross-sections of the retina of representative of *Crx*$^{Rdy/+}$ and WT cats at 6 weeks and 4 years of age are shown. Note that initially, while the inner and outer segments are not detectable (causing the total retina to be thinner than that of *Crx*$^{Rdy/+}$ and WT cats at 6 weeks), the rest of the retinal layers appear normally developed. With disease progressive the layers start to remodel and become harder to identify. However, the retina of *Crx*$^{Rdy/Rdy}$ cats does not thin so severely with age as that of the *Crx*$^{Rdy/+}$ cats. The retina seems to initially thin then thicken.

(B) Thicknesses of retinal layers in the dorsal region. Top panels show the different retinal layers' thicknesses in the dorsal area of *Crx*$^{Rdy/Rdy}$, *Crx*$^{Rdy/+}$ and WT cats over the course of the disease. The *Crx*$^{Rdy/Rdy}$ cat retina does not develop a similar degeneration as that of the *Crx*$^{Rdy/+}$ cat. **Bottom panels show comparison of the total retina (TR), receptor+ (REC+) and inner retina (IR) from *Crx*$^{Rdy/Rdy}$, *Crx*$^{Rdy/+}$ and WT cats** during disease progression. Note the maintenance of the TR but thinning of REC+ and thickening of the IR in the *Crx*$^{Rdy/Rdy}$ cat.

TR; Total retina, REC+; Receptor+, IR; Inner retina, INL; Inner retina layer, GCC; Ganglion cell complex.

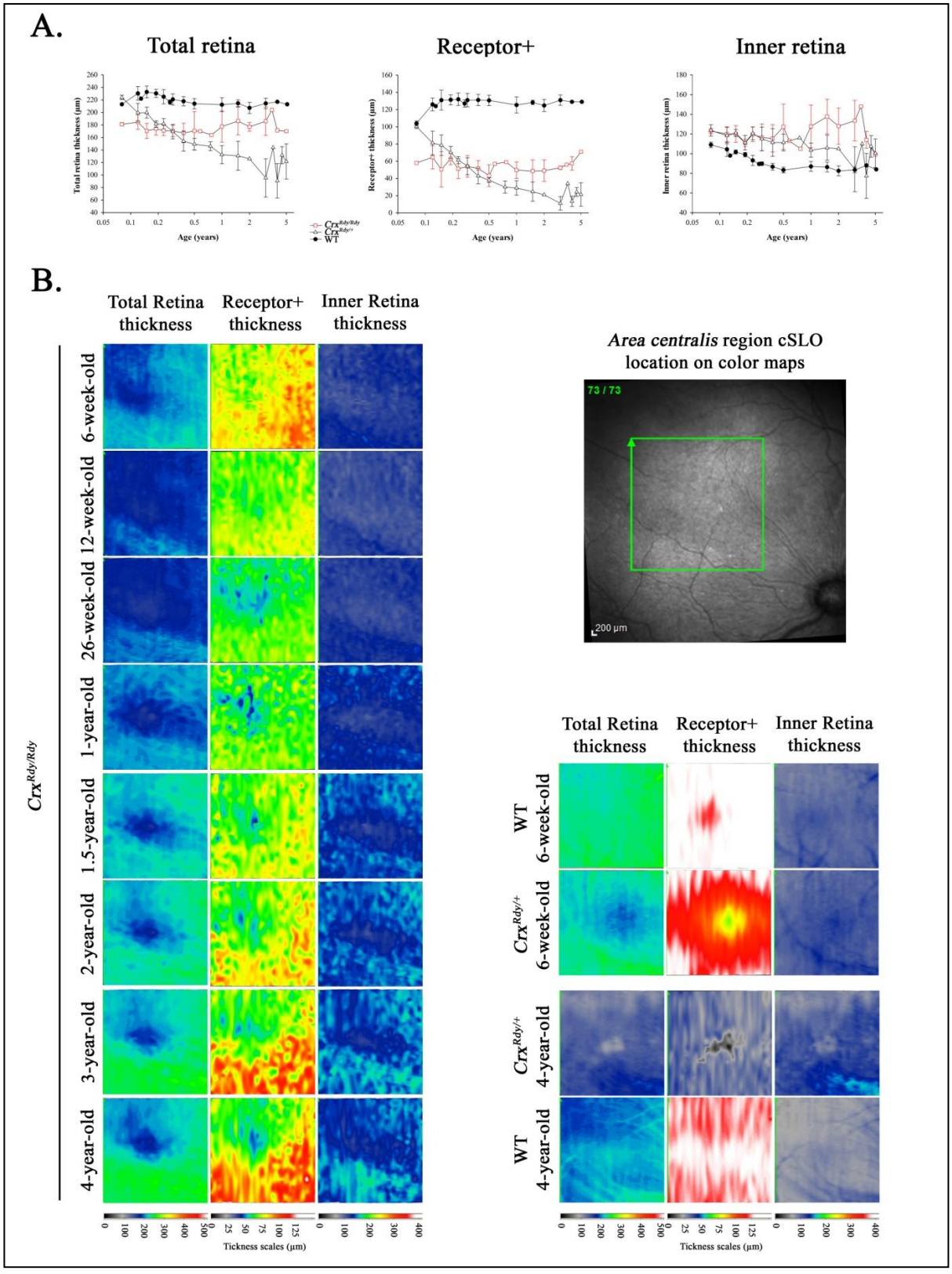

Figure 4.6. Spectral Domain – Optical Coherence Tomography (SD-OCT) *in vivo* retinal morphology analysis of the *area centralis*.

Figure 4.6 (cont'd)
(A) Thicknesses of retinal layers in the *area centralis* region.
The total retina (TR), receptor+ (REC+) and inner retina (IR) thicknesses in *Crx*$^{Rdy/Rdy}$, *Crx*$^{Rdy/+}$ and WT cats are shown during disease progression. The TR and IR of *Crx*$^{Rdy/Rdy}$ cats were thinner than those of *Crx*$^{Rdy/+}$ and WT cats before maturation. However, unlike with the *Crx*$^{Rdy/+}$ cat, their TR, REC+ and IR thicknesses remain stable, and the IR actually has a tendency to thicken with age.
(B) Total retinal, Receptor+ and Inner retina thicknesses color map in the *area centralis*.
The left panel shows color (heat) maps for a representative *Crx*$^{Rdy/Rdy}$ cat from 6 weeks to 4 years of age. The right top panel shows the retinal location of the color map. The bottom right panel shows the color map for representative *Crx*$^{Rdy/+}$and WT cats at 6 weeks and 4 years of age. Note the thinner TR and REC+ in the *Crx*$^{Rdy/Rdy}$ cat from an early age. The IR is thicker than that of the *Crx*$^{Rdy/+}$ and WT cats. With disease progression, thickening surrounding the center of the *area centralis* can be seen in the *Crx*$^{Rdy/Rdy}$ cat, leading to slight TR and REC+ thickening, which is in contrast with the severe thinning of retinal layers in the *Crx*$^{Rdy/+}$ cats at 4 year of age.

The SD-OCT findings were confirmed by histology and IHC (Figs. 4.7 and 4.8). Careful examination of plastic embedded semi-thin sections (Fig. 4.7 and Appendix V – Fig. 4.S8) confirmed the lack of normal development of photoreceptor inner and outer segments, although all other retinal layers seemed to develop properly. Only very small rudimentary inner segments are present in the *Crx*$^{Rdy/Rdy}$ cat retina (visible on high magnification histology and electron microscopy images). Those are surrounded and in contact with RPE villosities (Appendix V – Fig. 4.S8). On SD-OCT, as well as histology and immunohistochemistry sections, as mentioned earlier, the outer nuclear layer had a bilayered appearance at a young age. Progressive disorganization of the retinal layers developed with age. Initially, the lamination of the retina seemed normal (see Fig. 4.7A), but as early as 6 weeks of age some abnormal tissue can be seen between the ONL and INL nuclei. Additionally, it was noted that the shape and appearance of the chromatin of the ONL nuclei changed such that it was not so dense as in healthy photoreceptor nuclei. By 2 and 3.5 years of age, there was a complete disorganization of the retinal layers although retinal thickness was maintained with the exception of at the very center of the *area centralis*, which was thinned in most animals (Fig. 4.7).

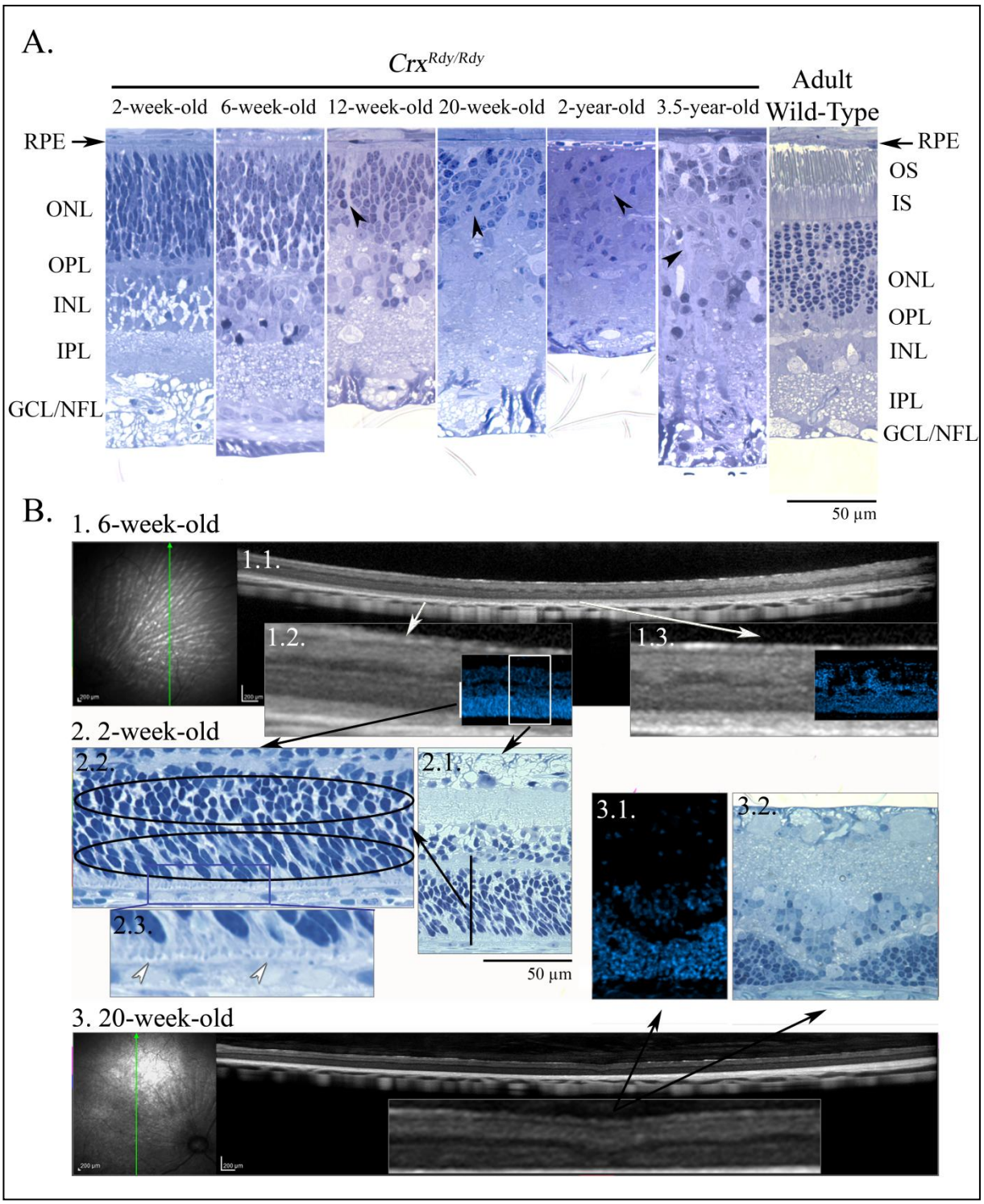

Figure 4.7. Representative histologic sections and morphologic characteristic in the *Crx*$^{Rdy/Rdy}$ cats.

With the exception of the inner segment and outer segment layers, all retinal layers were present.

Figure 4.7 (cont'd)

(A) Representative plastic sections of retina from centro-dorsal regions in *Crx*$^{Rdy/Rdy}$ cats and an adult WT cat.

Note the absence of photoreceptor inner and outer segment during maturation and at adulthood. The retinal thickness is preserved over time (although there is some individual variation). The preservation of thickness is accounted for by activation of the inner retinal components with development of advanced glial scaring. The *black arrowheads* indicated the Müller cell processes advancing between the ONL cell bodies.

OS, photoreceptor outer segment; IS, photoreceptor inner segment; ONL, Outer Nuclear Layer; OPL, Outer Plexiform Layer; INL, Inner Nuclear Layer; IPL, Inner Plexiform Layer; GCL/NFL, Ganglion Cell Layer/Nerve Fiber Layer; RPE, Retinal Pigmentary Epithelium

(B) SD-OCT, Histology and DAPI fluorescent staining (1) 6-week-old, (2) 2-week-old and 20-week-old *Crx*$^{Rdy/Rdy}$ cats.

As in (A), all retinal layers were present except the inner segment and outer segment layers. Only small rudimentary inner segments could be seen (2.3.: white arrow head). The photoreceptor nuclei (ONL) developed into a bilayered arrangement with nuclei in the outer portion being elongated while those in the inner portion were circular (1 and circled nuclei in 2.1). Progressive disorganization of the retinal layers developed (1.3., 3.1. and 3.2.), and the ONL thinned with most severe thinning in the center of the *area centralis* (3.).

To further investigate structural changes, immunolabeling of key photoreceptor structural and phototransduction proteins was performed on frozen retinal sections using markers to identify retinal cell types (Fig. 4.8, Appendix W – Fig. 4.S9 and Appendix a – Table 4.S4). At none of the ages tested did any cells label with human cone arrestin (hCAR) (hCAR labels both cone types), S-opsin (SO, short wavelength-opsin) or ML-opsin (MLO, medium/long wavelength-opsin) in the *Crx*$^{Rdy/Rdy}$ cat. Additionally, no photoreceptors ware labeled with calbindin, which labels cones in normal cats (Appendix W - Figs. 4.S9A and 4.S9B).[29] There was some RetP1 (a marker for rods) labeling in the *Crx*$^{Rdy/Rdy}$ cat, although this was severely decreased at all ages and abnormally distributed. The very short vestigial inner segments labeled, as did some photoreceptor cell bodies indicating mislocalization of rhodopsin, which was apparent from as early as 2 weeks of age. By 3.5 years of age, only few remaining ONL nuclei were labeled for rhodopsin (Fig. 4.8A).

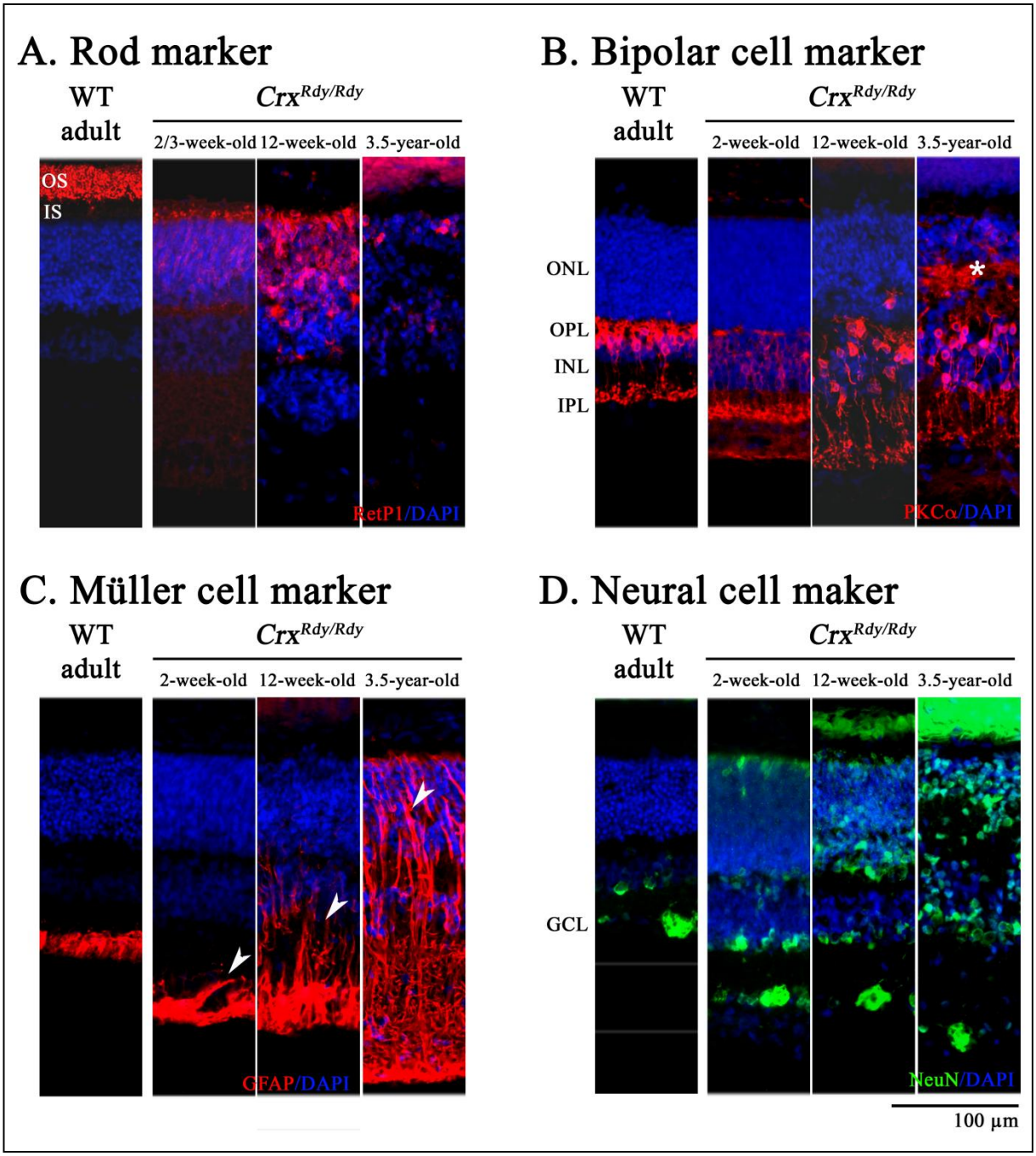

Figure 4.8. Immunolabeling of the *Crx*$^{Rdy/Rdy}$ cat central retinal region for (A) rod, (B) rod bipolar, (C) Müller cell and (D) Neural cell markers.
(A) In the *Crx*$^{Rdy/Rdy}$ cat, as early as 2 week of age, RetP1 (which labels rod outer segments (OS) in normal cats) can be seen labeling the very small inner segments (IS) and the ONL cell bodies. This mislocalization of rhodopsin persisted until adulthood, at which time only few rod positive nuclei were detectable. Cones labeling was absent at all ages tested in the *Crx*$^{Rdy/Rdy}$ retina**.**

Figure 4.8 (cont'd)
(B) Rod bipolar cells can be seen labeled by PKCα in 2-week-old *Crx*$^{Rdy/Rdy}$ retinas. By 12 weeks of age, the rod bipolar cells seemed to start sprouting towards the ONL. By 3.5 years of age, some major modifications happened, and the rod bipolar cells dendrites have invaded the ONL (indicated by the *white star*) forming a matrix within the latter.
(C) During disease progression, Müller cells became highly activated, and extensive GFAP labeled can be seen in the *Crx*$^{Rdy/Rdy}$ retina. At 3.5 years of age the GFAP positive Müller cell processes had extensively invaded all layers of the retina (spreading of the activated Müller cells is indicated by the *white arrows*).
(D) Labeling with NeuN antibody showed apparently normal labeling of ganglion cells and some INL cells, but there was also some abnormal labeling through the ONL nuclei.
OS; Photoreceptor outer segment, IS; Photoreceptor inner segment, ONL; Outer nuclear layer, OPL; Outer plexiform layer, INL; Inner nuclear layer, IPL; Inner plexiform layer, GCL; ganglion cell layer.

Immunolabeling for rod bipolar cells (using an anti-PKCα antibody) showed that in the *Crx*$^{Rdy/Rdy}$ kittens there initially appear to be normal numbers of PKCα expressing cells in the INL. Sprouting of PKCα labeled dendrites can be seen by 12 weeks of age, and by 3.5 years of age they were stretched and invaded the outer retina creating a matrix within the ONL (Fig. 4.8B). Other inner retinal cells were investigated using calbindin labeling (Appendix W - Fig. 4.S9B). It showed what seemed to be normal labeling of the inner retinal cells such as amacrine, horizontal and ganglion cells in the *Crx*$^{Rdy/Rdy}$ retina.

Immunolabeling for glial fibrillary acidic protein (GFAP) was markedly increased indicating Müller cell activation. At 2 weeks of age only very minor activation of Müller cells was seen, but by 12 weeks of age they were invading the INL and had extended toward the ONL. By 3.5 years of age, GFAP labeling was present within all retinal layers, indicative of extensive Müller cell activation characteristic of retinal scaring and remodeling (Fig. 4.8C).[30-32]

NeuN, a neuronal marker, labeled ganglion cells as in normal retina but it also abnormally labeled inner retinal cells and ONL nuclei at all age tested in the *Crx*$^{Rdy/Rdy}$ retina (Fig. 4.8D).

Immunolabeling indicated the presence of the retinal pigmentary epithelium (RPE65 antibody) in all ages tested and in all retinal regions (Appendix I - Fig. 4.S9C).

Crx labeling was present at 12 weeks and 3.5 years of age in $Crx^{Rdy/Rdy}$ retina and seems to be more extensive in older animals (Appendix I - Fig. 4.S9D).

4.4.5. $Crx^{Rdy/Rdy}$ retinas had a marked reduction of transcript levels for cone and rod specific genes and changes in expression levels of transcription factors involved in the photoreceptor development/fate cascade

To investigate molecular changes underlying $Crx^{Rdy/Rdy}$ retinal pathology, we assessed mRNA levels of selected CRX target genes in retinal subregions of 2-week-old $Crx^{Rdy/rdy}$, $Crx^{Rdy/+}$ and WT kittens (Appendix B - Fig. 4.S2). This included investigation of cone specific genes such as cone arrestin (*arrestin3, Arr3*), *medium-long wavelength opsin* (*MOP*), *short wavelength opsin* (*SO*), and a rod specific gene like *rhodopsin* (*Rho*). Transcription factors involved in the photoreceptor development cascade were also investigated (Fig. 4.9, Appendix b - Table 4.S5): total *Crx* (WT and mutant), *homeobox protein* (*Otx2*), *neural retina leucine zipper protein* (*Nrl*), *photoreceptor-specific nuclear receptor* (*Nr2e3*), *thyroid hormone receptor β2* (*Trβ2*) and the *nuclear receptor* (*Rorβ*) were measured.

Table 4.1. gives a summary of the results showing relative expression changes between $Crx^{Rdy/Rdy}$, $Crx^{Rdy/+}$ and WT kittens.

mRNA	*Crx*$^{Rdy/Rdy}$ *vs* *Crx*$^{Rdy/+}$	*Crx*$^{Rdy/Rdy}$ *vs* WT	*Crx*$^{Rdy/+}$ *vs* WT
Arr3	27.4x less	1724.1x less	62.9x less
SO	15.8x less	62.7x less	4.0x less
MOP	Not detectable in *Crx*$^{Rdy/Rdy}$	Not detectable in *Crx*$^{Rdy/Rdy}$	4.3x less
Rho	10.9x less	32.5x less	3.0x less
total *Crx*	No significant difference	1.8x more	1.8x more
Otx2	No significant difference	2.4x more	1.9x more
Nrl	2.3x less	No significant difference	No significant difference
Nr2e3	2.1x less	1.9x less	No significant difference
Trβ2	No significant difference	1.4x more	No significant difference
Rorβ	1.3x more	1.3x more	No significant difference

Table 4.1. Summary of the results by indicating fold expression changes for each mRNA between *Crx*$^{Rdy/Rdy}$, *Crx*$^{Rdy/+}$ and WT kittens.

The *Crx*$^{Rdy/Rdy}$ and *Crx*$^{Rdy/+}$ kitten retinas had significantly decreased levels of cone and rod opsin mRNA compared to the WT cats (Fig. 4.9, for all P values, see Appendix c – Table 4.S6). *Arr3*, *SO* and *Rho* expression was respectively 27.4, 15.8, 10.9 times higher in *Crx*$^{Rdy/+}$ kitten's retina compared to *Crx*$^{Rdy/Rdy}$ kitten's retina. *MOP* was not detectable in *Crx*$^{Rdy/Rdy}$ kitten's retina. To investigate the effect of the mutation on the *Crx* expression itself we evaluated expression of the total transcript. In both the *Crx*$^{Rdy/Rdy}$ and *Crx*$^{Rdy/+}$ kitten's retinas total levels of *Crx* were at a significantly higher level (1.8 times higher) than the levels of WT *Crx* transcript in the WT kitten's retina. No significant difference between total *Crx* expression levels in the *Crx*$^{Rdy/Rdy}$ and *Crx*$^{Rdy/+}$ kitten's retina was detected. *Otx2,* a transcription factor involved in photoreceptor development, was expressed at 2.4 and 1.9 times higher respectively in the *Crx*$^{Rdy/Rdy}$ and *Crx*$^{Rdy/+}$ kitten's retinas compared to the WT kitten's retina. Total *Crx* and *Otx2* were significantly increased compared to WT retinas, but there was no significant difference between the levels in the *Crx*$^{Rdy/Rdy}$ and *Crx*$^{Rdy/+}$ kitten's retinas. *Nrl* expression was

downregulated by 2.3 times in the $Crx^{Rdy/Rdy}$ compared to the $Crx^{Rdy/+}$ kitten's retina while there was no significant difference compared to the WT levels. *Nr2e3* was expressed at 2.1 and 1.9 times lower levels in the $Crx^{Rdy/Rdy}$ compared to the $Crx^{Rdy/+}$ kitten's retina and WT kitten's retina while there was no significant difference between the $Crx^{Rdy/+}$ and WT kitten's retinas. *Trβ2* was expressed at a 1.4 times higher levels in the $Crx^{Rdy/Rdy}$ compared to the WT kitten's retina while no difference was significant between the $Crx^{Rdy/+}$ and the $Crx^{Rdy/Rdy}$ or WT kitten's retinas. *Rorβ* was expressed at a 1.3 times higher levels in the $Crx^{Rdy/Rdy}$ compared to the $Crx^{Rdy/+}$ kitten's retina and WT kitten's retina while no difference was significant between the $Crx^{Rdy/+}$ and WT kitten's retinas.

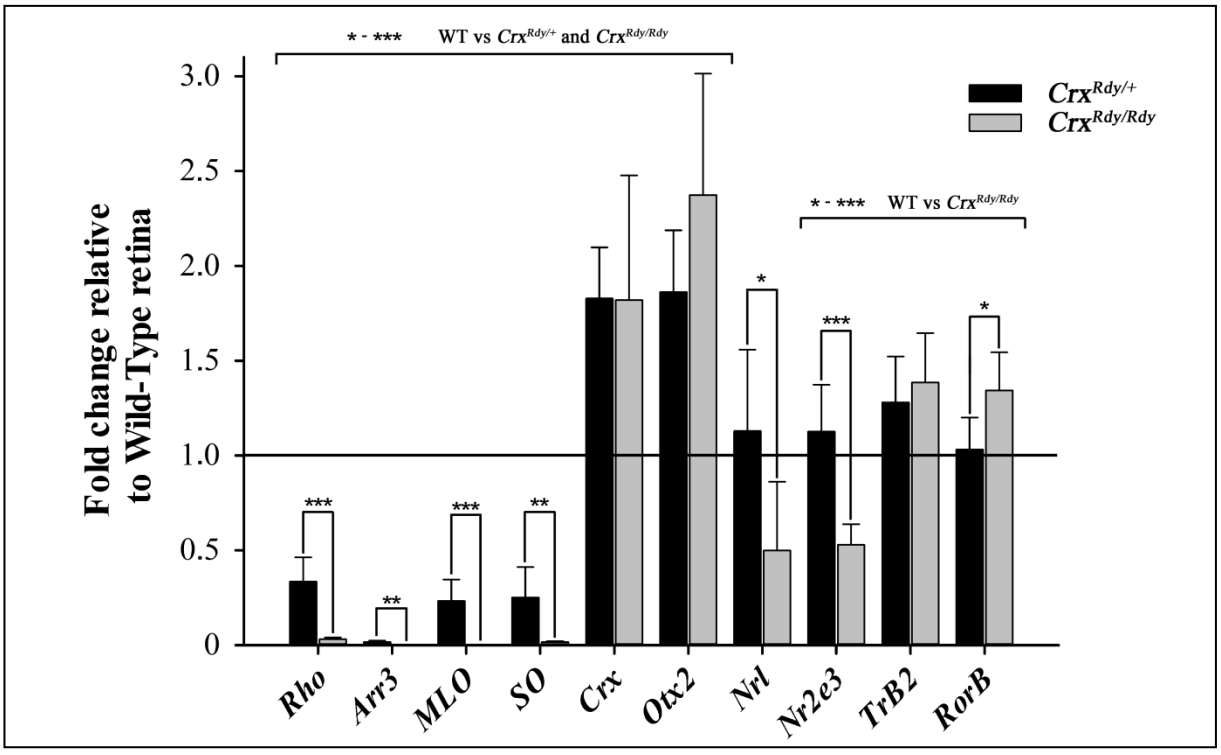

Figure 4.9. Changes in mRNA expression in $Crx^{Rdy/Rdy}$ retinas compared to $Crx^{Rdy/+}$ retinas – levels are normalized to WT retinas.

Figure 4.9 (cont'd)
qRT-PCR overall (average of the areas assessed) mRNA expression levels of *arrestin3* (*Arr3*, specific to cones), *medium-long wavelength opsin* (*MOP*, specific to M/L cones), *short wavelength opsin* (*SO*, specific to S cones), *rhodopsin* (*Rho*, specific to rods), total *Crx* (WT and mutant), *homeobox protein* (*Otx2*), *neural retina leucine zipper protein* (*Nrl*), *photoreceptor-specific nuclear receptor* (*Nr2e3*), *thyroid hormone receptor β2* (*Trβ2*) and the nuclear *receptor* (*Rorβ*) in $Crx^{Rdy/Rdy}$ and $Crx^{Rdy/+}$ retina in 2-week-old kittens retinas relative to levels in WT retinas.
The $Crx^{Rdy/Rdy}$ and $Crx^{Rdy/+}$ kitten retinas had significantly decreased levels of cone and rod opsin mRNA compared to the WT cats. In contrast, the expression of total *Crx* and *Otx2* were significantly increased compared to WT retinas. *Nrl* and *Nr2e3* were expressed at lower levels in the $Crx^{Rdy/Rdy}$ compared to the $Crx^{Rdy/+}$ and WT kitten's retinas while *Trβ2* and *Rorβ* were expressed at higher levels compared to the WT kitten's retinas. P-values comparing the means $Crx^{Rdy/Rdy}$, $Crx^{Rdy/+}$ and WT expression levels are $^{\dagger}P \leq 0.1$,$*P < 0.05$, $**P < 0.01$, and $***P < 0.001$.

To confirm the specific over expression of the mutant Crx product we performed Western blot assays (Fig. 4.10). This assay confirmed that the mutant Crx protein was at 3 times higher levels in the $Crx^{Rdy/Rdy}$ retinas than the WT Crx protein was in the WT retinas ($P = 0.005$) (Fig. 4.10B).

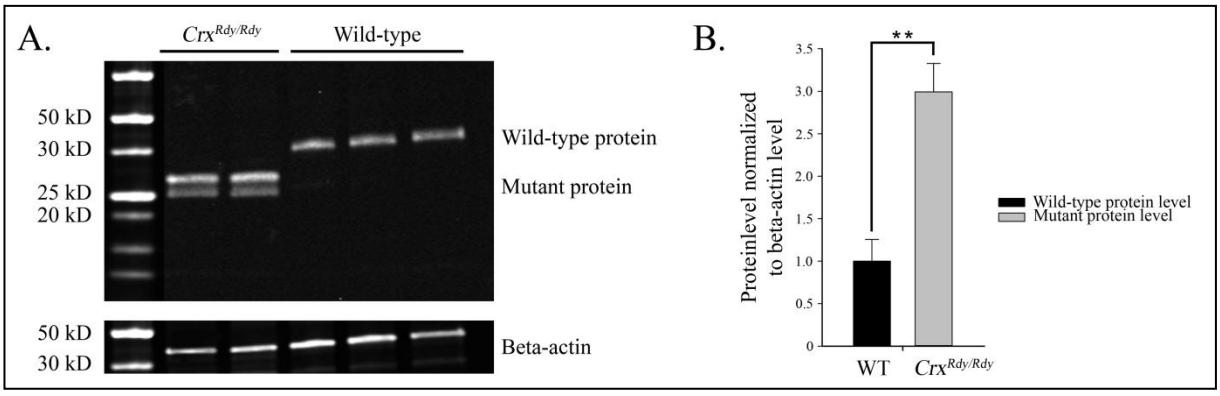

Figure 4.10. Western blot analysis for Crx nuclear protein.
(A) Western blot for nuclear Crx protein (immunolabeled with antibody 119b1). The amount of Crx protein present in retinal nuclear extract was investigated by Western blot from 2-week-old $Crx^{Rdy/Rdy}$ and WT kittens. In the $Crx^{Rdy/Rdy}$ kitten's retina only the truncated mutant Crx protein is present while as expected only the full length Crx protein is present in the WT kitten's retina. Beta-actin was used as protein loading control.
(B) Quantification of normal and mutant protein levels in $Crx^{Rdy/Rdy}$ and wild-type kittens.
Crx protein levels were normalized to beta-actin levels, and the $Crx^{Rdy/Rdy}$ kitten protein levels shown normalized to the Crx levels in the WT retinas. The level of truncated protein was higher in the $Crx^{Rdy/Rdy}$ kitten retina than the level of WT protein in the WT kittens. $**P < 0.01$

4.5. DISCUSSION

This study adds to previous studies characterizing the *Rdy* cat. While some phenotyping of the heterozygous $Crx^{Rdy/+}$ cat had been previously performed, there had been no studies reporting on the homozygous $Crx^{Rdy/Rdy}$ cat.[17-20, 33] In keeping with previous studies of Class III *CRX* mouse mutant models, the $Crx^{Rdy/Rdy}$ cat showed an over expression of the mutant Crx transcript that we predict exerts a dominant negative effect. The *Rdy* feline model offers important advantages due to the presence of a macula-like retinal region allowing for further characterization of the phenotype of Class III *CRX* mutations. Compared to other models the $Crx^{Rdy/Rdy}$ cat phenotype has certain unique features.

4.5.1. The $Crx^{Rdy/Rdy}$ kitten develops significant globe enlargement without glaucoma

The $Crx^{Rdy/Rdy}$ cat has a significant increase in axial globe length predominantly as a result of an increase in posterior segment length (Fig. 4.1). This was not associated with any increase in IOP (Fig. 4.2A).[34] Refraction (Fig. 4.2B) revealed that the globes had extreme myopia.[35-38] Abnormal globe length is a well-recognized feature in animals with abnormal visual input.[39, 40] The increase in globe size may be responsible for the choroidal thinning that was noted in the homozygous cats (Fig. 4.4).[41] The chicken has been used extensively for the study of myopia induced by visual deficits. Some models with enlarged globes have developed splits in Bruch's membrane (laquer cracks), which is also a feature of human high myopes. Further studies of the choroidal thinning in the $Crx^{Rdy/Rdy}$ cat are needed to see if splits in Bruch's membrane also develop.[42-48] The large degree of globe enlargement in the $Crx^{Rdy/Rdy}$ cat may make it a useful model for studying the mechanism of developmental myopia.

4.5.2. The *Crx*$^{Rdy/Rdy}$ kitten is a model for severe *CRX*-LCA retinopathies

The *Crx*$^{Rdy/Rdy}$ cat phenotype is characterized by blindness from birth, with a sluggish PLR, and no dazzle reflex or menace response. We suspected that the remaining PLR was driven by melanopsin containing ganglion cells and IHC showed very well conserved ganglion cells (Fig. 4.8D). Ophthalmoscopic features of the model included the development of tapetal hyperreflectivity, which is considered an indicator of generalized retinal thinning. However, there was not a significant decrease in total retinal thickness so the tapetal hyperreflectivity may have resulted from the almost total lack of cone and rod opsins that in a normal eye would absorb photons passing through the retina. The *Crx*$^{Rdy/Rdy}$ cat only developed very short inner segments that express rhodopsin (Fig. 4.8A) before photoreceptor maturation became halted. The photoreceptor nuclei consisted of two populations with different nuclear morphology: one which population had oval-shaped nuclei comparable to the appearance in an immature retina while the other showed a more mature morphology (round nuclei). It appeared that the normal migration of cell bodies of photoreceptors that occurs during maturation of the retina did not occur. The lack of photoreceptor maturation was reflected in the complete lack of detectable ERG responses (Fig. 4.3). Interestingly, there was not a rapid photoreceptor degeneration as occurs in the *Crx*$^{Rdy/+}$ cat, although some evidence of degeneration and cell migration occurred. There was initially relatively normal stratification of the retinal layers, but over time there was extensive activation of Müller cells and sprouting and migration of bipolar cells. This retinal remodeling resulted in some thickening of the inner retinal layers, which counteracted the thinning of the outer retain and thus preserved the overall retinal thickness (Figs. 4.5, 4.6, 4.7, 4.8B and 4.8C and Appendices R, S, T and U – Figs. 4.S4, 4.S5, 4.S6 and 4.S7).[30-32, 49] This retinal remodeling was more severe than in the *Crx*$^{Rdy/+}$ feline phenotype [17] but was similar to the *E168d2/d2* homozygous mouse.[50] The relative lack of overall retinal thinning may account for the striking

persistence of retinal vasculature until advanced disease stages (Figs. 4.4, 4.5, 4.6 and 4.7). The *area centralis* had slightly different changes compared to the peripheral retina with thinning of the total retina and receptor+ layers (Fig. 4.6). There was an earlier and marked loss of photoreceptor nuclei in the center of the *area centralis*.

The phenotype of the $Crx^{Rdy/Rdy}$ cat is quite different to that of the heterozygote, not being simply a more severe version. The $Crx^{Rdy/Rdy}$ cat has some similarities with the engineered *knockout* $Crx^{-/-}$ or Crx^{Rip} mice models [3, 21] with respectively some absence of outer segments at any time with rhodospin expression level decreased and some very small inner segments tips (Fig. 4.7 and Appendix V – Fig. 4.S8), and some absence of ERG response from an early age (Fig. 4.3) with mild retinal thickness changes and absence of cone marker expression. Although some similarities to other models, the $Crx^{Rdy/Rdy}$ cat presents with a particular phenotype that does not resemble any other.

The absence of photoreceptor development with no OS and very vestigial IS might be responsible for the relatively slow photoreceptor nuclei loss compared to the $Crx^{Rdy/+}$ cat. In the $Crx^{Rdy/+}$ cats, the degeneration of photoreceptors expressing phototransduction proteins and retinal degeneration can result from altered phototransduction cascade dynamics and mislocalization of opsins.[51-56]

4.5.3. Molecular mechanism underlying $Crx^{Rdy/Rdy}$ phenotype

The Rdy mutation introduces a premature stop codon [16] in *Crx* with the mutant transcript escaping nonsense-mediated decay and resulting in overexpression of the mutant allele (Fig. 4.8 and 4.9).[9, 57, 58]

Lack of normal Crx activity resulted in a marked decrease in cone and rod transcripts in the $Crx^{Rdy/Rdy}$ cat retinas. It also had effects on the levels of other transcription factors involved in

photoreceptor development. *Crx, Otx2* and *Rorβ* showed an increase in expression. The increase in *Otx2* expression may be due to a retroactive feedback mechanism compensating for the lack of other transcription factors. *Nrl* and *Nr2e3* expression level was decreased, perhaps contributing to the partial failure in maturation of the photoreceptor nuclei. Despite the slightly increased expression of *Trβ2*, which is involved in cone maturation, there was a lack of cone opsin expression and failure in cone maturation. Interpretation regarding the transcription factors' expression changes are still very difficult as the mechanism of interactions is still not completely understood and complex (Fig. 4.11).[2, 21]

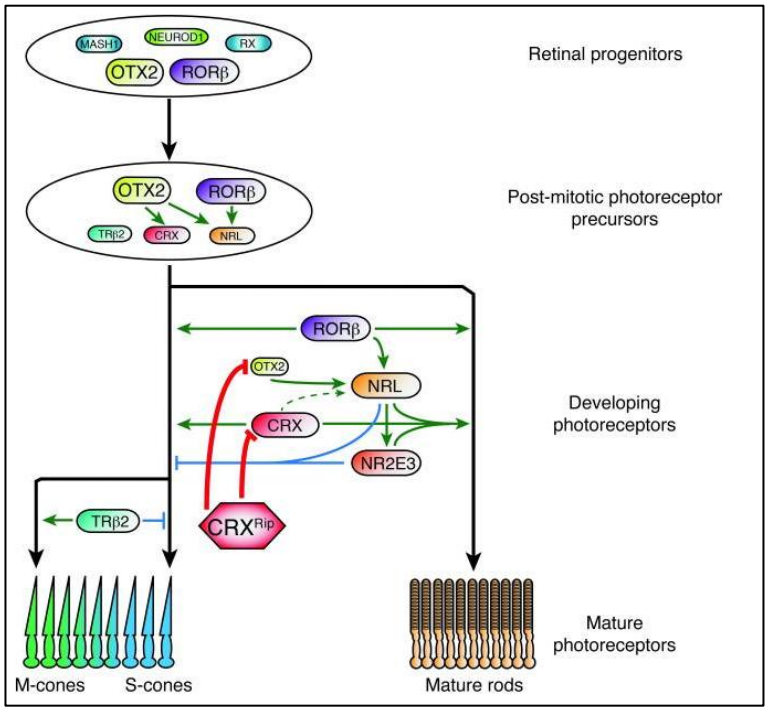

Figure 4.11. The molecular mechanism of congenital blindness caused by dominant *CRX* frameshift mutations from Roger et al, 2014.

The $Crx^{Rdy/Rdy}$ cat provides a large animal model for investigating scleral growth factors implicated in myopia development and for the severe dominant *CRX* mutations associated with over expression of a mutant transcript with an antimorphic effect.

4.6. ACKNOWLEDGEMENTS

The authors would like to thank Dr. Cheryl Craft for the donation of the hCAR antibody, Dr. Debra Thompson for the donation of the RPE65 antibody, Dr. Alicia Withrow for her help with thick sections, Dr. Wenjuan Ma for statistical advice and the RATTS group for their help with animal handling and anesthesia as well as our collaborator on this project Dr. Shiming Chen and Dr. Nicholas Tran.

Supported by National Institutes of Health Grants EY012543 and EY025272-01A1 (SC), EY002687 (P30 Core Grant) (Washington University Department of Ophthalmology and Visual Sciences (WU-DOVS)), EY013360 (T32 Predoctoral Training Grant) (WU), unrestricted funds from Research to Prevent Blindness (WUDOVS), Foundation Fighting Blindness (SC), Hope for Vision (SC), George H. Bird and ‘‘Casper’’ Endowment for Feline Initiatives (LMO and SMPJ), Michigan State University Center for Feline Health and Well-Being (LMO and SMPJ), and Myers-Dunlap Endowment (SMPJ).

APPENDICES

APPENDIX O – Figure 4.S1

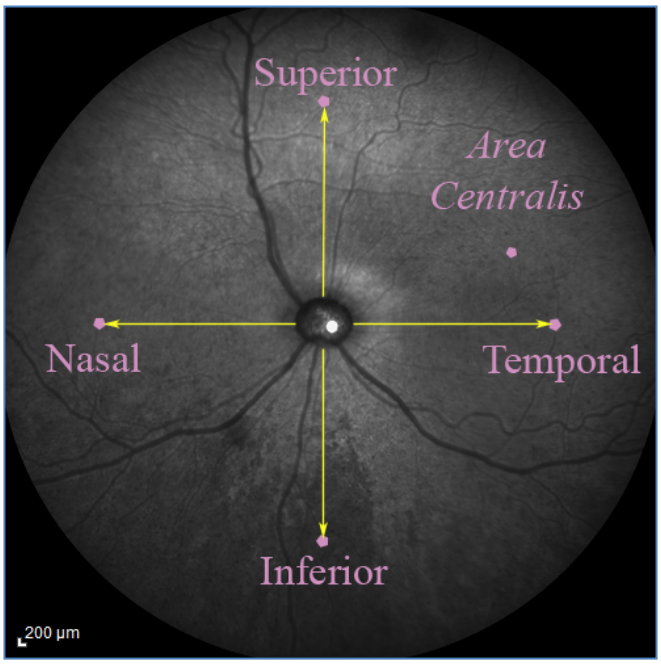

Figure 4.S1. Retinal regions imaged by SD-OCT and regions biopsied for histologic sections. Cross sectional retinal images were captured for measurement of retinal layer thicknesses at the following regions (as indicated on the fundus image by an asterisk): the *area centralis*; 4 optic nerve diameters from the optic nerve edge superiorly, inferiorly, temporally and nasally. Similarly, 3 to 3.5 mm retina-sclera biopsies were taken in the same area from processing to obtain histologic sections.

APPENDIX P – Figure 4.S2

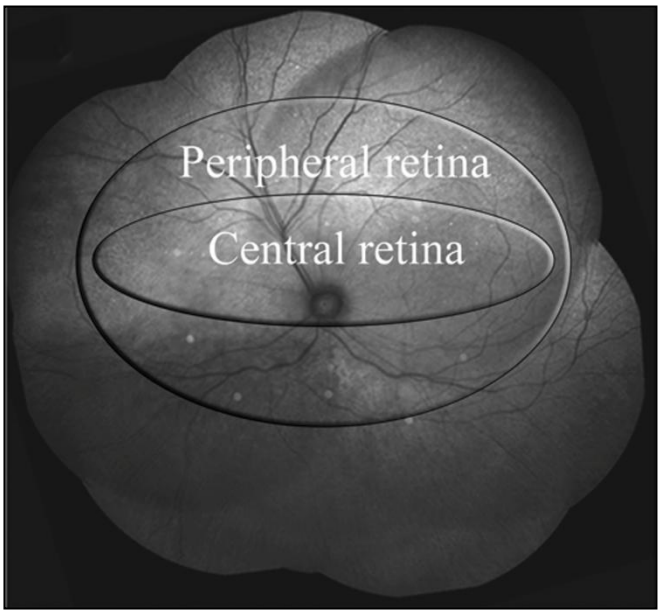

Figure 4.S2. Sites of retinal sampling for qRT-PCR (from Chapter 2).[17] Due to the small globe size of 2-week-old kittens, retina was collected from two regions as indicated (central and peripheral retinal regions).

APPENDIX Q – Figure 4.S3

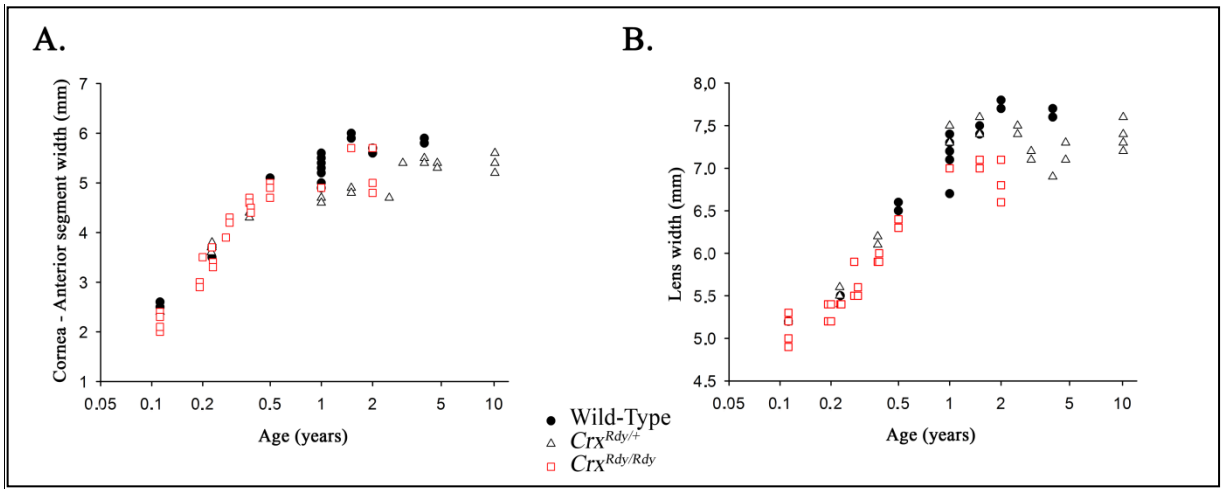

Figure 4.S3. Globe lengths.
(A) Scatter plot of the cornea-anterior segment width versus the age. No difference was present between the cornea-anterior segment width of the *Crx*$^{Rdy/Rdy}$ cat compared to that of the *Crx*$^{Rdy/+}$ and WT cats at any age tested.
(**B) Scatter plot of the lens width versus the age.** No difference was found between the lens width of the *Crx*$^{Rdy/Rdy}$ cat compared to that of the *Crx*$^{Rdy/+}$ and WT cats at any age tested.

APPENDIX R – Figure 4.S4

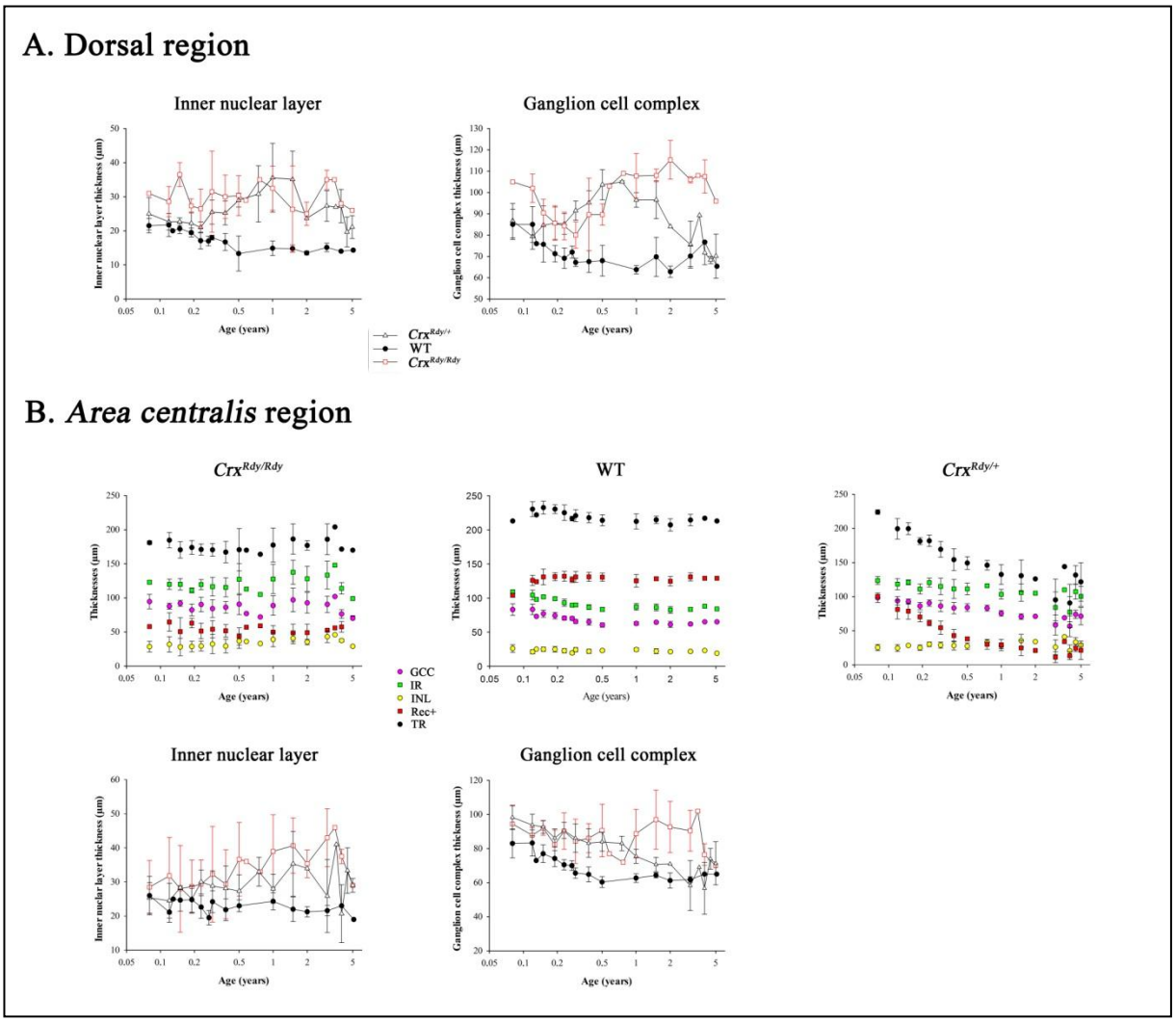

Figure 4.S4. Thicknesses of retinal layers in the dorsal and *area centralis* region.
(A) Dorsal region. The *Crx*$^{Rdy/Rdy}$ cat shows a thickening of the INL and GCC as occurs in the *Crx*$^{Rdy/+}$ cats, but in the homozygote the increased thickness is maintained with age.
(B) *Area centralis* region. As for the dorsal region (Fig. 4.5) the *Crx*$^{Rdy/Rdy}$ cats do not exhibit thinning of the retinal layers with disease progression in contrast to the *Crx*$^{Rdy/+}$ cats. The INL has a tendency to thicken, and the GCC thickness is maintained.
TR; Total retina, REC+; Receptor+, IR; Inner retina, INL; Inner retina layer, GCC; Ganglion cell complex.
.

APPENDIX S – Figure 4.S5

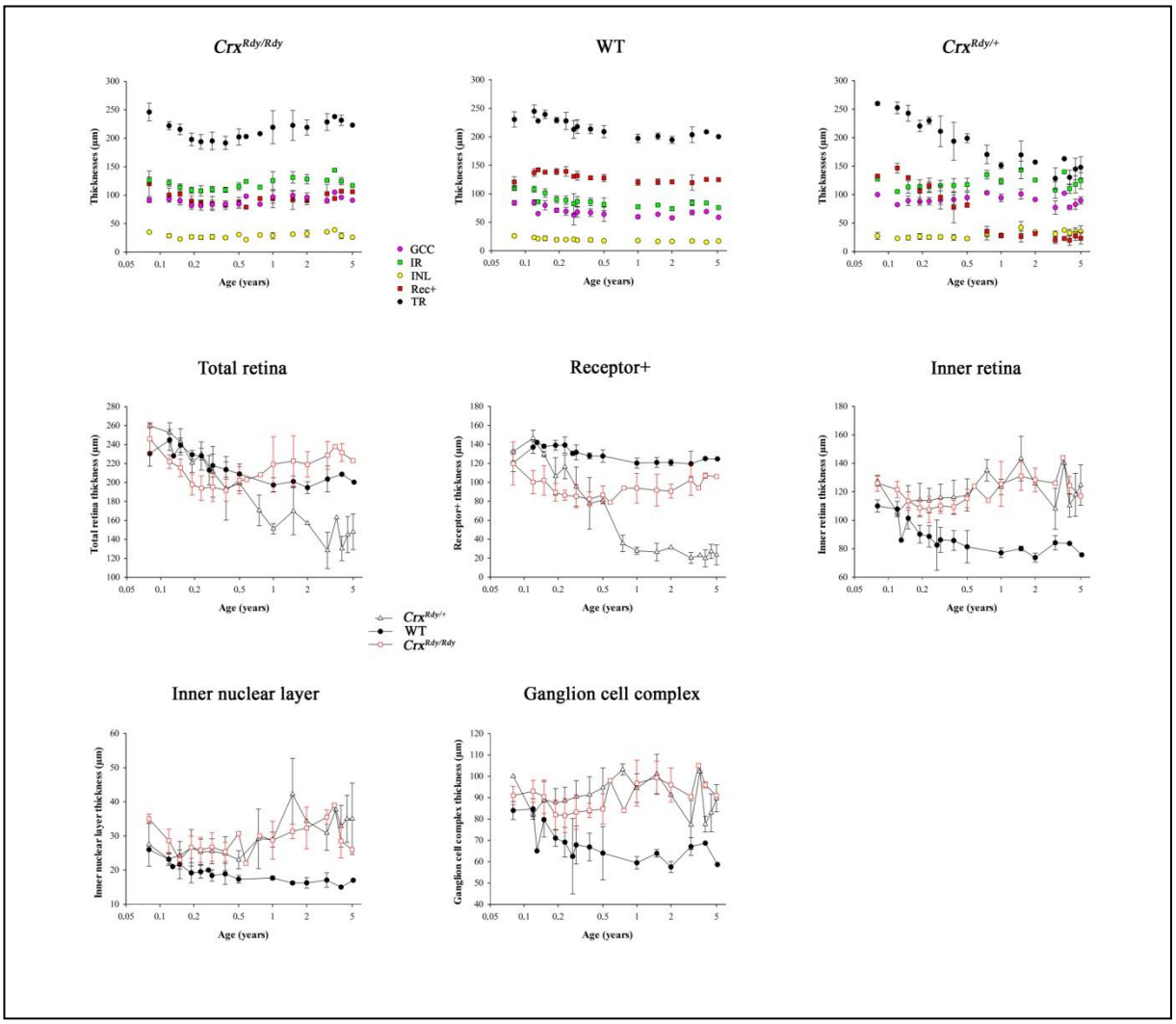

Figure 4.S5. Thicknesses of retinal layers in the temporal region.
As for the other regions retinal layer thicknesses are maintained in the *Crx*$^{Rdy/Rdy}$ cats in contrast to the severe thinning that occurs in the *Crx*$^{Rdy/+}$ cats. In the *Crx*$^{Rdy/Rdy}$ cats the INL, GCC and IR have a tendency to thicken while the TR initially thins then thickens after which the thickness is maintained. The REC+ thinned a bit but is maintained over time.
TR; Total retina, REC+; Receptor+, IR; Inner retina, INL; Inner retina layer, GCC; Ganglion cell complex.

APPENDIX T – Figure 4.S6

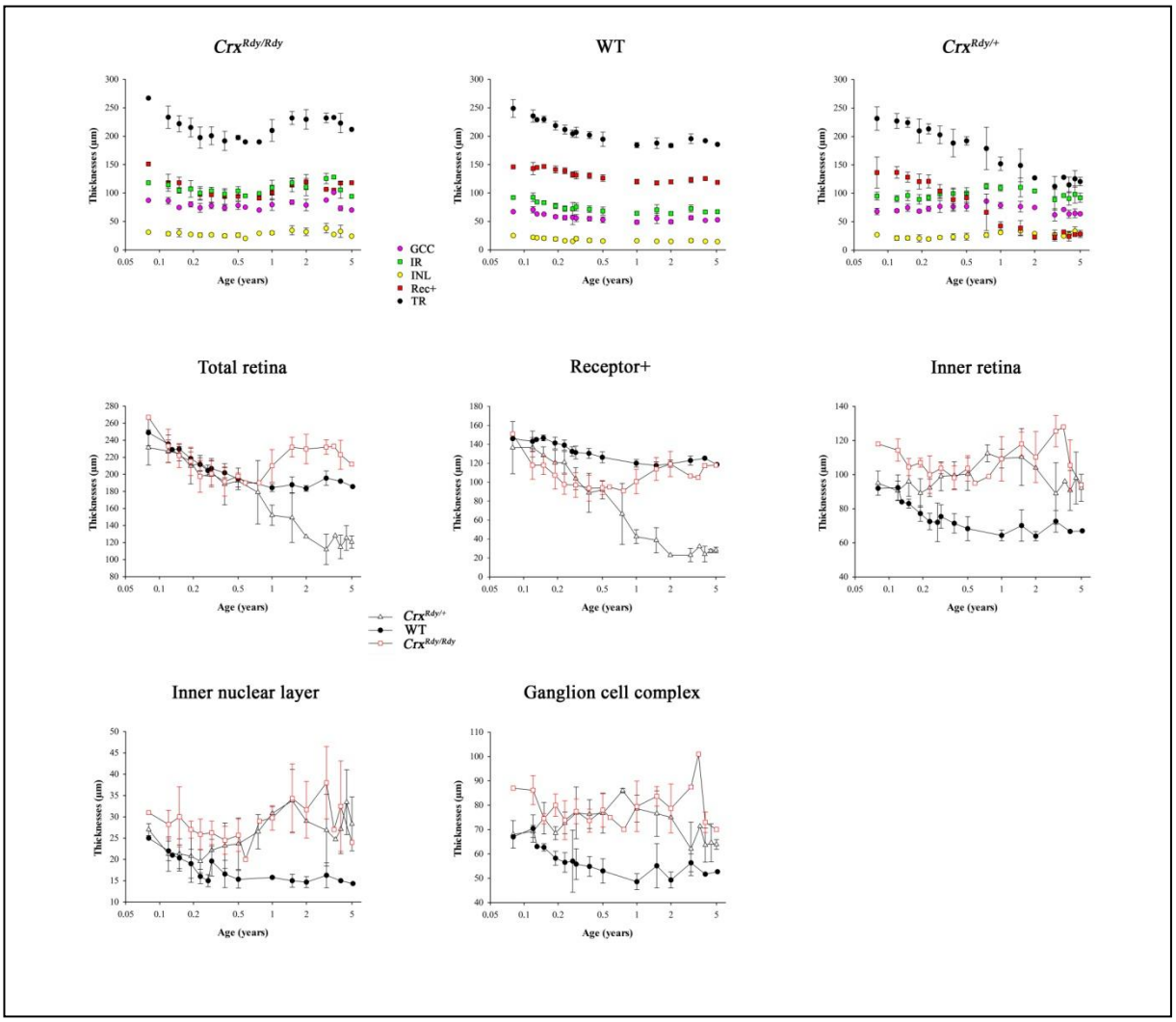

Figure 4.S6. Thicknesses of retinal layers in the nasal region.
As for the other regions retinal layer thicknesses are maintained in the *Crx*$^{Rdy/Rdy}$ cats in contrast to the severe thinning that occurs in the *Crx*$^{Rdy/+}$ cats In the *Crx*$^{Rdy/Rdy}$ cats the INL, GCC and IR have a tendency to thicken while the TR initially thins then thickens after which the thickness is maintained. The REC+ thinned a bit but is maintained over time.
TR; Total retina, REC+; Receptor+, IR; Inner retina, INL; Inner retina layer, GCC; Ganglion cell complex.

APPENDIX U –Figure 4.S7

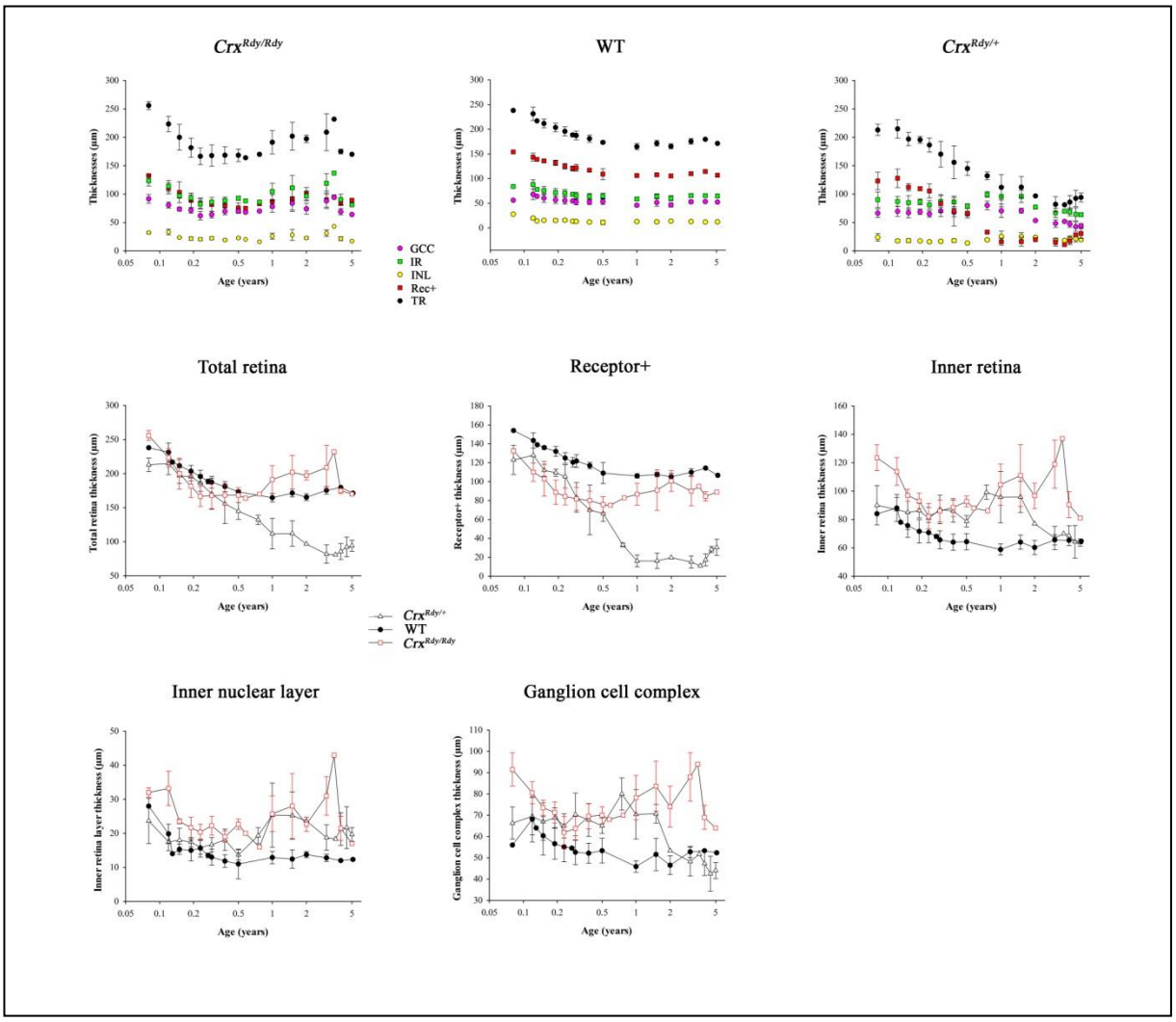

Figure 4.S7. Thicknesses of retinal layers in the ventral region.
As for the other regions retinal layer thicknesses are maintained in the *Crx*$^{Rdy/Rdy}$ cats in contrast to the severe thinning that occurs in the *Crx*$^{Rdy/+}$ cats. The INL, GCC and IR thicknesses are maintained. The REC+ and TR thinned a bit but then thickened over time.
TR; Total retina, REC+; Receptor+, IR; Inner retina, INL; Inner retina layer, GCC; Ganglion cell complex

APPENDIX V – Figure 4.S8

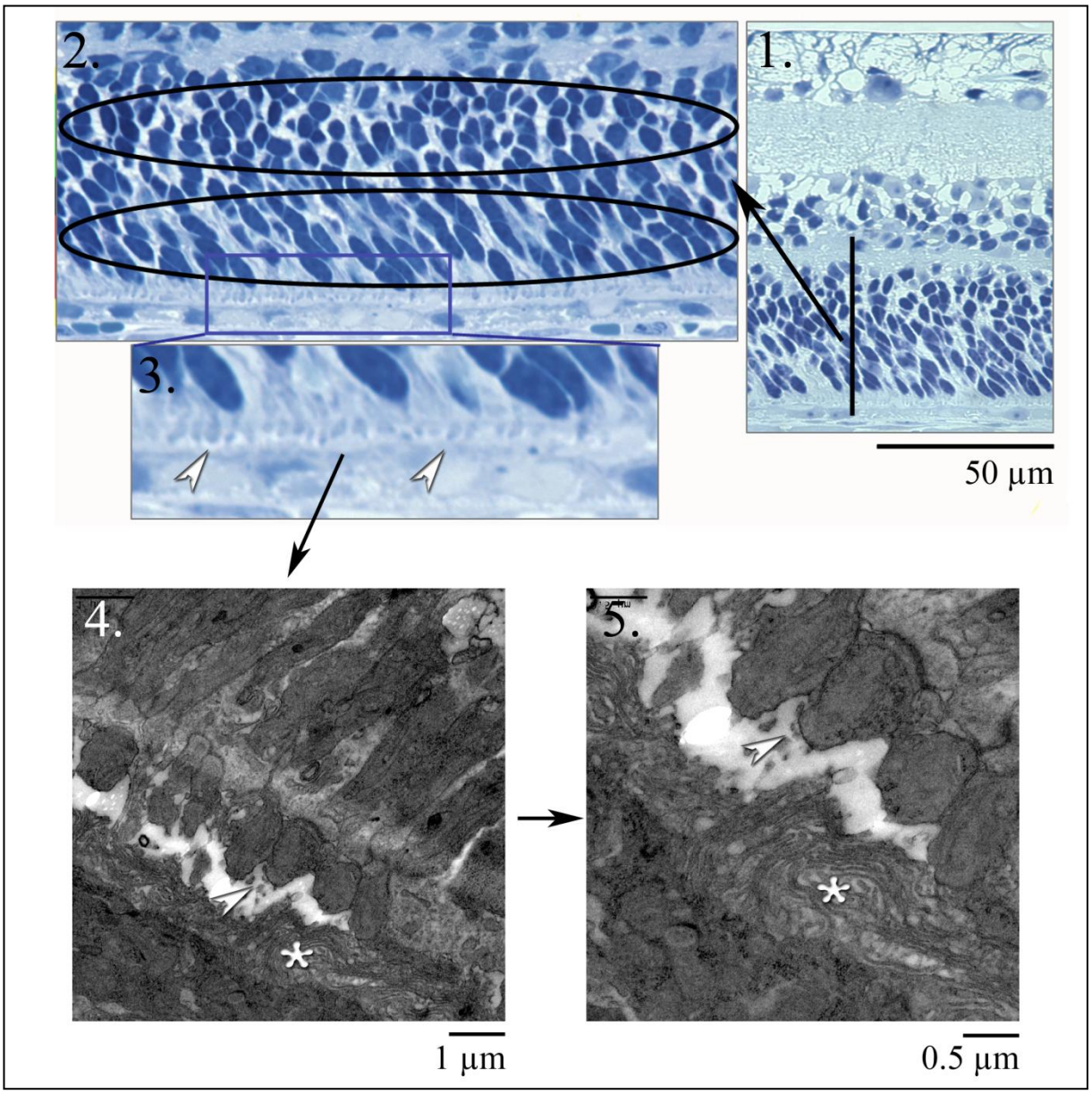

Figure 4.S8. Regular histologic and electron microscopy images of a 2-week-old *Crx*$^{Rdy/Rdy}$ cat.

Note the absence of photoreceptor outer segment layers on all images. Some very small rudimentary inner segments develop, indicated by white arrowheads (2. and 3.). Electron microscopy images showed similar rudimentary inner segments protruding through the external limiting membrane into the subretinal space, indicated by white arrowheads. The rudimentary inner segments are surrounded and in contact with RPE villosities, indicated by the white stars.

APPENDIX W – Figure 4.S9

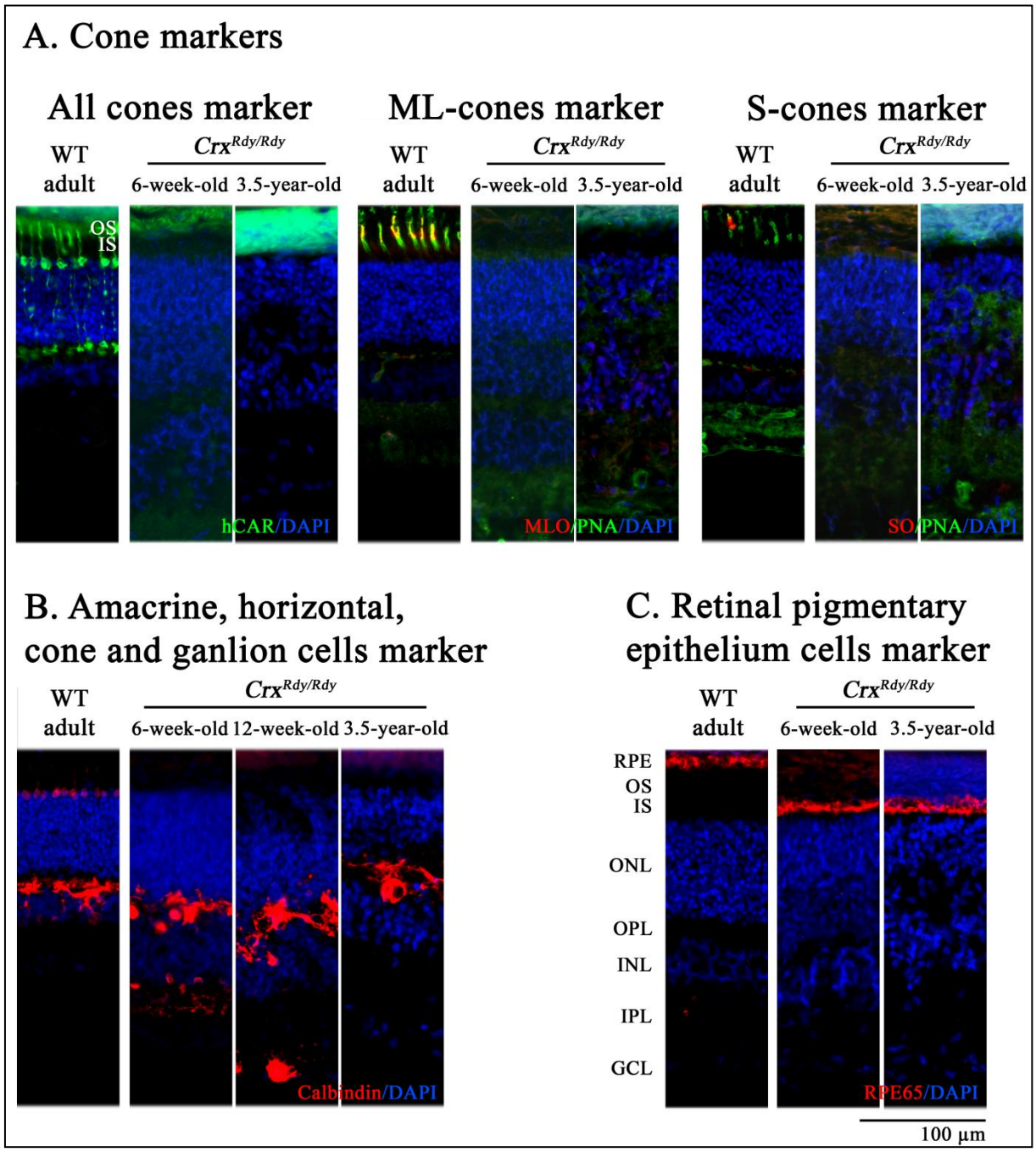

Figure 4.S9. Immunolabeling of the *Crx*$^{Rdy/Rdy}$ cat central retina frozen sections for (A) cones' markers, (B) inner retina cells's markers, (C) retinal pigmentary epithelium cell marker and (D) Crx antibody.

Figure 4.S9 (cont'd)

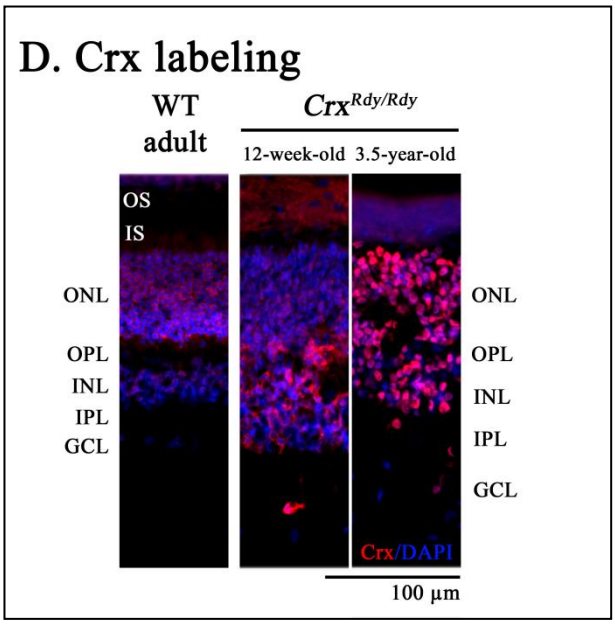

At any age tested, an absence of cones labeling was noted in the *Crx*$^{Rdy/Rdy}$ retina **(A)**. Human cone arrestin (hCAR) antibody that labels the entire cone cell bodies as seen in the WT adult retina was not detected. Labeling for medium/long wavelength opsin (MLO) or short wavelength opsin (SO) was also absent. This absence of cone labeling was also present with calbindin antibody labeling **(B)** (see the top row nuclei of the ONL labeled in red in the WT adult retina which is cone labeling). Calbindin labeling showed apparently normal labeling of the inner retinal cells such as amacrine, horizontal and ganglion cells in the *Crx*$^{Rdy/Rdy}$ retina at any age tested. Yet, it was difficult to assess precise morphology of those cell populations. **(C)** Retinal pigmentary epithelium labeled with RPE65 antibody was also present at any age tested. The Crx expression was present at high level especially in adult *Crx*$^{Rdy/Rdy}$ retina **(D)**.
OS; Photoreceptor outer segment, IS; Photoreceptor inner segment, ONL; Outer nuclear layer, OPL; Outer plexiform layer, INL; Inner nuclear layer, IPL; Inner plexiform layer, GCL; ganglion cell layer.

APPENDIX X – Table 4.S1.

Crx$^{Rdy/Rdy}$			WT			*Crx*$^{Rdy/+}$		
Age (years)	**GL both eyes**	**C-AC, L, PS both eyes**	**Age (years)**	**GL both eyes**	**C-AC, L, PS both eyes**	**Age (years)**	**GL both eyes**	**C-AC, L, PS both eyes**
0.074	1		0.071	3		0.038	1	
0.082	1		0.074	1		0.071	2	
0.112	3	3	0.09	3		0.074	2	
0.118	2		0.109	3		0.09	2	
0.148	1		0.112	1	1	0.109	3	
0.165	1		0.118	2		0.112	1	1
0.192	1	1	0.123	2		0.118	2	
0.2	1	1	0.129	2		0.129	1	
0.227	1	1	0.137	3		0.137	2	
0.23	2	1	0.14	1		0.165	1	
0.274	1	1	0.142	1		0.175	2	
0.288	2	1	0.148	1		0.194	1	
0.297	2		0.165	1		0.197	2	
0.337	2	1	0.175	3		0.2	1	
0.384	2	1	0.192	1		0.225	2	1
0.412	1		0.194	1		0.227	1	1
0.474	1		0.197	1		0.233	1	
0.499	2	2	0.2	1		0.236	1	
0.567	1		0.203	1		0.238	1	
0.778	1		0.225	1		0.274	1	
1	2	1	0.227	2	1	0.288	4	
1.5	1	1	0.233	1		0.297	2	
2	2	2	0.236	1		0.329	1	
			0.238	2		0.337	1	
			0.271	1		0.377	3	1
			0.274	1		0.384	3,5	
			0.288	3		0.412	2	
			0.297	2		0.499	3	

Table 4.S1. Experiments and numbers of animal for globe length in *Crx*$^{Rdy/Rdy}$, *Crx*$^{Rdy/+}$ and WT cats

Table 4.S1 (cont'd)

			0.329	2		0.567	1	
			0.337	2		0.775	1	
			0.377	3		1	4	1
			0.384	1		1.5	1	1
			0.412	2		2.5	1	1
			0.479	1		3	6	1
			0.499	1	1	4	2	2
			0.567	2		4.5	2	
			0.775	1		4.75	1	1
			1	9	5	5	2	
			1.5	2	1	9	2	
			2	1	1	10.1	2	2
			6	1				
Total different animals								
	6	5		24	9		30	12

GL both eyes: Axial globe length measurements in both eyes of one individual.
C-AC, L, PS both eyes: Cornea-Anterior chamber width, Lens width and Posterior Segment in both eyes of one individual.

APPENDIX Y – Table 4.S2.

IOP

Age (years)	*Crx*$^{Rdy/Rdy}$	WT
0.6		2
0.8	2	
0.9		1
2.5	1	
4.1	1	1
6.2	1	
Total different animals	**6**	**5**

Refraction

Age (years)	*Crx*$^{Rdy/Rdy}$	WT	*Crx*$^{Rdy/+}$
0.6		2	
0.8	2		1
0.9		1	
1.4			1
2.5	2		
3.2		1	
3.7			1
4.1	1	1	
4.6			1
6.2	1		
6.6			1
6.7			1
Total different animals	**6**	**5**	**6**

qRT-PCR

Age (weeks)	*Crx*$^{Rdy/Rdy}$	WT	*Crx*$^{Rdy/+}$
2	3	3	3

Western

Age (weeks)	*Crx*$^{Rdy/Rdy}$	WT
2	2	3

Table 4.S2. Experiments and numbers of animal for IOP, refraction, qRT-PCR, Western blot, immunohistochemistry and histology in *Crx*$^{Rdy/Rdy}$, *Crx*$^{Rdy/+}$ and WT cats

Table 4.S2 (cont'd)

		Immunohistochemistry	Histology
Age (years)	**Age (weeks)**	***Crx*$^{Rdy/Rdy}$**	***Crx*$^{Rdy/Rdy}$**
0.04	2	2	2
0.12	6	2	2
0.23	12	2	2
0.38	20	3	3
2		1	1
3.5		1	1

APPENDIX Z – Table 4.S3.

Age (years)	Age (weeks)	Fluorescein angiography	ERG	SD-OCT
0.08	4		2	2
0.12	6		6	4
0.15	8		2	2
0.19	10		4	3
0.23	12		5	8
0.29	15		4	4
0.34	17.5		1	
0.38	20		7	6
0.5	26	2		3
0.58				1
0.77				1
1		1		4
1.5				3
2		1		3
3		1		2
3.5				1
4		1		2
5				1
Total different animals		**4**	**10**	**12**

Table 4.S3. Experiments and numbers of animal for fluorescein angiography, ERG and SD-OCT in *Crx*$^{Rdy/Rdy}$ cats

APPENDIX a – Table 4.S4.

Antibody – Source	Type	Primary Dilution	Secondary Antibody – Source	Secondary Dilution
Hcar (Human cone arrestin) Dr. Cheryl Craft; LUMIJ, University of Southern California, Los Angeles, CA, USA	Polyclonal rabbit	1:10,000	Alexa Fluor 488 Goat anti-rabbit IgG Life technologies, Carlsbad, CA, USA	1:500
PNA (Biotinylated Peanut Agglutinin) Vector Labs Inc., Burlin-game, CA, USA	Biotinylated Lectin	1:500	Alexa Fluor 488 Streptavadin Life technologies, Carlsbad, CA, USA	1:500
ML-opsin (Anti-Opsin, Red/Green; Medium/ Long wavelength cone opsin) Millipore Corp., Billerica, MA, USA	Polyclonal rabbit	1:1,000	Alexa Fluor 568 or 594 Goat anti-rabbit IgG Life technologies, Carlsbad, CA, USA	1:500
S-opsin (Anti-Opsin, Blue; Short wavelength cone opsin) Millipore Corp., Billerica, MA, USA	Polyclonal rabbit	1:1,000	Alexa Fluor 568 or 594 Goat anti-rabbit IgG Life technologies, Carlsbad, CA, USA	1:500
RetP1 (Rhodopsin Ab-1) Thermo Scientific, Rockford, IL, USA	Monoclonal mouse	1:2	Alexa Fluor 594 Goat anti-mouse IgG Life technologies, Carlsbad, CA, USA	1:500
GFAP (Anti-Glial Fibrillary Acidic Protein) Cell Signaling Technology Inc., Danvers, MA, USA	Monoclonal mouse	1:300	Alexa Fluor 594 Rabbit anti-mouse IgG Life technologies, Carlsbad, CA, USA	1:500
PKCα (Protein Kinase C-alpha) BD Biosciences, San Jose, CA, USA	Monoclonal mouse	1:500	Alexa Fluor 594 Goat anti-mouse IgG Life technologies, Carlsbad, CA, USA	1:500
Calbindin Swant, Marly, Switzerland	Monoclonal mouse	1:500	Alexa Fluor 568 Goat anti-mouse IgG Life technologies, Carlsbad, CA, USA	1:500
NeuN (Neuron-Specific Nuclear Protein) Millipore Corp., Billerica, MA, USA	Monoclonal mouse	1:2,000	Alexa Fluor 488 Goat anti-mouse IgG Life technologies, Carlsbad, CA, USA	1:500
RPE65 (Retinal pigmentary epithelium-specific 65kDA protein) Dr. Debra Thompson; Kellogg eye center, University of Michigan, Ann Arbor, MI, USA	Monoclonal mouse	1:500	Alexa Fluor 568 Goat anti-mouse IgG Life technologies, Carlsbad, CA, USA	1:500
Crx (Cone rod homebox) Sigma-Aldrich, St Louis, MO, USA	Monoclonal mouse	1:20,000	Alexa Fluor 568 Goat anti-mouse IgG Life technologies, Carlsbad, CA, USA	1:500

Table 4.S4. List of antibodies used for IHC – their origins and dilutions

APPENDIX b – Table 4.S5.

Primer name	Forward primer	Reverse primer	Amplicon size (bp)
Arr3	5' CGTTGTCCTGTATTCCCTAGAC 3'	5' GCTAGAGGCCAGATTAGTATCAC 3'	190
Rho	5' GGTGCCCTACGCCAGCGTG 3'	5' CAGTGGGTTCTTGCCACAG 3'	190
MOP	5' TGTCTCCTTGTGTGGGATCA 3'	5' GTACGAGCTGCCACTGAACA 3'	257
SO	5' AGTCAGCCTCAACCCAGAA 3'	5' CACCATCTCCATGATGCAAG 3'	326
Crx Total	5' AAGACTCAGTACCCGGATGTGTA 3'	5' GGGGCTGTAGGAGTCTGAGAT 3'	223
OTX2	5' GCTAGACGTGCTGGAAGCTC 3'	5' GGGCTGGAGAGGTCTTCTTT 3'	209
Nrl	5' CCCACAGCTACTACCCAGGA 3'	5' TCACACCACTCCCTCTCCTC 3'	207
Nr2e3	5' CATCCCCATACTCCTCCTCA 3'	5' GAGGCAGGGACCACTGTATG 3'	198
TrB2	5' GACTCCGAACTTGTCGCATT 3'	5' TTTGGTTGATGTTGCTGTGG 3'	197
RorB	5' GAGGAATGCAGATGTTCAAGG 3'	5' GCTTCTGGACCTTCCTTGGT 3'	177
Tuba1b	5' GCTCTATTGCCTGGAACACG 3'	5' CATCTTCCTTGCCCGTGATG 3'	230
GAPDH	5' GGTCTTCACCACCATGGAGA 3'	5' TGGACTGTGGTCATGAGTCC 3'	237

Table 4.S5. Primer sequences for qRT-PCR assays

APPENDIX c – Table 4.S6.

	$Crx^{Rdy/Rdy}$ *vs* WT	$Crx^{Rdy/Rdy}$ *vs* $Crx^{Rdy/+}$	$Crx^{Rdy/+}$ *vs* WT
Arr3	P = 0.004	P = 0.003	P = 0.002
Rho	P = 0.004	P ≤ 0.001	P ≤ 0.001
MOP	P ≤ 0.001	P = 0.001	P = 0.002
SO	P = 0.004	P = 0.010	P = 0.026
Crx Total	P = 0.032	P = 0.792	P = 0.002
OTX2	P ≤ 0.001	P = 0.119	P ≤ 0.001
Nrl	P = 0.058	P = 0.029	P = 0.603
Nr2e3	P ≤ 0.001	P ≤ 0.001	P = 0.295
TrB2	P = 0.030	P = 0.507	P = 0.069
RorB	P = 0.049	P = 0.021	P = 0.822

Table 4.S6. *P* values for qRT-PCR assays results
Significant values are indicated in red.
Note only *P* values for the overall retina sample are given. Indeed, difference per region was not considered interpretable as the risk of Type II error was quite high.

REFERENCES

REFERENCES

1. Furukawa T, Morrow EM, Cepko CL. Crx, a novel otx-like homeobox gene, shows photoreceptor-specific expression and regulates photoreceptor differentiation. *Cell.* 1997;91:531-541.

2. Hennig AK, Peng GH, Chen S. Regulation of photoreceptor gene expression by Crx-associated transcription factor network. *Brain Res.* 2008;1192:114-133.

3. Morrow EM, Furukawa T, Raviola E, Cepko CL. Synaptogenesis and outer segment formation are perturbed in the neural retina of Crx mutant mice. *BMC Neurosci.* 2005;6:5.

4. Chau KY, Chen S, Zack DJ, Ono SJ. Functional domains of the cone-rod homeobox (CRX) transcription factor. *J Biol Chem.* 2000;275:37264-37270.

5. Chen S, Wang QL, Nie Z, et al. Crx, a novel Otx-like paired-homeodomain protein, binds to and transactivates photoreceptor cell-specific genes. *Neuron.* 1997;19:1017-1030.

6. Peng GH, Chen S. Crx activates opsin transcription by recruiting HAT-containing co-activators and promoting histone acetylation. *Hum Mol Genet.* 2007;16:2433-2452
.
7. Corbo JC, Lawrence KA, Karlstetter M, et al. CRX ChIP-seq reveals the cis-regulatory architecture of mouse photoreceptors. *Genome Res.* 2010;20:1512-1525.

8. Livesey FJ, Furukawa T, Steffen MA, Church GM, Cepko CL. Microarray analysis of the transcriptional network controlled by the photoreceptor homeobox gene Crx. *Curr Biol.* 2000;10:301-310.

9. Tran NM, Zhang A, Zhang X, Huecker JB, Hennig AK, Chen S. Mechanistically Distinct Mouse Models for CRX-Associated Retinopathy. *PLoS Genet.* 2014;10:e1004111.

10. Sohocki MM, Sullivan LS, Mintz-Hittner HA, et al. A range of clinical phenotypes associated with mutations in CRX, a photoreceptor transcription-factor gene. *Am J Hum Genet.* 1998;63:1307-1315.

11. Hull S, Arno G, Plagnol V, et al. The phenotypic variability of retinal dystrophies associated with mutations in CRX, with report of a novel macular dystrophy phenotype. *Invest Ophthalmol Vis Sci.* 2014;55:6934-6944.

12. Stone EM. Leber congenital amaurosis - a model for efficient genetic testing of heterogeneous disorders: LXIV Edward Jackson Memorial Lecture. *Am J Ophthalmol.* 2007;144:791-811.

13. Koenekoop RK. An overview of Leber congenital amaurosis: a model to understand human retinal development. *Surv Ophthalmol.* 2004;49:379-398.

14. Huang L, Xiao X, Li S, et al. CRX variants in cone-rod dystrophy and mutation overview. *Biochem Biophys Res Commun.* 2012;426:498-503.

15. Tran NM, Chen SM. Mechanisms of Blindness: Animal Models Provide Insight Into Distinct CRX-Associated Retinopathies. *Dev Dyn.* 2014;243:1153-1166.

16. Menotti-Raymond M, Deckman KH, David V, Myrkalo J, O'Brien SJ, Narfstrom K. Mutation discovered in a feline model of human congenital retinal blinding disease. *Invest Ophthalmol Vis Sci.* 2010;51:2852-2859.

17. Occelli LM, Tran NM, Narfstrom K, Chen S, Petersen-Jones SM. CrxRdy Cat: A Large Animal Model for CRX-Associated Leber Congenital Amaurosis. *Invest Ophthalmol Vis Sci.* 2016;57:3780-3792.

18. Leon A, Hussain AA, Curtis R. Autosomal dominant rod-cone dysplasia in the Rdy cat. 2. Electrophysiological findings. *Exp Eye Res.* 1991;53:489-502.

19. Curtis R, Barnett KC, Leon A. An early-onset retinal dystrophy with dominant inheritance in the Abyssinian cat. Clinical and pathological findings. *Invest Ophthalmol Vis Sci.* 1987;28:131-139.

20. Leon A, Curtis R. Autosomal dominant rod-cone dysplasia in the Rdy cat. 1. Light and electron microscopic findings. *Exp Eye Res.* 1990;51:361-381.

21. Roger JE, Hiriyanna A, Gotoh N, et al. OTX2 loss causes rod differentiation defect in CRX-associated congenital blindness. *J Clini Invest.* 2014;124:631-643.

22. Swaroop A, Wang QL, Wu W, et al. Leber congenital amaurosis caused by a homozygous mutation (R90W) in the homeodomain of the retinal transcription factor CRX: direct evidence for the involvement of CRX in the development of photoreceptor function. *Hum Mol Genet.* 1999;8:299-305.

23. Pignatelli V, Cepko CL, Strettoi E. Inner retinal abnormalities in a mouse model of Leber's congenital amaurosis. *J Comp Neurol.* 2004;469:351-359.

24. Hood DC, Lin CE, Lazow MA, Locke KG, Zhang X, Birch DG. Thickness of receptor and post-receptor retinal layers in patients with retinitis pigmentosa measured with frequency-domain optical coherence tomography. *Invest Ophthalmol Vis Sci.* 2009;50:2328-2336.

25. Mowat FM, Gornik KR, Dinculescu A, et al. Tyrosine capsid-mutant AAV vectors for gene delivery to the canine retina from a subretinal or intravitreal approach. *Gene Ther.* 2014;21:96-105.

26. Schneider CA, Rasband WS, Eliceiri KW. NIH Image to ImageJ: 25 years of image analysis. *Nat Methods.* 2012;9:671-675.

27. RStudio Team (2015). RStudio: Integrated Development for R. RStudio I, Boston, MA URL http://www.rstudio.com/.

28. Staurenghi G, Sadda S, Chakravarthy U, Spaide RF, International Nomenclature for Optical Coherence Tomography P. Proposed lexicon for anatomic landmarks in normal posterior segment spectral-domain optical coherence tomography: the IN*OCT consensus. *Ophthalmology.* 2014;121:1572-1578.

29. Pasteels B, Rogers J, Blachier F, Pochet R. Calbindin and calretinin localization in retina from different species. *Vis. Neurosci.* 1990;5:1-16.

30. Ekstrom P, Sanyal S, Narfstrom K, Chader GJ, van Veen T. Accumulation of glial fibrillary acidic protein in Muller radial glia during retinal degeneration. *Invest Ophthalmol Vis Sci.* 1988;29:1363-1371.

31. Sarthy PV, Fu M. Transcriptional activation of an intermediate filament protein gene in mice with retinal dystrophy. *DNA.* 1989;8:437-446.

32. Linberg KA, Fariss RN, Heckenlively JR, Farber DB, Fisher SK. Morphological characterization of the retinal degeneration in three strains of mice carrying the rd-3 mutation. *Vis Neurosci.* 2005;22:721-734.

33. Chong NH, Alexander RA, Barnett KC, Bird AC, Luthert PJ. An immunohistochemical study of an autosomal dominant feline rod/cone dysplasia (Rdy cats). *Exp Eye Res.* 1999;68:51-57.

34. Rusanen E, Florin M, Hassig M, Spiess BM. Evaluation of a rebound tonometer (Tonovet) in clinically normal cat eyes. *Vet Ophthalmol.* 2010;13:31-36.

35. McMullen RJ, Jr., Davidson MG, Gilger BC. The effect of 1% tropicamide-induced mydriasis and cycloplegia on spherical refraction of the adult horse. *Vet Ophthalmol.* 2014;17:120-125.

36. Twelker JD, Mutti DO. Retinoscopy in infants using a near noncycloplegic technique, cycloplegia with tropicamide 1%, and cycloplegia with cyclopentolate 1%. *Optom Vis Sci.* 2001;78:215-222.

37. Schaeffel F, Feldkaemper M. Animal models in myopia research. *Clin Exp Optom.* 2015;98:507-517.

38. Konrade KA, Hoffman AR, Ramey KL, Goldenberg RB, Lehenbauer TW. Refractive states of eyes and associations between ametropia and age, breed, and axial globe length in domestic cats. *Am J Vet Res.* 2012;73:279-284.

39. Whitmore WG. Congenital and developmental myopia. *Eye (London, England)* 1992;6 (Pt 4):361-365.

40. Ritchey ER, Zelinka C, Tang J, et al. Vision-guided ocular growth in a mutant chicken model with diminished visual acuity. *Exp Eye Res.* 2012;102:59-69.

41. Rada JA, Shelton S, Norton TT. The sclera and myopia. *Exp Eye Res.* 2006;82:185-200.

42. Liang H, Crewther DP, Crewther SG, Barila AM. A role for photoreceptor outer segments in the induction of deprivation myopia. *Vis Res.* 1995;35:1217-1225.

43. Troilo D, Quinn N, Baker K. Accommodation and induced myopia in marmosets. *Vis Res.* 2007;47:1228-1244.

44. Montiani-Ferreira F, Fischer A, Cernuda-Cernuda R, et al. Detailed histopathologic characterization of the retinopathy, globe enlarged (rge) chick phenotype. *Mol Vis.* 2005;11:11-27.

45. Montiani-Ferreira F, Kiupel M, Petersen-Jones SM. Spontaneous lacquer crack lesions in the retinopathy, globe enlarged (rge) chick. *J Comp Pathol.* 2004;131:105-111.

46. Inglehearn CF, Morrice DR, Lester DH, et al. Genetic, ophthalmic, morphometric and histopathological analysis of the Retinopathy Globe Enlarged (rge) chicken. *Mol Vis.* 2003;9:295-300.

47. McBrien NA, Gentle A. Role of the sclera in the development and pathological complications of myopia. *Prog Retin Eye Res.* 2003;22:307-338.

48. Gollender M, Thorn F, Erickson P. Development of axial ocular dimensions following eyelid suture in the cat. *Vis Res.* 1979;19:221-223.

49. Hippert C, Graca AB, Barber AC, et al. Muller glia activation in response to inherited retinal degeneration is highly varied and disease-specific. *PloS one.* 2015;10:e0120415.

50. Tran NM, Chen S. Mechanisms of blindness: Animal models provide insight into distinct CRX-associated retinopathies. *Dev Dyn.* 2014;243:1153-1166.

51. Hollingsworth TJ, Gross AK. Defective trafficking of rhodopsin and its role in retinal degenerations. *Int Rev Cell Mol Biol.* 2012;293:1-44.

52. Gao J, Cheon K, Nusinowitz S, et al. Progressive photoreceptor degeneration, outer segment dysplasia, and rhodopsin mislocalization in mice with targeted disruption of the retinitis pigmentosa-1 (Rp1) gene. *Proc Natl Acad Sci U S A.* 2002;99:5698-5703.

53. Hollingsworth TJ, Gross AK. The severe autosomal dominant retinitis pigmentosa rhodopsin mutant Ter349Glu mislocalizes and induces rapid rod cell death. *J Biol Chem.* 2013;288:29047-29055.

54. Bandyopadhyay M, Kono M, Rohrer B. Explant cultures of Rpe65-/- mouse retina: a model to investigate cone opsin trafficking. *Mol Vis.* 2013;19:1149-1157.

55. Rana T, Shinde VM, Starr CR, et al. An activated unfolded protein response promotes retinal degeneration and triggers an inflammatory response in the mouse retina. *Cell Death Dis.* 2014;5:e1578.

56. Athanasiou D, Aguila M, Bevilacqua D, Novoselov SS, Parfitt DA, Cheetham ME. The cell stress machinery and retinal degeneration. *FEBS lett.* 2013;587:2008-2017.

57. Nichols LL, 2nd, Alur RP, Boobalan E, et al. Two novel CRX mutant proteins causing autosomal dominant Leber congenital amaurosis interact differently with NRL. *Hum Mutat.* 2010;31:E1472-1483.

58. Terrell D, Xie B, Workman M, et al. OTX2 and CRX rescue overlapping and photoreceptor-specific functions in the Drosophila eye. *Dev Dyn.* 2012;241:215-228.

CHAPTER 5

ADENO-ASSOCIATED VIRUS GENE AUGMENTATION THERAPY TRIAL FOR *CRX*-LCA DOMINANT NEGATIVE MUTATION IN THE $CRX^{RDY/+}$ FELINE MODEL

5.1. ABSTRACT

PURPOSE. Mutations in the retinal transcription factor cone-rod homeobox (*CRX*) gene are cause of severe dominant LCA retinopathies. There is currently no treatment for dominant negative LCA diseases. The $Crx^{Rdy/+}$ feline large animal model was reported to be a valuable model for Class III *CRX* mutations for mechanistic disease mechanisms as well as potential therapy development. In this model, the disease is characterized by a toxic effect of the mutant *Crx* mRNA/protein over the WT mRNA/protein. The aim of this project was to shift the ratio of mutant to WT mRNA/protein in order to slow down retinal degeneration and rescue some visual function. **METHODS.** 3-week-old $Crx^{Rdy/+}$ kittens received a subretinal injection of an adeno-associated viral (AAV) vector containing the human *CRX* cDNA sequence with an attached FLAG-sequence. Two different AAV serotypes were used: AAV2/5 and AAV2/8 with a single capsid mutation (Y733F). Transgene expression was driven by an ubiquitous promoter (*chicken ß-actin*, *CBA*) or a photoreceptor specific promoter (*G-protein-dependent receptor kinase, GRK1*). Outcome was assessed by fundus examination, electroretinography (ERG), optical coherence tomography and immunohistochemistry analyses. **RESULTS.** The ubiquitous promoter resulted in low levels of transgene expression. The vectors with a *GRK1* promoter provided strong expression. Mixture of AAV2/8 Y733F containing vectors with both promoters (ubiquitous and *GRK1*) resulted also in an increased combined transgene. No major adverse effects were noted. Only one kitten showed significant functional rescue as assessed by ERG. **CONCLUSIONS.** Subretinal delivery of vector in 3-week-old kittens was possible, but it could be challenging to specifically target the *area centralis*, which is the most rapid degenerating region in the $Crx^{Rdy/+}$ model. Some transgene expression as demonstrated by FLAG expression was present in most kittens, yet only one kitten showed functional rescue. Further optimization is necessary, and gene augmentation might not be sufficient to shift the mutant to WT *Crx* ratio to

reach consistent and sustainable rescue. It may be of value to combine it with other techniques aiming to downregulate the mutant *Crx* allele.

5.2. INTRODUCTION

Mutations in the cone-rod homeobox (*CRX*) gene are an important cause of severe, early onset retinal dystrophies, which rapidly progress to blindness.[1, 2] In children, they result in one form of dominantly inherited childhood vision loss classified as Leber congenital amaurosis (LCA)[3, 4] for which there is an unmet need for a therapy to slow or prevent vision loss.

LCA accounts for ~5% of all inherited retinopathies with a prevalence of between 1 in 30,000 to 81,000 newborns.[5, 6] Mutations in the *CRX* gene account for about 2% of LCA.[7] *CRX* encodes a transcription factor that is essential for photoreceptor development, maturation and post-development survival. The protein has a DNA-binding domain and transactivation domains.[8-12]

In the *Rdy* cat, a single basepair deletion (p.Pro185LysfsTer2) in *Crx* was identified as the cause of a severe, dominant, early-onset form of progressive retinal atrophy.[13] The *Rdy* mutation results in a frameshift and premature stop codon at codon 186 resulting in a similar truncation to the *Ed168d2* mouse model and several different Class III human *CRX* frameshift mutations.[13-15] The heterozygous *Rdy* ($Crx^{Rdy/+}$) cat has been shown to have a LCA phenotype strikingly similar to those. The truncated mRNA in *Rdy* cats, as well as in animal and *in vitro* models of similar truncating mutations, escapes non-sense mediated decay and is transcribed into a truncated protein.[2, 14, 15] In chapter 2, we demonstrated that $Crx^{Rdy/+}$ feline retinas, prior to degeneration, have higher levels of mutant *Crx* mRNA and protein than they have of the wild-type *Crx* mRNA and protein, which is in keeping with the findings in mouse models with similar mutations. The

Crx mutant protein in Class III *CRX* mutations has an antimorphic effect by binding the promoter of target genes but failing to transactivate them.[2, 14]

In addition, to being a valuable model for mechanistic disease investigation, the feline model is extremely important for preclinical assessment of therapy in humans. As described in chapter 1, the cat eye has similar globe dimensions[16, 17] as the human eye making it suitable for therapy delivery techniques that are used in human patients. Also, the distribution of photoreceptors across the feline retina is similar to the human retina unlike laboratory mice, which have a dorsal to ventral photoreceptor gradient.[18-24] The *area centralis* of the feline retina has a higher density of photoreceptors, including cones, analogous to the human macula. This is particularly valuable when investigating conditions such as *CRX*-LCA retinopathies, which present with early cone photoreceptors involvement. The phenotypic similarity, along with an identical proposed disease mechanism for the frameshift mutations affecting the transactivation domains of *CRX*, make the $Crx^{Rdy/+}$ feline model a valuable model to use for preclinical testing of therapies for *CRX*-LCA retinopathies.

In designing a therapeutic approach, phenotypic characteristics of animals with Class III *CRX* mutations have been taken into account. The *E168d2* mouse model has two distinct lines. In one line an intronic *Neo* cassette remains (*E168d2Neo* line), and this line has a lower level of mutant *Crx* transcript and protein than a second line where the *Neo* cassette has been excised (*E168d2*). The *E168d2Neo* line has a much milder phenotype than the *E168d2* line suggesting that increasing the ratio of wild-type to mutant *Crx* will improve the phenotype.[2, 15] Additionally, humans and animal models heterozygous for *null* mutations of *CRX* have been shown to have very mild or non-existent phenotype, indicating that haploinsufficiency does not explain the severe phenotype associated with frameshift mutations.[2, 12, 15, 25-28] Taken together these

observations confirm that the severe dominant CRX-related retinopathies are not due to haploinsufficiency but due to a deleterious effect of the mutant protein.

As a treatment strategy, we therefore hypothesize that increasing the ratio of wild-type to mutant *Crx* protein will result in a milder phenotype in animals heterozygous for antimorphic *Crx* mutations. The aim of this study was to start investigating whether increasing expression of wild-type *Crx* improves the retinal phenotype of $Crx^{Rdy/+}$ kittens, making this a useful approach for translational therapy that aims to slow down vision loss in *CRX*-LCA patients with similar frameshift antimorphic mutations.

5.3. MATERIALS AND METHODS

Using an adeno-associated viral vector construct that has been previously shown to efficiently target cone and rod photoreceptors in wild-type cats[29, 30] and kittens (personal communication) and both wild-type and *E168d2* mouse[31], *Crx* was expressed in the photoreceptors of $Crx^{Rdy/+}$ kittens. This will be aiming to increase the ratio of wild-type Crx protein to mutant Crx protein to reduce the antimorphic effect of the mutant protein.

5.3.1. Ethics statement

All procedures were performed in accordance with the ARVO statement for the Use of Animals in Ophthalmic and Vision Research and approved by the Michigan State University Institutional Animal Care and Use Committee.

5.3.2. Animals

Fifteen purpose-bred $Crx^{Rdy/+}$ kittens maintained as a colony at Michigan State University were included in this study. They were housed under 12L:12D cycles and fed by the queens and a

commercial feline dry diet (Purina kitten chow; Nestlé Purina, St Louis, MO. USA). Animals ranging from 3 weeks to 12 weeks of age were studied.

5.3.3. Subretinal injections and vectors delivered

AAV were delivered by subretinal injection in 3-4-week-old (21 to 26 days of age) *Crx*$^{Rdy/+}$ kittens, the earliest age in which a subretinal injection could be reproducibly performed.

Kittens were anesthetized with isoflurane (IsoFlo; Abbott Laboratories, North Chicago, IL, USA) delivered in oxygen. Pupils were dilated with tropicamide ophthalmic solution (Tropicamide UPS 1% Falcon Pharmaceuticals Ltd., Fort Worth, TX, USA). The kittens were placed in dorsal recumbency for the procedure. Subretinal injection was performed as previously described. [32]

A vitrectomy was not performed due to the small size of the eye. A sclerotomy with a 25 or 30G needle was performed at 2.5 mm from the limbus and an aqueocentesis with a 30G needle (except for one kitten). Visualization of the fundus was performed using a 10mm diameter cover slip (CS-No1-10, Bioscience Tools, Highland, CA, USA) coupled on the cornea with Optixcare eye lube (Waterdown, Ontario, Canada). The subretinal injection was performed with a 33G Hamilton syringe (Reno, NV, USA).[32] After injection, a subconjunctival injection of a mixture of 2 mg methylprednisolone acetate (Depo-Medrol 40 mg/mL, Zoetis, Kalamazoo, MI, USA or Pfizer Inc, NYC, NY, USA), 0.1 mg dexamethasone (Dexa-ject 2mg/mL, Henry Schein Animal Health, Dublin, OH, USA or Dexium, Bimeda, Inc., Le Sueur, MN, USA) and 1.2 mg Gentamicin (40mg/ml, Hospira Inc, Lake Forest, IL, USA or GentaFuse, Bulter Schein Animal Health, Dublin, OH, USA) for a total volume of 0.13 mL was given.

One eye was injected with a therapeutic AAV-FLAG-*CRX* vector and the contralateral eye as either injected with a therapeutic vector as well or was uninjected, or received a construct

of the similar serotype and promoter but delivering the GFP gene. The central retina was targeted and approximately 30-200µL was injected (Fig. 5.1).

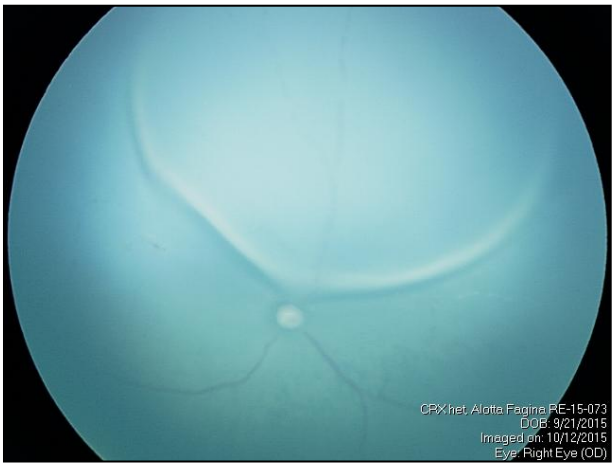

Figure 5.1. 175 µL subretinal injection in the central retinal region of a 3-week-old *Crx*$^{Rdy/+}$ kitten.

Several titers of vector were tested based on our preliminary studies and initial results (5x 10^{11}, 1x10^{12}, 5x10^{12} and 7.5x10^{12} vg/mL).

The different AAV vectors tested were AAV2/5 with an ubiquitous promoter and AAV2/8 Y733F (single mutant capsid tyrosine to phenylalanine mutation) with an ubiquitous (*Chicken ß-Actin CBA or Universoti of Florida UF*) or *GRK1* promoter (for details on injections, titers and volumes refer to Table 5.1 below).

After preliminary results and evidence of functional rescue in one eye in which the cornea was partially covered by its nictitans membrane, 5 kittens were kept in dim light conditions (0.04 to 3.45 cd/m^2) from eyelid opening (1 to 2 weeks of age) until euthanasia at 12 weeks of age.

ID	Age at injection (days)	Viral Construct injected in OD	Viral Construct injected in OS
AAV2/5 – Ubiquitous promoter			
OA01785531	**24**	**AAV2/5 *UF-SB-FLAG-hCRX* K2583**	**AAV2/5 sc-sm*CBA-hGFP***
		$5x10^{11}$vg/mL	$5x10^{11}$vg/mL
AAV2/8 Y733F mutant capsid			
AAV2/8 Y733F mutant capsid – Ubiquitous promoter			
OA02532731	**21**	**AAV2/8 Y733F, *UF-SB-FLAG-hCRX*, Ω4030**	-
		$1x10^{12}$vg/mL	
OA02532018	**28**	**AAV2/8 Y733F, *UF-SB-FLAG-hCRX*, Ω4030**	**AAV2/8 Y733F, *UF11-GFP*, I1838c**
		$5x10^{11}$vg/mL	$5x10^{11}$vg/mL
OA02525638	**24**	**AAV2/8 Y733F, *UF-SB-FLAG-hCRX*, Ω4030**	**AV2/8 Y733F, *UF11-GFP*, I1838c**
		$5x10^{11}$vg/mL	$5x10^{11}$vg/mL
AAV2/8 Y733F mutant capsid – *GRK1* promoter			
OA02532828	**21**	**AAV2/8 Y733F, *GRK1-FLAG-Crx*, K2822**	-
		$1x10^{12}$vg/mL	
OA02533517	**21**	**AAV2/8 Y733F, *GRK1-FLAG-Crx*, K2822**	-
		$1x10^{12}$vg/mL	
OA02496941	**26**	**AAV2/8 Y733F, *GRK1-FLAG-CRX*, P4376**	-
Dark conditions		$1x10^{12}$vg/mL	
OA02497929	**26**	**AAV2/8 Y733F, *GRK1-FLAG-CRX*, P4376**	-
Dark conditions		$1x10^{12}$vg/mL	
OA025001214	**26**	**AAV2/8 Y733F, *GRK1-FLAG-CRX*, P4376**	-

Table 5.1. List of animals, the vector and titer they received. Animals maintained in dark light conditions were indicated under their ID number.

Table 5.1 (cont'd)

Dark conditions		5x1012vg/mL	
OA02501046	26	A AAV2/8 Y733F, GRK1-FLAG-CRX, P4376	-
Dark conditions		$5x10^{12}$vg/mL	
OA02496779	**24**	**AAV2/8 Y733F, *GRK1-FLAG-CRX*, P4376**	-
Dark conditions		$7.5x10^{12}$vg/mL	
OA02496004	**24**	**AAV 8 733, *GRK1-FLAG-CRX*, P4376**	-
Dark conditions		$7.5x10^{12}$vg/mL	
ID	**Age at injection (days)**	**Viral Construct injected in OD**	**Viral Construct injected in OS**
AAV2/8 Y733F mutant capsid – Ubiquitous and *GRK1* promoters			
OA01790762	**24**	**AAV2/8 Y733F, *GRK1-FLAG-Crx*, K2822**	**AV2/8 Y733F, *UF11-GFP*, I1838c**
		$5x10^{11}$vg/mL	$5x10^{11}$vg/mL
OA02527420	**21**	**Mix Half/half AAV2/8 Y733F, *UF-SB-FLAG-hCRX*, Ω4030 AAV2/8 Y733F, *GRK1-FLAG-Crx*, K2822**	**Mix Half/half AAV2/8 Y733F, *UF-SB-FLAG-hCRX*, Ω4030 AAV2/8 Y733F, *GRK1-FLAG-Crx*, K2822**
		$1x10^{12}$vg/mL	$1x10^{12}$vg/mL
RSA 15-071 Died at recovery	**21**	**AAV2/8 Y733F, *UF-SB-FLAG-hCRX*, Ω4030**	**Mix Half/half AAV2/8 Y733F, *UF-SB-FLAG-hCRX*, Ω4030 AAV2/8 Y733F, *GRK1-FLAG-Crx*, K2822**
		$1x10^{12}$vg/mL	$1x10^{12}$vg/mL

5.3.4. Outcome evaluations

	Subretinal injection	Fundus imaging	ERG	cSLO	SD-OCT	Euthanasia	IHC
Age (weeks)	3	6,10,12	6, 10, 12	12	12	12	12

Table 5.2. Experimental design

5.3.4.1. Ophthalmic examination and fundus imaging

Eyes were examined regularly for any adverse response to the therapy such as inflammation or differential retinal degeneration between injected and uninjected regions and between treated and control eyes. Full ophthalmic examinations included indirect ophthalmoscopy daily up to 3 days post-operatively, then weekly until 6 weeks of age and finally at 10 and 12 weeks of age. Fundus photography (Ret-Cam II, Clarity Medical Systems, Inc., Pleasanton, CA, USA) was performed at 6, 10 and 12 weeks of age. Infrared and autofluorescence imaging with confocal scanning laser ophthalmoscopy (Spectralis OCT+HRA; Heidelberg Engineering Inc., Heidelberg, Germany) was performed before euthanasia at 12 weeks of age.

Animals injected with the *AAV*-GFP vector were monitored for GFP expression using wide-field fundus photography (RetCam II, Clarity Medical Systems, Inc., Pleasanton, CA, USA), and fluorescence was also monitored using a cSLO (confocal scanning laser ophthalmascope) (Spectralis® OCT+HRA, Heidelberg Engineering Inc., Heidelberg, Germany) at similar ages to the regular fundus imaging.

5.3.4.2. Retinal function assessment – Electroretinography (ERG)

Scotopic and photopic ERGs were recorded from kittens described previously in chapter 2.[14] The kittens were dark-adapted for 1 hour, and pupils were dilated with tropicamide ophthalmic solution, (Falcon Pharmaceuticals Ltd., Fort Worth, TX, USA). A Jet-lens monopolar electrode contact lens with a platinum needle skin reference electrode (Grass Technologies, Warwick, RI, USA) was placed 0.5 cm from the lateral canthus, and a ground electrode was placed over the occiput (Grass Technologies, Warwick, RI, USA). ERG a- and b-wave amplitudes and implicit times were measured in a standard fashion. Evidence of a positive effect

of therapy would be the presence of a cone-mediated response (not recordable from untreated kittens) and an improvement (lowering) of the threshold of dark-adapted responses and an increase in amplitudes compared to non-treated eyes.

5.3.4.3. Retinal morphology and CRX expression

5.3.4.3.1. *In vivo* Spectral Domain-Optical Coherence Tomography (SD-OCT)

SD-OCT imaging (Heidelberg Engineering) was used to capture single scan line and volume scan images from treated and untreated regions. The treated regions were assessed for retinal reattachment and any side effects from the procedure.[33] They were also assessed for evidence of photoreceptor morphology by examining the regions of the SD-OCT scan representing photoreceptor inner and outer segments and the ellipsoid zone.[33] Improvement in the definition of those layers was considered a positive outcome.

5.3.4.3.2. Immunohistochemistry (IHC)

After kittens were euthanized at 12 weeks of age (age of peak retinal function in wild-type kittens)[14], their eyes were removed and immersed in 4% paraformaldehyde (Electron Microscope Sciences, Hatfield, PA, USA) in phosphate-buffered saline (PBS, Sigma-Aldrich Corp., Saint Louis, MO, USA) on ice for 3 hours. They were then processed for immunohistochemistry and imaged as previously described[14, 30] (Table 5.3. lists the antibodies used). Treated and untreated region were examined for FLAG expression (marker of transgene and thus *CRX* expression) and hCAR, a cone photoreceptor marker to assess for evidence of rescue of photoreceptor maturation in the $Crx^{Rdy/+}$ kittens post *AAV* gene supplementary therapy.

Antibody – Source	Type	Primary Dilution	Secondary Antibody – Source	Secondary Dilution
FLAG (Anti-FLAG® M2) Sigma, St. Louis, MI, USA	Monoclonal mouse	1 :500	Alexa Fluor 568 Goat anti-mouse IgG, Life technologies, Carlsbad, CA, USA	1:500
hCAR (Human cone arrestin) Dr. Cheryl Craft; LUMIJ, University of Southern California, Los Angeles, CA, USA	Polyclonal rabbit	1:10,000	Alexa Fluor 488 Goat anti-rabbit IgG, Life technologies, Carlsbad, CA, USA	1:500

Table 5.3. List of antibodies used for IHC – their origins and dilutions

5.4. RESULTS

5.4.1. *Crx*$^{Rdy/+}$ kittens show retinal attachment after subretinal injection and only minor side effects

Summary of the volume and titer injected as well as side effects were detailed in Table 5.4 below. One kitten died during recovery and was excluded from the study.

ID	Eye	Vector injected	Titer, volume and location of the injection	Side effects/ Fluorescence on cSLO/SD-OCT	Scotopic ERG rescue	IHC FLAG /GFP labeling
AAV2/5 – Ubiquitous promoter						
OA01785531	OD	AAV2/5 *UF-SB-FLAG-hCRX* K2583	$5x10^{11}$vg/mL 50µL dorso-temporal (not sure all in, flattened bleb)	Retinal lesion and retinal tear at the injection site best seen on FAF	No rescue	Low FLAG expression
	OS	AAV2/5 sc-sm*CBA-hGFP*	$5x10^{11}$vg/mL 50µL temporal - *area centralis*	Retinal lesion at the injection site best seen on FAF, GFP fluorescence on FAF	N/A normal disease ERG progression	Low GFP expression in cones and off-target expression in Müller cells
AAV2/8 Y733F mutant capsid						
AAV2/8 Y733F mutant capsid – Ubiquitous promoter						
OA02532731	OD	AAV2/8 Y733F, *UF-SB-FLAG-hCRX*, Ω4030	$1x10^{12}$vg/mL 150µL nasal and very small temporal bleb	Retinal lesion at the injection site best seen on FAF, retina mild disorganization and thinning from injection	No rescue	Moderate FLAG expression
	OS	-	-	N/A	N/A normal disease ERG progression	None

Table 5.4. Details of outcomes for each kitten.

Table 5.4 (cont'd)

OA02532018	OD	AAV2/8 Y733F, *UF-SB-FLAG-hCRX*, Ω4030	$5x10^{11}$vg/mL 200µL in 3 blebs with were not easy to see including one far nasal and one dorsal	Retinal lesion at the injection site best seen on FAF, retina no very well reattached in few areas (mild folds)	No rescue	Low FLAG expression
	OS	AAV2/8 Y733F, *UF11-GFP*, I1838c	$5x10^{11}$vg/mL 100µL temporal	GFP fluorescence on FAF and nerve fibers fluorescence	N/A normal disease ERG progression	Strong GFP expression in photoreceptors
AAV2/8 Y733F mutant capsid						
AAV2/8 Y733F mutant capsid – Ubiquitous promoter						
OA02525638	OD	AAV2/8 Y733F, *UF-SB-FLAG-hCRX*, Ω4030	$5x10^{11}$vg/mL 200µL in 2 blebs 1dorso-temporal and one nasal	Retinal lesion and retinal tear at the injection site best seen on FAF	No rescue	Low FLAG expression
	OS	AAV2/8 Y733F, *UF11-GFP*, I1838c	$5x10^{11}$vg/mL 100µL temporal	GFP fluorescence on FAF and nerve fibers fluorescence	N/A normal disease ERG progression	Strong GFP expression in photoreceptors
AAV2/8 Y733F mutant capsid – *GRK1* promoter						
OA02532828	OD	AAV2/8 Y733F, *GRK1-FLAG-Crx*, K2822	$1x10^{12}$vg/mL 200µL dorsal about 100µL in the bleb	Retinal lesion at the injection site best seen on FAF, very few hyperfluorescent dots in the treated area seen on FAF	No rescue	Mild FLAG expression
	OS	-	-	N/A	N/A normal disease ERG progression	None
OA02533517	OD	AAV2/8 Y733F, *GRK1-FLAG-Crx*, K2822	$11x10^{12}$vg/mL 150µL temporal	Hyperfluorescent dots in the treated area seen on FAF	ERG rescue, improvement of amplitudes, implicit times and threshold (yet better at 10w then 12w)	Strong FLAG expression
	OS	-	-	N/A	N/A normal disease ERG progression	None

Table 5.4 (cont'd)

OA02496941	OD	AAV2/8 Y733F, *GRK1-FLAG-CRX*, P4376	$1x10^{12}$vg/mL 100µL dorso-nasal	Hyperfluorescent dots in the treated area seen on FAF, abnormalitis in the OPL layer	No rescue	IHC not performed
Dark conditions	OS	-	-	N/A	N/A normal disease ERG progression	IHC not performed
OA02497929	OD	AAV2/8 Y733F, *GRK1-FLAG-CRX*, P4376	$1x10^{12}$vg/mL 75µL dorsal	No abnormalities	No rescue	Strong FLAG expression
Dark conditions	OS	-	-	N/A	N/A normal disease ERG progression	None
OA025001214	OD	AAV2/8 Y733F, *GRK1-FLAG-CRX*, P4376	$5x10^{12}$vg/mL 100µL dorso-nasal	Hyperfluorescent dots in the treated area seen on FAF	No rescue	IHC not performed
Dark conditions	OS	-	-	N/A	N/A normal disease ERG progression	IHC not performed
OA02501046	OD	AAV2/8 Y733F, *GRK1-FLAG-CRX*, P4376	$5x10^{12}$vg/mL 100µL dorso-temporal miosis at the end	Retinal tear at the injection site, hyperfluorescent dots in the treated area seen on FAF and suspicious of IS/OS damage seen as layer irregularities	No rescue	Strong FLAG expression
Dark conditions	OS	-	-	N/A	N/A normal disease ERG progression	None
OA02496779	OD	AAV2/8 Y733F, *GRK1-FLAG-CRX*, P4376	$7.5x10^{12}$vg/mL 100µL dorsal	Hyperfluorescent dots in the treated area seen on FAF	Very mild ERG rescue seen as a very small b-wave in OD compared to OS	Moderate FLAG expression
Dark conditions	OS	-	-	N/A	N/A normal disease ERG progression	None

Table 5.4 (cont'd)

OA02496004	OD	AAV2/8 Y733F, *GRK1-FLAG-CRX*, P4376	$7.5x10^{12}$vg/mL 100µL nasal (50µL in vitreous)	Retinal lesion at the injection site best seen on FAF	Very mild ERG rescue seen as a very small b-wave in OD compared to OS	IHC not performed
Dark conditions	OS	-	-	N/A	N/A normal disease ERG progression	IHC not performed
AAV2/8 Y733F mutant capsid – Ubiquitous and *GRK1* promoters						
OA01790762	OD	AAV2/8 Y733F, *GRK1-FLAG-Crx*, K2822	$5x10^{11}$vg/mL 50µL dorsal (20µL in vitreous)	Small retinal lesion and retinal tear at the injection site best seen on FAF, hyperfluorescent dots in the treated area seen on FAF	No rescue	Moderate FLAG expression
	OS	AV2/8 Y733F, *UF11-GFP*, I1838c	$5x10^{11}$vg/mL 50µL dorsal (50µL subretinal and 40µL in vitreous)	GFP fluorescence on FAF and nerve fibers fluorescence	N/A normal disease ERG progression	Strong GFP expression in photoreceptors
OA02527420	OD	Mix Half/half AAV2/8 Y733F, *UF-SB-FLAG-hCRX*, Ω4030 AAV2/8 Y733F, *GRK1-FLAG-Crx*, K2822	$1x10^{12}$vg/mL 175µL dorsal	Retinal lesion at the injection site best seen on FAF	No rescue	Strong FLAG expression
	OS	Mix Half/half AAV2/8 Y733F, *UF-SB-FLAG-hCRX*, Ω4030 AAV2/8 Y733F, *GRK1-FLAG-Crx*, K2822	$1x10^{12}$vg/mL 175µL dorso-nasal	Retinal lesion at the injection site best seen on FAF, hyperfluorescent dots in the treated area seen on FAF	N/A normal disease ERG progression	Strong FLAG expression

Most of the kittens received a subretinal injection of 50 to 100µL. Bigger blebs were more challenging to perform and had increased risk of not reattaching normally. Ophthalmic examination showed that in all cases the retina reattached within a couple of days. At 9 weeks post-injection (12 weeks of age), SD-OCT retinal high-resolution cross-section images confirmed

that there was retinal reattachment in all eyes injected. No major retinal disorganization of the retinal layers secondary to the retinal detachment was noted, with the exception of two eyes that had some mild folds probably due to lack of proper reattachments (Fig. 5.2A) and two eyes that had some disorganization and thinning of the retina (Fig. 5.2B). The proper re-attachment post-injection allows us to believe that the surgery technique used is valuable as it allows proper sub-retinal injection without performing vitrectomy and so without being too invasive. Yet, it was noticed during surgery that, due to gauge size of the needle being used, the retinotomy created was big enough to allow some minor leakage from the sub-retinal injection site to the vitreous. The injection site had a retinal scaring in most of the kittens, which appeared as a dark lesion on fundus autofluorescence (FAF) (Fig. 5.2C). A couple of eyes also presented with a persistent retinal tear at the injection site (Fig. 5.2D).

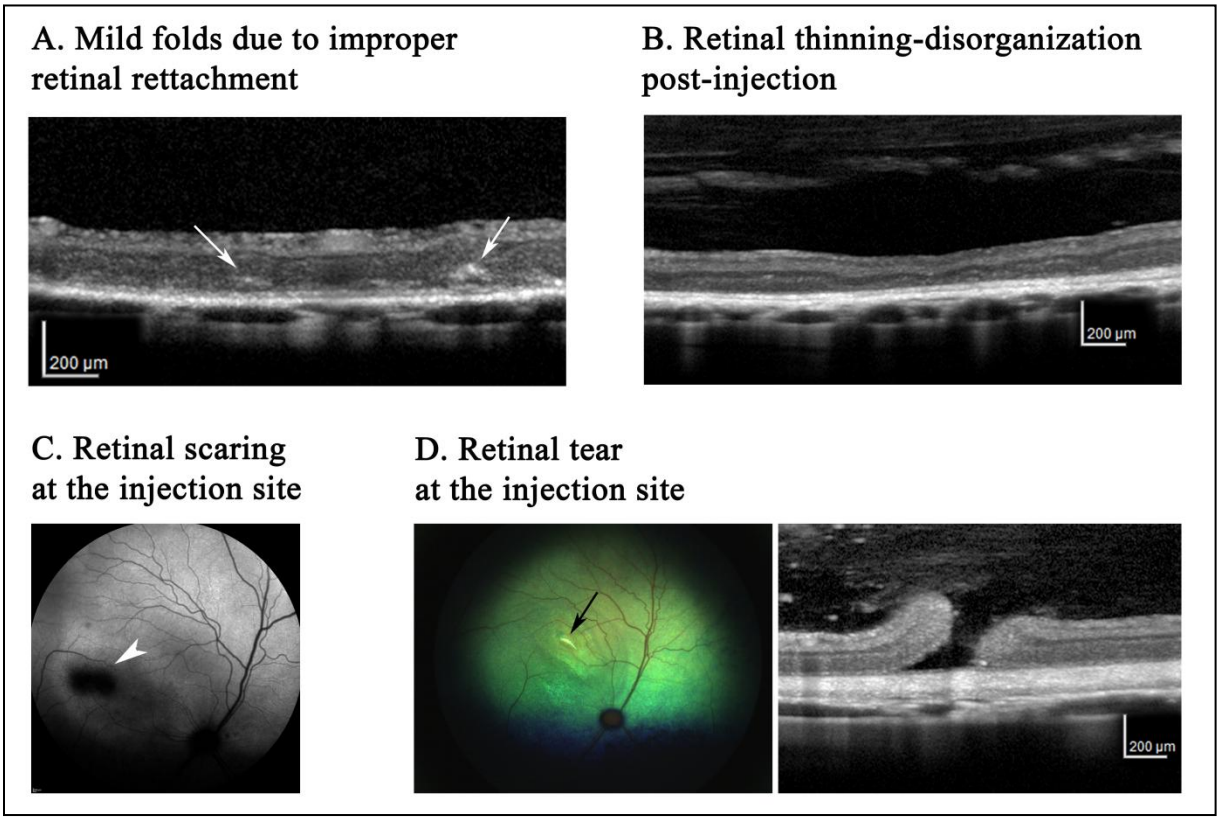

Figure 5.2. Side effects of subretinal injections.

Figure 5.2 (cont'd)
(A) SD-OCT cross retinal section showing improper retinal reattachment. This can lead to the formation of some folds or elevations of the retina (as indicated by the *white arrows*) (separation between the photoreceptor outer segment layer and the retinal pigmentary epithelium).
(B) SD-OCT cross retinal section showing retinal thinning and disorganization. This can occur following toxicity or improper retinal reattachment post-injection.
(C) Fundus autofluorescence cSLO image showing retinal/sclera scaring at the injection site (white arrowhead)**.**
(D) RetCam fundus image (right image) **and SD-OCT cross retinal** (left image) **section showing remnant retinal tear post-injection** (indicated by the *black arrow*)**.**

No major inflammation was seen. One kitten had some conjunctivitis due to canthal suture rubbing. Few kittens had some canthal suture dehiscence due to the excessive mother bathing. Four eyes had some corneal to iris synechias, and two had focal cataracts, which were thought to be due to technical error during the aqueocentesis.

Due to a surgical technique error, one kitten (OA02533517) had some damage to its nictitans membrane muscle. This did not seem to create any discomfort at any time but was covering 2/3 of its cornea.

5.4.2. Functional rescue

Photopic ERG responses were not detectable from any of the treated eyes, suggesting either no cone rescue or rescue that was below the threshold for ERG detection. Among the 15 treated eyes (14 cats), only one cat showed significant rescue of the scotopic ERG (2 cats showed a very minor increase in b-wave compared to the untreated eye). The cat (OA02533517) showing scotopic ERG response showed minor rescue at 6 weeks of age but more pronounced rescue at 10 and 12 weeks of age with improvement of amplitudes and implicit times as well as lower threshold ERG responses compared to the untreated eye. These ERG amplitudes were small compared to those of age-matched WT kittens (Fig. 5.3B). Interestingly, this was not the cat with

the bigger or more central bleb (Fig. 5.3A), and it also showed some hyperfluorescent dots on FAF. It received a 150µL bleb of $1x10^{12}$vg/mL AAV2/8 Y733F *GRK1-FLAG-Crx*, dorso-temporally. This was also the cat presented that had a nictitans membrane prolapsed due to a technical error. Based on this result, we hypothesized that reduced light exposure may have a beneficial effect on therapy. Subsequently, a cohort of kittens was kept under a dim red light following subretinal injections, however, no functional rescue was observed in those kittens.

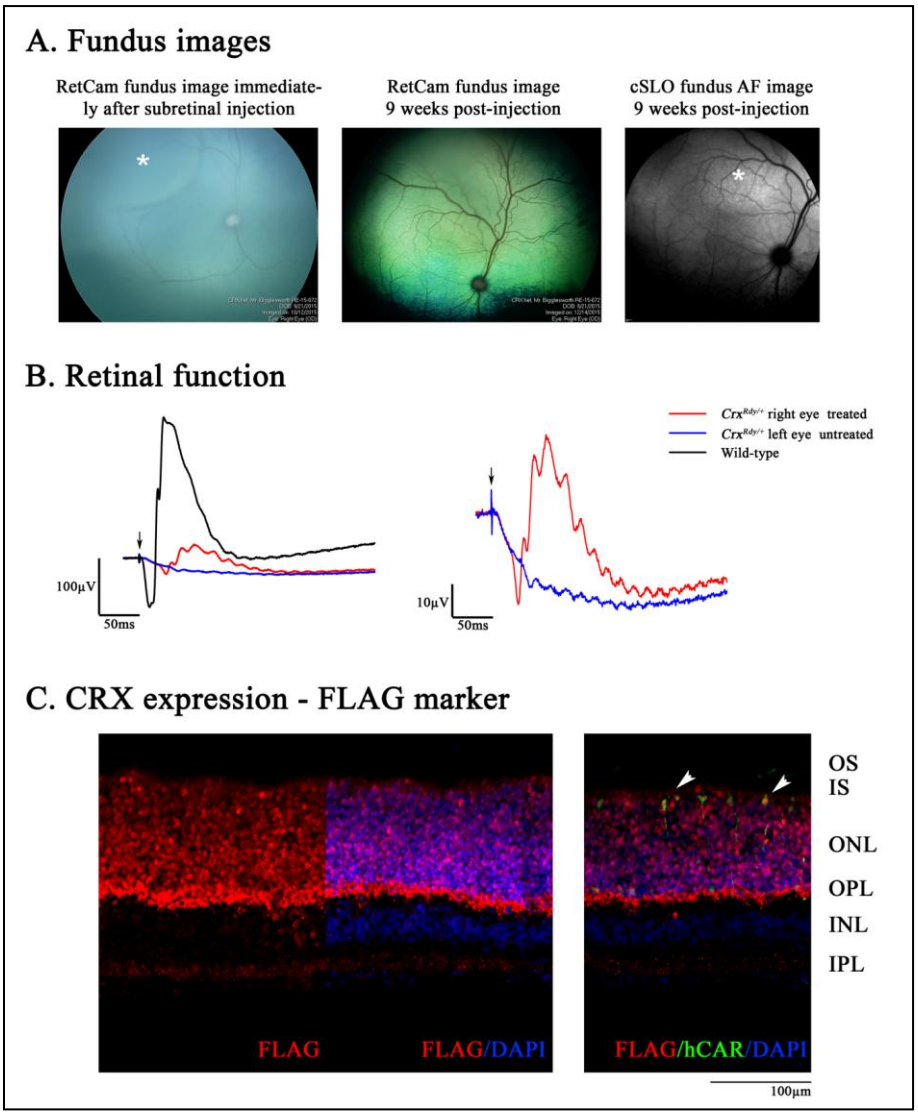

Figure 5.3. Summary of the outcome assessment from kitten OA02533517, which presented with functional rescue.

Figure 5.3 (cont'd)
(A) Fundus images. Left image: RetCam fundus image of a subretinal injection of 150µL of $1x10^{12}$vg/mL AAV2/ 8 Y733F *GRK1-FLAG-Crx* in the dorso-temporal retinal region in a 3-week-old $Crx^{Rdy/+}$ kitten indicated by the *white star*. **Middle image:** Follow-up RetCam fundus image of the same kitten at 12 weeks of age (9 weeks post-injection) showing no fundus lesion. **Right image:** cSLO autofluorescent image (AF) showing some changes in the bleb area (*white star*) seen as some hyperfluorescent dots.
(**B) Functional rescue in the treated eye.** Dark-adapted ERG raw tracings at 12 weeks of age from the treated right eye (OD) and untreated left eye (OS) of kitten OA02533517 and a wild-type control kitten at the same age for a 2.8 $cd.m^2$ light stimulus in scotopic condition. The **right tracings** show some rescue in OD, yet the amplitude is still very decreased compared to WT kitten. The **left tracings**, on a different scale, showed that, even though small, the rescue is significant compared to the untreated eye.
The black arrow indicated the light stimulus.
(C) **Immunohistochemistry of the treated right eye retina**. IHC showed strong expression of FLAG (therefore of CRX) in the treated region. hCAR labeled cones but no improvement in their IS/OS (indicated by the *white arrowheads*) development was noted.
IS/OS; photoreceptor inner/outer segments, ONL; outer nuclear layer, OPL; outer plexiform layer, INL; inner nuclear layer, IPL; inner plexiform layer.

5.4.3. Morphological rescue and molecular expression of the vector

No obvious improvement of photoreceptor inner and outer segments was observed on SD-OCT cross retinal section. Yet, as stated above most of the kittens did not show any severe retinal thinning or disorganization as a consequence of the AVV subretinal injection, which was confirmed by a finding on IHC.

Both use of the AAV2/5 sc sc-smCBA-hGFP in one eye and AAV2/8 Y733F *UF11-GFP* at $5x10^{11}$vg/mL in 3 eyes led to strong fluorescence revealed by autofluorescence imaging by 488nm cSLO imaging. IHC showed very different targeting of both vectors in kittens. The AAV2/5 sc-sm*CBA-hGFP* injected eyes showed some expression in cone photoreceptor but not in rods and some significant off-target expression in Müller cell. The AAV2/8 Y733F *UF11-GFP* injected eyes had high transgene GFP expression in both cones and rods in the 3 eyes injected, and 2 of the eyes showed mild off-target expression to amacrine and ganglion cells (Fig. 5.4A).

Additionally, it seems that there was less hCAR labeling in the center of the bleb, possibly indicating an adverse effect of transgene or viral vector presence.

All eyes injected with either construct or promoter showed some FLAG expression suggestive of *CRX* transgene expression (see details in Table 5.4). Yet, important variation existed between results from different serotypes and promoters. AAV2/5 *UF-SB-FLAG-hCRX* only resulted in low transgene expression. AAV2/8 Y733F with a ubiquitous promoter induced low to moderate transgene expression in the photoreceptors. The construct with a *GRK1* promoter or a combination of vectors with ubiquitous and *GRK1* promoters led to a stronger transgene expression (Fig. 5.4C). The use of the AAV2/8 Y733F combined to a *GRK1* promoter seemed to be associated with hyperfluorescent dots of fundus autofluoresccence cSLO images (Fig. 5.4B).

Most eyes did not show any changes in hCAR labeling compared to historical data [14], although a few eyes (Fig. 5.4D) seemed to have a stronger labeling of cones by hCAR in the treated versus the untreated regions.

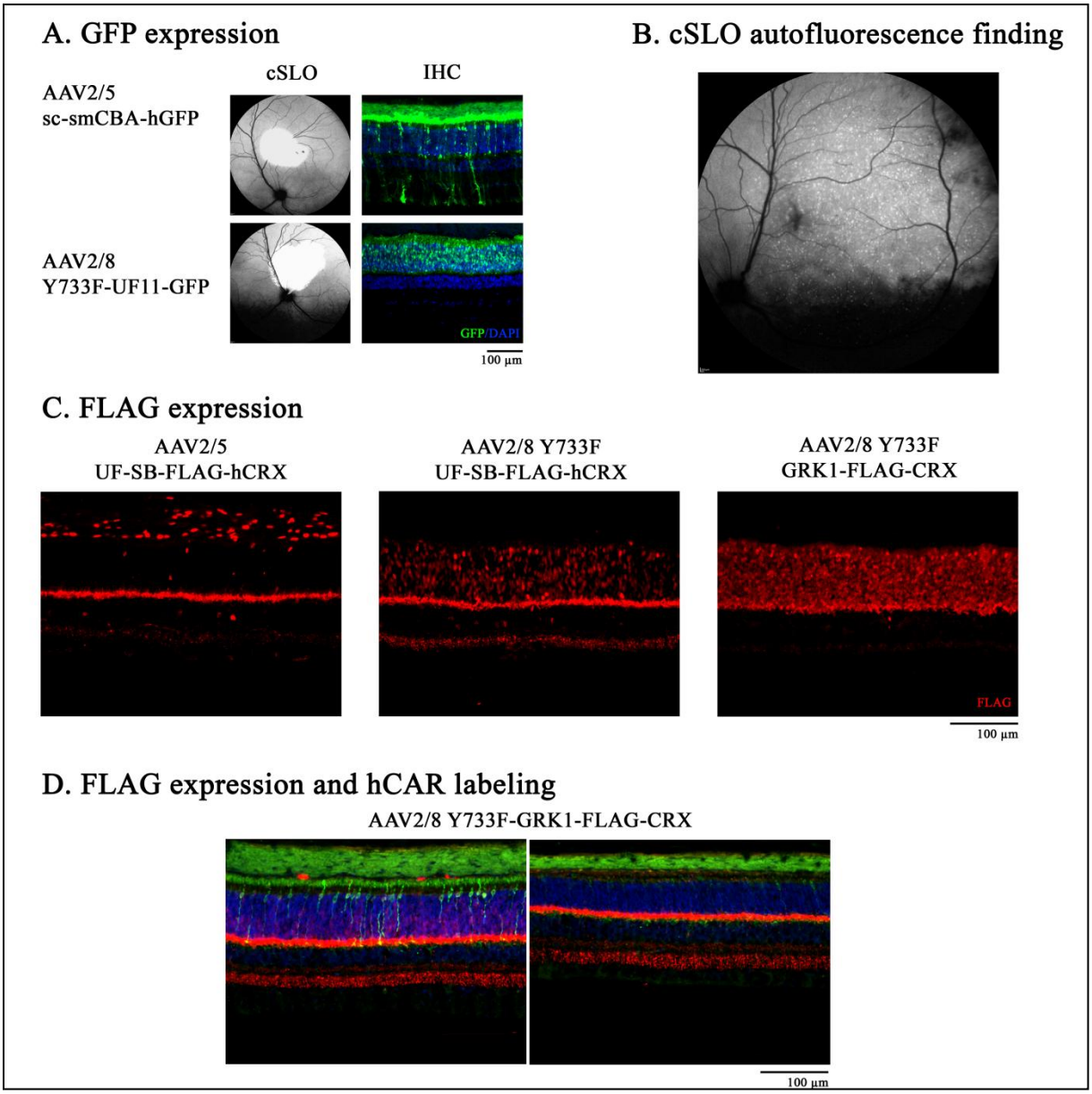

Figure 5.4. Molecular expression.
(A) GFP expression was present on cSLO imaging for both serotype AAV vectors at similar intensities, yet on IHC the AAV2/8 Y733F had a much higher GFP transgene expression of photoreceptors with less off-target expression.
(B) cSLO imaging of the bleb for injection with AAV2/8 Y733F combined to the GRK1 promoter led to the appearance of hyperfluorescent dots of FAF in the treated region.
(C) Immunolabeling for FLAG marker of CRX expression. The FLAG expression was extremely low when the AAV2/5 *UF-SB-FLAG-hCRX* was used at a titer of $5x10^{11}$vg/mL while it was moderate when using the AAV2/8 Y733F *UF11-GFP* at a titer of $1x10^{12}$vg/mL and strong while using AAV2/8 Y733F *GRK1-FLAG-Crx* at a titer of $1x10^{12}$vg/mL.
(D) Combined FLAG/hCAR labeling. Some eyes showed brighter hCAR (green) labeling in the treated region (left region) compared to the untreated region (right image).

5.5. DISCUSSION

Subretinal injections were successfully achieved in all kittens although it was difficult to precisely target the region including the *area centralis*. We wanted to target this region because it is the first region to degenerate in the $Crx^{Rdy/+}$ cat, and therefore any preservation of structure, as assessed by SD-OCT or IHC/EM, would have been easier to detect and obvious at an earlier age.[14] The subretinal injection treated no more than one quarter of the retinal area for the biggest bleb so it is conceivable that a mild degree of rescue would not result in a detectable improvement in the full-field electroretinogram. Multifocal or focal ERG to allow comparison of treated versus non treated retina would be of interest as well as developing some vision testing devices. Increasing the volume of fluid injected subretinally is not an option, because if the bleb is too large, we have found that retinal reattachment is not accurate, and retinal folds form (unpublished observations). A delay in reattachment could lead to retinal damage; we have noticed that delay in reattachment of large detachments can lead to cone loss[24] (unpublished observations). The effect of retinal detachment is not benign and has been extensively studied. Early changes include modification in rod terminals and rod bipolar spherules connection notably to horizontal cells altering the synapse complex, changes in ON- and OFF-bipolar cells.[24, 34-40] One way of transducing a larger retinal area is to do 2 or more separate subretinal injections allowing the treatment of larger retinal surface with lesser side effects.

The FLAG tag enabled the detection of which cells were expressing the transgene. IHC for Crx could not be used since it would not be possible to distinguish between the transgene (human CRX) and the endogenous Crx. FLAG expression was detected in all retinas suggesting that the appropriate cells had been transduced. One possibility for the apparent lack of rescue could be that the FLAG protein altered the function of the *CRX* transgene itself.

When used with an ubiquitous promoter, both the injections with the AAV2/5 and AAV2/8 Y733F serotypes resulted in low FLAG and therefore CRX expression. The use of AAV2/8 Y733F with a photoreceptor targeting promoter *GRK1* improved transgene expression and led to strong FLAG expression. Additionally, eyes receiving a combination of AAV2/8 Y733F containing both the ubiquitous and *GRK1* promoters seemed to have an even better effect with a stronger FLAG expression as seen by IHC. Those results need yet to be taken with caution. Indeed, the AAV2/5 *UF-SB-FLAG-hCRX* (ubiquitous promoter) was only tested at a low titer of $5x10^{11}$vg/mL and such in only one eye. Similarly, the use of AAV2/8 Y733F *UF-SB-FLAG-hCRX* (ubiquitous promoter) at a low $5x10^{11}$vg/mL titer only led to mild transgene expression compared to moderate FLAG expression when used at $1x10^{12}$vg/mL titer. The use of AAV2/8 Y733F *GRK1-FLAG-CRX* (photoreceptor specific promoter) showed some strong expression from a titer to 1 to 7.5 $x10^{12}$vg/mL. The transgene expressions obtained in this study are therefore only mildly comparable between serotypes and promoters as they were not all used at the same titers. It is necessary to perform a better dose-response study to compare transgene expression between different titers but also different serotypes and promoters. Investigation of various serotype-promoters and mutant capsid vectors specifically in the cats as a particular species is of value, and investigation in kittens (different retinal maturation stage) would be valuable as well. This is supported by the fact that target species, serotypes, mutant capsid, promoter and well as self-complementary AAV have been shown to make a difference in cell targeting.[29, 30, 32, 41, 42]

Only one kitten showed significant functional rescue. It is not clear why the ERG rescue achieved in the one kitten could not be repeated. In this animal, due to a surgical technique error, the nictitans was damaged resulting in partial coverage the cornea, which may have limited light exposure. Working on the hypothesis that reducing light exposure could improve the degree of

rescue, we tested a cohort of kittens with the same vector and kept them in dim lighting conditions, but this did not result in significant functional rescue. The bleb created in the kitten with rescue was quite peripheral (dorso-temporal). As the progression of the degeneration starts in the central retina and spreads to the periphery (following the pattern of retinal maturation), in theory the peripheral injection was in a region that was at an earlier stage of degeneration than the central retinal region treated in the rest of the kittens.

The lack of rescue could be caused by not being able to shift the mutant to WT: *Crx* allele ratio to sufficiently counteract the toxic effect of the mutant protein. There was no improvement in photoreceptor inner and outer segment morphology detectable on SD-OCT and on retinal sectioning (IHC). Many of the blebs did not include the *area centralis*. As a result, for the duration that the animals were kept there would be little loss of retinal layer thickness, so a mild preservation of thickness would not be detectable.[14] A few animals had stronger hCAR labeling in the injected area that might indicate a mild treatment-related improvement in cone health and maturation but not sufficient to lead to normal maturation or to improve function sufficiently to be detectable by full-field ERG.

In conclusion, subretinal injection in the 3-week-old kitten was possible, but it proved to be difficult to specifically include the *area centralis* at that age. Some transgene expression was detectable in the photoreceptors of most kittens when using an AVV2/8 Y733F mutant capsid with a *GRK1* promoter or a combination, but only one kitten had detectable functional rescue. Further refinement of the rAAV to optimize photoreceptor targeting is necessary. Gene augmentation therapy using AAV might not be sufficient to decrease the mutant to WT Crx ratio and achieve the degree of rescue that is required. It may be of value to combine it with other techniques that aim to downregulate the mutant *Crx* allele. This highlights the difficulties of

treating dominant disease, where the expression of the mutant allele has a strong deleterious effect.[16, 43, 44]

2.6. ACKNOWLEDGEMENTS

The authors would like to thank Dr. Cheryl Craft for the donation of the hCAR antibody and Dr. William Hauswirth and Sanford Boye for providing adeno-associated viral vectors.

Supported by Myers-Dunlap Endowment and Michigan State University College of Veterinary Medicine Endowed Research Funds.

REFERENCES

REFERENCES

1. Hull S, Arno G, Plagnol V, et al. The phenotypic variability of retinal dystrophies associated with mutations in CRX, with report of a novel macular dystrophy phenotype. *Invest Ophthalmol Vis Sci.* 2014;55:6934-6944.

2. Tran NM, Zhang A, Zhang X, Huecker JB, Hennig AK, Chen S. Mechanistically Distinct Mouse Models for CRX-Associated Retinopathy. *PLoS Genet.* 2014;10:e1004111.

3. Leber T. Über retinitis pigmentosa und angeborene Amaurose. *Graefe Arch Clin Exp Ophthalmol* 1869;15:1-25.

4. Schappert-Kimmijser J, Henkes HE, Van Den Bosch J. Amaurosis congenita (Leber). *Arch Ophthalmol.* 1959;61:211-218.

5. Stone EM. Leber congenital amaurosis - a model for efficient genetic testing of heterogeneous disorders: LXIV Edward Jackson Memorial Lecture. *Am J Ophthalmol.* 2007;144:791-811.

6. Koenekoop RK. An overview of Leber congenital amaurosis: a model to understand human retinal development. *Surv Ophthalmol.* 2004;49:379-398.

7. Huang L, Xiao X, Li S, et al. CRX variants in cone-rod dystrophy and mutation overview. *Biochem Biophys Res Commun.* 2012;426:498-503.

8. Hennig AK, Peng GH, Chen S. Regulation of photoreceptor gene expression by Crx-associated transcription factor network. *Brain Res.* 2008;1192:114-133.

9. Chau KY, Chen S, Zack DJ, Ono SJ. Functional domains of the cone-rod homeobox (CRX) transcription factor. *J Biol Chem.* 2000;275:37264-37270.

10. Furukawa T, Morrow EM, Cepko CL. Crx, a novel otx-like homeobox gene, shows photoreceptor-specific expression and regulates photoreceptor differentiation. *Cell.* 1997;91:531-541.

11. Morrow EM, Furukawa T, Raviola E, Cepko CL. Synaptogenesis and outer segment formation are perturbed in the neural retina of Crx mutant mice. *BMC neuroscience* 2005;6:5.

12. Chen S, Wang QL, Xu S, et al. Functional analysis of cone-rod homeobox (CRX) mutations associated with retinal dystrophy. *Hum Mol Genet.* 2002;11:873-884.

13. Menotti-Raymond M, Deckman KH, David V, Myrkalo J, O'Brien SJ, Narfstrom K. Mutation discovered in a feline model of human congenital retinal blinding disease. *Invest Ophthalmol Vis Sci.* 2010;51:2852-2859.

14. Occelli LM, Tran NM, Narfstrom K, Chen S, Petersen-Jones SM. CrxRdy Cat: A Large Animal Model for CRX-Associated Leber Congenital Amaurosis. *Invest Ophthalmol Vis Sci*. 2016;57:3780-3792.

15. Tran NM, Chen SM. Mechanisms of Blindness: Animal Models Provide Insight Into Distinct CRX-Associated Retinopathies. *Dev Dyn.* 2014;243:1153-1166.

16. Petersen-Jones SM, Annear MJ, Bartoe JT, et al. Gene augmentation trials using the Rpe65-deficient dog: contributions towards development and refinement of human clinical trials. *Adv Exp Med Biol*. 2012;723:177-182.

17. Vakkur GJ, Bishop PO. The Schematic Eye in the Cat. *Vis Res.* 1963;61:357-381.

18. Østerberg G. Topography of the layer of rods and cones in the human retina. *Acta Ophthalmol.* 1935;13:11-103.

19. Curcio CA, Sloan KR, Kalina RE, Hendrickson AE. Human photoreceptor topography. *J Comp Neurol.* 1990;292:497-523.

20. Jeon CJ, Strettoi E, Masland RH. The major cell populations of the mouse retina. *J Neurosci.* 1998;18:8936-8946.

21. Applebury ML, Antoch MP, Baxter LC, et al. The murine cone photoreceptor: a single cone type expresses both S and M opsins with retinal spatial patterning. *Neuron.* 2000;27:513-523.

22. Steinberg RH, Reid M, Lacy PL. The distribution of rods and cones in the retina of the cat (Felis domesticus). *J Comp Neurol.* 1973;148:229-248.

23. Provis JM, Dubis AM, Maddess T, Carroll J. Adaptation of the central retina for high acuity vision: cones, the fovea and the avascular zone. *Prog Retin Eye Res.* 2013;35:63-81.

24. Linberg KA, Lewis GP, Shaaw C, Rex TS, Fisher SK. Distribution of S- and M-cones in normal and experimentally detached cat retina. *J Comp Neurol.* 2001;430:343-356.

25. Nichols LL, 2nd, Alur RP, Boobalan E, et al. Two novel CRX mutant proteins causing autosomal dominant Leber congenital amaurosis interact differently with NRL. *Hum Mutat.* 2010;31:E1472-1483.

26. Swaroop A, Wang QL, Wu W, et al. Leber congenital amaurosis caused by a homozygous mutation (R90W) in the homeodomain of the retinal transcription factor CRX: direct evidence for the involvement of CRX in the development of photoreceptor function. *Hum Mol Genet.* 1999;8:299-305.

27. Furukawa T, Morrow EM, Li T, Davis FC, Cepko CL. Retinopathy and attenuated circadian entrainment in Crx-deficient mice. *Nat Genet.* 1999;23:466-470.

28. Silva E, Yang JM, Li Y, Dharmaraj S, Sundin OH, Maumenee IH. A CRX null mutation is associated with both Leber congenital amaurosis and a normal ocular phenotype. *nvest Ophthalmol Vis Sci.* 2000;41:2076-2079.

29. Minella AL, Mowat FM, Willett KL, et al. Differential targeting of feline photoreceptors by recombinant adeno-associated viral vectors: implications for preclinical gene therapy trials. *Gene Ther.* 2014;21:913-920.

30. Mowat FM, Gornik KR, Dinculescu A, et al. Tyrosine capsid-mutant AAV vectors for gene delivery to the canine retina from a subretinal or intravitreal approach. *Gene Ther.* 2014;21:96-105.

31. Tran NMA. Understanding CRX-Associated Retinopathies Using Animal Models. Washington University; 2013:174.

32. Petersen-Jones SM, Bartoe JT, Fischer AJ, et al. AAV retinal transduction in a large animal model species: comparison of a self-complementary AAV2/5 with a single-stranded AAV2/5 vector. *Mol Vis.* 2009;15:1835-1842.

33. Staurenghi G, Sadda S, Chakravarthy U, Spaide RF, International Nomenclature for Optical Coherence Tomography P. Proposed lexicon for anatomic landmarks in normal posterior segment spectral-domain optical coherence tomography: the IN*OCT consensus. *Ophthalmology.* 2014;121:1572-1578.

34. Linberg KA, Lewis GP, Matsumoto B, Fisher SK. Immunocytochemical evidence that rod-connected horizontal cell axon terminals remodel in response to experimental retinal detachment in the cat. *Mol Vis.* 2006;12:1674-1686.

35. Linberg KA, Lewis GP, Fisher SK. Retraction and remodeling of rod spherules are early events following experimental retinal detachment: an ultrastructural study using serial sections. *Mol Vis.* 2009;15:10-25.

36. Sakai T, Tsuneoka H, Lewis GP, Fisher SK. Remodelling of retinal on- and off-bipolar cells following experimental retinal detachment. *Clin Exp Ophthalmol.* 2014;42:480-485.

37. Lewis GP, Chapin EA, Luna G, Linberg KA, Fisher SK. The fate of Muller's glia following experimental retinal detachment: nuclear migration, cell division, and subretinal glial scar formation. *Mol Vis.* 2010;16:1361-1372.

38. Fisher SK, Lewis GP, Linberg KA, Verardo MR. Cellular remodeling in mammalian retina: results from studies of experimental retinal detachment. *Prog Retin. Eye Res.* 2005;24:395-431.

39. Marc RE, Murry RF, Fisher SK, Linberg KA, Lewis GP. Amino acid signatures in the detached cat retina. *nvest Ophthalmol Vis Sci.* 1998;39:1694-1702.

40. Fisher SK, Lewis GP, Linberg KA, Barawid E, Verardo MR. Cellular Remodeling in Mammalian Retina Induced by Retinal Detachment. In: Kolb H, Fernandez E, Nelson R (eds), *Webvision: The Organization of the Retina and Visual System.* Salt Lake City (UT); 1995.

41. Boyd RF, Sledge DG, Boye SL, et al. Photoreceptor-targeted gene delivery using intravitreally administered AAV vectors in dogs. *Gene Ther.* 2016;23:223-230.

42. Beltran WA, Boye SL, Boye SE, et al. rAAV2/5 gene-targeting to rods:dose-dependent efficiency and complications associated with different promoters. *Gene Ther.* 2010;17:1162-1174.

43. Annear MJ, Mowat FM, Bartoe JT, et al. Successful Gene Therapy in Older Rpe65-Deficient Dogs Following Subretinal Injection of an Adeno-Associated Vector Expressing RPE65. *Hum Gene Ther.* 2013;24:883-893.

44. Acland GM, Aguirre GD, Ray J, et al. Gene therapy restores vision in a canine model of childhood blindness. *Nat Genet.* 2001;28:92-95.

CHAPTER 6

CONCLUSIONS AND FUTURE DIRECTIONS

6.1. CONCLUSIONS ON THE *CRX*-LCA FELINE MODELS AND THERAPY TRIAL

The cone-rod homeobox transcription factor CRX mediates photoreceptor development and survival by regulating the expression of many photoreceptor genes. *CRX* mutations are mostly associated with dominant retinopathies**:** Leber congenital amaurosis (adLCA), cone-rod dystrophy (adCRD) and retinitis pigmentosa (adRP), with a remarkable heterogeneity in age of onset and severity. The precise mechanism by which these mutations cause dominant disease is not totally understood, and no treatment is available.

Recently, *in vitro* and animal model studies have been developed to study the pathogenic mechanisms of *CRX* mutations. We have been studying a spontaneously occurring feline model. This model has a severe phenotype analogous to autosomal dominant LCA characterized by early-onset of a severe cone-led retinal dystrophy leading to blindness. Our preliminary work on the feline model – Crx^{Rdy}, which carries p.Pro185LysfsTer2, a spontaneous antimorphic frameshift mutation in the final exon in *Crx* causing a premature stop codon at residue 186 – reveals that heterozygous $Crx^{Rdy/+}$ cats have a retinal phenotype similar to what have been classified as Class III *CRX* mutations in humans and mice. The severe phenotype (delayed retinal morphological and functional development, then degeneration and loss of vision) is the result of a dominant antimorphic effect of the mutant *Crx* allele over the wild-type allele. The phenotype is described in detail in young animals in chapter 2 of the current work with later disease stages being described in chapter 3. Older $Crx^{Rdy/+}$ cats have a severe retinal degeneration accompanied by extensive inner retinal and vascular remodeling. At very late stage disease RPE atrophy develops in the *area centralis*, somewhat similar to a macular dystrophy. The homozygous $Crx^{Rdy/Rdy}$ cats have a different phenotype with an early halting of photoreceptor maturation, a complete lack vision and yet only a slow degeneration of photoreceptors and considerable migration and remodeling of retinal cells. They develop globe enlargement, likely secondary to

the complete lack of vision, with expansion primarily of the posterior segment. Photoreceptor development halts after the development of small vestigial inner segments, and there is a complete lack of outer segment development, a lack of expression of photoreceptor specific genes and a total absence of retinal function. In contrast to the $Crx^{Rdy/+}$ cats, they do not develop marked retinal or vasculature thinning although they do undergo extensive retinal remodeling.

An attempt to improve the phenotype of the $Crx^{Rdy/+}$ cats by over-expressing wild-type *Crx* using AAV vector delivery resulted in minor evidence of rescue in one kitten. The lack of consistent improvements suggests that a strategy to concurrently reduce expression of the mutant allele will also be required.

6.2. FUTURE DIRECTIONS

6.2.1. Investigation of the underlying disease mechanisms

In the *Rdy* feline as well as in *knockin* mice models, the precise mechanism leading to the over expression of the mutant allele and its subsequent antimorphic effect is not fully understood. Investigation of the underlying mechanism is essential in order to understand these retinal dystrophies, suggest possible therapeutic interventions and perhaps also add to the understanding of dominant negative retinal dystrophies in general.[1-3]

More detailed investigation of the effect of the disease on gene expression at different stages of retinal maturation would be valuable using techniques such as transcriptome sequencing (RNA-seq)[4]. Newer techniques such as massively parallel single-cell RNA profiling could be used to investigate the altered transcriptome in individual retinal cell types. In addition further investigation of the action of Crx by chromatin immuno-precipitation (ChIP)[5] on retinal samples could be used to determine the targets of the mutant allele. It would be highly valuable in both the $Crx^{Rdy/+}$ and $Crx^{Rdy/Rdy}$ cats to compare such transcriptome analysis with those for the

comparable mouse model to see if the same pattern of expression occurs within different Class III CRX mutation models. Regional expression differences would be useful to investigate in the cat model, for example, comparing changes within the *area centralis* and the more peripheral retina. Such studies to investigate changes in a retinal region like the *area centralis* that is comparable to the human macula is not possible in the mouse models and could be important because of the early macular involvement in human patients. This could be achieved by investigating regional difference of protein expression by IHC and with the use of additional antibodies to characterize changes in retinal remodeling, notably at the synapse levels in younger animal and also to use markers for immature cells, especially in the $Crx^{Rdy/Rdy}$ cats. Electron microscopy at an early age could also be performed in the $Crx^{Rdy/Rdy}$ cat to further investigate ultrastructural features; an example of this would be to investigate whether the stunted inner segments start developing cilia. Moreover, investigations of the mechanisms of photoreceptor cell death and retinal remodeling would be valuable.[6-13]

Despite the lack of vision and photoreceptor outer segments the $Crx^{Rdy/Rdy}$ cat retains a slow PLR. Chromatic pupillometry to investigate whether this is driven by melanopsin expressing ganglion cells could be performed. Pupil responses could also be developed as an outcome measure for therapeutic rescue.

Investigation to determine the mechanism for mutant allele over expression and how the mutant protein impairs the ability of wild-type Crx to activate target gene expression would be important. It is possible that the mutant mRNA and mutant protein may be more stable. Therefore, more investigations on mRNA and protein stability could be performed in cell lines. Bioinformatics could also be used as a tool to try to predict the structural conformation and potential post-translational changes such as phosphorylation of the mutant Crx protein that could therefore affect its function and binding to target gene promoter.[14, 15]

Investigation of the globe expansion in the *Crx*$^{Rdy/Rdy}$ cat to further understand the mechanism by which myopia develops would be valuable. Investigation of the course of vitreous expansion as well as refractive error and sclera/choroidal changes can be performed by more SD-OCT and histologic studies, but more specifically by investigating molecular and gene changes during growth by scleral and ocular mRNA and microRNA analysis.[16-22]

6.2.2. Developing therapies for treatment of dominant negative *CRX*-LCA retinal dystrophies

Our long-term goal is to advance the understanding of *CRX*-linked dominant retinopathies and develop safe and effective treatments. In addition to the therapy trial tested in chapter 5, other approaches can be tested as described below.

6.2.2.1. Supplementation therapies: selecting *rAAV* serotypes and promoters that most efficiently transduce both cones and rods in wild-type kittens

Recombinant adeno-associated viral vectors rAAV-mediated gene transfer therapy in order to increase levels of normal Crx to compete with the mutant Crx protein is currently being tested as described in chapter 5.

To pursue developing and optimizing therapies for the *Crx*$^{Rdy/+}$ cats, selecting effective serotype-promoter combinations and its optimal titers is needed. The vector will need to efficiently target photoreceptor without leading to toxicity or off-target transgene expression. Newer generations of rAAV that increase the transduction efficiency need to be tested. For example, self-complementary vectors[23] that avoid the step of synthesizing a second DNA strand have been shown to have a more rapid and stronger transgene expression. Other advances include

modification in the viral vector packaging, which overcomes the limitations caused by barriers encountered by the viral vector when transducing the target cells (e.g. ubiquitination, nuclear accumulation). Those rAAV vectors containing capsid amino-acid substitutions[24-26] (substitutions which allow rAAV to avoid ubiquitination and proteosome degradation during intracellular transport) will also be interesting to test in cats. Lastly, evaluation of rAAV vectors containing a different promoter to allow more precise tissue transduction should be considered e.g. G-protein-dependent receptor kinase (*GRK*) promoter[24] and interphotoreceptor retinoid-binding protein *(IRBP)* promoter[26, 27].

Once an optimal rAAV serotype-promoter combination is identified, it can be packaged with *hCRX-FLAG* to further test the gene supplementation approach in the $Crx^{Rdy/+}$ kittens.

6.2.2.2. Silencing therapies

6.2.2.2.1. Use of antisense gene silencing therapy to reduce the level of mutant *Crx* and rescue the retinal phenotype

It is likely that a combination of increasing expression of WT *Crx* will need to be combined with a strategy to reduce levels of the mutant protein. Toward the latter goal, allele-specific antisense oligonucleotides (ASOs) could be used.[28, 29] ASO have been used and proven successful in some inherited retinal degenerations such as the *CEP290*-LCA mouse model.[30-34]

Allele-specific antisense oligonucleotides (ASOs) are single strand nucleic acids that have a complementary sequence to the target mRNA. The ASO binds to the target mutant mRNA; RNase H enzyme recognizes the heteroduplex and binds to it. The enzyme then degrades the mRNA, leaving the DNA strand (ASO) intact[35] and therefore decreasing the production of mutant protein. Our preliminary investigations of ASOs to specifically target the mutant allele and leave the WT allele unaffected have not been successful so far.

6.2.2.2.2. Knockdown the mutant *Crx* allele using siRNA or shRNA

Both the use of siRNA and shRNA would aim at interfering with the mutant *Crx* allele and therefore decrease its negative effect. They have been used in retinal disease therapy in the past.[36-40] siRNA are small interfering RNA sequences that can be artificially synthesized and injected into the vitreous or subretinally. shRNA is produced by the cell. Therefore rAAV-*Crx*-shRNA knockdown vectors would have to be injected into the eye to enable the production of shRNA which would target the endogenous *Crx*. siRNA are simpler to produce but would require repeated injection. The rAAV-shRNA are more challenging to produce, but once introduced into a cell they should lead to continuous production of shRNA. These approaches have the potential disadvantage of also targeting wild-type *Crx* expression. Producing a "hardened" *Crx* allele that is also introduced by a rAAV vector and is functional and yet resistant to the shRNA would be a strategy to overcome this problem.

6.2.2.3. Other possible therapies

Over the last decade, new therapy techniques have been developed and could be tested in the Crx^{Rdy} cat to help rescue vision. One technique that is currently receiving much interest is CRISPR-Cas9 editing. [41-44] This technique aims to edit the gene of interest. One strategy would be to try and target the mutant allele and render it non-pathogenic, and another approach is to correct the mutation. Although this technique has been proven to be successful in retinal diseases[45, 46], it presents many potential difficulties including in vivo efficiency and the potential for significant off-target effects. In the case of the Crx^{Rdy} cat the correction of a one base-pair deletion would be challenging and would require extensive *in vitro* optimization before therapy

could be tried in animal models. Additionally, the delivery of the CRISPR-Cas9 complex requires AAV target optimization as for AAV gene supplementation.

Another potential therapy to be tested is retinal sheet or cell transplant.[47-52] For example, retinal sheet allograft has been tested in a feline *CEP290*-LCA model of progressive retinal dystrophy, showing integration but no ERG rescue.[53, 54] To be more effective genetic correction of iPS would be more valuable. This technique requires the development of induced pluripotent stem cell (iPS) using cells from the "patient" such as skin or adipocytes.[55] The iPS cells are then induced to form immature photoreceptor cells for transplantation or even developed into retinal organoids for transplantation. So far, growing iPS cells from adult cat cells has proven challenging.

6.2.3. Developing vision assessment in the cat

In comparison to the canine species, the feline species is harder to vision test in a reliable way. Indeed, cats are not consistently motivated by food or human interaction. Development of a similarly reliable test as published for dogs (Fig.1)[56, 57] is needed. Optokinetic testing could be developed by trying to adapt rodents' optokinetic device and additional maze test [58] to a bigger size using a computer screen. Other techniques or devices need to be developed in order to assess functional vision after therapy in addition to ERG testing.

REFERENCES

REFERENCES

1. Grayson C, Molday RS. Dominant negative mechanism underlies autosomal dominant Stargardt-like macular dystrophy linked to mutations in ELOVL4. *J Biol Chem.* 2005;280:32521-32530.

2. Barroso I, Gurnell M, Crowley VE, et al. Dominant negative mutations in human PPARgamma associated with severe insulin resistance, diabetes mellitus and hypertension. *Nature.* 1999;402:880-883.

3. Marivin A, Leyme A, Parag-Sharma K, et al. Dominant-negative Galpha subunits are a mechanism of dysregulated heterotrimeric G protein signaling in human disease. *Sci Signal.* 2016;9:ra37.

4. Ruzycki PA, Tran NM, Kefalov VJ, Kolesnikov AV, Chen S. Graded gene expression changes determine phenotype severity in mouse models of CRX-associated retinopathies. *Genome Biol.* 2015;16:171.

5. Corbo JC, Lawrence KA, Karlstetter M, et al. CRX ChIP-seq reveals the cis-regulatory architecture of mouse photoreceptors. *Genome Res.* 2010;20:1512-1525.

6. Morrow EM, Furukawa T, Raviola E, Cepko CL. Synaptogenesis and outer segment formation are perturbed in the neural retina of Crx mutant mice. *BMC Neurosci.* 2005;6:5.

7. Pignatelli V, Cepko CL, Strettoi E. Inner retinal abnormalities in a mouse model of Leber's congenital amaurosis. *J Comp Neurol.* 2004;469:351-359.

8. Chong NH, Alexander RA, Barnett KC, Bird AC, Luthert PJ. An immunohistochemical study of an autosomal dominant feline rod/cone dysplasia (Rdy cats). *Exp Eye Res.* 1999;68:51-57.

9. Sancho-Pelluz J, Arango-Gonzalez B, Kustermann S, et al. Photoreceptor cell death mechanisms in inherited retinal degeneration. *Mol. Neurobiol.* 2008;38:253-269.

10. Athanasiou D, Aguila M, Bevilacqua D, Novoselov SS, Parfitt DA, Cheetham ME. The cell stress machinery and retinal degeneration. *FEBS Lett.* 2013;587:2008-2017.

11. Arango-Gonzalez B, Trifunovic D, Sahaboglu A, et al. Identification of a common non-apoptotic cell death mechanism in hereditary retinal degeneration. *PloS one.* 2014;9:e112142.

12. Paquet-Durand F, Sahaboglu A, Dietter J, et al. How long does a photoreceptor cell take to die? Implications for the causative cell death mechanisms. *Adv Exp Med Biol.* 2014;801:575-581.

13. Sahaboglu A, Paquet-Durand O, Dietter J, et al. Retinitis pigmentosa: rapid neurodegeneration is governed by slow cell death mechanisms. *Cell Death Dis.* 2013;4:e488.

14. Chen S, Wang QL, Xu S, et al. Functional analysis of cone-rod homeobox (CRX) mutations associated with retinal dystrophy. *Hum Mol Genet.* 2002;11:873-884.

15. Valastyan JS, Lindquist S. Mechanisms of protein-folding diseases at a glance. *Model Mec.* 2014;7:9-14.

16. Metlapally R, Park HN, Chakraborty R, et al. Genome-Wide Scleral Micro- and Messenger-RNA Regulation During Myopia Development in the Mouse. *Invest Ophthalmol Vis Sci.* 2016;57:6089-6097.

17. Metlapally R, Wildsoet CF. Scleral Mechanisms Underlying Ocular Growth and Myopia. *Prog Mol Biol Transl Sci.* 2015;134:241-248.

18. Metlapally R, Gonzalez P, Hawthorne FA, Tran-Viet KN, Wildsoet CF, Young TL. Scleral micro-RNA signatures in adult and fetal eyes. *PloS one.* 2013;8:e78984.

19. Jobling AI, Gentle A, Metlapally R, McGowan BJ, McBrien NA. Regulation of scleral cell contraction by transforming growth factor-beta and stress: competing roles in myopic eye growth.*J Biol Chem.* 2009;284:2072-2079.

20. Yang J, Reinach PS, Zhang S, et al. Changes in retinal metabolic profiles associated with form deprivation myopia development in guinea pigs. *Sci Rep.* 2017;7:2777.

21. Zhou X, Ye J, Willcox MD, et al. Changes in protein profiles of guinea pig sclera during development of form deprivation myopia and recovery. *Mol Vis.* 2010;16:2163-2174.

22. Ritchey ER, Zelinka C, Tang J, et al. Vision-guided ocular growth in a mutant chicken model with diminished visual acuity. *Exp Eye Res.* 2012;102:59-69.

23. Petersen-Jones SM, Bartoe JT, Fischer AJ, et al. AAV retinal transduction in a large animal model species: comparison of a self-complementary AAV2/5 with a single-stranded AAV2/5 vector. *Mol Vis.* 2009;15:1835-1842.

24. Kay CN, Ryals RC, Aslanidi GV, et al. Targeting photoreceptors via intravitreal delivery using novel, capsid-mutated AAV vectors. *PloS one.* 2013;8:e62097.

25. Mowat FM, Gornik KR, Dinculescu A, et al. Tyrosine capsid-mutant AAV vectors for gene delivery to the canine retina from a subretinal or intravitreal approach. *Gene Ther.* 2014;21:96-105.

26. Boyd RF, Sledge DG, Boye SL, et al. Photoreceptor-targeted gene delivery using intravitreally administered AAV vectors in dogs. *Gene Ther.* 2016;23:400.

27. Dyka FM, Boye SL, Ryals RC, Chiodo VA, Boye SE, Hauswirth WW. Cone specific promoter for use in gene therapy of retinal degenerative diseases. *Adv Exp Med Biol.* 2014;801:695-701.

28. Crooke ST. Vitravene--another piece in the mosaic. *Antisense Nucleic Acid Drug Dev.* 1998;8:vii-viii.

29. El Harchaoui K, Akdim F, Stroes ES, Trip MD, Kastelein JJ. Current and future pharmacologic options for the management of patients unable to achieve low-density lipoprotein-cholesterol goals with statins. *Am J Cardiovasc Drugs.* 2008;8:233-242.

30. Garanto A, Chung DC, Duijkers L, et al. In vitro and in vivo rescue of aberrant splicing in CEP290-associated LCA by antisense oligonucleotide delivery. *Hum Mol Genet.* 2016;25:2552-2563.

31. Gerard X, Garanto A, Rozet JM, Collin RW. Antisense Oligonucleotide Therapy for Inherited Retinal Dystrophies. *Adv Exp Med Biol.* 2016;854:517-524.

32. Gerard X, Perrault I, Hanein S, et al. AON-mediated Exon Skipping Restores Ciliation in Fibroblasts Harboring the Common Leber Congenital Amaurosis CEP290 Mutation. *Mol Ther Nucleic Acids.* 2012;1:e29.

33. Collin RW, den Hollander AI, van der Velde-Visser SD, Bennicelli J, Bennett J, Cremers FP. Antisense Oligonucleotide (AON)-based Therapy for Leber Congenital Amaurosis Caused by a Frequent Mutation in CEP290. *Mol Ther Nucleic Acids.* 2012;1:e14.

34. Collin RW, Garanto A. Applications of antisense oligonucleotides for the treatment of inherited retinal diseases. *Curr Opin Ophthalmol.* 2017;28:260-266.

35. Bennett CF, Swayze EE. RNA targeting therapeutics: molecular mechanisms of antisense oligonucleotides as a therapeutic platform. *Ann Rev Pharmacol Toxicol.* 2010;50:259-293.

36. Mao H, Gorbatyuk MS, Rossmiller B, Hauswirth WW, Lewin AS. Long-term rescue of retinal structure and function by rhodopsin RNA replacement with a single adeno-associated viral vector in P23H RHO transgenic mice. *Hum Gene Ther.* 2012;23:356-366.

37. Georgiadis A. Viral vector-mediated RNA interference in the retina *Division of Molecular Therapy, Institute of Ophthalmology.* University College London 2009:227.

38. Gorbatyuk M, Justilien V, Liu J, Hauswirth WW, Lewin AS. Suppression of mouse rhodopsin expression in vivo by AAV mediated siRNA delivery. *Vis Res.* 2007;47:1202-1208.

39. O'Reilly M, Palfi A, Chadderton N, et al. RNA interference-mediated suppression and replacement of human rhodopsin in vivo. *Am J Hum Genet.* 2007;81:127-135.

40. Thakur A, Fitzpatrick S, Zaman A, et al. Strategies for ocular siRNA delivery: Potential and limitations of non-viral nanocarriers. *J Biol Eng*. 2012;6:7.

41. Jiang F, Doudna JA. CRISPR-Cas9 Structures and Mechanisms. *Ann Rev Biophys.* 2017;46:505-529.

42. Doudna JA, Charpentier E. Genome editing. The new frontier of genome engineering with CRISPR-Cas9. *Science.* 2014;346:1258096.

43. Wang H, La Russa M, Qi LS. CRISPR/Cas9 in Genome Editing and Beyond. *Ann Rev Biochem.* 2016;85:227-264.

44. Sander JD, Joung JK. CRISPR-Cas systems for editing, regulating and targeting genomes. *Nat Biotechnol.* 2014;32:347-355.

45. Yu W, Mookherjee S, Chaitankar V, et al. Nrl knockdown by AAV-delivered CRISPR/Cas9 prevents retinal degeneration in mice. *Nat Commun.* 2017;8:14716.

46. Peng YQ, Tang LS, Yoshida S, Zhou YD. Applications of CRISPR/Cas9 in retinal degenerative diseases. *Int J Ophthalmol.* 2017;10:646-651.

47. West EL, Pearson RA, MacLaren RE, Sowden JC, Ali RR. Cell transplantation strategies for retinal repair. *Prog Brain Res.* 2009;175:3-21.

48. Pearson RA, Hippert C, Graca AB, Barber AC. Photoreceptor replacement therapy: challenges presented by the diseased recipient retinal environment. *Vis Neurosci.* 2014;31:333-344.

49. Jayakody SA, Gonzalez-Cordero A, Ali RR, Pearson RA. Cellular strategies for retinal repair by photoreceptor replacement. *Prog Retin Eye Res.* 2015;46:31-66.

50. Lakowski J, Gonzalez-Cordero A, West EL, et al. Transplantation of Photoreceptor Precursors Isolated via a Cell Surface Biomarker Panel From Embryonic Stem Cell-Derived Self-Forming Retina. *Stem Cells.* 2015;33:2469-2482.

51. Seiler MJ, Aramant RB. Cell replacement and visual restoration by retinal sheet transplants. *Prog Retin Eye Res.* 2012;31:661-687.

52. Nistor G, Seiler MJ, Yan F, Ferguson D, Keirstead HS. Three-dimensional early retinal progenitor 3D tissue constructs derived from human embryonic stem cells. *J Neurosci Methods.* 2010;190:63-70.

53. Ivert L, Gouras P, Naeser P, Narfstrom K. Photoreceptor allografts in a feline model of retinal degeneration. *Graefe Arch Clin Exp Ophthalmol.* 1998;236:844-852.

54. Seiler MJ, Aramant RB, Seeliger MW, Bragadottir R, Mahoney M, Narfstrom K. Functional and structural assessment of retinal sheet allograft transplantation in feline hereditary retinal degeneration. *Vet Ophthalmol.* 2009;12:158-169.

55. Jumabay M, Bostrom KI. Dedifferentiated fat cells: A cell source for regenerative medicine. *World J Stem Cells.* 2015;7:1202-1214.

56. Gearhart PM, Gearhart CC, Petersen-Jones SM. A novel method for objective vision testing in canine models of inherited retinal disease. *Invest Ophthalmol Vis Sci*. 2008;49:3568-3576.

57. Garcia MM, Ying GS, Cocores CA, Tanaka JC, Komaromy AM. Evaluation of a behavioral method for objective vision testing and identification of achromatopsia in dogs. *Am J Vet Res.* 2010;71:97-102.

58. Kretschmer F, Sajgo S, Kretschmer V, Badea TC. A system to measure the Optokinetic and Optomotor response in mice. *J Neurosci Methods.* 2015;256:91-105.